2013

INVESTIGATING THERAPEUTIC OPTIONS FOR LAFORA DISEASE USING STRUCTURAL BIOLOGY AND TRANSLATIONAL METHODS

Amanda R. Sherwood
University of Kentucky, lilbunny321@hotmail.com

STUDENT AGREEMENT:

I represent that my thesis or dissertation and abstract are my original work. Proper attribution has been given to all outside sources. I understand that I am solely responsible for obtaining any needed copyright permissions. I have obtained and attached hereto needed written permission statements(s) from the owner(s) of each third-party copyrighted matter to be included in my work, allowing electronic distribution (if such use is not permitted by the fair use doctrine).

I hereby grant to The University of Kentucky and its agents the non-exclusive license to archive and make accessible my work in whole or in part in all forms of media, now or hereafter known. I agree that the document mentioned above may be made available immediately for worldwide access unless a preapproved embargo applies.

I retain all other ownership rights to the copyright of my work. I also retain the right to use in future works (such as articles or books) all or part of my work. I understand that I am free to register the copyright to my work.

REVIEW, APPROVAL AND ACCEPTANCE

The document mentioned above has been reviewed and accepted by the student's advisor, on behalf of the advisory committee, and by the Director of Graduate Studies (DGS), on behalf of the program; we verify that this is the final, approved version of the student's dissertation including all changes required by the advisory committee. The undersigned agree to abide by the statements above.

Amanda R. Sherwood, Student

Dr. Matthew Shawn Gentry, Major Professor

Dr. Michael Mendenhall, Director of Graduate Studies

INVESTIGATING THERAPEUTIC OPTIONS FOR LAFORA DISEASE USING STRUCTURAL BIOLOGY AND TRANSLATIONAL METHODS

DISSERTATION

A dissertation submitted in partial fulfillment of the requirements for the degree of Doctor of Philosophy in the College of Medicine at the University of Kentucky

By

Amanda Renee Sherwood

Lexington, Kentucky

Director: Dr. Matthew Gentry

Associate Professor of Molecular and Cellular Biochemistry

Lexington, Kentucky

2013

ABSTRACT OF DISSERTATION

INVESTIGATING THERAPEUTIC OPTIONS FOR LAFORA DISEASE USING STRUCTURAL BIOLOGY AND TRANSLATIONAL METHODS

Lafora disease (LD) is a rare yet invariably fatal form of epilepsy characterized by progressive degeneration of the central nervous and motor systems and accumulation of insoluble glucans within cells. LD results from mutation of either the phosphatase laforin, an enzyme that dephosphorylates cellular glycogen, or the E3 ubiquitin ligase malin, the binding partner of laforin. Currently, there are no therapeutic options for LD, or reported methods by which the specific activity of glucan phosphatases such as laforin can be easily measured. To facilitate our translational studies, we developed an assay with which the glucan phosphatase activity of laforin as well as emerging members of the glucan phosphatase family can be characterized. We then adapted this assay for the detection of endogenous laforin activity from human and mouse tissue. This laforin bioassay will prove useful in the detection of functional laforin in LD patient tissue following the application of therapies to LD patients. We subsequently developed an *in vitro* readthrough reporter system in order to assess the efficacy of aminoglycosides in the readthrough of laforin and malin nonsense mutations. We found that although several laforin and malin nonsense mutations exhibited significant drug-induced readthrough, the location of the epitope tag used to detect readthrough products dramatically affected our readthrough results. Cell lines established from LD patients with nonsense mutations are thus required to accurately assess the efficacy of aminoglycosides as a therapeutic option for LD. Using hydrogen-deuterium exchange mass spectrometry (DXMS), we then gained insight into the molecular etiology of several point mutations in laforin that cause LD. We identified a novel motif in the phosphatase domain of laforin that shares homology with glycosyl hydrolases (GH) and appears to play a role in the interaction of laforin with glucans. We studied the impact of the Y294N and P301L LD mutations within this GH motif on glucan binding. Surprisingly, these mutations did not reduce glucan binding as expected, rather enhancing the binding of laforin to glucans. These findings elucidate the mechanism by which laforin interacts with and acts upon glucan substrates, providing a target for the development of therapeutic compounds.

KEYWORDS: Lafora disease, laforin, malin, glucan phosphatase, neurodegeneration

Amanda Renee Sherwood

November 27, 2013

INVESTIGATING THERAPEUTIC OPTIONS FOR LAFORA DISEASE USING STRUCTURAL BIOLOGY AND TRANSLATIONAL METHODS

By

Amanda Renee Sherwood

Dr. Matthew Shawn Gentry
Director of Dissertation

Dr. Michael Mendenhall
Director of Graduate Studies

November 27, 2013
Date

ACKNOWLEDGEMENTS

Graduate school has been an arduous journey in which I faced challenges that seemed insurmountable. I truly learned the meaning of defeat and triumph, and I would not have made it without the unconditional support of my loved ones and close friends. Foremost, I would like to thank my parents, Paul and Karen. You never ceased to encourage me or simply listen to my frustrations. I'm sure I would not have succeeded without your unending patience and love.

I would like to acknowledge my mentor Dr. Matthew Gentry for giving me the opportunity to fulfill my aspirations and for driving me to become an independent scientist. Over the past five years, he navigated me through the ups and downs of research and challenged me to think critically, guiding me to formulate my own hypotheses and experiments. I appreciate his willingness to listen and his encouragement. I would also like to thank my dissertation committee members, Dr. Paul Murphy, Dr. Sabire Ozcan, Dr. Melinda Wilson, and my external examiner Dr. Michael Kilgore for valuable suggestions and feedback that have aided me in becoming a better scientist.

There are several people who helped me perform the experiments included in my dissertation I would like to acknowledge. I am indebted to Simon Hsu and Brian Wong, without whom I would not have been able to tackle such a large DXMS project. Casper Wilkens helped me optimize affinity electrophoresis conditions for laforin studies. Dr. Vikas Dukhande was always willing to share his cells with me, as well as lend an ear when I was frustrated. All members of the Gentry lab, past and present, were willing to donate reagents or a hand whenever it was needed, which I'm thankful for.

I would also like to thank Jennifer Vernia, Jackie Oh, and Jason Meyer for always taking the time to listen, comfort, and inspire. I can only hope one day to return the kindness and support you have shown me. And to Serge Cardinali, when writing this dissertation seemed particularly overwhelming, you kept me smiling and provided me with crucial Taco Bell refuelings.

Finally, I would like to acknowledge Dr. Daniel Noonan, Dr. Charles Waechter, and Dr. Paul Murphy, who always made time to critique my work and provide me with valuable feedback, and who went above and beyond in giving assistance, direction, and praise. In particular, I would like to thank Dr. Jeffrey Rush, without whose words of encouragement at a critical point in my career I might not have succeeded.

TABLE OF CONTENTS

Acknowledgments iii
List of Tables viii
List of Figures ix
Abbreviations xi
CHAPTER 1: INTRODUCTION AND BACKGROUND 1
Lafora disease: on overview 1
The role of laforin in glycogen metabolism 3
Malin and the regulation of enzymes involved in glycogen metabolism 6
CHAPTER 2: MATERIALS AND METHODS 14
Recombinant protein expression and purification 14
*p*NPP assay (abbreviated) 14
Malachite green assay (abbreviated) 15
Laforin antibody production 15
Cell culture and transfections 16
Cell lysate preparation and immunoprecipitation 16
Assessment of antibodies for the immunoprecipitation of overexpressed laforin 17
Assessment of antibodies for the immunoprecipitation of endogenous laforin 18
Antigen competition to confirm laforin antibody specificity 18
Assessment of antibody impact on recombinant laforin activity 19
Immunoprecipitation of overexpressed laforin for activity assay 19
Immunoprecipitation and activity assay of endogenous laforin from HepG2 cells 20
Immunoprecipitation and activity assay of endogenous laforin from mouse skeletal muscle and human skin tissue 20
Creation of laforin and malin nonsense mutant constructs 22
Laforin half-life determination 23
Immunofluorescence cell staining 23

Statistical analysis 24
Generation of laforin mutants for DXMS 24
Carbohydrate binding assays 25
Native glycogen gel electrophoresis 25
Optimization of pepsin digestion of laforin 26
Hydrogen-deuterium exchange of laforin 27
Homology modeling of laforin 30
CHAPTER 3: A MALACHITE GREEN-BASED ASSAY TO ASSESS GLUCAN PHOSPHATASE ACTIVITY 32
Introduction 32
Results 34
Discussion 37
CHAPTER 4: A BIOASSAY FOR LAFORA DISEASE AND LAFORIN GLUCAN PHOSPHATASE ACTIVITY 46
Introduction 46
Results 47
Discussion 51
CHAPTER 5: EFFECTS OF AMINOGLYCOSIDES ON NONSENSE MUTATIONS IN LAFORIN AND MALIN AS A THERAPEUTIC OPTION FOR LAFORA DISEASE 64
Introduction 64
Results 66
Discussion 70
CHAPTER 6: HYDROGEN- DEUTERIUM EXCHANGE MASS SPECTROMETRY PROVIDES INSIGHT INTO THE IMPACT OF LAFORA DISEASE MUTATIONS ON THE STRUCTURE AND MECHANISM OF LAFORIN 86
Introduction 86
Results 90
The glycosyl hydrolase motifs of laforin and choice of Lafora disease mutants to study using DXMS 90
Biochemical characterization of wild-type laforin and laforin mutants 92

Optimization of laforin digestion for DXMS 95
DXMS experiments and structural insights of wild-type laforin 96
The substrate preference of laforin 97
The binding dynamics of laforin with glycogen 99
The DXMS method elucidates the pathogenesis of LD mutations in laforin 101
Insights into the binding mechanism of laforin 102
Effects of LD mutations in the GH1-like region on laforin binding dynamics 103
Homology model of laforin reveals spatial binding dynamics 105
Discussion 108
Insights into the structure and mechanism of laforin 108
Insight into the molecular etiology of LD mutations 112
CHAPTER 7: DISCUSSION AND FUTURE DIRECTIONS 147
Application of the laforin bioassay with Lafora disease patients 147
Structural aspects of laforin and the impact of disease mutations 149
APPENDIX 1: SUPPLEMENTARY PROTOCOLS 156
pNPP assay 156
Malachite green standard curve and assay 160
REFERENCES 166
VITA 186

LIST OF TABLES

Table 5.1: Summary of laforin and malin nonsense mutant expression and readthrough results 84

LIST OF FIGURES

Figure 1.1: Laforin and malin 9
Figure 1.2: Glucans and the role of laforin in Lafora disease 10
Figure 1.3: Model depicting the proposed role of the laforin-malin complex and its interactions in glycogen metabolism 12
Figure 3.1: Experimental design of assays and phosphatases chosen for study 39
Figure 3.2**:** The *p*NPP and malachite green assays reveal specific glucan phosphatase activity only in glucan phosphatases 42
Figure 3.3: *p*NPP and malachite green assay results reported using total protein 44
Figure 4.1: Laforin exhibits phosphatase activity both bound to and free of the antibody-agarose complex 54
Figure 4.2: Laforin antibody selection 56
Figure 4.3: Immunoprecipitation and activity assay of recombinant and overexpressed laforin 58
Figure 4.4: Immunoprecipitated endogenous laforin exhibits specific glucan phosphatase activity 60
Figure 4.5: Endogenous laforin activity from mouse and human tissue lysate 61
Figure 5.1: Laforin and malin nonsense mutations chosen for study 75
Figure 5.2: Response of C-terminally FLAG-tagged laforin nonsense mutants to readthrough-promoting compounds 77
Figure 5.3: Response of C-terminally FLAG-tagged malin nonsense mutants to readthrough-promoting compounds 79
Figure 5.4: Response of N-terminally FLAG-tagged laforin and malin nonsense mutants to readthrough-promoting compounds 81
Figure 5.5: Determination of endogenous laforin half-life 83
Figure 6.1: Amide hydrogen exchange and DXMS experimental layout 115
Figure 6.2: The characteristic regions of the DSP domain 116
Figure 6.3: The glycosyl hydrolase family 1 active site pattern in the R motif of laforin 117
Figure 6.4: Biochemical characterization of Ni-NTA purified wild-type laforin and mutants 119
Figure 6.5: Purification of recombinant wild-type laforin for DXMS and peptide coverage map 121
Figure 6.6: Mass spectra of residues 98-111 of wild-type laforin 123
Figure 6.7A: DXMS results of wild-type laforin and SEX4 without substrate 125
Figure 6.7B: DXMS results of wild-type laforin and SEX4 without substrate 126
Figure 6.8: DXMS results of wild-type laforin with structurally varied glucan substrates 128
Figure 6.9: Peptides within the CBM of laforin that exhibit deuteration changes after glycogen binding 130
Figure 6.10: Peptides within the DSP of laforin that exhibit deuteration changes after glycogen binding 131
Figure 6.11: Maximal percent decreases in deuteration of SEX4 and laforin upon substrate binding 133

Figure 6.12: The laforin W32G CBM mutant and DSP mutant G240S validate the DXMS method 135
Figure 6.13: The DSP of C266S laforin exhibits disrupted glycogen binding 137
Figure 6.14: The Y294N and P301L mutants exhibit strengthened glycogen binding 139
Figure 6.15: Peptides within the R motif of the Y294N and P301L mutants that exhibit decreases in deuteration after glycogen binding 141
Figure 6.16: Homology model of the CBM of wild-type laforin with binding dynamics 143
Figure 6.17: Homology model of the DSP of wild-type laforin with binding dynamics 144
Figure 6.18: Alteration of the binding dynamics of laforin resulting from the P301L mutation 146
Figure 7.1: The role of the GH-like motif in the variable loop of LSF2 154

ABBREVIATIONS

BSA, bovine serum albumin; C-FLAG, C-terminal FLAG tag; CBM, carbohydrate-binding module; CF, cystic fibrosis; CFTR, cystic fibrosis transmembrane conductance regulator; CSF, cerebrospinal fluid; cTP, chloroplast targeting peptide; DiFMUP, 6,8-difluoro-4-methylumbellyferyl phosphate; DSP, dual-specificity phosphatase; DTT, dithiothreitol; DXMS, hydrogen-deuterium exchange mass spectrometry; FDP, fluorescein diphosphate; FPLC, fast protein liquid chromatography; GH, glycosyl hydrolase; HEK, human embryonic kidney, HRP, horseradish peroxidase; LB, Lafora body; LD, Lafora disease; LSF2; Like SEX4 2; mRIPA, modified RIPA buffer; N-FLAG, N-terminal FLAG tag; NEM, *N*-ethylmaleimide; OMFP, 3-*O*-methylfluorescein phosphate; PAS, periodic acid Schiff; pcDNA3.1 FLAG, pcDNA3.1 with N-terminal FLAG tag; PME, progressive myoclonus epilepsy; *p*NPP, *para*-nitrophenylphosphate, PP1, protein phosphatase 1; PPM, metallo-dependent protein phosphatase, PPP, phosphoprotein phosphatase; PTEN, phosphatase and tensin homolog; PTP, protein tyrosine phosphatase; PTPMT1, protein tyrosine phosphatase localized to mitochondrion 1; SEX4, Starch Excess 4; TBS, Tris-buffered saline; TCEP, tris(2-carboxyethyl)phosphine; TCPTP, T-cell protein tyrosine phosphatase; VHR, VH1-related dual-specificity phosphatase.

CHAPTER 1: BACKGROUND AND INTRODUCTION

Lafora disease: an overview.

Lafora disease (LD; OMIM #254780) is a fatal autosomal recessive disorder characterized by myoclonic, tonic-clonic, and focal-occipital seizures accompanied by progressive degeneration of the central nervous and motor systems (*13, 68*). Other symptoms include dementia, visual hallucinations, ataxia, absence and grand mal seizures along with epilepsy triggered by stimulus (*105*). Patients with LD develop normally until they present with a tonic-clonic seizure during adolescence. Subsequently, patients exhibit the described seizure types that increase in frequency and severity with age (*105*). The initial seizure is also followed by rapid concurrent neurodegeneration, and patient death occurs overwhelmingly within ten years of disease onset due to complications such as status epilepticus, aspiration pneumonia, or respiratory failure (*105*). There is significant neuronal loss across the CNS upon death with no signs of inflammation (*52*). The progressive escalation of epileptic symptoms places LD within the progressive myoclonus epilepsy (PME) family, which is comprised of five major disorders (*14, 62, 83*). Together, the PMEs constitute ≈1% of all epilepsies (*105*).

Due to the progressive nature of neurodegeneration, the frequency of myoclonic seizures, and the variety of seizure types that can present, PMEs are often difficult to diagnose at onset (*105*). However, a distinguishing characteristic of LD is the presence of hyperphosphorylated and poorly branched glycogen-like accumulations called Lafora bodies (LBs) in the cytoplasm of cells in all tissues. The spherical and insoluble LB inclusions are 3-40 μm in size, and can grow large enough to occupy the entire cytoplasm. Despite the presence of LBs in a variety of tissues throughout the body, non-neurological symptoms are uncommon (*105*), likely because CNS neurons are unable to undergo cell division to replace lost cells. Due to their size, LBs may act as a physical block preventing crucial cellular trafficking events in neurons, which transport intracellular cargos over larger distances than other cells. Alternatively, LBs may act as an unusable energy sink,

reducing the availability of free glucose to neurons, which are highly energy dependent and thus sensitive to perturbations in energy availability (*54*). Although the etiology of LD has yet to be fully elucidated, the presence of LBs in neurons is hypothesized to be responsible for the non-apoptotic neural cell death and seizures observed in patients (*27, 129, 176*).

LD results from recessive mutations in the autosomal *EPM2A* (*epilepsy, progressive myoclonus type 2A*) and *EPM2B* (*epilepsy, progressive myoclonus type 2B*) genes encoding the dual-specificity phosphatase laforin and the E3 ubiquitin ligase malin, respectively (*29, 55, 107*). Defects in laforin account for 70% of LD cases and defects in malin 27% of cases, with mutations found across both proteins (*134, 141*) (Figure 1.1A and B). Mutations in laforin and malin have been demonstrated to disrupt activity, substrate binding, interaction partner binding, and localization (*29, 42, 141*).

The accumulation of LBs within cells and the absence of normal cellular glycogen indicate defects in glycogen metabolism, linking epilepsy and neurodegeneration to the disruption of metabolism. LD is a rare disease (*105*), however, there is a strong connection between metabolic defects and many other types of epilepsies (*119*), with epilepsy affecting almost 3 million Americans at an estimated annual cost of $15.5 billion (*1*). Insight into the molecular etiology of LD and the disruption of glycogen metabolism may reveal a metabolic link shared with other forms of epilepsy.

There are currently no available therapies for LD outside of palliative therapeutics that allow the symptoms of LD to be managed for a short period (*105, 107*). Permanent therapeutic options for LD including *EMP2A/EPM2B* gene replacement or treatment with Trojan horse liposomes (also called PEGylated immunoliposomes) containing the gene for laforin or malin are both being explored (*115*). As LD is an invariably fatal disorder, we assessed additional therapeutic options for LD. We explored the efficacy of aminoglycosides, compounds that have been shown to produce readthrough of disease-causing nonsense mutations (*94*), in rescuing nonsense mutations in laforin and malin. We also explored the impact of

LD point mutations on laforin structure and activity for the development of LD mutation-specific therapies.

The role of laforin in glycogen metabolism.

Two groups searching for genes mutated in LD patients simultaneously discovered the *EPM2A* gene that encodes the protein laforin (*106, 132*). This gene was later discovered to be conserved in all vertebrates as well as a subset of protists and invertebrates (*55*). Laforin is expressed in all human tissues, although higher expression is observed in brain, skeletal muscle, heart, and liver (*133*). Laforin is a bimodular protein, containing an N-terminal carbohydrate-binding module (CBM) representative of the CBM20 family (*18, 25, 166*) and a C-terminal dual-specificity phosphatase (DSP) domain featuring the canonical DSP active site motif $Dx_{30}HCxxGxxRS/T$ (CX_5R) (*106*) (Figure 1.1A).

Dual-specificity phosphatases (DSPs) are a class of phosphatases whose members dephosphorylate a diverse array of substrates including phosphoserine, threonine, and tyrosine residues, phosphatidylinositols, ribo/deoxyribonucleotide 5'-triphosphates, pyrophosphate/triphosphate, or phosphorylated glucans (*2, 109, 154*). DSPs are members of the larger protein tyrosine phosphatase (PTP) family that all utilize a cysteine-dependent mechanism to hydrolyze phosphoester bonds. This mechanism is dependent on the conserved CX_5R active site motif common to all PTP phosphatases (*2*). Consistent with its designation as a DSP, laforin exhibits *in vitro* phosphatase activity against phosphoserine, threonine, and tyrosine residues of various exogenous substrates (*52*). In addition to this activity, laforin can utilize the artificial substrates 3-O-methylflourescein phosphate (OMFP) and *para*-nitrophenylphosphate (*p*NPP) (*42, 55*).

Laforin is the founding member of a small group of DSPs called the glucan phosphatases. Of the 128 human phosphatases, laforin is the only phosphatase with a CBM, and the only phosphatase possessing activity against phosphorylated carbohydrates (*55, 172*). CBMs are noncatalytic domains divided into 67 families based on evolutionary relationships, polypeptide folds, and substrate preferences according to the Carbohydrate-Active Enzymes (CAZY) database (*18, 25*). The

CBM20 family constitutes one of the most characterized CBM families, featuring glycosylhydrolases and glucotransferases from bacteria, fungi, and plants (*18, 81, 82*). The CBM20 domain that it possesses allows laforin to bind glycogen both *in vivo* and *in vitro* and to dephosphorylate this glucose polymer (*55, 152, 166*).

Glucans are complex carbohydrates featuring glucose moieties linked by glycosidic bonds. Glycogen is a water-soluble glucan produced in the cytoplasm of most archaebacteria, bacteria, fungi, and animal species functioning as an energy storage molecule. Glycogen features glucose residues joined by α-1,4-glycosidic linkages formed by glycogen synthase, and also possesses α-1,6-glycosidic linkages at regular branch points formed by branching enzyme (*121*) (Figure 1.2A). These regular α-1,6 branch points are crucial for the water solubility of glycogen (*54*). It has been observed that glycogen naturally contains low levels of phosphate, but the role of this phosphate in glycogen in addition to the enzymes responsible for its introduction has not been determined (*54, 96*).

Interestingly, when laforin is mutated, cells begin to accumulate LBs, insoluble glucan deposits that possess higher amounts of phosphate than glycogen and exhibit irregular branching like that seen in other insoluble glucose polymers such as amylopectin, a component of plant starch (*54, 124, 149*) (Figure 1.2B and C). Following this discovery, subsequent work established that laforin dephosphorylates glucans such as glycogen and amylopectin *in vitro* (*152, 172*). LD mutations in laforin abolish *in vitro* and *in vivo* glucan binding as well as *in vitro* glucan phosphatase activity (*55, 141*). Recently, it has been demonstrated that as phosphate levels increase in glycogen, glycogen becomes insoluble (*149, 152*). As other human phosphatases lack the ability to dephosphorylate glucans (*172*), these findings indicate that laforin's role in cells is to remove phosphate from cellular glycogen to prevent the formation of LBs (*54*).

Additional *in vivo* work supports the role of laforin in binding cellular glycogen to prevent LB formation. As it possesses a CBM, laforin co-localizes with glycogen granules, with mutations in the CBM disrupting this co-localization (*166*). In addition to laforin interaction with phosphorylated glucans *in vitro* (*55*), a study

employing mice overexpressing catalytically inactive laforin showed that laforin preferentially binds LBs over glycogen (*28*). These studies utilized overexpressed laforin to examine subcellular localization, and currently no study has described the localization of endogenous laforin in a vertebrate. However, endogenous laforin localization was reported for the red algae *Cyanidioschyzon merolae*. In *C. merolae*, laforin co-localized with the outer surface of the starch granules present within *C. merolae* as demonstrated by immunogold electron microscopy (*55*). Thus, the binding of laforin to glycogen in vertebrates is supported by data from both *in vivo* and *in vitro* systems.

It is currently not understood if LB formation is the result of an overactive polyglucosan biosynthetic pathway or a disrupted degradative metabolic pathway. Recent work reported that phosphate is incorporated into glycogen by glycogen synthase at a rate of ≈1 phosphate per 10,000 glucose residues during glycogen synthesis (*151*). However, a subsequent report questioned the role of glycogen synthase in glycogen phosphorylation (*113*). Regardless of the mechanism by which phosphate is introduced into glycogen, it is likely that laforin is responsible for removing this phosphate to maintain glycogen solubility (*54, 151*). It has been observed that tissues with the highest laforin expression in the body are also the tissues that exhibit the highest proportion of LBs in LD (*49*). These tissues, including neurons, cardiac muscle, and liver, also display increased laforin expression in normal individuals (*52*). In addition, the phosphate content of LBs isolated from muscle and hepatic tissue of *EPM2A* knockout mice is higher than the phosphate content of glycogen from wild-type mice (*50, 150, 152*). Most importantly, laforin can remove phosphate from LBs observed to form in a laforin knockout mouse model (*50, 149, 152*). The failure of laforin to remove phosphate covalently attached to glucose moieties may disrupt packing within glycogen, thus altering its solubility. Alternatively, increased glycogen phosphate may block the action of glycogen branching enzyme during glycogen synthesis that is necessary for glycogen solubility (*55, 136*) (Figure 1.2D).

Laforin protein levels are regulated by the ubiquitin-proteasome system (*58*), and a direct correlation has also been described between laforin protein levels

and cellular glycogen content. Investigation into mouse models that accumulate higher or lower levels of glycogen revealed that laforin protein expression is upregulated as muscle glycogen stores increase (*167*). This result suggests that glycogen and laforin levels are closely linked. In addition, laforin levels in the brains of adult mice have also been seen to increase with age, indicating that laforin may have a vital role in the maturation of the CNS. While these links have been described, exact mechanisms regulating these fluctuations in laforin protein levels are unknown.

Impaired protein clearance may also be involved in the neuronal cell death observed in LD patients. Cells overexpressing mutant laforin exhibit impaired clearance of misfolded proteins with the appearance of ubiquitin-positive perinuclear aggresomes (*51*). These aggregates of proteins marked for proteasomal degradation are also present in the neurons of both LD patients and laforin-deficient mice (*161*). Furthermore, disruption of exon 4 of the *EPM2A* gene in mice often leads to cell death prior to the formation of LBs, and those neurons that do develop LBs in these mice often do not deteriorate (*50*). Upregulation of the unfolded protein response due to endoplasmic reticulum stress is seen when laforin is mutated or missing (*95, 161*), indicating that laforin or a possible binding partner play a role in cellular protein clearance. The fact that malin, an E3 ubiquitin ligase, is mutated in LD also provides support that LD is a disease of impaired protein clearance as the ubiquitination pathway is involved in protein turnover by the proteasome. Therefore, neuronal cell death in LD might be driven by a combination of LBs and impaired protein clearance.

Malin and the regulation of enzymes involved in glycogen metabolism.

Malin consists of a single subunit featuring an N-terminal consensus RING-finger domain, which is characteristic of a distinct class of E3 ubiquitin ligases (*19, 71, 158*), followed by 6 NHL (NCL-1, HT2A, and LIN-41 proteins) repeats (Figure 1.1B). NHL domains typically form a six-bladed β-propeller that is involved in

protein-protein interactions, much like WD40 repeats (*143*). Like laforin, malin is conserved in all vertebrates (*122*).

Malin has been shown to act as an E3 ubiquitin ligase in cell culture, binding directly to and polyubiquitinating laforin to trigger the degradation of laforin by the proteasome (*58*). The NHL domain of malin was required for the interaction of malin with laforin in this study (*58*). The ubiquitination of laforin by malin was also recapitulated *in vitro* using purified components (*58*). In addition, it has been observed that the inhibition of proteasome activity by MG-132 results in increased laforin levels, indicating that laforin levels are regulated by the proteasome. In agreement with these findings, mutations in malin lead to increased levels of laforin in both LD patients and mice (*40, 157, 159, 163*). Currently, it is unknown what triggers malin ubiquitination of laforin, but *in vitro* biochemical and *in vivo* LD patient data both support this ubiquitination event.

Through binding to laforin, malin has also been shown to ubiquitinate several proteins involved in glycogen metabolism to trigger their degradation. Among these proteins are the muscle isoform of glycogen synthase (GS) (*163*) and protein targeting to glycogen (PTG), the glycogen targeting subunit of protein phosphatase type 1 (*147, 174*). Ubiquitination of glycogen synthase and PTG by the laforin-malin complex led to a decrease in protein levels as well as a decrease in cellular glycogen levels. The laforin-malin complex has also been demonstrated to ubiquitinate glycogen debranching enzyme (GDE/AGL) and AMP-activated kinase (AMPK) (*30, 111, 147*). Interestingly, AMPK, a cellular energy sensor, phosphorylates laforin to increase the formation of the laforin-malin complex (*147*). Recent work indicates that the laforin-malin complex also interacts with and ubiquitinates neuronatin, a protein that stimulates glycogenesis, thus promoting the proteasomal degradation of the protein. These results suggest that in the presence of an inactive laforin-malin complex, neuronatin accumulates and overstimulates glycogen synthesis (*135*). The function of laforin as a scaffold is independent of its function as a glucan phosphatase, as inactive C266S laforin is still able to interact with malin and allow ubiquitination of GS and PTG (*147, 174*). These findings indicate that in addition to its role in dephosphorylating glycogen, laforin acts as a

scaffold to allow malin to regulate protein levels of enzymes involved in glycogen metabolism (Figure 1.3).

The work examining the ubiquitination of GS, PTG, GDE, and AMPK by laforin and malin involved overexpression of the enzymes studied. Despite complementary work from multiple labs, the levels of GS, PTG, and GDE in tissues did not change between 3-month old malin knockout mice and wild-type mice (*40, 157*). In addition, 3-6 month old mice lacking laforin did not exhibit increased levels of GS or PTG in muscle or brain (*149*). However, one study found dramatically higher levels of GS in the brains of 11-month old malin-deficient mice (*159*). The age of the mice studied may thus be playing a role in these conflicting results. Additionally, PTG levels were found to be increased in primary fibroblasts from LD patients (*162*). These results indicate that the functional significance of laforin-malin mediated ubiquitination of enzymes involved in glycogen metabolism is not completely elucidated.

The downregulation of laforin by malin is puzzling with regard to LD pathogenesis, as LD occurs due to the loss of function of either malin or laforin. Why one protein that inhibits LD (i.e. malin) triggers the degradation of the second protein (i.e. laforin) is still unresolved, but malin-directed ubiquitination of laforin is supported by *in vitro* biochemical data, *in vivo* mouse models, and LD patient data (*29, 40, 58*). While it has been demonstrated that laforin and malin play a role in glycogen metabolism, controversial findings and missing links make it difficult to determine the relationship between the disruption of proper glycogen metabolism and the neuronal damage leading to the devastating symptoms of LD.

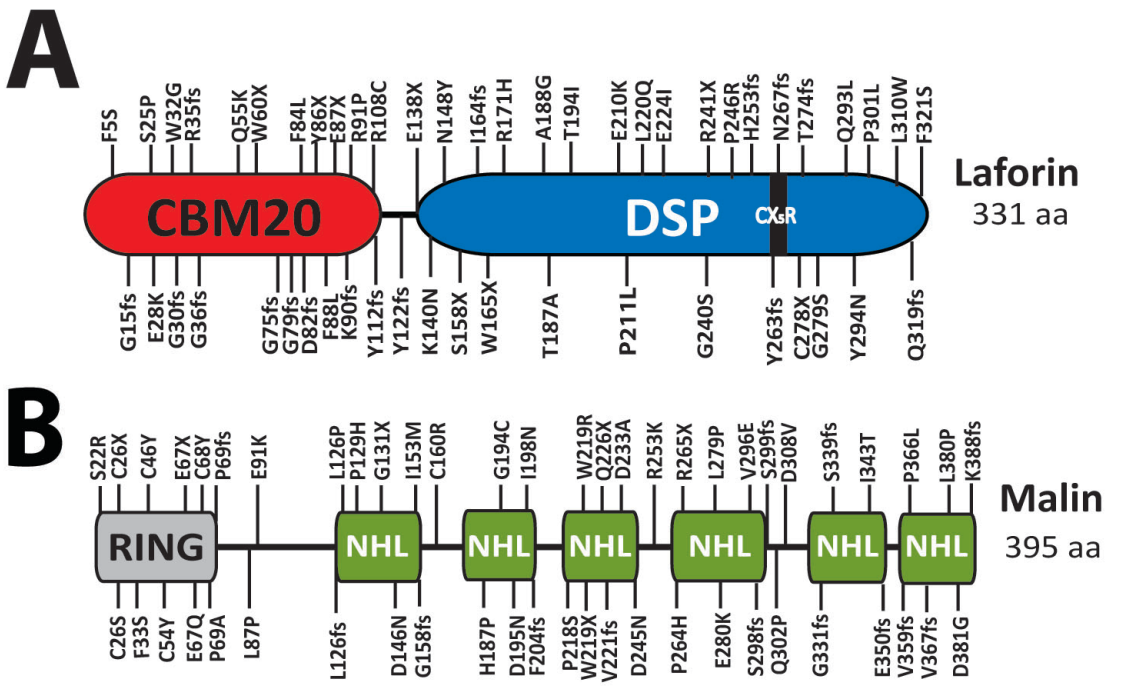

Figure 1.1. Laforin and malin. A. Schematic of laforin. Laforin possesses an N-terminal carbohydrate binding module family 20 (CBM20) domain and a C-terminal dual-specificity phosphatase (DSP) domain featuring the canonical DSP $Dx_{30}HCxxGxxRS/T$ (CX_5R) active site motif, indicated by a black bar. The Asp, Cys, and Arg residues of this motif are all required for dephosphorylation. The Arg residue interacts with the phosphate of the substrate while the Asp residue functions as a general acid to promote expulsion of the phosphate leaving group. The Cys residue generates a nucleophilic attack on the phospho-substrate, forming a phospho-enzyme intermediate (*38*). The Gly residue contributes to active site architecture, and the His and Ser/Thr residues decrease the pKa of the active site Cys (*2*). Known LD point mutations are equally distributed across the domains of laforin (*78*). **B.** Schematic of malin. Malin consists of an N-terminal consensus RING domain followed by six NHL repeats. Known LD point mutations are equally distributed across the domains of the protein (*78*).

A

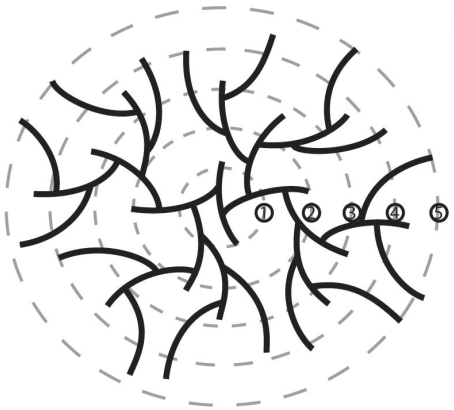

B

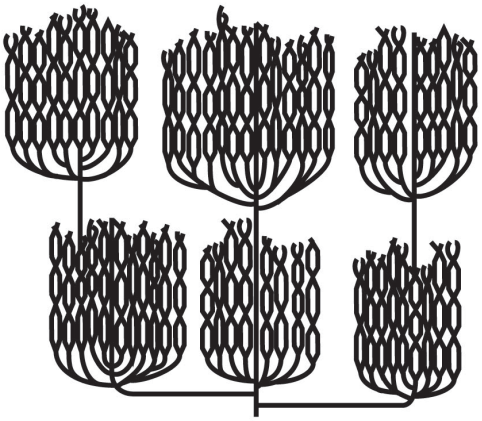

C

	residues/ branch	branching pattern	water soluble	phosphate content (w/w)
Glycogen	12-14	continuous	yes	0.064-0.25%
Amylopectin	12-25	discontinuous	no	0.1-0.5%
Lafora body	12-30+	discontinuous	no	0.35-1.0%

D

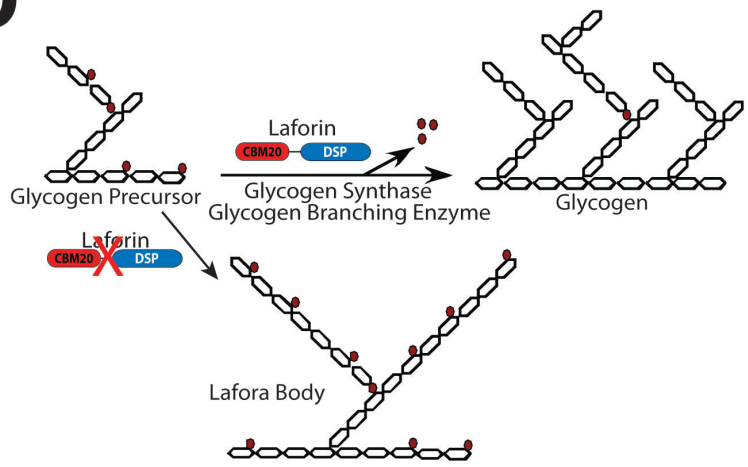

Figure 1.2. Glucans and the role of laforin in Lafora disease. The three-dimensional structure of glycogen and amylopectin cannot be determined experimentally due to their heterogeneity. The depicted models of glycogen and amylopectin structure are widely accepted (*24, 61*). In each model, unbroken lines indicate glucan chains. **A.** Glycogen consists of chains of glucose moieties linked by α-1,4-glycosidic bonds, with regular branch points formed by α-1,6-glycosidic linkages. These α-1,6 branch points generate sequential tiers in glycogen, five of which are shown. These tiers are organized in a continuous manner that allows glycogen to remain water soluble. **B.** Amylopectin also consists of glucose residues linked by α-1,4-glycosidic bonds, but branch points formed by α-1,6-glycosidic linkages are discontinuous. Adjacent glucan chains can then interact and form double helices, causing amylopectin to become crystalline and thus insoluble in water. **C.** Chart comparing the biochemical and physical properties of glycogen, amylopectin, and Lafora bodies. **D.** Model of Lafora body formation caused by the loss of laforin activity. Glycogen synthesis involves the concerted efforts of glycogen synthase and branching enzyme covalently linking glucose moieties (hexagons). Glycogen normally contains a small amount of covalently linked phosphate (red circles) that is present as both phosphomonoester (adjacent to glucose hexagons) and phosphodiester (between glucose hexagons) linkages. This phosphate may be introduced in error by glycogen synthase during glycogen synthesis, subsequently blocking the action of branching enzyme. Laforin then dephosphorylates glycogen, likely allowing branching enzyme to form the branches in glycogen necessary for water solubility. In the absence of laforin, phosphate accumulates and glycogen becomes less branched, eventually forming a Lafora body (adapted from Gentry et. al) (*54*).

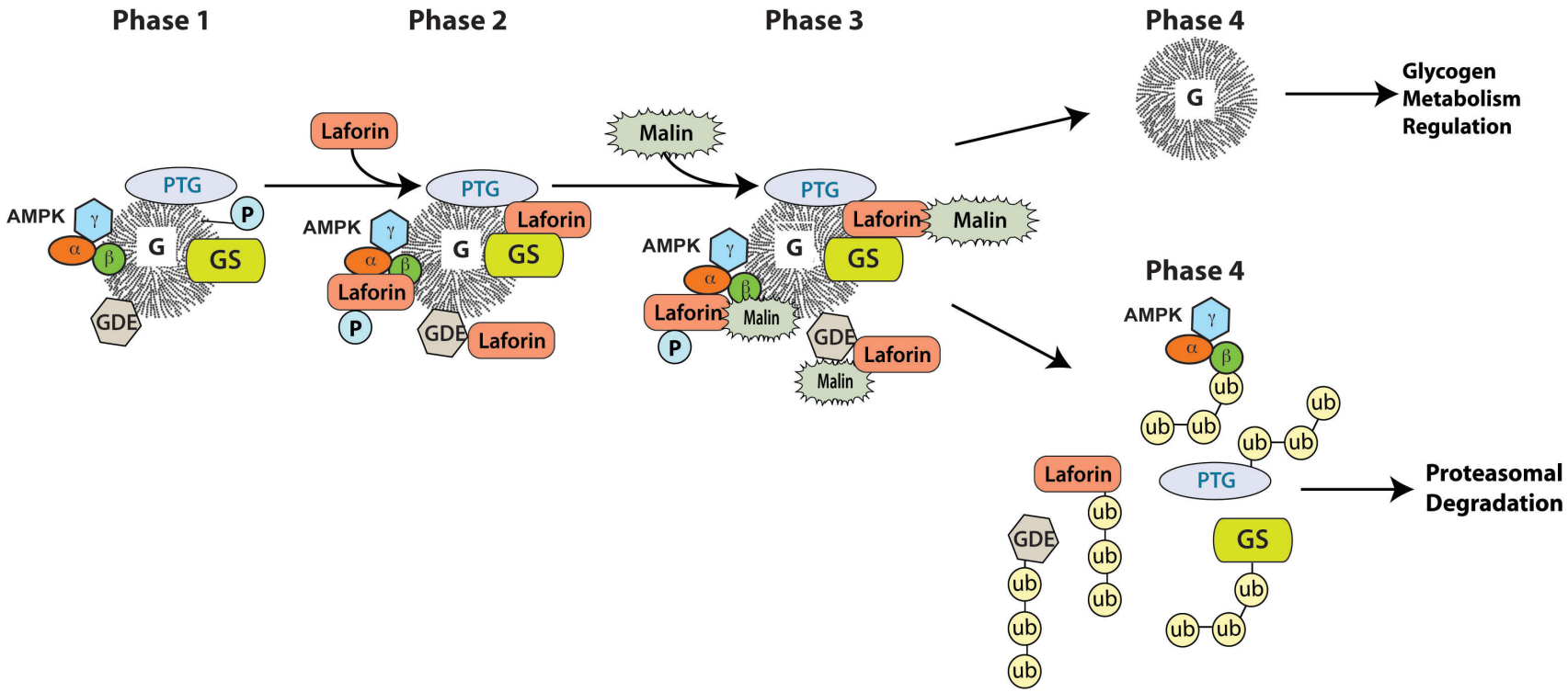
Phase 1
Phase 2
Phase 3
Phase 4
Glycogen
Metabolism
Regulation
Laforin
Malin
PTG
AMPK
γ
α
β
G
GS
GDE
P
ub
Phase 4
Proteasomal
Degradation

Figure 1.3. Model depicting the proposed role of the laforin-malin complex and its interactions in glycogen metabolism. In phase 1, the heterotrimeric AMP-activated protein kinase (AMPK), protein targeting to glycogen (PTG), glycogen synthase (GS), and glycogen debranching enzyme (GDE) bind to glycogen. Laforin binds glycogen via its CBM in phase 2 and dephosphorylates glycogen. In addition, APMK phosphorylates laforin, which has been shown to increase formation of the laforin-malin complex (*147*). In phase 3, malin binds to laforin and laforin acts as a targeting subunit to direct malin ubiquitination of PTG, GS, and AMPK. Laforin is also ubiquitinated by malin. In addition, malin ubiquitinates GDE, but the role of laforin in this event is unknown. These ubiquitination events lead to the degradation of laforin, AMPK, GS, GDE, and PTG in phase 4 to regulate glycogen metabolism. Work from multiple labs has demonstrated a discrepancy in the alteration of PTG, GS, and GDE levels in LD mouse models. Therefore the validity of this model is currently in question. For simplicity purposes, the spatial-temporal nature of protein interactions is not depicted and many of them are unknown.

CHAPTER 2: MATERIALS AND METHODS

Recombinant protein expression and purification.

Wild-type laforin, C266S laforin, VHR, and Dullard were cloned previously into the pET21a vector featuring a C-terminal HIS_6 tag (EMD Chemicals, Darmstadt, Germany) (*39, 89, 166*). Proteins were expressed in *Escherichia coli* BL21 (DE3) CodonPlus RIL cells (Stratagene, Santa Clara, CA). The transformed cells were grown in a laboratory shaker at 37°C in 2xYT medium until they reached an OD of 0.8 at 600 nm. Following induction with 0.4 M isopropyl β-D-1-thiogalactopyranoside for 12 hours at 22°C, proteins were affinity-purified from bacterial extracts using Ni^{2+}-agarose (Qiagen, Hilden, Germany) affinity chromatography (*58*) for enzymatic/binding assays. Further purification of monomeric laforin to near homogeneity for DXMS studies was then performed using gel filtration chromatography with an AKTA Fast Protein Liquid Chromatography (FPLC) system (GE Healthcare, Little Chalfont, UK) using a HiLoad 16/60 Superdex 200 size exclusion column (GE Healthcare). The FPLC-purified laforin was then concentrated to 4 mg/mL using an Amicon 30k concentrator (Millipore, Billerica, MA) and subjected to DXMS. All purifications were performed in HIS buffer (300 mM NaCl, 50 mM Tris-HCl, 15% glycerol, 3 mM tris(2-carboxyethyl)phosphine (TCEP), pH 8), using HIS buffer containing 0.5% Triton X-100 for initial cell lysis. Bacterial cells were lysed under pressure and lysates centrifuged (20,000*g*, 45 min, 4°C) to remove insoluble matter. Following incubation with Ni^{2+}-agarose (2 hours, 4°C), detergent was removed by repeated washes with HIS buffer and proteins eluted using HIS buffer containing 300 mM imidazole (30 min, 4°C).

***p*NPP assay (abbreviated; see Appendix 1 for full protocol).**

This assay measures general phosphatase activity against the small molecule *para*-nitrophenylphosphate (*p*NPP). Each 50 μl reaction replicate consisted of 1X phosphatase buffer (0.1 M sodium acetate, 0.05 M Bis-Tris, 0.05 M Tris-HCl, 2 mM dithiothreitol (DTT), pH 5), 50 mM *p*NPP, and 50-1000 ng of recombinant enzyme.

Reactions were incubated at 37°C for 10 min prior to the addition of 200 μl of 0.25 N NaOH to terminate the reactions. The absorbance of each reaction at 410 nm was read and enzyme activity calculated using Beer's Law (*138*).

Malachite green assay (abbreviated; see Appendix 1 for full protocol).

This assay utilizes the phosphorylated glucan polymer amylopectin in conjunction with malachite green reagent to specifically measure glucan phosphatase activity. Each 20 μl reaction replicate consisted of 1X phosphatase buffer (pH 7), 45 μg amylopectin, and 50-1000 ng of recombinant enzyme. Reactions were incubated at 37°C for 10 min prior to the addition of 20 μl of 0.1 M *N*-ethylmaleimide (NEM) to terminate the reactions. 80 μl of malachite green reagent was added and each reaction incubated at room temperature for 40 min before the absorbance at 620 nm was read (*138*). Enzyme activity was calculated by comparison of free phosphate to a standard curve.

Laforin antibody production.

We collaborated with the NIH NeuroMab Facility (Davis, CA) to generate and characterize mouse monoclonal IgG1 antibodies raised against full-length wild-type human laforin-HIS_6. We also generated rabbit IgG polyclonal antibodies (Cocalico Biologicals Inc, Reamstown, PA) against full-length wild-type human laforin-HIS_6. Laforin was expressed in *Escherichia coli* BL21 (DE3) CodonPlus RIL cells (Stratagene) and then purified from soluble bacterial extracts using Ni^{2+}-agarose (Qiagen) affinity chromatography. Eluted laforin (1.2 mg/mL) was supplemented with 20% glycerol and used for antibody production.

Mouse monoclonal antibodies against laforin (NeuroMab N84/1 and N84/37.1; 30 μg/mL) were purified from tissue culture supernatant collected from cultured mouse hybridomas. The supernatant was filtered through a 0.22 μm filter (Millipore) and then affinity purified using either a HiTrap Protein A HP or HiTrap Protein G HP column in conjunction with an antibody purification kit (GE Healthcare). Rabbit polyclonal antibodies against laforin (rabbits #113 and #139;

0.6 mg/mL) were obtained from exsanguination serum filtered through a 0.22μm filter and affinity purified with protein A using the Montage Antibody Purification Kit with PROSEP-A Media (Millipore). We also created a rabbit polyclonal antibody against a laforin peptide (amino acids 18-32; 21st Century Biochemicals Inc, Marlboro, MA) and obtained peptide affinity-purified α-laforin antibody (#4860; 50 μg/mL).

Cell culture and transfections.

Human embryonic kidney 293 (HEK293) and HepG2 cells were maintained in high glucose Dulbecco's modified Eagle's medium (DMEM; Gibco, Grand Island, NY) supplemented with 2 mM L-glutamine (Gibco), 5% fetal bovine serum (Gibco), and 100 units/mL penicillin/streptomycin (Gibco). Cells were incubated at 37°C in an atmosphere of 5% CO_2. Twenty-four hours before transfection, HEK293 cells were split into 10 cm dishes. The following day, at approximately 80% confluence, HEK293 cells were transiently transfected with 10 μg of laforin or malin plasmids using 30 μl of PEI-MAX (Polysciences Inc., Warrington, PA). For readthrough experiments, HEK293 cells were then incubated for 4 hours at 37°C to allow for recovery, after which the cells were cultured for 18 hours in the presence of gentamicin (Sigma-Aldrich, St. Louis, MO), amikacin (Sigma-Aldrich), PTC124 (Selleck Chemicals, Houston, TX), or DMSO (Sigma-Aldrich) at the indicated concentrations. As PTC124 exhibits the greatest level of solubility in DMSO, the effects of both PTC124 and the DMSO vehicle were studied. The amount of DMSO used to deliver the largest concentration of PTC124 in each experiment was then used as a matched control.

Cell lysate preparation and immunoprecipitation.

For readthrough experiments, cells were washed twice with ice-cold Tris-buffered saline (TBS) and then lysed in 500 μl ice-cold modified RIPA (mRIPA) buffer (150 mM NaCl, 50 mM Tris-HCl (pH 8), 0.4 mM EDTA, 10 mM NaF, 1% Nonidet P-40 (NP-40), 10% glycerol) supplemented with protease inhibitors (*58*).

Lysates were centrifuged (10,000*g*, 10 min, 4°C) to remove insoluble matter. The protein concentration of supernatant samples was determined using the Bradford protein assay (Bio-Rad, Hercules, CA). N-terminally FLAG-tagged proteins were immunoprecipitated (2 hours, 4°C) using 35 μl M2 α-FLAG agarose (Sigma-Aldrich). Lysate and immunoprecipitation samples were then heated (15 min, 95°C) in sample buffer (50 mM Tris-HCl (pH 6.8), 2% SDS, 10% glycerol, 1% β-mercaptoethanol, and 0.02% bromophenol blue). Immunoprecipitation (IP) and whole cell lysate (WCL) samples were subjected to Western analysis using mouse α-FLAG peroxidase-conjugated antibody (1:3000 M2 α-FLAG HRP; Sigma-Aldrich). Blots were developed with SuperSignal West Pico Chemiluminescent Substrate (Thermo Scientific, Waltham, MA).

Assessment of antibodies for the immunoprecipitation of overexpressed laforin.

Full-length human wild-type laforin cloned into a modified pcDNA3.1 vector (Invitrogen, Carlsbad, CA) featuring an N-terminal FLAG tag (pcDNA3.1 FLAG) (*166*) was first expressed in HEK293 cells grown to 80% confluence. 24 hours post-transfection, cells were rinsed twice with 5 mL TBS and lysates collected in 300 μl ice-cold modified mRIPA supplemented with protease inhibitors (*58, 160*). After centrifugation to clear the lysates (10,000*g*, 10 min, 4°C), 10 μl of each laforin antibody was then incubated while rocking with supernatants (1 hour, 4°C) prior to the addition of 35 μl Protein A Sepharose slurry (Sigma-Aldrich). Supernatants were then incubated while rocking (1 hour, 4°C) prior to centrifugation (5,000*g*, 2 min, 4°C) to collect the Sepharose beads.

After removing the supernatant by vacuum, the Sepharose was washed twice by the addition of 1 mL of mRIPA buffer followed by centrifugation (5,000*g*, 2 min, 4°C), with the supernatant removed after each step. The supernatant from the final wash was removed and the Sepharose resuspended in 50 μl protein sample dye. After boiling the samples (10 min, 95°C) and collecting the supernatant from the

Sepharose, 40 μl of Sepharose supernatant (IP) and 2.7 μg cell lysate (WCL) was analyzed by Western blot using 1:3000 M2 α-FLAG HRP.

Assessment of antibodies for the immunoprecipitation of endogenous laforin.

For each antibody tested, HepG2 cells grown to 90% confluence in three 100 mm plates were collected in 500 μl mRIPA buffer supplemented with protease inhibitors. 10 μl of each laforin antibody was then incubated with the lysates (2 hours, 4°C) followed by rocking with 35 μl Protein A Sepharose (2 hours, 4°C). 40 μl of IPs and 50 μg of WCL samples were analyzed by Western blot using 1:1000 of either α-laforin antibody N84/37.1 or #113 (*137*) to avoid same species cross-reactivity of the secondary antibody. Either 1:3000 goat α-mouse HRP (Invitrogen) or 1:3000 goat α-rabbit HRP (Calbiochem, Billerica, MA) secondary was used.

Antigen competition to confirm laforin antibody specificity.

To confirm the specificity of α-laforin antibody N84/37.1, 200 ng of recombinant laforin, 60 μg of HepG2 cell lysate, and 40 μl of pcDNA3.1 FLAG laforin immunoprecipitated with rabbit α-laforin antibody #139 were loaded twice onto a denaturing gel and then subjected to electrophoresis. Following Western transfer, the membrane was divided into identical halves. One half was probed with 1 μl α-laforin antibody N84/37.1 (1:10,000 dilution), while the other was probed with 1 μl α-laforin antibody N84/37.1 (1:10,000) that had been incubated with 400 μg of recombinant laforin (2 hours, 4°C). To confirm α-laforin antibody #113 specificity, a separate gel was loaded twice with 200 ng recombinant laforin, 25 μg of lysate from HEK293 cells transfected with pcDNA3.1 FLAG laforin, and 40 μg of HepG2 lysate. Each membrane half was immunoblotted with either 1 μl α-laforin antibody #113 (1:10,000) or 1 μl α-laforin antibody #113 (1:10,000) incubated first with 3.5 mg recombinant laforin (2 hours, 4°C). Either 1:3000 goat α-mouse HRP or 1:3000 goat α-rabbit HRP secondary was used.

Assessment of antibody impact on recombinant laforin activity.

For *p*NPP assays, 100 ng of recombinant wild-type laforin was first incubated with 2 μl α-laforin antibody #113 (30 min, 4°C) followed by the addition of 10 μl Protein A Sepharose (30 min, 4°C). For malachite green assays, 100 ng of recombinant laforin was incubated with 1 μl α-laforin antibody #113 (30 min, 4°C) followed by 3 μl of Protein A Sepharose (30 min, 4°C). Reaction components were then added to the immunoprecipitated laforin and reactions incubated at 37°C for 10 minutes prior to termination. 100 ng of inactive C266S laforin was used as a control. As commercial preparations of Protein A Sepharose can contain contaminating phosphate, malachite green assays were performed with 3 μl of Protein A Sepharose in the absence of laforin.

Immunoprecipitation of overexpressed laforin for activity assay.

Two 100 mm plates of HEK293 cells grown to 80% confluence were transfected with pcDNA3.1 FLAG wild-type laforin, inactive C266S laforin, or empty vector (*166*). After 24 hours, lysates were collected in 500 μl mRIPA supplemented with protease inhibitors for each construct. Lysates were then incubated with 10 μl of α-laforin antibody #113 (1 hour, 4°C) prior to the addition of 35 μl of Protein A Sepharose (1 hour, 4°C). 50 μl of mRIPA buffer was then added to resuspend the Protein A Sepharose, giving a final volume of 80 μL. 10 μl and 5 μl of immunoprecipitated laforin was used for *p*NPP and malachite green assays (2 hours, 37°C), respectively. 20 μl of the Protein A Sepharose was also boiled (15 min, 95°C) and analyzed by Western blot with 1:1000 α-laforin antibody N84/37.1. 15 μg of WCL was probed with 1:5000 mouse α-β actin (Sigma-Aldrich). Primary antibodies were probed with 1:3000 goat α-mouse HRP secondary antibody.

For FLAG peptide elution assays, HEK293 cells were transfected with pcDNA3.1 FLAG human wild-type laforin, inactive C266S laforin, or wild-type VHR (*58*). After 24 hours, cells were lysed in 500 μl mRIPA buffer supplemented with protease inhibitors and the lysates incubated with 35 μl M2 α-FLAG agarose (Sigma-Aldrich; 2 hours, 4°C). After washing the agarose beads twice with mRIPA buffer,

half of the collected agarose beads was subjected to incubation with 100 μg/mL FLAG peptide (Sigma-Aldrich; 12 hours, 4°C). Laforin eluate was then obtained by centrifugation of the α-FLAG agarose (5,000*g*, 3 min, 4°C) and collection of the supernatant. Immunoprecipitated laforin bound to α-FLAG agarose or FLAG-peptide eluate was then subjected to *p*NPP and glucan phosphatase assays.

Immunoprecipitation and activity assay of endogenous laforin from HepG2 cells.

1.4 x 10^6 HepG2 liver cells/plate were plated in four 150 mm plates and grown to 90% confluence. The lysate of two plates was immunoprecipitated with either α-laforin antibody #113 in conjunction with Protein A Sepharose or only Protein A Sepharose as a control. HepG2 lysates were first collected in 2 mL HIS buffer supplemented with protease inhibitors. Lysates were cleared by centrifugation (5,000*g*, 10 min, 4°C), filtered through a 0.22 μm filter, and 60 μl of α-laforin antibody #113 was then added to the supernatant (1 hour, 4°C). 150 μl of Protein A Sepharose was then added (1 hour, 4°C) and the beads washed three times with 1 mL of 1X phosphatase buffer (pH 7) to remove contaminating cellular phosphate.

From the final volume of 80 μL of immunoprecipitated laforin, *p*NPP and malachite green assays were then performed in quadruplicate with 10 μl and 5 μl of immunoprecipitated laforin as described previously, with reactions incubated for 1.5 and 18 hours at 37°C, respectively. 20 μl of the Protein A Sepharose was boiled (15 min, 95°C) and analyzed by Western blot with 1:1000 α-laforin antibody N84/37.1 (*137*). 80 μg of WCL was probed with 1:5000 mouse α-β actin. Primary antibodies were probed with 1:3000 goat α-mouse HRP secondary antibody.

Immunoprecipitation and activity assay of endogenous laforin from mouse skeletal muscle and human skin tissue.

For the mouse tissue experiments, 0.1 g of skeletal muscle collected from a wild-type C57BL/6 mouse was homogenized in 4 mL of HIS buffer supplemented

with protease inhibitors. The mouse muscle lysate was then cleared by centrifugation (5,000*g*, 10 min, 4°C), filtered through a 0.22 μm filter, and the supernatant collected. This process resulted in 4 mL of 3.8 mg/mL of soluble mouse skeletal muscle lysate. Similarly, soluble human skin tissue lysate from a normal adult (Novus Biologicals, Littleton, CO) was diluted in HIS buffer supplemented with protease inhibitors. Then, 0.02 - 1.0 mg of mouse skeletal muscle lysate and 0.1 - 0.75 mg of human skin tissue lysate was immunoprecipitated with 20 μl of α-laforin antibody #113 (1 hour, 4°C) in conjunction with 60 μl of Protein A Sepharose (1 hour, 4°C) in a final volume of 500 μL. As a negative control, mouse lysate supernatant and human lysate was immunoprecipitated with only Protein A Sepharose. The Protein A Sepharose was then washed three times with 1 mL of 1X phosphatase buffer (pH 7).

The final volume of 60 μL of immunoprecipitated mouse or human laforin was divided into three 20 μL aliquots, with one aliquot utilized in malachite green assays, a second utilized in immunoblotting experiments, and a third aliquot reserved for any necessary subsequent experiments. Malachite green assays were performed in quadruplicate with 5 μl of the immunoprecipitated laforin for each replicate, with reactions incubated for 12 hours at 37°C. As a control, muscle tissue from a laforin deficient mouse was prepared as above and malachite green assays were performed following the same protocol. The laforin-deficient samples were utilized to define the amount of contaminating phosphate from the immunoprecipitation protocol. The immunoblotting aliquot was generated by boiling 20 μl of α-laforin-Protein A Sepharose from the immunoprecipitation. The mouse tissue aliquot was then analyzed by Western blot with 1:1000 α-laforin antibody M01 (Abnova, Walnut, CA), which is specific for an epitope in both mouse and human laforin (amino acids 101-199, which share 99% identity). The human skin cell lysate was processed in the same manner and was analyzed by Western blot with 1:1000 α-laforin antibody N84/37.1 (*137*). Primary antibodies were probed with 1:3000 goat α-mouse HRP secondary antibody.

Creation of laforin and malin nonsense mutant constructs.

Human wild-type laforin and malin cDNAs were cloned previously into a modified pcDNA3.1 vector (Invitrogen) featuring either an N-terminal or C-terminal FLAG epitope tag (*58*). Each of the four most commonly occurring nonsense mutations in laforin or malin were introduced into the corresponding template using QuikChange PCR-based site-directed mutagenesis (Stratagene). Laforin nonsense mutants were generated using the following primer pairs: Y86X (C-G substitution) forward primer 5'-CGCGTGGACACGTTCTGGTA**G**AAGTTCCTTA-AGCGGGAGCC-3', Y86X reverse primer 5'-GGCTCCCGCTTAAGGAACTT**C**TACCAGA-ACGTGTCCACGCG-3'; S158X (C-G substitution) forward primer 5'-GCAGGCCACCA-AGCCATGCATTATT**G**AAGAATTCTACCAAATATCTGGCTG-3', S158X reverse primer 5'-CAGCCAGATATTTGGTAGAATTCTT**C**AATAATGCATGGCTTGGTGGCCTGC-3'; R241X (C-T substitution) forward primer 5'-CCAGATATGAGCACCGAAGGC**T**GA-GTACAGATGCTGCCCCAG-3', R241X reverse primer 5'-CTGGGGCAGCATCTGTAC-TC**A**GCCTTCGGTGCTCATATCTGG-3'; C278X (C-A substitution) forward primer 5'-CGCTCCACCGCGGCTGTCTG**A**GGCTGGCTCCAGTATGTG-3', C278X reverse primer 5'-CACATACTGGAGCCAGCC**T**CAGACAGCCGCGGTGGAGCG-3'. Malin nonsense mutants were generated using the following primer pairs: E67X (G-T substitution) forward primer 5'-CGCGCACTCTGGCCCTC**T**AGTGCCCATTCTGCAGG-3', E67X reverse primer 5'-CCTGCAGAATGGGCACT**A**GAGGGCCAGAGTGCGCG-3'; G131X (G-T substitution) forward primer 5'-CCCTGGTCAACCCCACC**T**GACTGGCGCTTTGTCCCAAG-3', G131X reverse primer 5'-CTTGGGACAAAGCGCCAGTC**A**GGTGGGGTTGACCAGGG-3'; W219X (G-A substitution) forward primer 5'-GGAGGCCAATTCTCCTTACCTT**A**GGGTGTGG-AGACCACCCCTCAG-3', W219X reverse primer 5'-CTGAGGGGTGGTCTCCACACCC**T**A-AGGTAAGGAGAATTGGCCTCC-3'; R265X (C-T substitution) forward primer 5'-GCTCATCTGTGCAATCCC**T**GAGGGGTGGCAGTGTCTTGG-3', R265X reverse primer 5'-CCAAGACACTGCCACCCCTC**A**GGGATTGCACAGATGAGC-3'. The nucleotide depicted in bold indicates the mutation site.

Laforin half-life determination.

8.9 x 10^6 HEK293 cells/plate and 6.5 x 10^6 HepG2 cells/plate were seeded onto 150 mm plates containing DMEM and incubated for 24 hours at 37°C. Fresh media was then added to each plate and the cells incubated for 30 min at 37°C. 200 μg/mL cycloheximide (Acros Organics, Lafayette, CO) was then added to the cells, after which 0 hour time point replicates were immediately collected. Cells incubated with cycloheximide for 0, 1, 4, 8, 12, or 24 hours were washed twice with TBS and then lysed in 1 mL of HIS buffer supplemented with protease inhibitors. Lysates were then centrifuged (10,000*g*, 10 min, 4°C) and the supernatants filtered through a 0.22 μm syringe filter. The filtered supernatants were frozen at -20°C until all time points were collected. After thawing at 0°C, the protein concentration of the supernatants was determined via Bradford assay, sample dye added, and the samples heated (15 min, 95°C). Following Western transfer of samples, membranes were incubated with N84/37.1 α-laforin antibody used at a 1:1000 dilution (*137*). Samples were also probed with 1:5000 α-cyclin D1 (Cell Signaling Technology, Danvers, MA) or 1:5000 α-β actin. Following incubation with primary antibodies, blots were then probed with 1:3000 goat α-mouse HRP or goat α-rabbit HRP secondary antibodies.

Immunofluorescence cell staining.

HEK293 cells were seeded onto 18 mm glass coverslips in DMEM and incubated at 37°C overnight. The next day, the media was removed and the cells rinsed with TBS. Coverslips were then incubated in 4% paraformaldehyde in TBS (15 min, 22°C) and rinsed three times with TBS. Cells were then permeabilized using 1% Triton X-100 in TBS (15 min, 4°C) and rinsed three times with TBS. The coverslips were then moved to a humidified chamber (22°C) and blocked with 1% fetal bovine serum in TBS (30 min, 22°C). Used at a concentration of 1:200 in blocking solution, either α-laforin antibody N84/37.1 or rabbit polyclonal α-laforin antibody #139 (*137*) was added to the coverslips (1 hour, 22°C). Rabbit #139 pre-immune serum was also tested to assess non-specific antibody binding. Coverslips

were then washed five times with 0.05% Tween-20 in TBS prior to the addition of 1:200 fluorescein-conjugated goat α-mouse or goat α-rabbit antibody (Invitrogen; 45 min, 22°C) in blocking solution. Coverslips were then washed five times with 0.05% Tween-20 in TBS and any remaining liquid removed prior to mounting of the coverslips in Vectashield mounting media with DAPI (Vector Laboratories, Inc., Burlingame, CA). The coverslip edges were then sealed with nail polish. Cells were imaged on a Zeiss Axiovert 200M inverted fluorescence microscope using a 100x oil objective (Carl Zeiss Microimaging, Thornwood, NY) and an Orca ER camera (Hamamatsu Corp. Bridgewater, NJ).

Statistical analysis.

The percent readthrough of nonsense mutations was calculated by dividing the mean signal of full-length laforin or malin following treatment by the mean signal of full-length laforin or malin prior to treatment using densitometry. Signal intensities were quantified using ImageJ software. Data are expressed as the percent change in means ± SEM. One-way ANOVA analysis was applied to determine statistical significance using sample-matched β actin signals as a covariate. Statistical significance was accepted at $p < 0.05$.

Generation of laforin mutants for DXMS.

Wild-type human laforin cloned into the pET21a vector (*166*) was used as a template for QuikChange PCR-based site-directed mutagenesis (Stratagene) in order to generate the following LD point mutants for study: W32G, G240S, Y294N, and P301L. C266S laforin cloned into the pET21a vector had been generated previously (*166*). The primers pairs used for mutagenesis were as follows: W32G (T-G substitution) forward 5'- CGAGCTGGGGCGT**G**GGGAGCCGCGCGGTG-3', W32G reverse 5'- CACCGCGCGGCTCCC**C**ACGCCCCAGCTCG-3'; G240S (G-A substitution) forward 5'- CCAGATATGAGCACCGAA**A**GCCGAGTACAGATG-3', G240S reverse 5'- CATCTGTAC-TCGGC**T**TTCGGTGCTCATATCTGG-3'; Y294N (T-A substitution) forward 5'- GAGGA-AGGTGCAG**A**ATTTCCTCATGGCC-3', Y294N reverse 5'- GGCCATGAGGAAAT**T**CTGC-

ACCTTCCTC-3'; P301L (C-T substitution) forward 5'-CTCATGGCCAAGAGGC**T**GGC-TGTCTACATTGAC-3', P301L reverse 5'- GTCAATGTAGACAGCC**A**GCCTCTTGGCCA-TGAG-3'.

Carbohydrate binding assays.

Following incubation of 30 μL of amylose resin (New England Biolabs, Ipswich, MA) with 1% w/v BSA in HIS buffer, 2 μg of wild-type laforin or laforin mutants in 200 μL HIS buffer were added, rocked for 1 hr at 4°C, and then the resin pelleted by centrifugation (5000*g*, 2 min). The same amount of protein used for assay was used to create input samples. Protein in the supernatant of samples was precipitated (12 hours, -20°C) with 800 μL acetone, centrifuged (5000*g*, 2 min), and then the acetone evaporated. The protein pellet was then resuspended in mRIPA and sample dye added. The amylose was centrifuged (5000*g*, 2 min), resuspended in mRIPA, and sample dye added. The input (I), supernatant (S), and pellet (P) fractions were analyzed by Western blot using 1:2000 mouse monoclonal α-HIS_6 primary antibody (Neuromab, Davis, CA) and 1:3000 goat α-mouse HRP (Invitrogen) secondary antibody.

Native glycogen gel electrophoresis.

Wild-type laforin and mutants were analyzed for glycogen binding affinity by native gel affinity electrophoresis (*110*). 5-10 μg of proteins were prepared in 1X phosphatase buffer (pH 7) and NativePage sample buffer (Invitrogen) and then loaded onto 10% acrylamide native gels (pH 8.8) or the same gels with 0.03% w/v glycogen from rabbit liver (Type III; Sigma-Aldrich) added. The rabbit glycogen (15 mg) was first dissolved in 5 mL of ddH_2O to create a 3 mg/mL (0.3% w/v) stock, and 1 mL of this stock was used in the preparation of a 10 mL gel. Native electrophoresis was then performed (3 hours, 150 V, 4°C) in a Bio-Rad Mini PROTEAN Tetra gel system using Tris-Borate running buffer (0.25 M Tris base, 0.12 M boric acid, pH 8.8) with 2 mM DTT added. NativeMark (Invitrogen) protein standard was used to provide reference proteins. Samples ran on a native gel without polysaccharide in

the same gel tank served as a control. Proteins were visualized by coommassie blue staining.

Optimization of pepsin digestion of laforin.

Prior to performing on-exchange for DXMS, the digestion conditions for a protein must be optimized to yield full peptide coverage across the protein (*23*). This process involves testing different concentrations of denaturant in the "exchange quench" solution, different concentrations of reducing agent used to eliminate disulfide bonds, and determining the type of protease column needed as well as the flow rate over the protease column. To begin, the concentrations of protein per sample, the reducing agent TCEP, and the denaturant guanidine hydrochloride (GuHCl) present during digestion of laforin were varied. Full coverage of wild-type laforin required 10 μg of protein per sample with a ratio of 5.3μl:10.6μl:4μl of protein:buffer:exchange quench solution (5.3% v/v formic acid, 15% v/v glycerol, 0.8 M GuHCl, 39 mM TCEP, pH 2.4) while also using a 30 mg/mL porcine pepsin-immobilized protease column (16 μl bed volume) (Sigma-Aldrich; immobilized on Poros 20 AL medium from PerSeptive Biosystems) with a flow rate of 20 μL/min. Procedures detailing the subsequent pepsin proteolysis of a protein for DXMS have been described previously (*63, 114*).

For each digestion test, protein was diluted in purification buffer on ice to mock dilution in D_2O-based buffers during deuterium exchange, after which ice-cold quench solution was added (final sample concentration of 0.5M GuHCl and 10 mM TCEP) in order to denature the protein for proteolysis and mock quench of exchange. Quenching exchange involves a low temperature and pH, as amide hydrogen-solvent exchange is dependent on these variables (*53*). Lowering solution pH to 2.2-2.5 and temperature to 0°C thus reduces back-exchange of a deuterium label during sample processing. Quenching of the samples was allowed to proceed on ice for 30 s, after which samples were immediately frozen on dry ice and stored at -80°C until analysis.

Prior to digestion and MS analysis, the denatured protein samples were placed into the sample basin of the cryogenic autosampler module of the DXMS apparatus containing dry ice. Once thawed at 0°C, individual samples (20 μL) were immediately injected and pumped through the pepsin column (48 s exposure to protease). The subsequent peptides were collected on a C18 trap (Michrom MAGIC, Auburn, CA) and then separated using a C18 reversed phase HPLC column (Michrom MAGIC) to minimize overlap. Following separation, the peptides were eluted using a linear acetonitrile gradient of 0.05% v/v trifluoroacetic acid/ 8% v/v acetonitrile to 0.01% v/v trifluoroacetic acid/ 48% v/v acetonitrile performed over 30 minutes. Eluted peptides were then electrosprayed directly into an OrbiTrap Elite Mass Spectrometer (Thermo Fisher) in either MS1 profile mode or data-dependent MS/MS mode.

In order to identify pepsin-generated peptides, a data-dependent data acquisition proceeds as a primary MS1 profile scan for parent peptide ion mass identification, and data-dependent MS/MS scans for fragment peptide ion sequence identification are then acquired. Proteome Discoverer software (Thermo Scientific) was used to determine the sequence of the parent peptide ions and their chromatographic retention times from the acquired MS/MS data. The conditions described above yielded the highest number of overlapping peptides with the most complete primary acid sequence coverage and were subsequently used for DXMS sample preparation.

Hydrogen-deuterium exchange of laforin.

DXMS experiments, measuring the location and rate of deuterium uptake via the difference in peptide mass between pre- and post-incubation in D_2O buffer, were performed as previously described (*63, 77, 114*). Initially, wild-type laforin without substrate was prepared in three states of deuteration: nondeuterated (ND), deuterated, and fully deuterated (FD). The ND samples were prepared exactly as those used for digestion optimization (see previous section), and provide a baseline for each peptide prior to deuterium exposure. The FD samples provide the

"maximum" level of deuteration for each peptide at equilibrium, allowing for correction of any back exchange of a deuterium label with hydrogen prior to sample analysis. Back exchange correction for each peptide was determined using the methods of Zhang and Smith (*178*):

$$\text{deuteration level (\%)} = \frac{m(P) - m(N)}{m(F) - m(N)} \times 100$$

where *m(P)*, *m(N)*, and *m(F)* are the centroid value of the partially deuterated, nondeuterated, and fully deuterated peptide spectras, respectively. FD samples were obtained by incubating protein (24 hours, 0°C) in D_2O containing 0.8% v/v formic acid, which denatures the protein to allow all amide hydrogens to exchange with deuterium.

The deuterated laforin samples were incubated in D_2O buffer at 0°C for 10, 30, 100, 300, 1000, 3000, and 10000 s (166.67 min) prior to quenching exchange. This was done in order to reveal areas of the protein that are exposed to solvent versus those buried within the interior, as well as to determine the rate of uptake and thus the degree of solvent accessibility/secondary structure. Samples incubated with glucan substrate at matching time points then provide insight into laforin structural dynamics or protection from deuteration due to substrate binding. Each deuterated sample contained 10 μg laforin protein diluted into ice-cold D_2O buffer (300 mM NaCl, 50 mM Tris-HCl, 3 mM TCEP, pD (read) 7.1) with or without glucan present, the final ratio being 5.3μl:10.6μl:4μl for protein:D_2O buffer:exchange quench solution (5.3% v/v/ formic acid, 15% v/v glycerol, 2.5M GuHCl, 39 mM TCEP, pH 2.4).

In initial wild-type laforin substrate-binding studies, several structurally distinct glucans were utilized, including amylopectin from potato starch (Sigma-Aldrich; 5 mg/mL), glycogen from rabbit liver (Type III, Sigma-Aldrich; 5 mg/mL), and β-cyclodextrin (Sigma-Aldrich, 5 mM). Prior to exchange experiments, wild-type laforin was incubated (1 hour, 4°C) with amylopectin, glycogen, or β-cyclodextrin in protein buffer. Laforin was then incubated in D_2O buffer or D_2O buffer containing the same glucans to generate deuterated samples, which were incubated at 0°C for

the same time points as detailed above prior to the addition of quench solution. All samples for each condition were prepared on the same day. Pepsin digestion, peptide separation by chromatography, and mass spectral acquisition was performed as described in the previous section. As this process is fully automated, the time between protein loading onto the pepsin column and mass spectral acquisition remained constant (~30 min) for all samples. For the initial wild-type substrate-binding studies, an LCQ Classic (Thermo Fisher) electrospray ion trap-type mass spectrometer and an electrospray Q-TOF mass spectrometer (Waters Corp, Milford, MA) were used. Data from all sample sets were acquired from a single automated run of 8 hours. Mass spectrometry data were acquired in both MS1 profile mode and data-dependent MS1:MS2 mode. Exchange of laforin with and without glucan was performed twice, with all samples prepared in triplicate. As the glycogen results were the strongest and also most physiologically relevant, the binding of all laforin mutants was subsequently analyzed using only glycogen.

Wild-type laforin and mutant DXMS samples were run on an OrbiTrap Elite Mass Spec (Thermo Fisher). These samples were prepared as above, with the exception that the total protein per sample was 10-fold more dilute than for the LCQ to yield optimal peptide detection by the OrbiTrap Elite. The instrument was operated in the positive ESI with a sheath gas flow of 8 units, a voltage of 4.5kV, a capillary temperature of 200°C, and an S-lens RF of 67%. The resolution of the survey scan was set at 60,000, at m/z 400 with a target value of $1x10^6$ ions and 3 microscans. The maximum injection time for MS/MS was varied between 25 and 200 ms. Dynamic exclusion was 30 s and early expiration was disabled. The isolation window for MS/MS fragmentation was set to 2, and the five most abundant ions were selected for product ion analysis.

In order to identify the potential sequences of parent peptide ions from the collected MS/MS data, the program SEQUEST (Thermo Fisher) was utilized for LCQ data and Proteome Discoverer for the OrbiTrap Elite data. DXMS Explorer (Sierra Analytics, Modesto, CA) (*65, 77*) data reduction software was used to confirm peptide identifications for the correct comparison of undeuterated and deuterated

peptides. All selected peptides first passed the quality control threshold established by the software and then were manually checked for the mass envelope fitting with the calculated mass envelope for data reduction. The highest signal/noise ion was picked if multiple ionization charges (1,2, or 3) of a peptide were detected. Normally, the peptide with the lowest charge state gave the best signal. Percent deuteration was calculated as the number of deuterium ions incorporated into a given peptide at a fixed time, divided by the maximum level incorporated at equilibrium of FD samples. Ribbon maps were created from individual peptide graphs depicting regional levels of deuterium incorporation and represent the average percent change in deuteration at each time point with a standard deviation of <2% between experiments.

Homology modeling of laforin.

A BLASTp search of the nonredundant GenBank human database with the CBM of laforin (residues 1-112) identified the CBM of *Geobacillus stearothermophilus* cyclodextrin glycosyltransferase (Protein Data Bank ID: 1CYG) (*92*) as the closest match (5×10^{-26}). A BLASTp search of the DSP of laforin (residues 152-331) identified *Arabidopsis thaliana* Starch Excess 4 (SEX4; Protein Data Bank ID: 3NME) (*160*) as the closest match (9×10^{-5}). We confirmed the identification of these structural templates with HHpred (*145, 146*), which queries alignment and structural databases such as Pfam, SMART, PDB, CDD, and HMMTigr. HHpred identified cyclodextrin glycosyltransferase (1CYG) in the top three hits (2×10^{-22}) for the CBM of laforin and SEX4 as the highest hit (5.1×10^{-38}) for the DSP of laforin. The sequences of the top five HHpred hits for both the CBM and DSP of laforin were then aligned with laforin using PROfile Multiple Alignment with predicted Local Structure 3D (PROMALS3D) (*118*). The resulting alignments were manually inspected for positional matching of residues known to be critical for CBM and DSP function. SWISS-MODEL was then used to generate homology models of the CBM and DSP domains of laforin, and the models were assessed using Anolea, Gromos, QMEAN6, DFire, and Verify3D (*5, 31, 97*). Multiple models were generated and each model was analyzed to determine which HHpred hits generated the best models. For

the CBM and DSP of laforin, cyclodextrin glucanotransferase and SEX4 yielded the best homology models, respectively. Images were generated using PyMol (DeLano Scientific, San Francisco, CA; http://pymol.sourceforge.net).

CHAPTER 3: A MALACHITE GREEN-BASED ASSAY TO ASSESS GLUCAN PHOSPHATASE ACTIVITY

Introduction.

Lafora disease (LD), a fatal neurodegenerative disorder, results from mutation of the glucan phosphatase laforin (*55, 105, 106*). Currently, various therapies for LD such as gene replacement and gene delivery using PEGylated immunoliposomes are being explored (*57*). We test the efficacy of aminoglycosides, compounds shown to promote the readthrough of nonsense mutations (*94*), in rescuing nonsense mutations in laforin (see Chapter 5: Effects of Aminoglycosides on Nonsense Mutations in Laforin and Malin as a Therapeutic Option for Lafora Disease). Detecting the activity of functional laforin following the application of these various treatments will aid in the evaluation of their efficacy. However, a means by which the phosphatase activity of laforin can be separated from the activity of other cellular phosphatases has yet to be established. As laforin is the only known phosphatase possessing a carbohydrate binding module (CBM) (*55*), we hypothesize that we can separate the activity of laforin from other cellular phosphatases using a phosphatase assay specifically utilizing a glucan substrate.

The human genome encodes for 13 phosphoprotein phosphatases (PPP family), 10 phosphoprotein metallo-dependent phosphatases (PPM family), 28 aspartate-dependent phosphatases (HAD family), and 105 protein tyrosine phosphatases (PTP family) (*153*). These enzymes dephosphorylate phosphoserine and threonine residues of protein substrates, while the PTPs can also act upon phosphotyrosine residues (*153*). Laforin is a member of the dual-specificity phosphatases (DSPs) (*55, 106, 133*), a class of phosphatases within the larger PTP family. The DSPs include phosphatases with a heterogeneous array of substrates, including phosphoserine, threonine, and tyrosine residues of proteins as well as phosphatidylinositols, glycerophospholipids, mRNA, and glucans (*3, 109, 116, 154*). As there are several families of cellular phosphatases, we chose several enzymes representative of each phosphatase family and the DSP class to test alongside laforin with the glucan phosphatase assay that we developed.

Laforin is the founding member of a group within the DSPs known as the glucan phosphatases (*55, 173*). Laforin is the only glucan phosphatase found in the genomes of all mammals, some invertebrates, and some protists, while additional glucan phosphatases exist in plants (*55, 56, 109, 126, 152, 173*). In addition to laforin, we included two glucan phosphatases recently discovered in plants in our study, *Arabidopsis thaliana* Starch Excess4 (SEX4), and *Arabidopsis thaliana* Like Sex Four 2 (LSF2). These enzymes were included in order to test the applicability of the glucan phosphatase assay we developed in characterizing emerging glucan phosphatases.

Prior to testing laforin and the other phosphatases that we selected for glucan phosphatase activity, we confirmed that these enzymes were active utilizing an *in vitro* assay with an artificial substrate. Many DSPs possess *in vitro* phosphatase activity towards phosphate esters of serine, threonine, and tyrosine residues of synthetic peptides (*2, 103, 108*), as well as towards synthetic small molecule substrates such as *para*-nitrophenylphosphate (*p*NPP), 3-*O*-methylfluorescein phosphate (OMFP), fluorescein diphosphate (FDP), and 6,8-difluoro-4-methylumbellyferyl phosphate (DiFMUP) (*103, 108*). We chose the *p*NPP assay to assess the general activity of the phosphatases in our study due to its simplicity and wide applicability. Hydrolysis of the aryl phosphate moiety from the small molecule *p*NPP converts this colorless substrate into *para*-nitrophenol, which reacts with a strong base to form the bright yellow phenolate ion that can be observed by reading the absorbance at 410 nm (Figure 3.1A).

Using a synthetic small molecule such as *p*NPP, one can determine the dephosphorylation kinetics and specificity constants/catalytic efficiencies of a phosphatase, and then compare these values to other phosphatases. This type of analysis can also provide valuable insights into the substrate of the phosphatase. A prime example of this methodology was work on the DSP tumor suppressor phosphatase and tensin homolog (PTEN). *In vitro* experiments using recombinant PTEN revealed it to be ~1000-fold less active against the phosphotyrosine analog *para*-nitrophenyl phosphate (*p*NPP) than typical tyrosine-specific PTPs. These

results prompted the search for other substrates that ultimately led to the important discovery that PTEN is a phosphoinositide lipid phosphatase (*100*).

In addition to utilizing the *p*NPP assay to measure generic phosphatase activity, we developed an *in vitro* assay to measure the specific glucan phosphatase activity of the enzymes included in our study. While most *in vitro* phosphatase assays utilize artificial substrates, assays that assess phosphatase activity against biologically relevant substrates have been reported (*67, 101, 103, 173*). Malachite green is a useful reagent in this regard, allowing the colorimetric detection of picomolar amounts of phosphate liberated from substrates due to the formation of a phosphomolybdate malachite green complex that can be measured at 620 nm (*67, 93, 103*) (Figure 3.1B). In addition to the advantages of simplicity and sensitivity, malachite green assays have been utilized to detect phosphate released from an array of endogenous substrates such as proteins and lipids (*101, 103*).

Herein, we describe a glucan phosphatase assay that utilizes malachite green in conjunction with the phosphorylated glucose polymer amylopectin. We demonstrate that this glucan phosphatase assay allows for the comparison of activity between glucan phosphatases, and will likely be useful in the characterization of emerging glucan phosphatases. This assay also effectively separates enzymes with glucan phosphatase activity from those that lack the activity.

Results.

We included several glucan phosphatases in our study. We purified human wild-type laforin and a catalytically inactive mutant as an experimental control (C266S), *A. thaliana* SEX4, and *A. thaliana* LSF2 as described previously (*55, 126*). We also purified or purchased phosphatases from a variety of different organisms and phosphatase families (*17, 123, 140, 164*). We utilized the PPP family member *Oryctolagus cuniculus* protein phosphatase 1 (PP1) (*109*), the human HAD family member Dullard (*89, 109*), and the *Escherichia coli* PPM family member alkaline phosphatase (*33*) (Figure 3.1C). We also employed enzymes from within the PTP family: classical PTPs such as human T-cell PTP (TCPTP) (*6, 109*) and *Yersinia pestis*

YopH (*60, 179*), and DSPs such as vaccinia virus VH1-related DSP (VHR) (*55*) and murine PTP localized to mitochondrion 1 (PTPMT1) (*175*) (Figure 3.1C). The phosphatases above have previously been shown to possess phosphatase activity against substrates such as *p*NPP, phosphorylated peptides, phosphorylated glucans, or phospholipids (*6, 33, 55, 60, 89, 126, 173, 175*).

To ensure that each phosphatase we included in our work was active, we first performed phosphatase assays with each using the small molecule *p*NPP (see Appendix 1: Supplementary Protocols, *p*NPP assay). Aliquots of 5X assay buffer (100 mM sodium acetate, 50 mM Bis-Tris, 50 mM Tris) were prepared for each pH to be tested, and enzymes were diluted with 1X assay buffer of the optimal pH containing 1 mM dithiothreitol (DTT) to a final enzyme concentration ranging from 50 to 1000 ng/µl. Each reaction replicate (at least 3) was performed in a final volume of 50 µl, and consisted of 33 µl H_2O, 10 µl 5X assay buffer at the optimal enzyme pH, 1 µl 100 mM DTT, and 5 µl 0.5 M *p*NPP. We added 1 µl of diluted enzyme to each replicate tube, began timing the reaction, vortexed the tube, and then placed it at 37˚C.

We repeated this methodology every 15 seconds until enzyme was added to each replicate. After a reaction time of 10 minutes at 37˚C, we added 200 µl of 0.25 N NaOH and vortexed the tubes to quench the reactions, and read the absorbance (*A*) of each replicate at 410 nm. We then utilized Beer's Law ($A=\varepsilon lc$, where the path length l = 1 cm) and the molar absorption coefficient (ε) of the phenolate ion under our reaction conditions (17,800 M^{-1} cm^{-1}) to determine the concentration in moles per liter (c) of phenolate ion generated per reaction. We calculated the activity of each enzyme, expressed as µmol phosphate released/ min/ µmol protein. Although it is common to report phosphatase activity in terms of total protein, a true comparison of activities must be made using moles of protein (Figure 3.2A). However, we have also provided our results in terms of total protein (Figure 3.3A) for comparison with previously published activity data (Figure 3.1C). All of the phosphatases tested exhibited activity against *p*NPP (Figure 3.2A) that closely

reflected previously published data at the optimal pH for each enzyme (Figure 3.1C and 3.3A).

Next, we employed a malachite green assay to assess specific glucan phosphatase activity of the above enzymes at optimal pH using the phosphorylated glucan amylopectin as the substrate (see Appendix 1: Supplementary Protocols, Malachite green standard curve and assay). First, we prepared the malachite green reagent. We began with 1 volume of 4.2% ammonium molybdate tetrahydrate in 4 N HCl, added 3 volumes of 0.045% malachite green carbinol hydrochloride, stirred the solution for 30 minutes, filtered the solution with grade 5 Whatman filter paper, and then sterile-filtered the reagent. Prior to performing experiments with this reagent, a standard curve should be generated (see Appendix 1). Next, we prepared the amylopectin to be used as the phosphoglucan substrate. Amylopectin is largely water insoluble, and therefore it must be solubilized via heating or ethanol. We prepared a suspension of 5 mg/mL of amylopectin in H_2O, heated the suspension at 70˚C for 30 minutes (the suspension will go from opaque to clear; vortexing aids solubility), and stored this solution at room temperature.

Before beginning the malachite green assay, we first added 0.01% v/v Tween 20 from a 10% stock to an aliquot of malachite green reagent. Tween 20 stabilizes the formation of the malachite green phosphomolybdate complex and prevents sedimentation of the complex for up to 48 hours (*80*). We then prepared 5X assay buffer (100 mM sodium acetate, 50 mM Bis-Tris, 50 mM Tris) for each pH to be tested and diluted enzymes with 1X assay buffer of the optimal pH with 1 mM dithiothreitol (DTT) added to a final enzyme concentration ranging from 50 to 1000 ng/µl. Each reaction (at least 3 replicates) was then performed in a final volume of 20 µl consisting of 4 µl H_2O, 4 µl 5X assay buffer at the optimal enzyme pH, 2 µl 100 mM of DTT, and 9 µl of 5 mg/mL amylopectin. We added 1 µl of diluted enzyme to each reaction tube, began timing the reaction, vortexed the tube, and then placed the tube at 37˚C.

This methodology was repeated every 15 seconds until enzyme was added to each replicate. The reactions were incubated at 37˚C for 10 minutes before 20 µl 0.1M *N*-ethylmaleimide (NEM) was added to terminate all PTP reactions. NEM is a

thiol-modifying reagent that irreversibly inhibits PTPs without affecting malachite green phosphomolybdate color formation (*101*). For non-PTPs, addition of malachite green reagent was used to terminate the reaction (*67*). Following NEM addition to the PTP reaction tubes, 80 µl of the malachite green reagent containing Tween20 was then added. After malachite green reagent was added to every reaction tube, the tubes were vortexed and placed at room temperature. All reactions were incubated for 40 minutes before measuring the absorbance at 620 nm (*80*) and calculating the pmoles of phosphate released/min/nmol protein using the standard curve.

Using the above methodology, we found that only wild-type laforin, SEX4, and LSF2 exhibited glucan phosphatase activity, while all other phosphatases that we tested possessed very little to no activity (Figure 3.2B). We also reported our results in terms of total protein (Figure 3.3B). To assess the relative activity of the phosphatases tested towards amylopectin, we compared phosphate liberation from amylopectin to *p*NPP activity and found that only the glucan phosphatases were effective at dephosphorylating amylopectin, with laforin being the most efficient (Figure 3.2B and 3.3B, numbers above the bars). Thus, only the glucan phosphatases possess the ability to release phosphate from amylopectin. The glucan phosphatase assay described is a simple method to characterize emerging members of the unique and growing family of glucan phosphatases, as has been done with the recently characterized glucan phosphatase LSF2 (*127*).

Discussion.

With the recent discovery of a unique class of dual-specificity phosphatases that dephosphorylate glucans, we report an *in vitro* assay tailored for the detection of phosphatase activity against phosphorylated glucans. We demonstrate that in contrast to a general phosphatase assay utilizing a synthetic substrate, only phosphatases that possess glucan phosphatase activity liberate phosphate from the phosphorylated glucan amylopectin using the described assay. This assay is simple and cost-effective, providing reproducible results that clearly establish the presence

or absence of glucan phosphatase activity. The assay described will be a useful tool in characterizing emerging members of the glucan phosphatase family.

Our glucan phosphatase assay also reveals that of representative phosphatases from every cellular phosphatase family, only glucan phosphatases are able to dephosphorylate amylopectin. This assay will prove useful in the detection of functional laforin activity in patient cells following application of future therapies for Lafora disease if a means to enrich laforin protein levels for assay can be established. In the following chapter, we explore an immunoprecipitation-based method for the detection of endogenous laforin protein levels and activity.

A

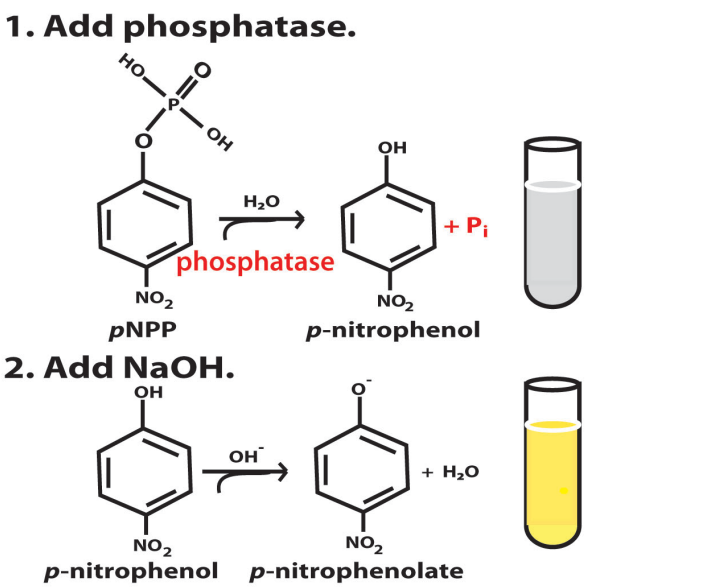

B

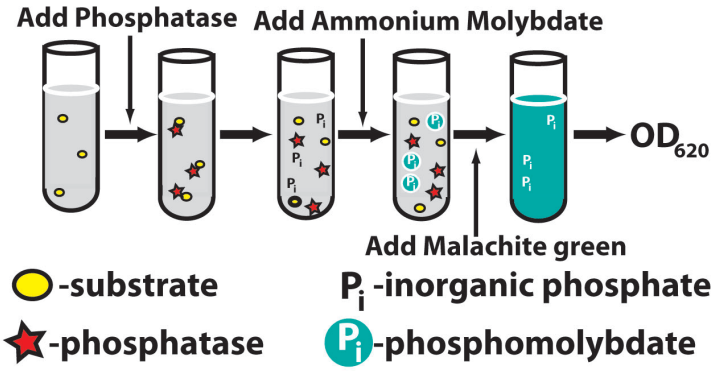

C

Phosphatase	Organism	Family	Substrate	Reported *p*NPP Activity
C266S Laforin	*H. sapiens*	DSP	Inactive	Inactive[2]
Wild type Laforin	*H. sapiens*	DSP	Glucans	5.5[1]
Alkaline Phosphatase	*E. coli*	PPM	pSer, pThr, pTyr, r/dNTP	7.0[1]
YopH	*Y. enterolitica*	PTP	pTyr	131[20]
PTPMT1	*M. musculus*	DSP	Phosphatidylglycerol	0.7[1]
Dullard	*H. sapiens*	Aspartate	pSer, pThr	2.0[1]
LSF2	*A. thaliana*	DSP	Glucans	-
SEX4	*A. thaliana*	DSP	Glucans	4.0[2]
VHR	*Vaccinia virus*	DSP	pSer, pThr, pTyr	14.0[1]
TCPTP	*H. sapiens*	PTP	pTyr	100.0[1]
PP1	*O. Cuniculus*	PPP	pSer, pThr	11.0[1]

Figure 3.1. Experimental design of assays and phosphatases chosen for study. **A.** The *p*NPP assay**.** Hydrolysis of the aryl phosphate moiety from the small molecule *para*-nitrophenylphosphate (*p*NPP) converts this colorless substrate into *para*-nitrophenol, which forms the bright yellow phenolate ion under alkaline conditions (pK_a of 7.2). The presence of the soluble phenolate ion can be observed by reading the absorbance at 410 nm. When performing this colorimetric assay under saturation conditions of substrate as we have done, it is possible to calculate the rate of dephosphorylation as well as kinetic constants such as k_{cat} and K_M (*103, 108*). While *p*NPP is an artificial substrate, the small size of this molecule restricts interaction to a low number of residues, allowing resolution of active site conformation changes due to mutation (*108*). Phosphatase assays involving this substrate can also be performed in a continuous or discontinuous fashion. Continuous enzyme assays, allowing hydrolysis products to be quantified without disturbing the reaction, are superior to discontinuous assays in the efficiency of determining kinetic constants (*103*). However, for the purpose of this work, discontinuous assay under saturated conditions was sufficient (10 times the K_m) (*108*), providing the initial (linear) rate of the reaction for phosphatase activity comparison. **B.** The malachite green assay utilizing amylopectin as a substrate**.** As phosphate monoesters in amylopectin are hydrolyzed, the free phosphate forms a complex with the ammonium molybdate in the malachite green reagent. At low pH, the basic malachite green dye forms a complex with phosphomolybdate and shifts to its absorption maximum. This complex is stabilized for up to 48 hours by detergents such as Tween 20 (*80*), allowing for easy colorimetric detection that is linear with as little as 50 to 1000 pmol of P_i following measurement of the absorbance at 620 nm (*67*). While it is not possible to calculate enzyme kinetics using the heterogeneous amylopectin polymer, use of amylopectin as a substrate allows for the detection of glucan phosphatase activity. For both the malachite green and *p*NPP assay, dithiothreitol (DTT) was used as the reducing agent to maintain enzyme activity as malachite green is sensitive to 2-mercaptoethanol (*101*). **C.** List of phosphatases used in the *p*NPP and malachite green assays**.** Phosphatases across families and within families were chosen to obtain a representative and diverse

collection of cellular enzymes for study. Included in the list is the family and organism of origin, the known substrates, and the reported specific activity against *p*NPP (μmol/min/mg) for each enzyme.

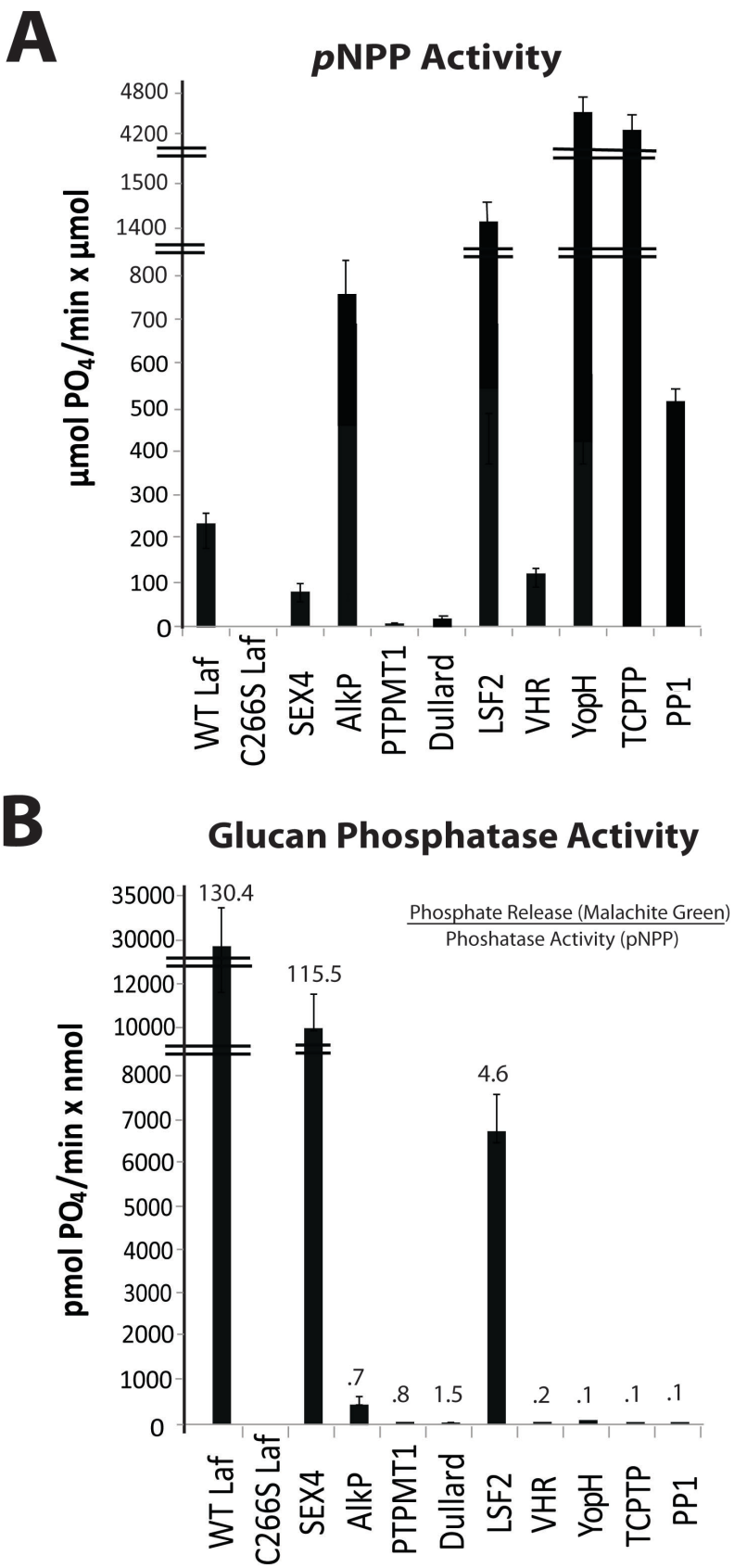
A
pNPP Activity
µmol PO4/min x µmol
4800
4200
1500
1400
800
700
600
500
400
300
200
100
0
WT Laf
C266S Laf
SEX4
AlkP
PTPMT1
Dullard
LSF2
VHR
YopH
TCPTP
PP1
B
Glucan Phosphatase Activity
Phosphate Release (Malachite Green)
Phoshatase Activity (pNPP)
pmol PO4/min x nmol
35000
30000
12000
10000
8000
7000
6000
5000
4000
3000
2000
1000
0
130.4
115.5
4.6
.7
.8
1.5
.2
.1
.1
.1
WT Laf
C266S Laf
SEX4
AlkP
PTPMT1
Dullard
LSF2
VHR
YopH
TCPTP
PP1

Figure 3.2. The *p*NPP and malachite green assays reveal specific glucan phosphatase activity only in glucan phosphatases. A. *p*NPP activity**.** The activity of each phosphatase utilized in our study against the synthetic substrate *p*NPP in μmol phosphate released per minute per μmol protein. Each assay was independently repeated with four replicates. Error bars; S.E. **B.** Glucan phosphatase activity**.** The specific activity of the same phosphatases against phosphorylated amylopectin in pmol phosphate released per minute per nmol protein. Each assay was independently repeated with four replicates. The numbers above the bars are the ratio of phosphate release (malachite green assay) to the phosphatase activity (*p*NPP assay) for each enzyme. Error bars; S.E.

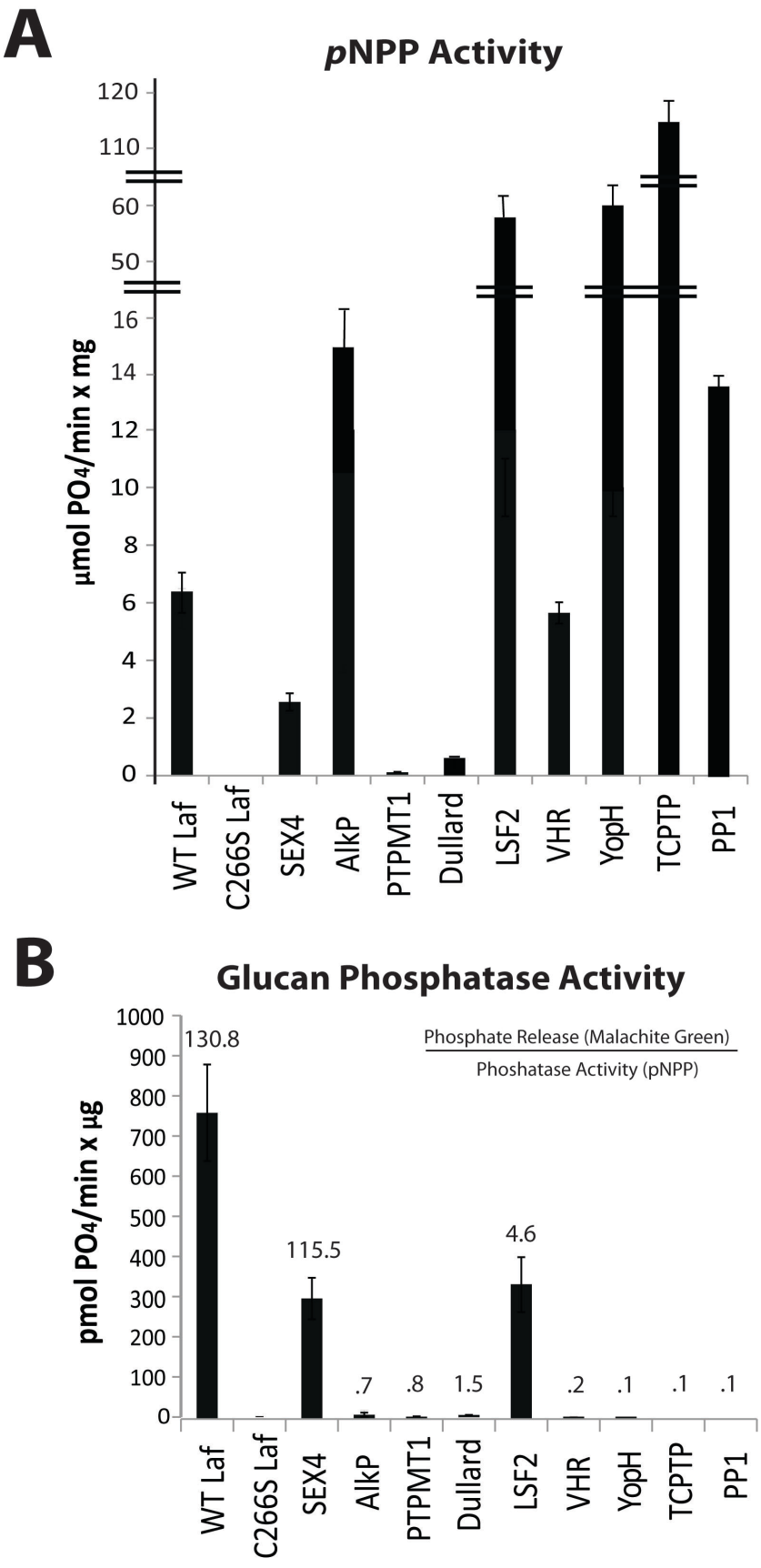
A
pNPP Activity
µmol PO4/min x mg
120
110
60
50
16
14
12
10
8
6
4
2
0
WT Laf
C266S Laf
SEX4
AlkP
PTPMT1
Dullard
LSF2
VHR
YopH
TCPTP
PP1
B
Glucan Phosphatase Activity
Phosphate Release (Malachite Green)
Phoshatase Activity (pNPP)
pmol PO4/min x µg
1000
900
800
700
600
500
400
300
200
100
0
130.8
115.5
4.6
.7
.8
1.5
.2
.1
.1
.1
WT Laf
C266S Laf
SEX4
AlkP
PTPMT1
Dullard
LSF2
VHR
YopH
TCPTP
PP1

Figure 3.3. *p*NPP and malachite green assay results reported using total protein. A. *p*NPP activity**.** The activity of each phosphatase utilized in our study against the synthetic substrate *p*NPP in μmol phosphate released per minute per mg protein. **B.** Glucan phosphatase activity**.** The specific activity of the same phosphatases against phosphorylated amylopectin in pmol phosphate released per minute per μg protein.

CHAPTER 4: A BIOASSAY FOR LAFORA DISEASE AND LAFORIN GLUCAN PHOSPHATASE ACTIVITY

Introduction.

To date, Lafora disease (LD) can only be managed for a short period using palliative therapeutics designed to limit the severity and frequency of epileptic episodes (*37, 107*). More permanent therapeutic options for the alleviation of the LD phenotype, including *EPM2A* or *EPM2B* gene replacement using neutral PEGylated immunoliposomes (*139*) and readthrough of nonsense mutations using aminoglycosides and functionally-related compounds (see Chapter 5: Effects of Aminoglycosides on Nonsense Mutations in Laforin and Malin as a Therapeutic Option for Lafora Disease), are currently being explored. Additionally, results from LD mouse models suggest that downregulation of glycogen metabolism to inhibit the formation of Lafora bodies (LBs) is an additional treatment option (*156, 159*).

As therapeutic options for LD become available and enter clinical trials, it will be necessary to assess the efficacy of these therapies. Currently, the quantitated neurological and electrophysiological states of LD patients are the only means by which therapeutics may be assessed for efficacy, and these methods are subject to varied response and must be assessed long-term (*14, 105, 107*). Building upon our previous work developing an assay by which laforin activity can be separated from that of other cellular phosphatases (see Chapter 3: A Malachite Green-Based Assay to Assess Glucan Phosphatase Activity), we developed a simple and sensitive bioassay for endogenous laforin activity as a biochemical means of assessing the efficacy of future LD therapies.

We demonstrate that this bioassay can measure the activity of endogenous laforin from either human or mouse tissue, providing rapid results. This bioassay can therefore be utilized with tissue from LD mouse models or LD patients following the application of LD therapies. This assay can also be utilized at any time after treatment administration, and is suitable for both the detection of endogenous laforin protein concentrations and, more importantly, the assessment of enzymatic activity. Furthermore, we demonstrate that this bioassay is specific for laforin, the

only human enzyme known to possess glucan phosphatase activity (*55, 138*) (Chapter 3). As this bioassay utilizes the glucan amylopectin, which possesses similar biophysical characteristics to LBs (Figure 1.2C), this assay also potentially measures the activity of functional laforin against LBs.

Results.

In order to generate a bioassay for endogenous laforin activity, we first optimized assay conditions using overexpressed human laforin. The basis of this bioassay is to immunoprecipitate laforin and then assess its glucan phosphatase activity. Therefore, it was crucial to determine if the activity of laforin bound to an α-laforin antibody-agarose complex is inhibited. Our experimental design was to first express FLAG-tagged wild-type laforin, immunoprecipitate laforin using α-FLAG agarose, and then perform activity assays of laforin both bound to and eluted from the immunoprecipitation complex (Figure 4.1A).

We employed two assays to assess laforin function following immunoprecipitation. First, we used the *p*NPP assay, which utilizes the exogenous phosphatase substrate *para*-nitrophenylphosphate (*p*NPP), to assess general phosphatase activity. We also used a malachite green assay utilizing the phosphorylated glucan polymer amylopectin to determine biologically relevant glucan phosphatase activity (*138, 173*) (see Chapter 3). As a control for these assays, we used a DSP that dephosphorylates proteinaceous substrates, vaccinia virus VH1-related DSP (VHR) (*39, 55, 138*). VHR possesses *p*NPP activity, but cannot liberate phosphate from amylopectin (*138, 173*) (Figure 3.2A and B). We also utilized an enzymatically inactive laforin mutant in which the catalytic cysteine residue is mutated to serine (C266S), abolishing enzymatic activity against *p*NPP and amylopectin (*55, 138*) (Figure 3.2A and B). We found that following immunoprecipitation with FLAG-agarose, FLAG-laforin both bound to and eluted from FLAG-agarose exhibited *p*NPP and malachite green activity (Figure 4.1B and C). Therefore, the activity of laforin is not impacted by immunoprecipitation.

Conversely, C266S laforin did not demonstrate *p*NPP or malachite green activity and VHR demonstrated only *p*NPP activity, each as expected.

We then analyzed seven monoclonal and polyclonal α-laforin antibodies for the ability to immunoprecipitate overexpressed human laforin. Following immunoprecipitation of FLAG-laforin with each α-laforin antibody, we separated the immunoprecipitated proteins by SDS-PAGE and immunoblotted using α-FLAG. We found that the best antibodies for the immunoprecipitation of overexpressed laforin were the Protein A purified α-laforin antibodies N84/37.1, #113, and #139 (Figure 4.2A).

Next, we sought to assess the detection limit of each α-laforin antibody using serial dilutions of recombinant human laforin. A range of recombinant laforin protein from 20 μg to 0.02 ng per lane was loaded onto identical gels and then subjected to SDS-PAGE. Following Western transfer, each blot was then incubated with one of the seven α-laforin antibodies. The α-laforin antibodies #113 and N84/37.1 were among the best antibodies for blotting, easily detecting as little as 200 ng of recombinant laforin (Figure 4.2B). While equally efficient at immunoprecipitating overexpressed laforin as α-laforin antibody #113 (Figure 4.2A), α-laforin antibody #139 was less efficient at detecting recombinant laforin (Figure 4.2B).

Laforin antibodies were then tested for the ability to immunoprecipitate endogenous laforin from HepG2 liver cells, as laforin is present in many tissues of the human body, including brain, heart, skeletal muscle, liver, and kidney (*106, 133*). HepG2 cell lysates were incubated with each α-laforin antibody followed by incubation with Protein A Sepharose. The amount of laforin immunoprecipitated by each α-laforin antibody was then assessed following SDS-PAGE and immunoblot using either α-laforin antibody #113 or N84/37.1. We found that only the polyclonal α-laforin antibodies (#113 and #139) were able to efficiently immunoprecipitate endogenous laforin (Figure 4.2C). Based on our findings, α-laforin antibody N84/37.1 was selected for blotting and α-laforin antibody #113 for immunoprecipitation purposes.

We confirmed that the N84/37.1 and #113 α-laforin antibodies were indeed specific to laforin using antigen competition. We incubated both of the antibodies with recombinant laforin prior to performing a Western blot of recombinant, overexpressed, and endogenous laforin (Figure 4.2D). Both N84/37.1 and #113 α-laforin antibodies exhibited a drastic reduction in blotting signal when these antibodies were incubated first with recombinant laforin (Figure 4.2D). Additionally, preimmune serum from rabbits #113 and #139 was analyzed to confirm that α-laforin antibody production was due to immunization with the laforin antigen (data not shown).

As α-laforin antibody #113 is polyclonal, one concern of our design was that polyclonal antibody binding to laforin could inhibit enzymatic activity. Therefore, we tested if laforin bound by polyclonal α-laforin antibodies displays reduced phosphatase activity. We incubated recombinant laforin with α-laforin antibody #113 followed by Protein A Sepharose and then performed both *p*NPP and malachite green assays. We compared the activity of Sepharose-bound laforin with laforin lacking antibody and Sepharose, and found that the immunoprecipitation of recombinant laforin with polyclonal α-laforin antibody #113 did not inhibit *p*NPP or glucan phosphatase activity (Figure 4.3A, left and middle panels). It should be noted that the malachite green assay detects phosphate released from amylopectin as well as any free phosphate present in assay reagents. Therefore, we performed malachite green assays with only Protein A Sepharose in the absence of laforin to confirm that the Protein A Sepharose was not a source of phosphate contamination (Figure 4.3A, right panel). These results demonstrate that laforin is active both bound and free from the polyclonal antibody-Sepharose complex.

We then attempted to assess the activity of laforin overexpressed in cell culture and immunoprecipitated with α-laforin antibody #113. We first expressed wild-type and inactive C266S FLAG-laforin in HEK293 cells, immunoprecipitated laforin with α-laforin antibody #113 in conjunction with Protein A Sepharose, and then assessed the activity of the immunoprecipitated laforin. *p*NPP and malachite green assays were performed with 10 μl and 5 μl of immunoprecipitated laforin,

respectively. We found that only wild-type FLAG-laforin exhibited *p*NPP activity (Figure 4.3B, left panel) and glucan phosphatase activity (Figure 4.3B, right panel), with very low background from C266S FLAG-laforin (Figure 4.3B, right panel). These data indicate that our experimental design can function when using cell lysate and can also differentiate between active and inactive laforin.

Next, we determined if we could immunoprecipitate endogenous laforin from HepG2 liver cells and detect its phosphatase activity. We grew HepG2 cells to 90% confluence and lysed them in the same buffer used to purify recombinant laforin for antibody production, as this buffer provided us with higher yields of immunoprecipitated endogenous laforin than other buffers (data not shown). We found that we could immunoprecipitate at least ~20 ng of laforin from HepG2 cells using α-laforin antibody #113 in conjunction with Protein A Sepharose (Figure 4.4A).

After immunoprecipitating endogenous laforin, we performed *p*NPP and malachite green assays with the Sepharose-bound laforin. We found that the Protein A Sepharose control exhibited a similar *p*NPP absorbance as Protein A Sepharose with bound laforin (Figure 4.4B). We then pre-cleared the HepG2 cell lysates with Protein A Sepharose in addition to immunoprecipitating with Protein A Sepharose incubated first with BSA, but control *p*NPP activity was not diminished (data not shown). These results indicate that the *p*NPP assay is not suitable for use as a bioassay, likely due to the interaction of Protein A Sepharose with other cellular phosphatases. In contrast to these results, the Protein A Sepharose control exhibited very little background when the malachite green assay was utilized, with only immunoprecipitated laforin exhibiting robust glucan phosphatase activity (Figure 4.4C). Thus, the malachite green assay with amylopectin substrate, when used in conjunction with the α-laforin antibody #113, is specific for the quantification of endogenous laforin activity.

Finally, we tested our bioassay for the detection of endogenous laforin activity in both mouse and human tissue lysate. We generated and obtained lysates from C57BL/6 mouse skeletal muscle and human skin tissue, respectively. Next, we

immunoprecipitated laforin from different amounts of lysate based on total protein, ranging from 0.02 mg – 1.0 mg of mouse skeletal muscle lysate and from 0.1 mg – 0.75 mg of human skin tissue lysate. We divided the immunoprecipitated laforin into three 20 μl aliquots to use the material for Western analysis, malachite green assays, and a third aliquot to repeat both assays. We detected ~4 ng of laforin in the 1.0 mg lane of mouse skeletal muscle lysate (Figure 4.5A). Since we divided the immunoprecipitation from the 1.0 mg sample into three aliquots, we immunoprecipitated ~12 ng total from 1.0 mg of the lysate. Similarly, we detected ~10 ng of laforin from the 0.75 mg sample of human skin lysate (Figure 4.5B). Thus, we immunoprecipitated ~30 ng in total from the 0.75 mg sample. We then tested the immunoprecipitated laforin for glucan phosphatase activity using the assay established above. Laforin immunoprecipitated from at least 0.5 mg of total protein from mouse skeletal muscle lysate and from at least 0.3 mg of total protein from human skin lysate demonstrated robust glucan phosphatase activity above the Protein A Sepharose control (Figure 4.5C and D). Therefore, we successfully immunoprecipitated endogenous laforin from both mouse and human tissue and measured its glucan phosphatase activity.

Discussion.

We sought to characterize α-laforin antibodies capable of detecting and immunoprecipitating endogenous laforin in order to generate a bioassay for laforin activity. First, we explored the conditions for the immunoprecipitation and assay of overexpressed laforin while also determining if antibody binding to laforin could inhibit laforin activity. We began by testing the activity of overexpressed FLAG-laforin immunoprecipitated using α-FLAG agarose, and found that overexpressed laforin did demonstrate *p*NPP and glucan phosphatase activity. This activity was not impacted by whether laforin was bound to or eluted from the FLAG-agarose.

We then identified two α-laforin antibodies, N84/37.1 and #113, that were capable of detecting and immunoprecipitating endogenous laforin, respectively. Following immunoprecipitation of overexpressed laforin with α-laforin antibody

#113, we found that binding of this polyclonal antibody to laforin did not negatively impact activity. These results reflected those obtained with recombinant laforin, where α-laforin antibody #113 and Protein A Sepharose binding did not impact either *p*NPP or malachite green activity. Following immunoprecipitation of endogenous laforin using α-laforin antibody #113, we found that the *p*NPP assay gave significant background, likely due to the interaction of another cellular phosphatase with the Protein A Sepharose. However, using the malachite green assay with amylopectin substrate, we showed that glucan phosphatase activity was specific to successful immunoprecipitation of endogenous laforin. Finally, we demonstrated that this methodology can be successfully employed using mouse or human tissue lysate. Therefore, this assay is can be utilized with tissue from both LD mouse models and LD patients.

It is important to note that Western analysis alone is likely not sufficient to accurately assess if a given treatment is yielding functional laforin. Western analysis is unable to discriminate between wild type and mutant laforin, unless the antibody epitope is itself mutated. Therefore, one needs an enzymatic assay to quantify the activity of functional laforin rather than just total protein. The assay that we have developed faithfully reports the activity of functional endogenous laforin.

While we utilized finite supplies of a polyclonal α-laforin antibody in our study, we found that rabbit polyclonal antibodies created in different animals were as successful in the immunoprecipitation of endogenous laforin as α-laforin antibody #113. Thus, after a brief assessment for quality, stocks of polyclonal antibodies against laforin could be continuously maintained. The bioassay we have developed in this work will no doubt prove useful in the assessment of future therapeutic interventions for LD.

Laforin is widely expressed in tissues throughout the human body (*106, 133*). Prior to PCR analysis, LD was diagnosed using light microscopy of a skin biopsy in conjunction with hematoxylin eosin or periodic acid Schiff (PAS) staining (*37, 105*). A similar skin biopsy of LD patients following therapeutic intervention in conjunction with the immunoprecipitation method we have identified would allow

for detection of endogenous laforin activity. Alternatively, this bioassay could be utilized on cerebrospinal fluid (CSF) collected from patients, as seizures disrupt the blood-brain barrier.

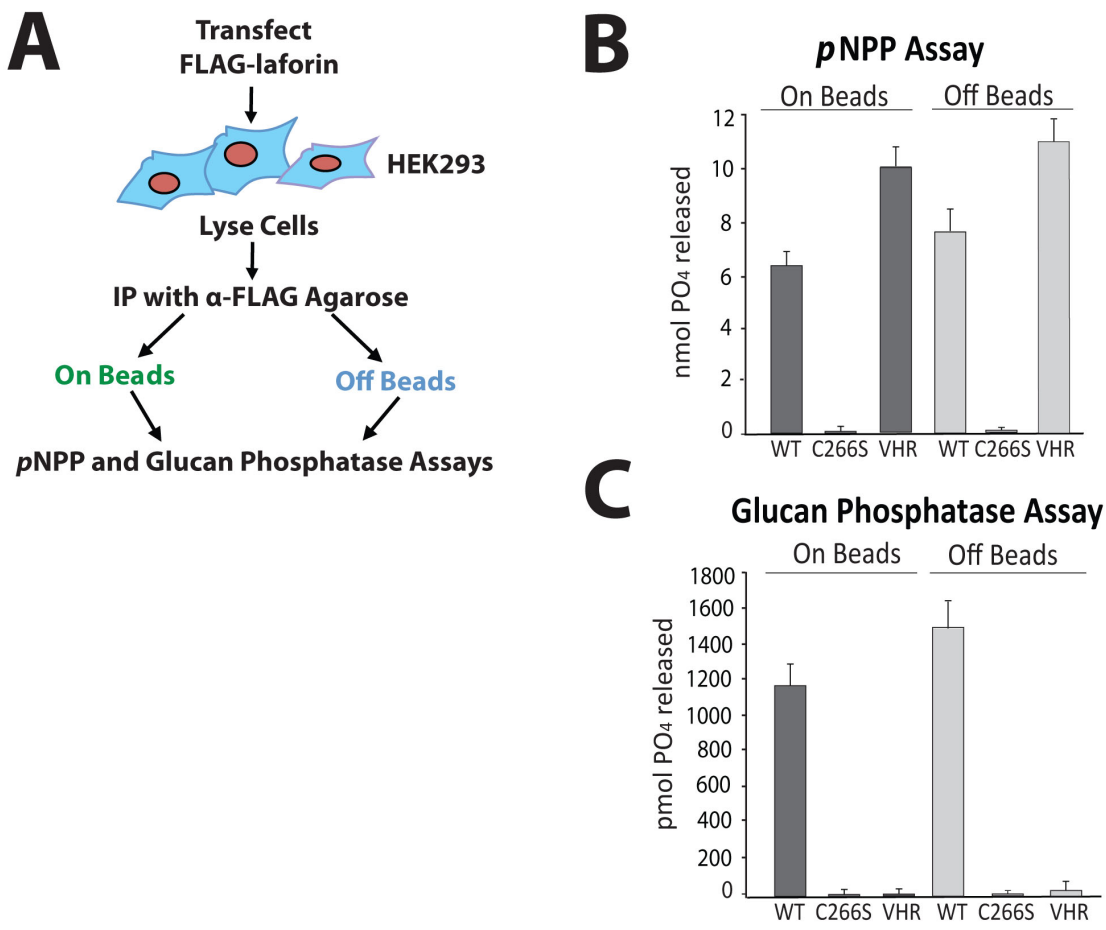
A
Transfect
FLAG-laforin
HEK293
Lyse Cells
IP with α-FLAG Agarose
On Beads
Off Beads
pNPP and Glucan Phosphatase Assays
B
pNPP Assay
On Beads
Off Beads
nmol PO4 released
0
2
4
6
8
10
12
WT C266S VHR WT C266S VHR
C
Glucan Phosphatase Assay
On Beads
Off Beads
pmol PO4 released
0
200
400
600
800
1000
1200
1400
1600
1800
WT C266S VHR WT C266S VHR

Figure 4.1. Laforin exhibits phosphatase activity both bound to and free of the antibody-agarose complex. A. Schematic of experimental design**.** Before attempting to test endogenous laforin, we first optimized our experimental conditions using overexpressed laforin. We immunoprecipitated FLAG-laforin and assessed its *p*NPP and glucan phosphatase activity both bound to and free of the FLAG antibody-agarose complex ("on beads" and "off beads") in order to determine if antibody binding to laforin inhibits activity. **B.** *p*NPP assay of immunoprecipitated FLAG-laforin**.** FLAG-tagged human wild-type laforin, catalytically inactive C266S laforin, and wild-type VHR were expressed in HEK293 cells and immunoprecipitated with α-FLAG agarose. VHR, a DSP that acts upon protein substrates and not glucan substrates, was included as a control. Immunoprecipitated proteins were either left bound to the antibody-agarose complex ("on beads") or eluted from the complex using FLAG peptide ("off beads"). The absorbance of reactions at 410 nm was measured. Error bars indicate ± SEM. **C.** Glucan phosphatase assay of immunoprecipitated FLAG-laforin**.** The absorbance of reactions at 620 nm was measured. Error bars indicate ± SEM. Proteins are as indicated as in Figure 4.1B. The experiments above were performed a minimum of three times, with reactions performed in quadruplicate.

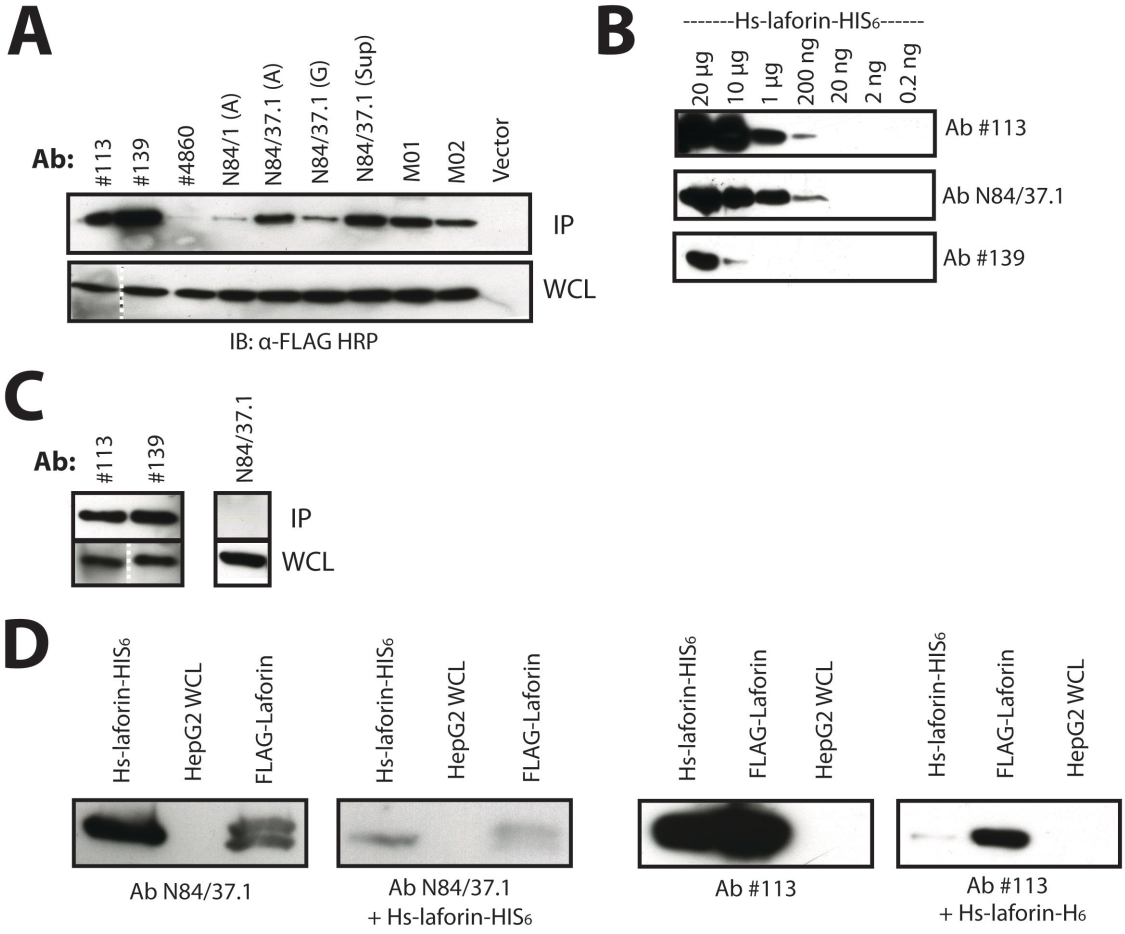
A
Ab:
#113
#139
#4860
N84/1 (A)
N84/37.1 (A)
N84/37.1 (G)
N84/37.1 (Sup)
M01
M02
Vector
IP
WCL
IB: α-FLAG HRP
B
-------Hs-laforin-HIS6------
20 µg
10 µg
1 µg
200 ng
20 ng
2 ng
0.2 ng
Ab #113
Ab N84/37.1
Ab #139
C
Ab:
#113
#139
N84/37.1
IP
WCL
D
Hs-laforin-HIS6
HepG2 WCL
FLAG-Laforin
Ab N84/37.1
Ab N84/37.1
+ Hs-laforin-HIS6
Ab #113
Ab #113
+ Hs-laforin-H6

Figure 4.2. Laforin antibody selection. A. Immunoprecipitation of overexpressed laforin using available antibodies**.** FLAG-laforin was immunoprecipitated using a variety of α-laforin antibodies in conjunction with Protein A Sepharose. We tested protein A-purified rabbit polyclonal α-laforin antibodies #113, #139, #4860, protein A- and G-purified mouse monoclonal α-laforin antibodies N84/1 and N84/37.1 from NeuroMabs, and several commercially available mouse monoclonal α-laforin antibodies (M01 and M02, Abnova). "(A)" or "(G)" indicates affinity purification of an antibody with either protein A or protein G, respectively. "Sup" indicates unpurified tissue culture supernatant. Cells containing empty vector were immunoprecipitated with α-FLAG agarose. The depicted image is a representation. The dotted line indicates where an image portion is a composite of the same image due to the presence of molecular weight marker in between the lanes. **B.** Detection limit of laforin antibodies**.** Serial dilutions of recombinant laforin (20 μg to 0.2 ng) were probed with the α-laforin antibodies. Only α-laforin antibodies #113, N84/37.1, and #139 are shown, as they displayed the most sensitive detection of recombinant laforin. The depicted images are representations. **C.** Immunoprecipitation of endogenous laforin from HepG2 cultures**.** Only the polyclonal α-laforin antibodies #113 and #139 were able to immunoprecipitate endogenous laforin. While the other antibodies did not immunoprecipitate laforin, laforin was detected in their WCL samples. Only the result from α-laforin antibody N84/37.1 is shown to depict this negative result. The depicted images are a representation. The dotted line indicates where an image portion is a composite of the same image due to the presence of molecular weight marker in between lanes. **D.** The specificity of the N84/37.1 and #113 α-laforin antibodies were confirmed using antigen competition. Each antibody was incubated with recombinant laforin prior to immunoblotting recombinant (Hs-laforin-HIS_6), overexpressed (FLAG-laforin), and endogenous (HepG2 WCL) laforin. Representative images of matched blots are portions of the same exposure. Endogenous laforin was not visible at the exposures depicted. The above experiments were performed a minimum of three times.

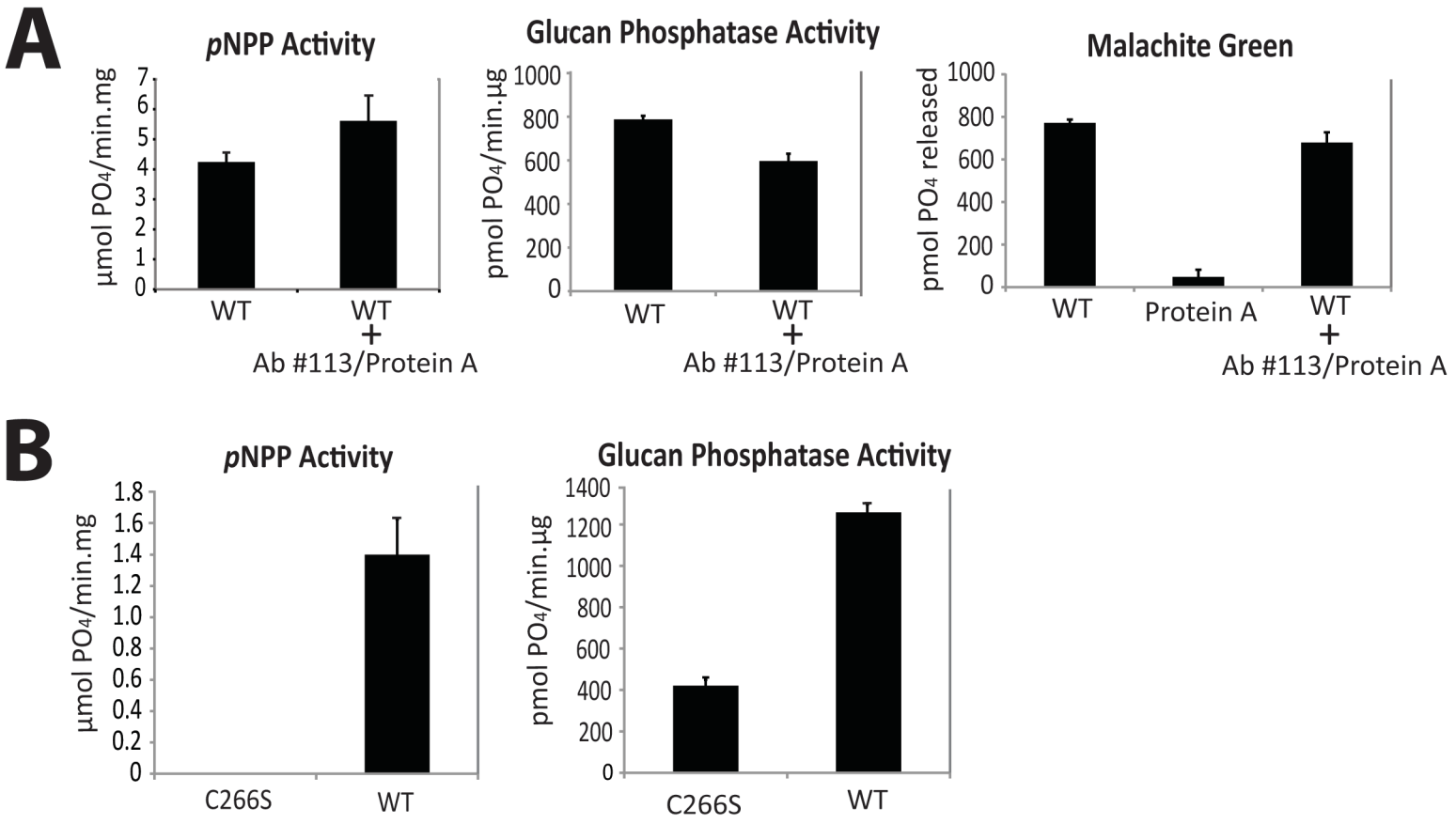
A
pNPP Activity
µmol PO4/min.mg
0
1
2
3
4
5
6
7
WT
WT
+
Ab #113/Protein A
Glucan Phosphatase Activity
pmol PO4/min.µg
0
200
400
600
800
1000
WT
WT
+
Ab #113/Protein A
Malachite Green
pmol PO4 released
0
200
400
600
800
1000
WT
Protein A
WT
+
Ab #113/Protein A
B
pNPP Activity
µmol PO4/min.mg
0
0.2
0.4
0.6
0.8
1.0
1.2
1.4
1.6
1.8
C266S
WT
Glucan Phosphatase Activity
pmol PO4/min.µg
0
200
400
600
800
1000
1200
1400
C266S
WT

Figure 4.3. Immunoprecipitation and activity assay of recombinant and overexpressed laforin. A. Recombinant laforin was incubated with α-laforin antibody #113 and Protein A Sepharose to determine the impact of antibody binding on activity. The phosphatase activity of non-incubated and incubated recombinant laforin was assayed using *p*NPP and malachite green assays. Identical malachite green reactions were carried out containing only Protein A Sepharose to test for the presence of phosphate contamination. Protein A Sepharose (Sigma-Aldrich) was utilized, as free phosphate was present in other commercial preparations (data not shown). Reactions containing inactive C266S recombinant laforin were utilized as a negative control. Error bars indicate ± SEM. **B.** Immunoprecipitated overexpressed laforin exhibits *p*NPP and glucan phosphatase activity**.** Human wild-type and inactive C266S FLAG-laforin was expressed in HEK293 cells and then immunoprecipitated using α-laforin antibody #113. In order to determine protein amounts, immunoprecipitated laforin was analyzed by SDS-PAGE and Western blotted alongside known amounts of recombinant human laforin. *p*NPP and glucan phosphatase activity of immunoprecipitated laforin was then determined using the amount of immunoprecipitated laforin calculated by comparison to the known recombinant protein amounts. Error bars indicate ± SEM. The experiments above were repeated a minimum of three times, with reactions performed in quadruplicate.

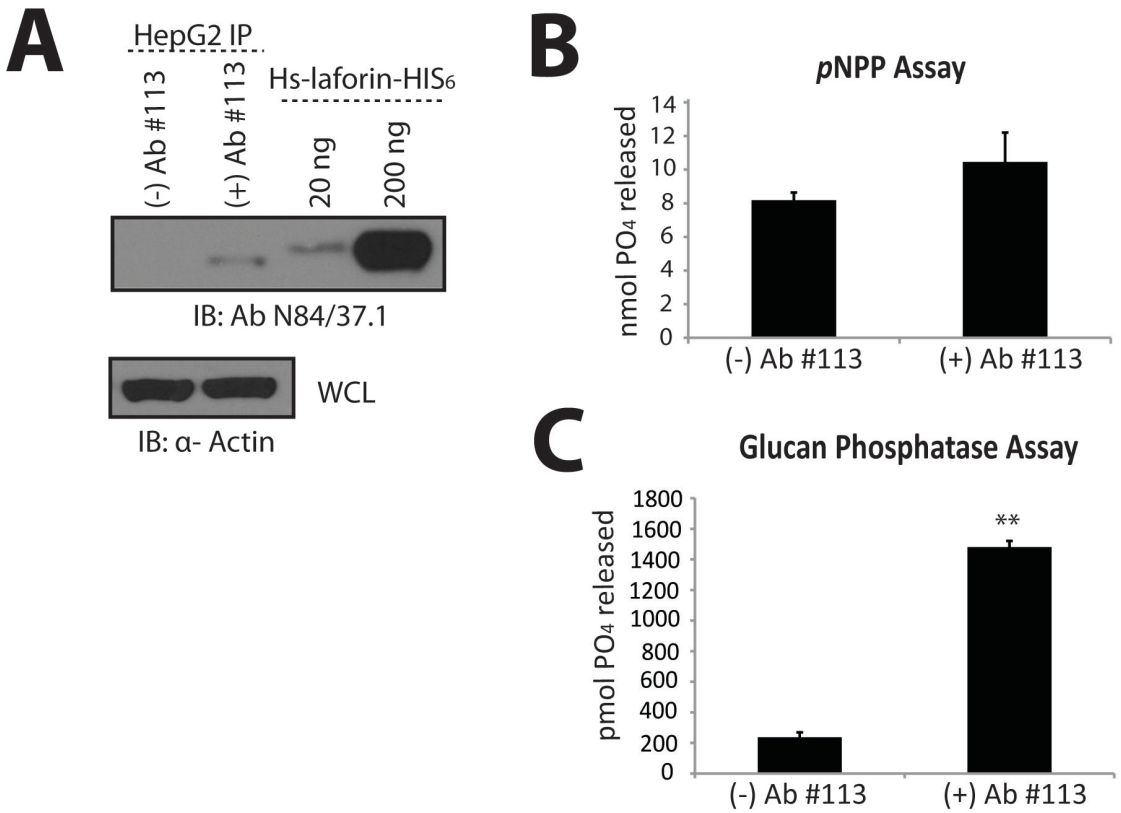

Figure 4.4. Immunoprecipitated endogenous laforin exhibits specific glucan phosphatase activity. Laforin was immunoprecipitated from HepG2 cells using α-laforin antibody #113 and Protein A Sepharose or Protein A Sepharose alone as a control. **A.** Western analysis of immunoprecipitated endogenous laforin from HepG2 cells. The laforin immunoprecipitate sample was divided into three equal aliquots and one aliquot was separated via SDS-PAGE, Western transferred, and immunoblotted with α-laforin antibody N84/37.1. Known amounts of recombinant laforin were ran alongside the immunoprecipitated laforin to allow for quantification of the immunoprecipitated laforin. The depicted image is a representation. **B.** *p*NPP assay of immunoprecipitated endogenous laforin from HepG2 cells. Error bars indicate ± SEM. **C**. Glucan phosphatase assay of immunoprecipitated endogenous laforin from HepG2 cells**.** Error bars indicate ± SEM. The experiments above were repeated a minimum of three times, with reactions performed in quadruplicate. A double asterisk indicates $p < 0.01$ following an independent-samples t-test.

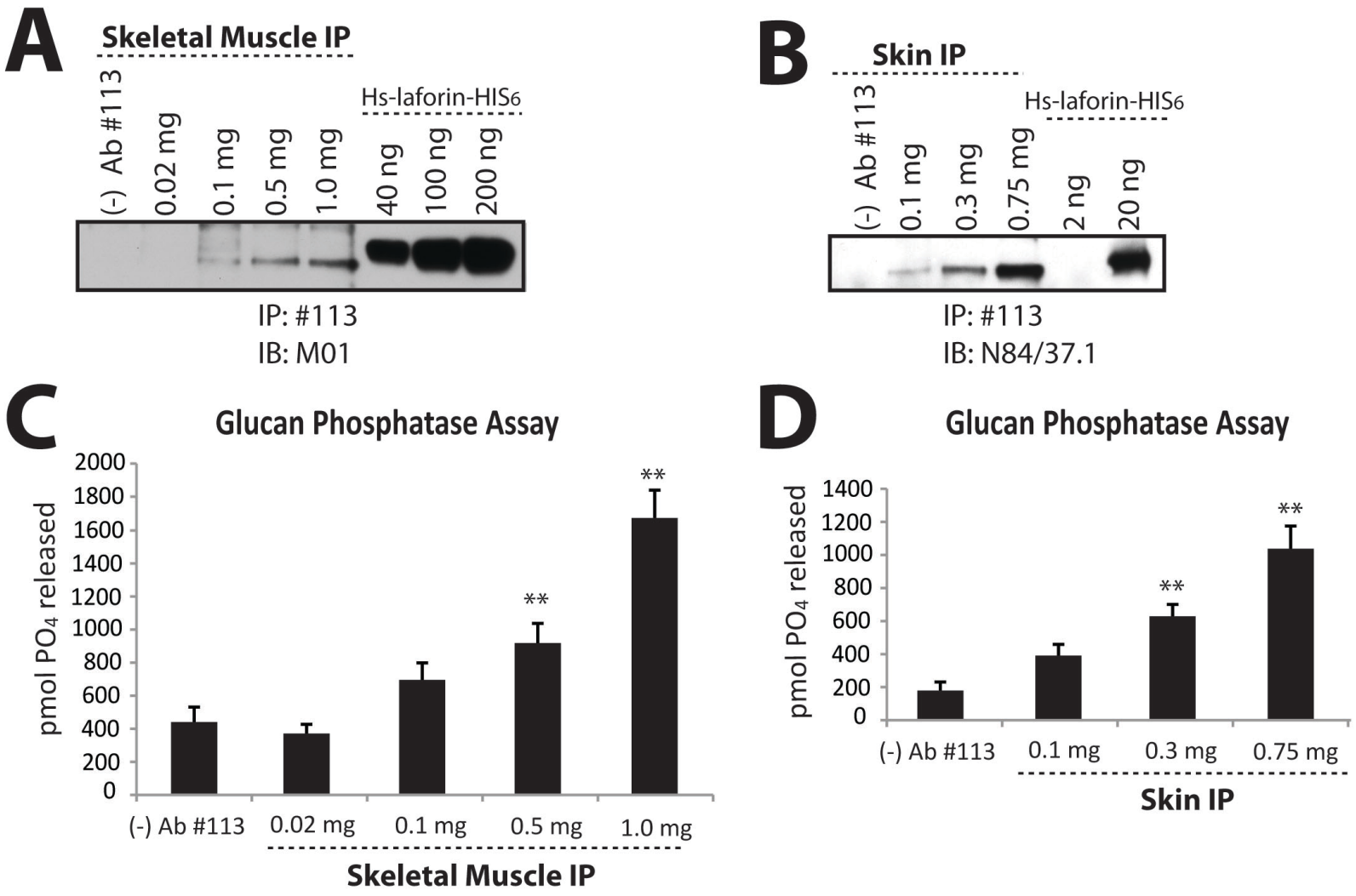
A
Skeletal Muscle IP
(-) Ab #113
0.02 mg
0.1 mg
0.5 mg
1.0 mg
Hs-laforin-HIS6
40 ng
100 ng
200 ng
IP: #113
IB: M01
B
Skin IP
(-) Ab #113
0.1 mg
0.3 mg
0.75 mg
Hs-laforin-HIS6
2 ng
20 ng
IP: #113
IB: N84/37.1
C
Glucan Phosphatase Assay
pmol PO4 released
2000
1800
1600
1400
1200
1000
800
600
400
200
0
**
**
(-) Ab #113
0.02 mg
0.1 mg
0.5 mg
1.0 mg
Skeletal Muscle IP
D
Glucan Phosphatase Assay
pmol PO4 released
1400
1200
1000
800
600
400
200
0
**
**
(-) Ab #113
0.1 mg
0.3 mg
0.75 mg
Skin IP

Figure 4.5. Endogenous laforin activity from mouse and human tissue lysate. Laforin was immunoprecipitated from increasing amounts of mouse skeletal muscle lysate and human skin lysate using α-laforin antibody #113 in conjunction with Protein A Sepharose and tested for glucan phosphatase activity. **A.** Western analysis of immunoprecipitated laforin from mouse skeletal muscle**.** Increasing amounts of mouse skeletal muscle lysate from 0.02 mg - 1.0 mg of total protein was used to immunoprecipitate laforin. The immunoprecipitate sample was divided into three equal aliquots and one aliquot was separated via SDS-PAGE, Western transferred, and immunoblotted with α-laforin antibody M01. Known amounts of recombinant laforin were ran alongside the immunoprecipitated laforin to allow for quantification of the immunoprecipitated laforin. As a negative control, antibody was excluded from a 1.0 mg sample (lane: (-) Ab#113). The depicted image is a representation. **B.** Western analysis of immunoprecipitated laforin from human skin lysate**.** Increasing amounts of human skin lysate from 0.1 mg - 0.75 mg of total protein was used to immunoprecipitate laforin. The immunoprecipitate sample was divided into three equal aliquots and one aliquot was separated via SDS-PAGE, Western transferred, and immunoblotted with α-laforin antibody N84/37.1. Known amounts of recombinant laforin were ran alongside the immunoprecipitated laforin to allow for quantification of the immunoprecipitated laforin. As a negative control, antibody was excluded from a 0.75 mg sample (lane: (-) Ab#113). The depicted image is a representation. **C.** Glucan phosphatase assay of laforin immunoprecipitated from mouse skeletal muscle. Increasing amounts of mouse skeletal muscle lysate from 0.02 mg - 1.0 mg of total protein was used to immunoprecipitate laforin. The immunoprecipitated sample was divided into three equal aliquots and one aliquot was used to perform glucan phosphatase assays in quadruplicate. Error bars indicate ± SEM. **D**. Glucan phosphatase assay of laforin immunoprecipitated from human skin. Increasing amounts of human skin lysate from 0.1 mg - 0.75 mg of total protein was used to immunoprecipitate laforin. The immunoprecipitated sample was divided into three equal aliquots and one aliquot

was used to perform glucan phosphatase assays in quadruplicate. Error bars indicate ± SEM. The experiments above were repeated a minimum of three times. A double asterisk indicates $p < 0.01$ following an independent-samples t-test.

CHAPTER 5: EFFECTS OF AMINOGLYCOSIDES ON NONSENSE MUTATIONS IN LAFORIN AND MALIN AS A THERAPEUTIC OPTION FOR LAFORA DISEASE

Introduction.

Lafora disease (LD) results from recessive mutations in the autosomal genes encoding either the glucan phosphatase laforin or the ubiquitin ligase malin (*EPM2A* and *EPM2B*, respectively) (*29, 55, 106, 107, 152*), with mutations in laforin accounting for 70% of LD cases and mutations in malin 27% of LD cases (*134*). Disease-causing mutations are distributed across the domains of each protein (*52*). Nonsense mutations are found in ~16% of LD patients with laforin defects and ~15% with malin defects, leading to truncated and nonfunctional protein products (*52, 141*). Currently, there is no long-term treatment option for LD outside of palliative therapeutics (*37, 107*). For the subset of LD patients with nonsense mutations in laforin or malin, aminoglycosides and their functional equivalents may lead to the production of functional protein that can inhibit the formation of LBs or possibly lead to their breakdown.

Aminoglycoside antibiotics, due to their availability and low cost, have been used since their discovery in the 1940s to treat a variety of serious bacterial infections such as tuberculosis (*48*). Aminoglycosides are known to function by binding to the prokaryotic ribosome and inhibiting protein synthesis. However, aminoglycosides can also bind weakly to the mammalian 40S ribosomal subunit, decreasing translation fidelity by causing the ribosome to "read through" nonsense mutations. This occurs due to the insertion of either the correct amino acid or one associated with a near-cognate aminoacyl tRNA (*94*). This translational readthrough process is regulated by several factors such as the stop codon itself and the sequence surrounding it (*86, 102*). Although aminoglycosides are unable to cross the blood-brain barrier (*148*), this barrier is often ruptured during seizures as occur in LD.

The aminoglycoside gentamicin, because of its well-characterized safety profile in humans, has been frequently assessed for the ability to read through nonsense mutations causing disease (*94*). Studies have evaluated the use of

gentamicin in cystic fibrosis (CF) cell lines containing nonsense mutations and in cells transfected with cystic fibrosis transmembrane conductance regulator (*CFTR*) constructs containing CF-causing nonsense mutations. In both cell models, gentamicin treatment promoted full-length, functional CFTR production of up to 20-35% of wild-type protein levels depending on the nonsense mutation sequence (*11, 73*). The results from these cell-based assays translated favorably into clinical trials involving CF patients, where intravenous gentamicin administration promoted functional CFTR production *in vivo* (*32, 171*).

Subsequent studies demonstrated that the aminoglycoside amikacin promotes greater production of functional CFTR than gentamicin in a CF mouse model at clinically relevant doses of both compounds (*41*). Although variability in nonsense mutation readthrough is seen with aminoglycosides depending on CF nonsense mutation sequence, as little as 5% of normal CFTR protein levels appears to be adequate for the alleviation of CF symptoms (*120*), which may prove similar with laforin and malin protein levels and LD. Given the predictive power of *in vitro* models for nonsense readthrough in CF patients, we hypothesized that gentamicin or amikacin-induced readthrough of LD-causing nonsense mutations *in vitro* may be a likely indicator of successful readthrough in LD patients.

While efficacious in terms of nonsense readthrough, aminoglycosides require parenteral administration, and severe side effects such as ototoxicity and nephrotoxicity limit their long-term application (*48*). Only 3 mg/kg of gentamicin and 15 mg/kg of amikacin can cause ≥20% nephrotoxicity in patients (*10*). In search of a safer alternative to aminoglycosides, recent work identified PTC124, a compound that also promotes nonsense readthrough but exhibits minimal side effects in humans at single doses of up to 100 mg/kg (*72, 169*). In clinical trials evaluating PTC124 efficacy in CF patients with nonsense mutations, PTC124 led to improvements in CFTR activity as well as phenotypic characteristics such as lung function and bodyweight (*87, 170*). PTC124 has even been shown to be safe and effective in promoting functional CFTR production in children with CF-causing nonsense mutations, with no adverse drug reactions after a 2-year follow-up (*130*).

Therefore, PTC124 is also a promising therapeutic candidate for LD patients, most of whom are children or adolescents.

We explored the efficacy of the aminoglycosides gentamicin and amikacin and the functional analog PTC124 in promoting readthrough of nonsense mutations in laforin and malin that cause LD. We utilized transient transfection of FLAG-tagged laforin and malin constructs containing nonsense mutations followed by analysis of full-length protein levels in order to generate an *in vitro* readthrough model. This readthrough model was based on previous work utilizing epitope tag-based *in vitro* readthrough systems (*21, 22*). Aminoglycoside and PTC124 treatment did lead to significant readthrough of several of the laforin and malin nonsense mutants studied. Surprisingly however, the location of the epitope tag impacted both the basal expression and drug-induced readthrough response of the laforin and malin constructs utilized. Therefore, cell lines established from LD patients with nonsense mutations will likely be required in order to assess the full efficacy of these compounds.

Results.

In order to assess the efficacy of aminoglycoside and PTC124-mediated readthrough of LD-causing nonsense mutations, we designed a cell culture model utilizing transient transfection of C-terminally FLAG-tagged (C-FLAG) laforin and malin constructs. Using these constructs, FLAG-tagged proteins will only be observed if readthrough of a nonsense mutation occurs. Four of the most common LD-causing nonsense mutations in both laforin and malin were selected from the LD mutation database (*79*) for study (Figure 5.1A and B).

The eight C-FLAG mutants were first expressed in HEK293 cells in order to assess basal readthrough levels. Western blot analysis of cell lysates was then performed using a monoclonal α-FLAG antibody. Although little to no basal readthrough was expected, most of the mutant constructs exhibited a variable level of basal readthrough between 20-100% of wild-type protein levels (Figure 5.1C).

Only R241X laforin, E67X malin, and R265X malin exhibited undetectable levels of basal readthrough.

Next, we evaluated the drug-induced readthrough of the four laforin and four malin C-FLAG nonsense mutants following gentamicin, amikacin, and PTC124 treatment. The concentrations of the three compounds utilized were those used in previous studies that were found to be therapeutic without causing significant toxicity (*41, 169*). However, to confirm that these concentrations were nontoxic and to assess if the drugs impacted wild-type laforin expression, wild-type laforin was expressed in HEK293 cells prior to treatment of the cells with gentamicin, amikacin, or PTC124 for 18 hours. Wild-type laforin protein levels remained constant before and after treatment, and thus there was no toxicity-induced decrease in laforin expression (Figure 5.2A). Additionally, there was no shift in the molecular weight of laforin that would have been indicative of readthrough of the true termination codon (Figure 5.2A). Since these drug concentrations were not toxic to cells, nor did they cause readthrough of the true termination codon, they were used in subsequent studies.

We then examined the level of drug-induced readthrough for the C-FLAG Y86X, S158X, R241X, and C278X laforin mutants. Each C-FLAG laforin nonsense mutant displayed varying levels of readthrough following treatment with a range of concentrations of gentamicin, amikacin, and PTC124 (Figure 5.2B-D). No full-length laforin was detected following R241X laforin expression in cells and application of any of the three readthrough-promoting compounds (data not shown). Similarly, Y86X laforin did not exhibit a significant readthrough response after application of any of the three readthrough-promoting compounds. Readthrough levels were <10% with 150-600 μM of gentamicin or amikacin treatment, with increasing concentrations of PTC124 from 15-45 μM leading to a decreasing trend in full-length laforin compared to untreated cells (Figure 5.2B).

C278X laforin displayed trending increases in readthrough of up to 50% above untreated C278X laforin levels with 150-600 μM gentamicin and 15-45 μM PTC124 treatment, although these results were not statistically significant (Figure

5.2C). Meanwhile, S158X laforin responded more favorably following gentamicin and amikacin treatment, with up to a 40% increase in readthrough observed with 150-600 μM gentamicin treatment and a significant increase in readthrough of 50% above untreated S158X laforin levels seen with 600 μM amikacin treatment (Figure 5.2D). Conversely, no significant increase in S158X readthrough was observed when cells were treated with PTC124.

As seen with C-FLAG wild-type laforin (Figure 5.2A), full-length C-FLAG wild-type malin protein levels were not negatively impacted by gentamicin, amikacin, or PTC124 treatment, nor did the drugs cause readthrough of the natural termination codon (Figure 5.3A). The C-FLAG malin nonsense mutants G131X and W219X demonstrated varying amounts of readthrough in response to gentamicin, amikacin, and PTC124 treatment (Figure 5.3B and C). Despite drug treatment, no full-length protein was detected for the C-FLAG E67X or R265X malin nonsense mutants (data not shown).

Conversely, C-FLAG G131X malin exhibited up to a 17% increase in readthrough with 150-600 μM gentamicin treatment and up to a 30% increase in readthrough above untreated G131X malin levels with increasing concentrations of PTC124 from 15-45 μM, although these results were not significant (Figure 5.3B). Similarly, W219X malin demonstrated levels of readthrough up to 40-65% above untreated W219X malin levels following treatment with 150-600 μM gentamicin and amikacin, although again, statistical significance was not achieved (Figure 5.3C).

Because prior work utilized epitope tags at either the N- or C-terminus of nonsense mutant constructs (*21, 22*), N-terminally FLAG-tagged (N-FLAG) constructs of the same laforin and malin nonsense mutants previously studied were constructed in order to determine if the location of the epitope tag impacts basal and/or drug-induced readthrough. Unlike the C-FLAG wild-type and nonsense mutant laforin and malin constructs whose protein products were observable in cell lysate, the N-FLAG proteins required enrichment via immunoprecipitation with α-FLAG agarose in order to detect N-FLAG wild-type and mutant laforin and malin.

Even using this immunoprecipitation strategy, the only truncated N-FLAG laforin mutant that was detectable following Western analysis was N-FLAG C278X laforin (Figure 5.4A). The level of the truncated mutant was only 4 ± 2% that of N-FLAG wild-type laforin levels. The truncated N-FLAG malin nonsense mutants exhibited 10-40% of N-FLAG wild-type malin expression levels (Figure 5.4A). Unlike the C-FLAG mutant constructs, no basal readthrough was observed for any of the N-FLAG laforin or malin nonsense mutants (Figure 5.4A).

Next, the N-FLAG laforin and malin nonsense mutants were treated with the same concentrations of gentamicin, amikacin, or PTC124 used previously to treat the C-FLAG mutants in order to assess drug-induced readthrough. Although the N-FLAG C278X laforin mutant and E67X and W219X malin mutant truncations were expressed (Figure 5.4A), no readthrough was observed following treatment with any of the three readthrough-promoting compounds (data not shown). Additionally, no drug-induced readthrough was observed for N-FLAG S158X laforin or R241X laforin (data not shown).

In contrast, the N-FLAG G131X malin mutant exhibited a 100% increase in readthrough above untreated G131X malin levels with 600 μM gentamicin treatment (Figure 5.4B), although this result was not statistically significant. Statistically insignificant readthrough of up to 24% was also observed with 15-45 μM PTC124 treatment, however, DMSO alone gave 18% readthrough (Figure 5.4B).

The N-FLAG R265X malin mutant demonstrated a significant increase in readthrough of 87% above untreated R265X malin levels with 600 μM gentamicin treatment. While amikacin treatment increased readthrough of R265X malin up to 67%, this readthrough was not statistically significant. Additionally, 45 μM PTC124 promoted a significant increase in readthrough of 80% in R265X malin (Figure 5.4C). However, this amount of PTC124 required a final volume of 0.06% v/v DMSO vehicle, and this amount of DMSO alone promoted readthrough of R265X of 60% although this result was not statistically significant (Figure 5.4C). Therefore, only 20% of the readthrough observed after 45 μM PTC124 treatment can be attributed to PTC124.

If full-length laforin or malin is produced in LD patients following readthrough-promoting therapy, treatments must occur at a frequency that allows the levels of these proteins to remain constant in cells for the alleviation of the LD phenotype. Therefore, we examined the half-life of endogenous laforin and malin protein. For this work, an antibody capable of detecting endogenous laforin in cell lysate (Neuromab mouse monoclonal α-laforin antibody N84/37.1) (*137*) was utilized. We assessed the levels of endogenous laforin in both HEK293 and HepG2 liver cells. Cells were treated for 0, 1, 4, 8, 12, and 24 hours with 200 μg/mL cycloheximide to inhibit protein synthesis and cell lysates then subjected to Western analysis.

Surprisingly, endogenous laforin levels remained stable over 24 hours of cycloheximide treatment (Figure 5.5). As cell death was observed at 24 hours, no longer time points were taken. As expected, the cyclin D1 control exhibited a half-life under 4 hours (*45*). After testing several commercially available monoclonal and polyclonal malin antibodies as well as malin polyclonal antibodies generated by our lab, endogenous malin could not be detected in cell lysate (data not shown). Finally, immunofluorescence experiments were performed with a rabbit polyclonal α-laforin antibody generated by our lab (#139) and the Neuromab α-laforin antibody N84/37.1 (*137*) to determine the applicability of these antibodies to detect endogenous laforin localization in human cell lines. The α-laforin antibody N84/37.1 was not able to detect endogenous laforin in HEK293 cells, while the rabbit polyclonal α-laforin antibody #139 demonstrated nonspecific binding (data not shown). Therefore, better antibodies are needed in order to detect the presence of laforin within patient cells.

Discussion.

Aminoglycosides and the functional analog PTC124 can cause the readthrough of nonsense mutations responsible for genetic diseases such as cystic fibrosis and Duchenne's muscular dystrophy, generating full-length, functional proteins with the promise of alleviating disease phenotypes (*94, 169*). In the hope of

facilitating a clinical trial involving readthrough therapy in LD patients, the efficacy of PTC124 and the aminoglycosides gentamicin and amikacin were tested in the readthrough of LD nonsense mutations in the genes encoding laforin and malin. Based on the dose-dependent response in full-length protein production seen both *in vitro* with gentamicin treatment of CFTR nonsense mutations (*73*) and *in vivo* with CF patients (*171*), a range of concentrations of gentamicin, amikacin, and PTC124 was tested in order to determine the presence of a dose-dependent readthrough response in full-length laforin and malin production.

An *in vitro* readthrough reporter system was created utilizing expression and treatment of FLAG-tagged laforin and malin LD nonsense mutants in HEK293 cells. Eight of the most common LD-causing nonsense mutations, four in laforin and four in malin, were chosen for study. These nonsense mutants represent two of the three mammalian translation termination codons (UGA and UAG). Previous work has demonstrated that the termination codon generated due to a nonsense mutation impacts the relative efficiency of termination in the order of UAA>UAG>UGA, which is reflected in the readthrough efficiency of UGA>UAG>UAA (*102*). Therefore, UGA laforin nonsense mutants (S158X, R241X, and C278X) and UGA malin nonsense mutants (G131X and R264X) were expected to exhibit greater readthrough than the UAG laforin nonsense mutant (Y86X) and UAG malin nonsense mutants (E67X and W219X).

Prior work utilizing *in vitro* readthrough reporter systems examined readthrough of nonsense-containing constructs possessing an epitope tag at either the N- or C-terminus (*21, 22*). These studies utilized epitope tags at only one location and did not assess how the epitope tag may affect readthrough. We investigated the impact of the FLAG epitope tag location on readthrough by creating N-terminally FLAG-tagged (N-FLAG) and C-terminally FLAG-tagged (C-FLAG) laforin and malin nonsense mutant constructs. We found that while the readthrough of the LD nonsense mutations in laforin and malin studied was dose-dependent and followed the UGA>UAG readthrough pattern, the location of the FLAG tag at either the N- or C-terminus of the proteins greatly impacted readthrough.

The readthrough of one nonsense mutant could not be studied using the readthrough reporter system that we developed. The N-FLAG R241X laforin mutant (nonsense sequence UGA) did not exhibit detectable expression, and both the N-FLAG and C-FLAG constructs did not demonstrate basal readthrough or induced readthrough following treatment with the three readthrough-promoting compounds (see Table 1 for a summary of all experimental results). A premature termination codon at least 50-55 nucleotides upstream of an exon-exon junction can trigger nonsense-mediated decay (NMD) of an mRNA (*88*). However, the R241X mutation is located a few nucleotides downstream of the final exon-exon junction in laforin (*106, 133*). Therefore, NMD likely cannot account for the lack of expression of the R241X laforin mutant, indicating that another mechanism may be acting to prevent expression.

Despite successful expression, several laforin and malin nonsense mutations failed to respond to treatment with gentamicin, amikacin, or PTC124. No basal or drug-induced readthrough was observed for the C-FLAG and N-FLAG E67X malin mutant (nonsense sequence UAG) (Table 1). While the C-FLAG Y86X laforin mutant (nonsense sequence UAG) exhibited low basal readthrough, it also did not demonstrate a significant readthrough response (Table 1). LD patients possessing these mutations may thus not be candidates for readthrough therapy.

Three of the laforin and malin nonsense mutants studied demonstrated promising trends in drug-induced readthrough response that were not statistically significant. The C-FLAG C278X laforin (nonsense sequence UGA), G131X malin (nonsense sequence UGA), and W219X malin (nonsense sequence UAG) mutants all exhibited increasing readthrough with increasing concentrations of gentamicin. Low concentrations of amikacin also led to an increase in readthrough with these mutants, while increasing amikacin concentrations diminished this response. The C278X laforin mutant alone demonstrated increasing readthrough with increasing PTC124 concentrations. In contrast to the C-FLAG constructs, the N-FLAG C278X laforin and W219X malin mutants did not exhibit basal or drug-induced readthrough (Table 1), indicating that the location of the FLAG tag is impacting mutant readthrough. However, C-FLAG and N-FLAG G131X malin constructs both

exhibited readthrough with gentamicin, indicating that this mutant may demonstrate a readthrough response in LD patients treated with gentamicin.

Two nonsense mutants demonstrated statistically significant drug-induced readthrough. The C-FLAG S158X laforin mutant (nonsense sequence UGA) demonstrated a statistically significant increase in readthrough of 50% following treatment with 600 μM amikacin (Table 1). N-FLAG R265X malin (nonsense sequence UGA) exhibited significant increases in readthrough of up to 87% with 600 μM gentamicin and 20% with 45 μM PTC124 (Table 1). However, the N-FLAG S158X laforin and C-FLAG R265X malin mutant constructs did not demonstrate basal or induced-drug readthrough. Therefore, the location of the FLAG tag is impacting the expression and readthrough of these mutants. However, the readthrough response of the S158X laforin and R265X malin nonsense mutants indicates that LD patients possessing these mutations may benefit from readthrough therapy.

While this work has established that the location of the FLAG tag is influencing readthrough response, the sequence of the nonsense mutation alone has been demonstrated to influence readthrough efficiency in the order of UGA>UAG>UAA (*74, 75, 102*). The basal and induced readthrough of the C-FLAG laforin and malin nonsense mutants generally followed this established pattern. We observed basal readthrough of C278X laforin (UGA) > S158X laforin (UGA) > Y86X laforin (UAG) and G131X malin (UGA) > W219X malin (UAG). This pattern was also reflected in the greater readthrough response of C278X laforin (UGA) ≥ S158X laforin (UGA) > Y86X laforin (UAG) observed with the three readthrough-promoting compounds utilized. However, W219X malin (UAG) exhibited a greater readthrough response than G131X malin (UGA). This may be due to sequences upstream and downstream of the nonsense codon, which can impact readthrough (*15*). The N-FLAG malin nonsense mutant truncations also exhibited expression levels of G131X (UGA) > R265X (UGA) > E67X (UAG) > W219X (UAG). In addition, only N-FLAG G131X and R265X malin exhibited a readthrough response. Although the majority of these results were not statistically significant, it is important to note that these results did follow the general readthrough pattern established in prior work.

Although the basal and induced readthrough of the laforin and malin LD nonsense mutants followed these established readthrough patterns, the C-FLAG laforin and malin mutants that were expressed showed basal readthrough of 20-100% (Table 1) where translation termination is found to have an estimated error rate of 0.01 to 0.1% (*47*). In addition, the expression, basal readthrough, and drug-induced readthrough results observed with the N-FLAG nonsense mutant constructs are in direct conflict with those obtained with the C-FLAG constructs (Table 1). These conflicting results indicate that the *in vitro* readthrough reporter system utilized here, although modeled after previous work, likely does not faithfully assess readthrough of LD-causing nonsense mutations.

As LD is a fatal disorder, the use of compounds that exhibit toxicity such as aminoglycosides can be justified for compassionate use in a clinical trial. Prior to the administration of these compounds to LD patients with nonsense mutations, such as those possessing the S158X laforin or R265X malin mutations, cell lines from these patients should be used first to assess drug efficacy and develop individualized therapies, as the readthrough of nonsense mutations has been found to be similar *in vitro* and *in vivo* (*15, 131*).

In the hope of facilitating such a clinical trial, the half-life of endogenous laforin protein was examined. By determining the half-life of this protein, the required frequency of readthrough-promoting treatment administration to LD patients in order to maintain laforin levels may be determined. We found that over a period of 24 hours of cycloheximide treatment, despite significant cell death, laforin levels remained stable. These results indicate that any full-length laforin generated as a result of treatment with readthrough-promoting compounds will likely remain stable over a period of days, allowing for less frequent dosing with compounds such as aminoglycosides, which possess the potential for toxic effects.

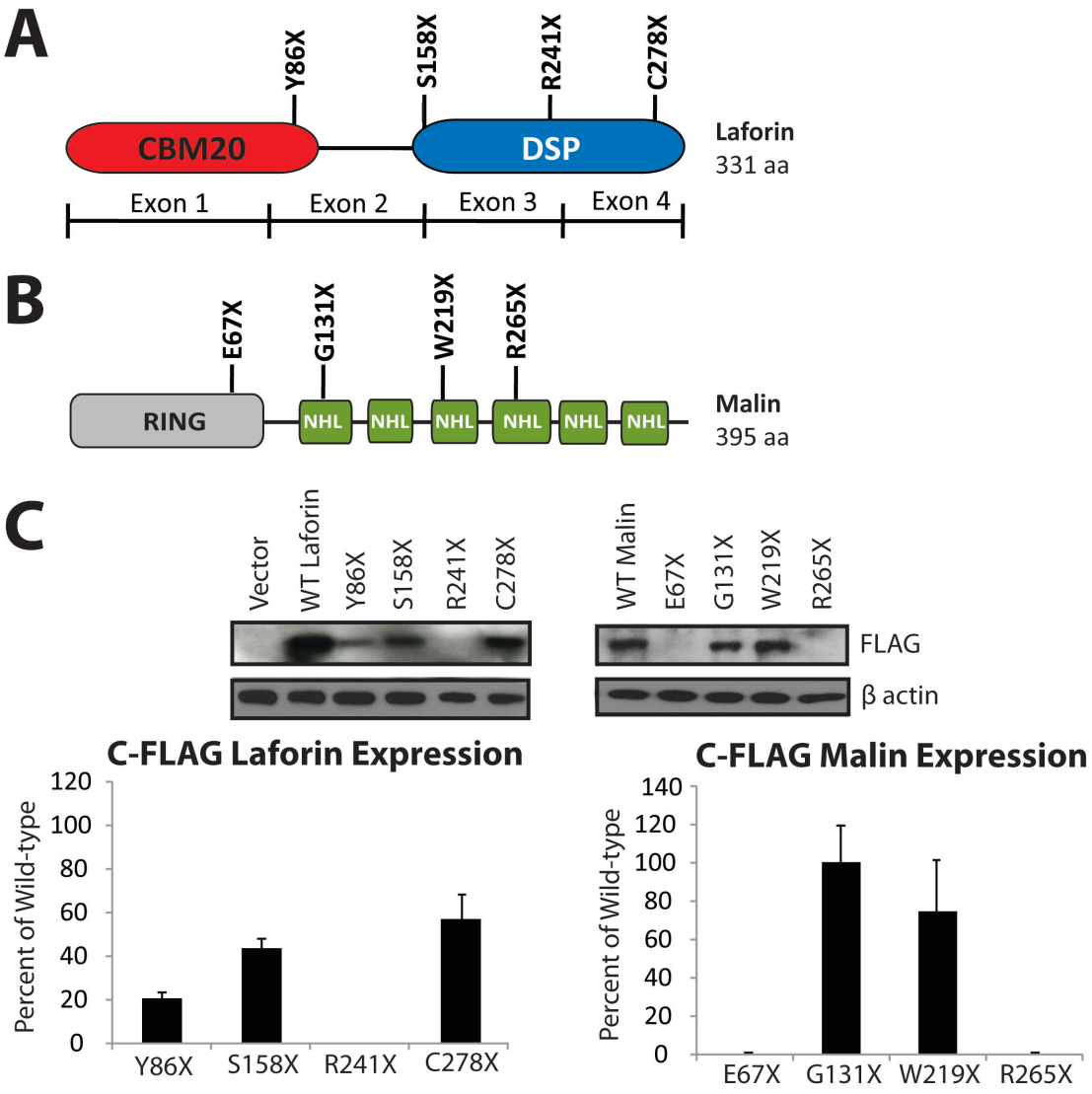
A
Y86X
S158X
R241X
C278X
CBM20
DSP
Laforin
331 aa
Exon 1
Exon 2
Exon 3
Exon 4
B
E67X
G131X
W219X
R265X
RING
NHL
NHL
NHL
NHL
NHL
NHL
Malin
395 aa
C
Vector
WT Laforin
Y86X
S158X
R241X
C278X
WT Malin
E67X
G131X
W219X
R265X
FLAG
β actin
C-FLAG Laforin Expression
Percent of Wild-type
120
100
80
60
40
20
0
Y86X
S158X
R241X
C278X
C-FLAG Malin Expression
Percent of Wild-type
140
120
100
80
60
40
20
0
E67X
G131X
W219X
R265X

Figure 5.1. Laforin and malin nonsense mutations chosen for study. A. Laforin schematic with nonsense mutations**.** Laforin possesses an N-terminal carbohydrate-binding module (CBM) family 20 domain and a C-terminal dual-specificity phosphatase (DSP) domain encoded by exons 1-2 and exons 3-4 of the *EPM2A* gene respectively (*106, 133*). LD-causing nonsense mutations in laforin that were utilized in this study are depicted. **B**. Malin schematic with nonsense mutations**.** Malin possesses an N-terminal RING-finger domain followed by six NHL repeats. The protein is encoded by a single exon (*29*). LD-causing nonsense mutations in malin that were utilized in this study are depicted. **C**. Basal readthrough of C-terminally FLAG-tagged laforin and malin nonsense mutants**.** Mutants were expressed for 24 hours in HEK293 cells and cell lysates immunoblotted for FLAG. The depicted image is a representation, showing an exposure at which the readthrough products of all expressed mutants are visible. Readthrough levels were quantitated by densitometric western blot analysis and presented as percent of wild-type ± SEM (n=3).

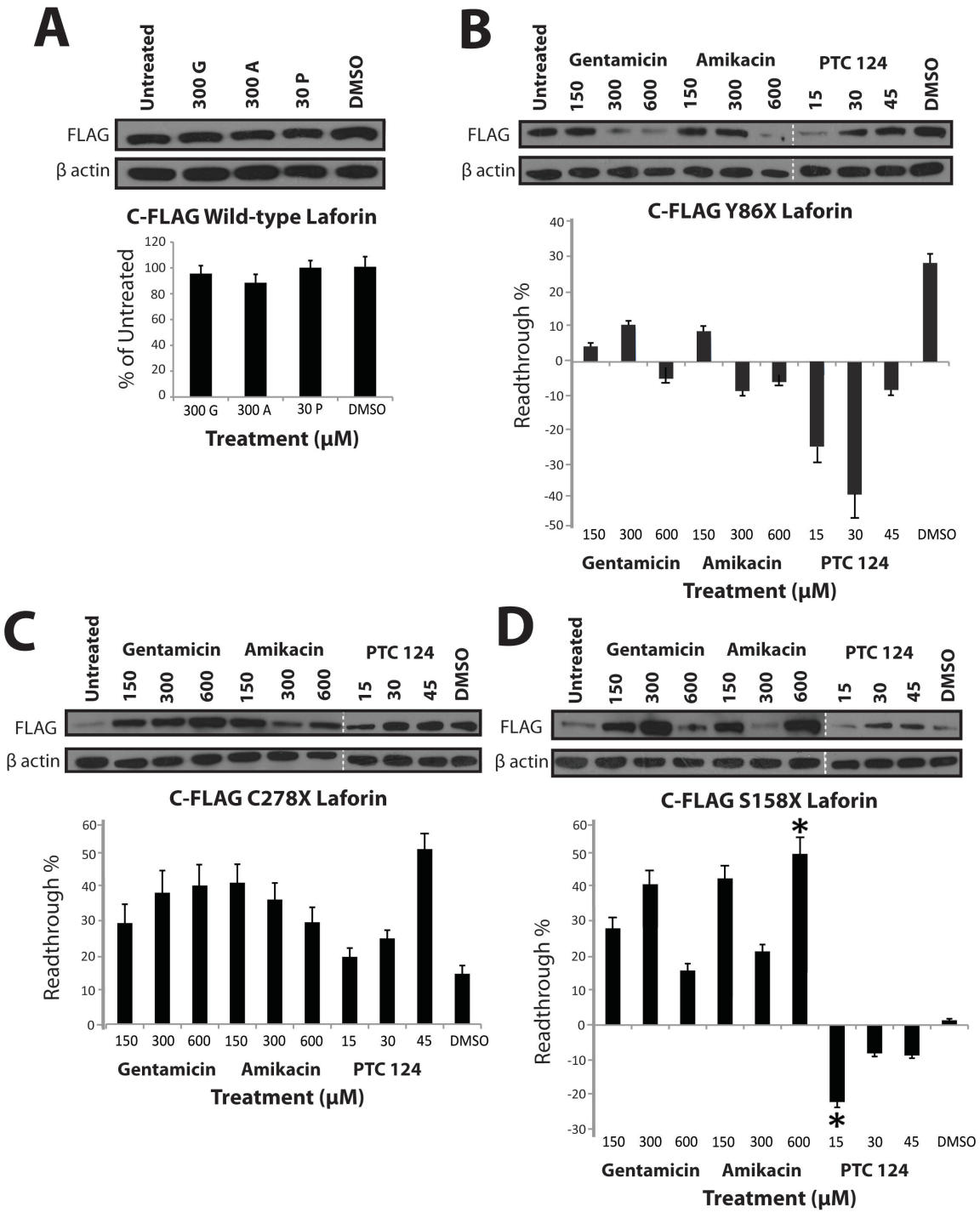
A
Untreated
300 G
300 A
30 P
DMSO
FLAG
β actin
C-FLAG Wild-type Laforin
% of Untreated
300 G
300 A
30 P
DMSO
Treatment (μM)
B
Untreated
Gentamicin
Amikacin
PTC 124
DMSO
FLAG
β actin
C-FLAG Y86X Laforin
Readthrough %
Gentamicin
Amikacin
PTC 124
Treatment (μM)
C
C-FLAG C278X Laforin
Readthrough %
Gentamicin
Amikacin
PTC 124
Treatment (μM)
D
C-FLAG S158X Laforin
Readthrough %
Gentamicin
Amikacin
PTC 124
Treatment (μM)

Figure 5.2. Response of C-terminally FLAG-tagged laforin nonsense mutants to readthrough-promoting compounds. A. Impact of readthrough-promoting compounds on wild-type laforin protein levels. C-terminally FLAG-tagged wild-type laforin was transiently transfected into HEK293 cells 4 hours prior to incubation of the cells with 300 μM gentamicin (G), 300 μM amikacin (A), 30 μM PTC124 (P), or 0.03% v/v DMSO vehicle for 18 hours. Cell lysates were immunoblotted for FLAG and expression levels quantitated using densitometric western blot analysis. Data are presented as percent of untreated laforin ± SEM (n=3). The depicted image is a representation. As a loading control, β actin was detected in all samples. **B-D.** Response of laforin nonsense mutants to readthrough-promoting compounds. C-terminally FLAG-tagged Y86X laforin **(B)**, C278X laforin **(C)**, and S158X laforin **(D)** were transiently transfected into HEK293 cells 4 hours prior to treatment with 150-600 μM gentamicin (G) or amikacin (A), 15-45 μM PTC124 (P), or 0.06% v/v DMSO vehicle for 18 hours. Cell lysates were immunoblotted for FLAG and readthrough levels quantitated using densitometric western blot analysis. Data are presented as the percent change in full-length laforin in treated samples compared to untreated (readthrough percent) ± SEM. Experiments were repeated at least three times and the depicted images are a representation. The white dotted line indicates where an image is a composite of portions of the same exposure. Statistical significance (indicated by an asterisk) was set at $p < 0.05$.

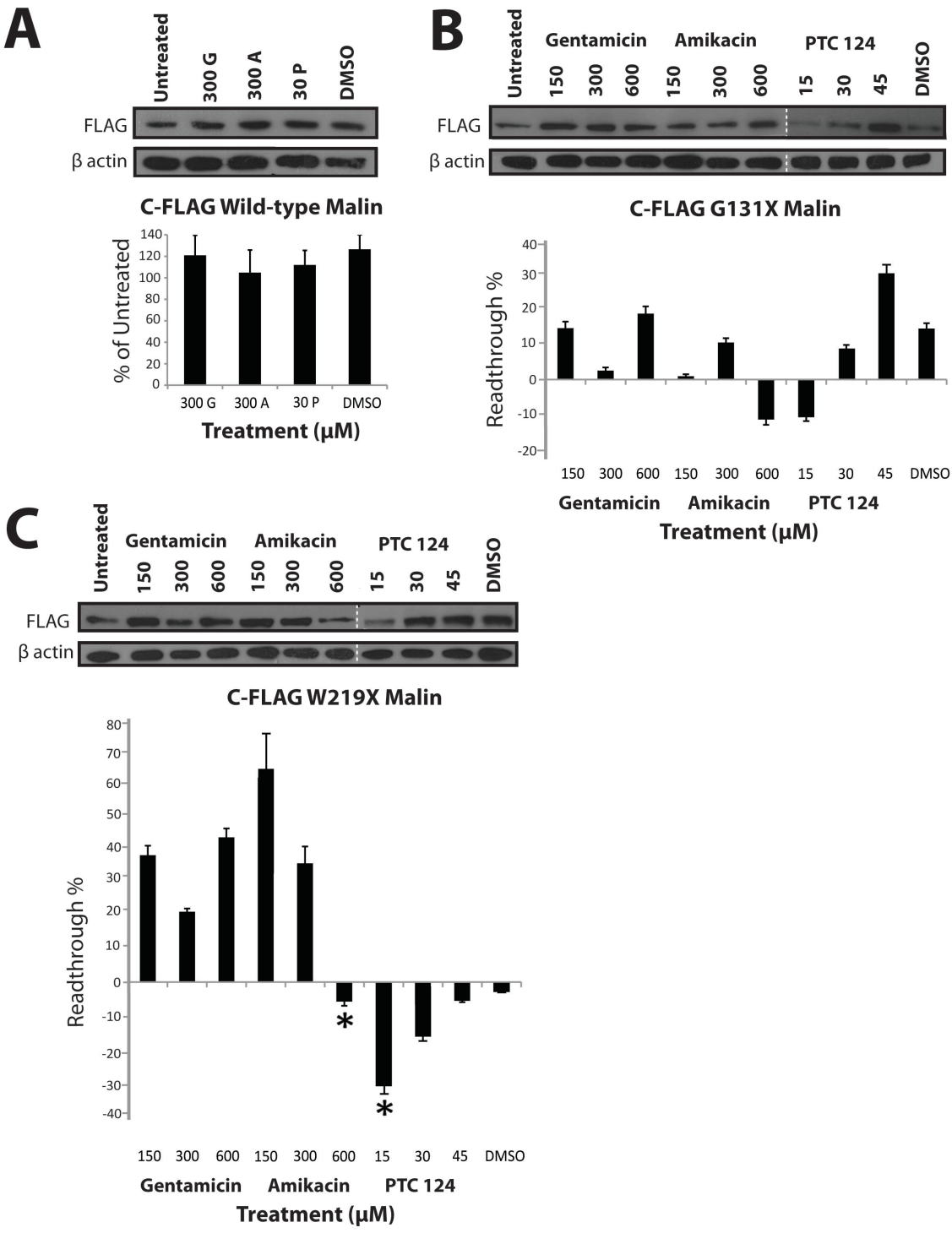
A
Untreated
300 G
300 A
30 P
DMSO
FLAG
β actin
C-FLAG Wild-type Malin
% of Untreated
300 G
300 A
30 P
DMSO
Treatment (μM)
B
Untreated
Gentamicin
Amikacin
PTC 124
150
300
600
150
300
600
15
30
45
DMSO
FLAG
β actin
C-FLAG G131X Malin
Readthrough %
Gentamicin
Amikacin
PTC 124
Treatment (μM)
C
Untreated
Gentamicin
Amikacin
PTC 124
FLAG
β actin
C-FLAG W219X Malin
Readthrough %
Gentamicin
Amikacin
PTC 124
Treatment (μM)

Figure 5.3. Response of C-terminally FLAG-tagged malin nonsense mutants to readthrough-promoting compounds. A. Impact of readthrough-promoting compounds on wild-type malin protein levels**.** C-terminally FLAG-tagged wild-type malin was transiently transfected into HEK293 cells 4 hours prior to incubation of the cells with 300 μM gentamicin (G), 300 μM amikacin (A), 30 μM PTC124 (P), or 0.03% v/v DMSO vehicle for 18 hours. Cell lysates were immunoblotted for FLAG and expression levels quantitated using densitometric western blot analysis. Data are presented as percent of untreated malin ± SEM (n=3). The depicted image is a representation. **B-C.** Response of malin nonsense mutants to readthrough-promoting compounds**.** C-terminally FLAG-tagged G131X malin **(B)** or W129X malin **(C)** were transiently transfected into HEK293 cells 4 hours prior to treatment with 150-600 μM gentamicin (G) or amikacin (A), 15-45 μM PTC124 (P), or 0.06% v/v DMSO vehicle for 18 hours. Cell lysates were immunoblotted for FLAG and readthrough levels quantitated using densitometric western blot analysis. Data are presented as the percent change in full-length malin in treated samples compared to untreated (readthrough percent) ± SEM. Experiments were repeated at least three times and the depicted images are a representation. The white dotted line indicates where an image is a composite of portions of the same exposure. Statistical significance (indicated by an asterisk) was set at $p < 0.05$.

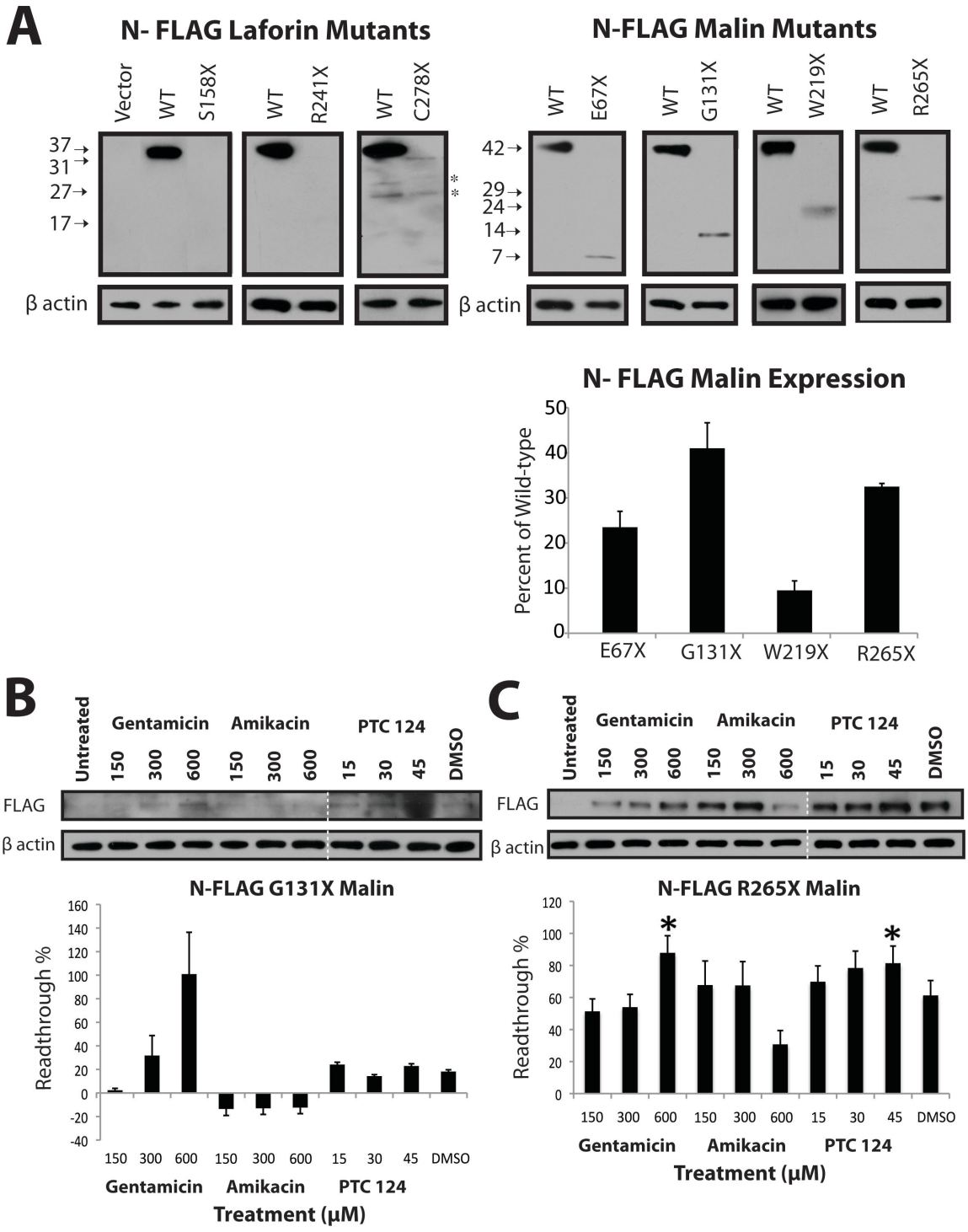
A
N- FLAG Laforin Mutants
Vector
WT
S158X
WT
R241X
WT
C278X
37
31
27
17
β actin
N-FLAG Malin Mutants
WT
E67X
WT
G131X
WT
W219X
WT
R265X
42
29
24
14
7
β actin
N- FLAG Malin Expression
Percent of Wild-type
50
40
30
20
10
0
E67X
G131X
W219X
R265X
B
Untreated
Gentamicin
Amikacin
PTC 124
150
300
600
150
300
600
15
30
45
DMSO
FLAG
β actin
N-FLAG G131X Malin
Readthrough %
160
140
120
100
80
60
40
20
0
-20
-40
150 300 600 150 300 600 15 30 45 DMSO
Gentamicin
Amikacin
PTC 124
Treatment (μM)
C
Untreated
Gentamicin
Amikacin
PTC 124
150
300
600
150
300
600
15
30
45
DMSO
FLAG
β actin
N-FLAG R265X Malin
Readthrough %
120
100
80
60
40
20
0
*
*
150 300 600 150 300 600 15 30 45 DMSO
Gentamicin
Amikacin
PTC 124
Treatment (μM)

Figure 5.4. Response of N-terminally FLAG-tagged laforin and malin nonsense mutants to readthrough-promoting compounds. A. Expression test of N-terminally FLAG-tagged laforin and malin nonsense mutants**.** Mutants were expressed for 24 hours in HEK293 cells and cell lysates immunoprecipitated with α-FLAG agarose. The depicted images are a representation and asterisks indicate nonspecific bands. Expression levels were quantitated by densitometric western blot analysis and presented as percent of wild-type ± SEM (n=3). Y86X was not included in the N-FLAG set of mutants. **B-C.** Response of malin nonsense mutants to readthrough-promoting compounds**.** N-terminally FLAG-tagged G131X malin **(B)** or W129X malin **(C)** were transiently transfected into HEK293 cells 4 hours prior to treatment with 150-600 μM gentamicin (G) or amikacin (A), 15-45 μM PTC124 (P), or 0.06% v/v DMSO vehicle for 18 hours. Cell lysates were immunoprecipitated with α-FLAG agarose and readthrough levels quantitated using densitometric western blot analysis. Data are presented as the percent change in full-length malin in treated samples compared to untreated (readthrough percent) ± SEM. Experiments were repeated at least three times and the depicted images are a representation. The white dotted line indicates where an image is composed of portions of the same exposure. Statistical significance (indicated by an asterisk) was set at $p < 0.05$.

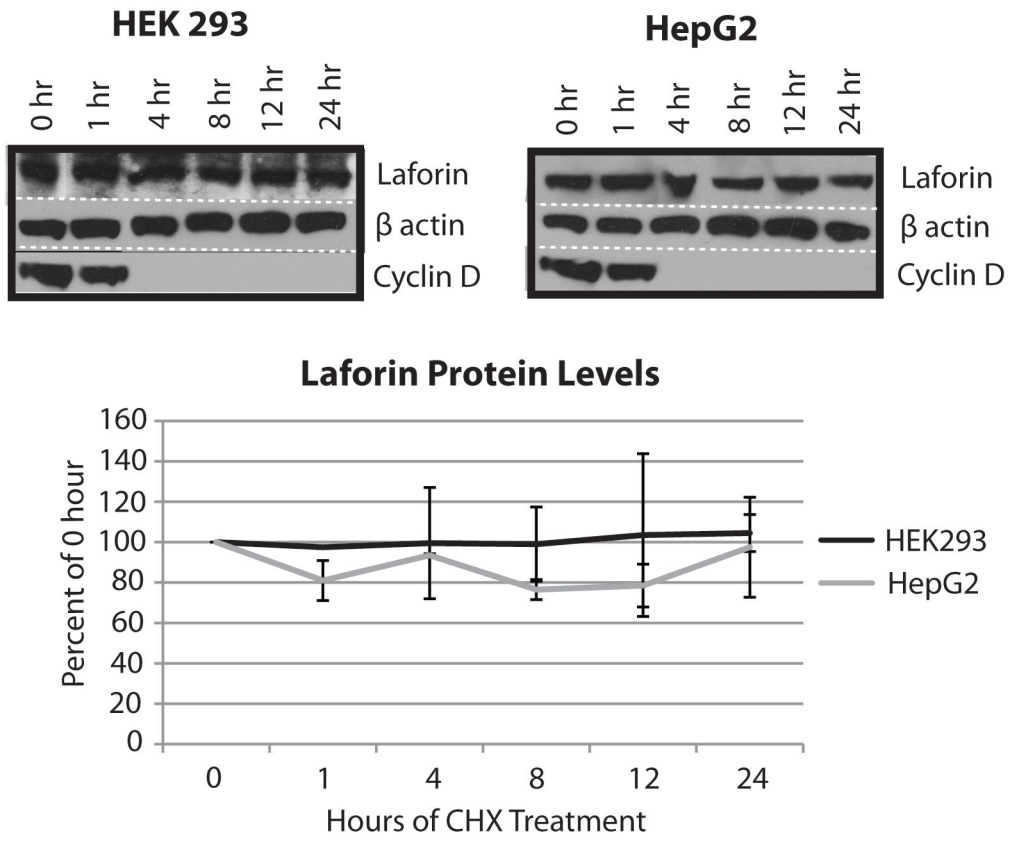

Figure 5.5. Determination of endogenous laforin half-life. HEK293 and HepG2 cells were treated with 200 μg/mL of cycloheximide (CHX) for 0-24 hours. Cell lysates were then immunoblotted using Neuromab α-laforin N84/37.1 antibody and laforin levels quantitated using densitometric western blot analysis. Data are presented as the percent change in laforin levels from 0 hours of treatment ± SEM (n=3). As a loading control, β actin was detected in all samples, while cyclin D1 was detected as an experimental control.

Mutant	Sequence	Tag	Expressed?	Mutant Expression (% of WT)	Basal Readthrough (% of WT)	Maximum Gentamicin Response (% Readthrough)	Maximum Amikacin Response (% Readthrough)	Maximum PTC124 Response (% Readthrough)
Y86X Laforin	UAG	C-FLAG	Yes	N/A	20.6 ± 2.7	9.8 ± 1.3	7.2 ± 0.9	-35.1 ± 1.1
S158X Laforin	UGA	C-FLAG	Yes	N/A	43.6 ± 4.3	41.6 ± 6.0	50.7 ± 5.0*	-7.0 ± 0.4
		N-FLAG	No	-	-	-	-	-
R241X Laforin	UGA	C-FLAG	No	N/A	-	-	-	-
		N-FLAG	No	-	-	-	-	-
C278X Laforin	UGA	C-FLAG	Yes	N/A	57.0 ± 11.2	40.5 ± 8.4	40.9 ± 7.7	35.1 ± 6.5
		N-FLAG	Yes	4.5 ± 2.1	-	-	-	-
E67X Malin	UAG	C-FLAG	No	N/A	-	-	-	-
		N-FLAG	Yes	23.5 ± 3.5	-	-	-	-
G131X Malin	UGA	C-FLAG	Yes	N/A	100.3 ± 18.8	17.4± 2.2	10.6 ± 1.1	15.3 ± 2.4
		N-FLAG	Yes	41.0 ± 5.6	-	100.9 ± 35.5	-12.4 ± 5.1	5.9 ± 2.0
W219X Malin	UAG	C-FLAG	Yes	N/A	74.6 ± 25.8	42.2 ± 4.0	64.2 ± 12.0	-3.2 ± 0.4
		N-FLAG	Yes	9.5 ± 2.1	-	-	-	-
R265X Malin	UGA	C-FLAG	No	N/A	-	-	-	-
		N-FLAG	Yes	32.5 ± 0.7	-	87.8 ± 10.7*	67.7 ± 15.0	20.0 ± 10.7*

Table 5.1. Summary of laforin and malin nonsense mutant expression and readthrough results. For each laforin or malin nonsense mutant, the sequence of the nonsense mutation is indicated. For the N-terminally FLAG-tagged (N-FLAG) and C-terminally FLAG-tagged (C-FLAG) construct of each mutant, the expression level, basal readthrough level, and highest level of readthrough for any concentration of gentamicin, amikacin, and PTC124 is indicated. The maximum PTC124 response is the final value after subtraction of the readthrough observed with DMSO vehicle. N/A indicates where a value could not be measured, while a dash indicates where a value could not be determined due to the lack of observable data.

CHAPTER 6: HYDROGEN-DEUTERIUM EXCHANGE MASS SPECTROMETRY PROVIDES INSIGHT INTO THE IMPACT OF LAFORA DISEASE MUTATIONS ON THE STRUCTURE AND MECHANISM OF LAFORIN

Introduction.

There are currently no therapeutic options for LD outside of palliative therapeutics designed to limit the frequency and severity of epileptic episodes (*105, 107*). Understanding the underlying biochemistry resulting from a specific LD point mutation in the development of the disease has been a major roadblock in devising strategies for the treatment of LD. While nonsense mutations in laforin may respond to readthrough-promoting compounds as explored in the previous chapter, future work is required using patient fibroblasts to assess the efficacy of these compounds for patient treatment. In regards to many of the point mutations in laforin, previous work has demonstrated loss of substrate binding and phosphatase activity (*52*, *141*). However, these studies did not determine the structural or mechanistic alterations in laforin responsible for the loss of function. Thus, we explored the possible alteration of the structure and binding behavior of laforin as a result of several LD-causing point mutations. Insights into the disrupted structure and mechanism of laforin will likely aid in the development of future therapies that stabilize the protein.

To date, there have been no structural or mechanistic studies of laforin, and the mechanism by which laforin interacts with and acts upon glucose polymers remains unknown. However, some insight into the possible structure and mechanism of laforin is provided by the recent crystal structure of another glucan phosphatase from *Arabidopsis* called Starch Excess 4 (SEX4) whose substrate is the plant carbohydrate starch (*55, 160*). Disruption of *SEX4* leads to starch accumulation in plants reminiscent of LD in humans at the cellular level (*55, 112*). While laforin consists of only a CBM and DSP domain, SEX4 possesses these domains in addition to a chloroplast targeting peptide (cTP) and a C-terminal domain (CT) required for the interaction of the CBM and DSP (*112*, *160*). While SEX4 and laforin share similar domains, their DSP and CBM domains are in opposite orientations (*54*). Thus, these

two proteins likely utilize different mechanisms to dephosphorylate thier substrates. In addition to information about the structure of glucan phosphatases provided by the crystal structure of SEX4, a technique known as hydrogen-deuterium exchange mass spectrometry (DXMS) has been used to analyze the structural dynamics (i.e., how the domains of the protein behave during substrate binding) and thus the mechanism of SEX4 (*77*).

DXMS measures the exchange of the backbone amide hydrogens of a protein with deuterium atoms in a D_2O-based aqueous environment. There are several groups of potentially exchangeable hydrogens in a protein, such as those found on the functional groups of amino acid side chains (-OH, -SH, NH_2, -COOH) which exchange too rapidly to be measured and do not retain deuterons during processing. Hydrogens attached directly to the α-carbon and side chains are covalent and do not exchange. However, the single amide hydrogen of an amino acid residue can undergo exchange at a measurable rate from hundreds of milliseconds to years under physiological conditions (Figure 6.1A), thus increasing the mass of the amino acid by one mass unit (*65, 90*). This increase in mass can then be detected using mass spectrometry.

The exchange of free amide hydrogens is governed by pH, temperature, and exposure to solvent (*142*). In a folded protein, free amide hydrogens present in unstructured regions and thus not involved in hydrogen bonding exhibit an exchange rate on the order of seconds, while those buried within the hydrophobic protein interior or involved in hydrogen bonding networks contributing to secondary structure will take days to months to fully exchange (*44*). Amide hydrogen exchange rates can thus provide information on the conformation of a folded protein. When DXMS is then performed with the endogenous substrate of a protein present, the binding dynamics of a protein can be assessed, which may indicate either structural changes occurring because of substrate binding or areas of the protein being protected from deuteration due to steric hindrance by the substrate (*23, 77*).

DXMS has been used extensively to study local and global protein dynamics as well as the site of protein-substrate interaction (*23, 43, 66, 168*). Use of DXMS allows the study of a protein's structure and substrate interactions (*12, 77*) in a more natural environment than that provided by the conditions necessary for x-ray crystallography-based structural studies, with which protein binding dynamics cannot be studied. In addition, DXMS allows the use of the endogenous substrate of a protein. Depending on the fragmentation pattern of a protein, DXMS provides a medium resolution of 5-10 amino acids. However, the technique can accommodate proteins of all sizes as well as complex interacting partners, unlike x-ray crystallography and NMR (*90, 155*). Following exposure of a protein to deuterated solvent, the pH of the solution is lowered to 2.5 and the temperature to 0°C, the pH and temperature minimum of acid (H^+) and base (OH^-) catalyzed hydrogen exchange (*9, 34, 155*). The protein is then fragmented by pepsin proteolysis and subjected to LC-MS/MS to detect resulting mass changes in peptides as a result of deuterium uptake (*90*) (Figure 6.1B).

The DXMS work involving SEX4 revealed that in addition to CBM interaction with the glucan substrate, specific regions in the DSP of SEX4 also interacted with the substrate (*77, 160*). This work provided the first evidence that the DSP domain of a glucan phosphatase contains residues that interact with glucans. These findings were confirmed upon the determination of the structure of a glucan phosphatase bound to glucans (*104*). The glucan-bound structure identified an aromatic channel in the DSP active site that was necessary for binding and dephosphorylating starch. Aromatic regions within carbohydrate binding modules are a common theme, as these domains allow a protein to bind a carbohydrate and then another domain to enzymatically modify the carbohydrate (*18, 35, 98*) An example of this domain architecture is seen in α-amylase (*59*). α-amylase contains an N-terminal hydrolase domain that cleaves glycosidic bonds and a C-terminal CBM. The CBM binds carbohydrates and the hydrolase domain then cleaves nearby glycosidic bonds. These aromatic residues allow carbohydrate binding proteins to engage their substrates and then release from the substrates. In fact, the K_d of most carbohydrate

binding proteins is in the millimolar range (*59*). This "poor" binding affinity is key to enzymatic activity because proteins that bind more tightly have decreased efficiency in cleaving carbohydrates. However, it is rare to observe an aromatic channel necessary for glucan binding within the active site of the enzymatic domain of a glucan binding enzyme, as is seen with glucan phosphatases (*104*).

The regions of the SEX4 DSP interacting with glucans following DXMS include the recognition domain, variable loop, the CX_5R motif (also called the PTP loop), and the D loop, all sequence motifs specific to DSPs (*2*). The recognition domain in DSPs contributes to the depth of the active site as well as substrate binding (*84, 177*). The variable loop also contributes to active site depth while helping to orient the CX_5R motif Arg residue in coordinating two of the phosphoryl oxygen atoms as required for proper phosphate removal, thus demonstrating close proximity to the substrate (*2, 177*). The D loop contains an Asp residue that functions as a general acid-base catalyst to allow the catalytic Cys residue in the CX_5R motif of the PTP loop to perform nucleophilic attack of the phosphorus atom of the phosphate moiety and dephosphorylate the substrate (*2*). This Asp residue makes direct contact with the substrate (*177*). While this region did not interact with glucans in SEX4 (*77*), the R motif is another sequence motif characteristic of DSPs that contains a highly conserved Arg residue (*2*). The above regions are all associated with the active site of SEX4 (*160*) (Figure 6.2). Unpublished work from our lab demonstrates that SEX4 possesses an aromatic platform within its DSP that is integral for binding and dephosphorylating starch. This work therefore suggests that glucan phosphatases are similar to other carbohydrate binding enzymes and likely undergo a very dynamic on/off interaction with carbohydrates. These results suggest that glucan phosphatases possess a K_d in the millimolar range to allow the enzyme to "scan" for phosphate within glycogen or starch.

Although crystallography and DXMS studies of SEX4 have provided insight into both the structure of a glucan phosphatase and a mechanism for substrate interaction, laforin has distinct architectural differences and unique binding dynamics from SEX4. The DSP and CBM domains of SEX4 and laforin lie in completely opposite orientations (Figure 6.3A and B) due to the convergent

evolution of these proteins (*56*), and laforin contains a predicted flexible linker between the DSP and CBM. Laforin also lacks structural elements such as the C-terminal domain of SEX4 critical for the folding of SEX4 (Figure 6.3A and B), as well as conserved residues in SEX4 necessary for CBM and DSP domain interaction (*160*). Finally, laforin possesses higher *in vitro* glucan phosphatase activity than SEX4 (*55*). As a crystal structure of laforin is not available, we utilized DXMS to determine the structural elements and binding dynamics of wild-type laforin. In addition, as DXMS has been used to study the conformational changes of proteins mutated in disease (*26, 36*), we explored the possible disruption of substrate binding and activity resulting from LD-causing point mutations within laforin. To facilitate these DXMS studies, we optimized a method to purify large quantities of nearly homogenous recombinant laforin.

Results.

The glycosyl hydrolase motifs of laforin and choice of Lafora disease mutants to study using DXMS.

We performed bioinformatics on the glucan phosphatases using multiple iterations of PSI-BLASTp and uncovered two regions within the DSP domains of glucan phosphatases that share remote homology to glycosyl hydrolase domains. Glycosyl hydrolases (GH) are enzymes that bind to and cleave glycosidic bonds, and are grouped into 115 families based on protein sequence and catalytic mechanism (*25, 69, 70*). GHs are more commonly found in bacterial, fungal, and plant genomes (*18, 25, 82*). The regions of the glucan phosphatase DSP domain that resemble GH domains are within the variable loop and R motif. Therefore, we investigated these regions further. The variable loop motif resembles a glycosyl hydrolase family 10 (GH10)-like active site sequence and the R motif resembles a glycosyl hydrolase family 1 (GH1)-like active site sequence.

Next we analyzed laforin orthologs from vertebrates to protists and found that these GH-like motifs are highly conserved from humans to red algae (Figure 6.3C), although human and red algal laforin share only 25% overall identity (*55*).

After establishing that these sequences are highly conserved in glucan phosphatases, Dr. Gentry tested the glucan phosphatases for glycosyl hydrolase activity against glucan substrates by quantifying glucose release and did not detect glycosyl hydrolase activity (data not shown). This result is not surprising given the remote homology of the SEX4 and laforin DSP domain with glycosyl hydrolases and the lack of conservation of the GH active site catalytic residues. However, it is surprising to identify a glucan binding motif within the DSP domain that is conserved from red algae to plants to humans.

Laforin and SEX4 are merely analogous in function given their different domain arrangement, possibly sharing function through convergent evolution (*56*). The fact that laforin and SEX4 share conservation of GH active site sequences in their DSP domains despite their evolutionary distance provides further evidence for an integral role of the GH-like regions in glucan interaction. The variable loop and R motif are highly conserved among proteinaceous DSPs (*2*) but feature little sequence homology between non-proteinaceous DSPs (*2, 160*). However, the variable loop and R motif are known to be closely associated with the active site in both proteinaceous and non-proteinaceous DSPs (*2, 177*). The variable loop and R motif are also adjacent to the active site in the crystal structure of SEX4 (*160*), indicating the importance of these regions in glucan phosphatase function. Interestingly, while the variable loop of proteinaceous DSPs such as VHR consists of a loop (*177*), the variable loop of SEX4 possesses α-helical structure (*160*) (Figure 6.3D) that may prove a general feature of glucan phosphatases. Cumulatively, our data indicate that the GH-like regions in the variable loop and R motif of laforin likely play an integral role in substrate presentation to the active site.

Interestingly, there are a number of LD missense mutations in the R motif of laforin. The discovery of the GH1-like region in the R motif of laforin prompted us to study LD-causing missense point mutants found in the R motif in order to determine the importance of these residues in glucan binding. We chose the Y294N and P301L disease mutations found within the R motif for study using *in vitro* activity and binding assays and DXMS. To validate our experimental approach, we also analyzed

well-characterized disease-causing mutations outside of the R motif: W32G and G240S. The W32G mutation in the CBM has been demonstrated to dramatically decrease glucan binding and activity. We included the G240S DSP mutation due to reports that G240S laforin retains phosphatase activity and glucan binding (*141*). The G240S mutation is a unique LD mutation in that laforin maintains both functionalities, but is no longer able to interact with protein targeting to glycogen (PTG), a protein involved in glycogen metabolism (*141*). It is thought that the loss of interaction between PTG and laforin leads to LD in these patients. In addition to W32G and G240S, we mutated the catalytic cysteine of laforin to serine in order to generate a catalytically inactive C266S mutant (*55*) as a control for biochemical assays and comparison for DXMS.

Biochemical characterization of wild-type laforin and laforin mutants.

We first assayed the general phosphatase activity of wild-type laforin and each laforin mutant utilizing the exogenous substrate *para*-nitrophenylphosphate (*p*NPP), which due to its small size can diffuse into the active site and thus measures only the functionality of the DSP (see Chapter 3, Figure 3.1A). *p*NPP assays have been used to define phosphatase activity in a variety of proteinaceous and non-proteinaceous phosphatases (*138, 173*). We also determined the specific activity of the same mutant laforin proteins against phosphorylated glucans using the malachite green assay with amylopectin as the substrate (see Chapter 3, Figure 3.1B). This modified malachite green assay requires binding of the glucan by the CBM to facilitate glucan dephosphorylation, thus measuring both glucan binding and the functionality of the CBM and DSP together. This assay has demonstrated loss of glucan phosphatase activity in both SEX4 and laforin when residues in their CBMs critical for substrate binding are mutated (*55*).

The *p*NPP and glucan phosphatase activity of wild-type laforin and the inactive C266S mutant (Figure 6.4A and B, respectively) are in agreement with previously determined values (*55, 138*). As previously reported, the Y294N and P301L mutations almost completely impaired *p*NPP activity while the G240S mutant still exhibited substantial activity (*46, 141*) (Figure 6.4A). As we predicted due to the

location of the W32G mutation in the CBM, we found that the W32G mutant also retained some *p*NPP activity (Figure 6.4A). These results indicate that the Y294N and P301L mutations may be disrupting DSP domain structure, thus generating an inactive enzyme.

Each of the laforin mutants displayed decreased glucan phosphatase activity (Figure 6.4B), although not entirely as predicted based on our previous understanding. Trp32 is a highly conserved CBM20 residue proposed to be crucial for binding (*166*) and disrupted glucan binding of the W32G mutation has been reported (*141*). The impaired W32G glucan phosphatase activity that we observed (Figure 6.4B) is in agreement with this previous work, and demonstrates the importance of CBM binding for glucan phosphatase activity. The G240S mutant has been reported to not disrupt glucan binding (*141*), and we found that this mutant exhibited 60% of wild-type glucan phosphatase activity (Figure 6.4B). The Y294N and P301L mutations are both reported to disrupt glucan binding through an unexplained mechanism (*141*), and we found that these mutants both exhibited decreased glucan phosphatase activity (Figure 6.4B). While we are able to explain some of these results with our current understanding of laforin, other aspects remain an enigma. Why do Y294N and P301L have no pNPP activity yet still possess reasonable glucan phosphatase activity? And how does the W32G mutant still dephosphorylate glucans when others have reported that this mutant does not bind glucans?

As the Y294N and P301L mutants did not exhibit *p*NPP activity, it is possible that glucan binding by the CBM is aiding in the binding of the DSP to glucan to allow limited glucan phosphatase activity. The glucan phosphatase activity of Y294N is similar to G240S while the activity of P301L is similar to W32G, indicating that Pro301 may play a more critical role in glucan phosphatase activity than Tyr294. Altogether, the agreement of our *p*NPP and glucan phosphatase assay results with previously reported results lends support to the above conclusions.

To specifically examine the relative binding affinity for glucans of wild-type laforin and the laforin mutants, we utilized two assays. First, we assessed if these proteins could bind the glucan amylose using an amylose resin pull-down assay.

Proteins with the ability to bind amylose will pellet with the amylose, while those unable to bind will remain in the supernatant. The W32G mutation abolished amylose binding (Figure 6.4C), indicating that the CBM is essential for glucan binding. The G240S mutation, which does not impact glucan binding, led to similar binding characteristics as wild-type laforin (Figure 6.4C). However, the Y294N and P301L mutations residing in the GH region of the R motif did not impact amylose binding (Figure 6.4C). These results were surprising, as previous work reported that Y294N and P301L are unable to bind glucans (*46*). With our amylose pull-down assay, wild-type laforin is found exclusively in the amylose pellet, while previous glycogen pull-down assays show that wild-type laforin is also found in the supernatant. This discrepancy may be due to the fact that glycogen is water soluble while amylose is water insoluble. Amylose therefore pellets more efficiently, demonstrating that our assay is superior for assessing glucan binding.

We examined the glucan binding affinity of these proteins further by assessing the degree of migration of each protein through a native glycogen gel. Proteins with the ability to interact with glycogen will exhibit impaired migration through a gel containing glycogen compared to a gel without glycogen present. Consistent with the results from the amylose pull-down assay, the W32G mutant migrated to the same degree in both a glycogen-free gel and a gel containing glycogen (Figure 6.4D), indicating a loss of glucan binding. The catalytically inactive C266S mutant, with a functional CBM, exhibits the same degree of impaired migration through a glycogen gel as wild-type laforin (Figure 6.4D). This result indicates that C266S laforin possesses the same binding affinity for glucans as wild-type laforin.

Surprisingly, the Y294N and P301L mutants displayed severely impaired migration through a glycogen gel compared to wild-type laforin (Figure 6.4D), indicating a much stronger interaction with glycogen than seen with wild-type laforin. The reduced glucan phosphatase activity of the Y294N and P301L mutants indicates that the Tyr294 and Pro301 residues are crucial for glucan phosphatase activity. However, while it was expected that these mutations would abolish glucan

binding, it appears that they actually cause a strengthened interaction with glycogen and thus may impair activity. These results were further explored using DXMS.

Optimization of laforin digestion for DXMS.

Before examining the binding dynamics of the Y294N and P301L mutants in the GH1-like domain of laforin, we utilized DXMS to assess wild-type laforin structural features and binding dynamics with various glucans. For this work, we tested the physiological substrate of laforin, glycogen, as well as amylopectin, as this glucan resembles LBs in regards to phosphate content and branching pattern (*54*) (Figure 1.2C). As glycogen and amylopectin are heterogeneous polymers, we also utilized β-cyclodextrin, a homogeneous, seven-ring, cyclic oligosaccharide in order to utilize a well-defined glucan substrate.

The initial wild-type laforin DXMS studies required purification of large yields (~20 mg) of monomeric wild-type laforin to >95% homogeneity (Figure 6.5A). In order to obtain 20-30 mg of laforin from a liter culture of *E. coli*, we found that the purification of laforin required the presence of glycerol and a detergent in the protein buffer (see Chapter 2 for detailed methods on laforin purification). Following purification of laforin from soluble bacterial extracts, we utilized fast protein liquid chromatography (FPLC) using a size-exclusion column to obtain >95% pure laforin monomer (Figure 6.5B).

The ability to obtain detailed exchange behavior of an entire protein using DXMS is largely determined by the protein sequence coverage and the density of the peptide fragments produced following proteolysis. DXMS analysis of laforin therefore required optimization of the digestion conditions of laforin by pepsin to yield full coverage of the protein (see Chapter 2 for detailed methods of the optimization of laforin digestion). The conditions we identified providing the greatest coverage of laforin gave 134 high-quality peptides with 100% laforin sequence coverage. We analyzed 27 laforin fragments of the optimal size in the subsequent DXMS experiments. These 27 peptides gave complete distribution

across laforin in order to provide suitable experimental resolution and full protein coverage for DXMS experiments (Figure 6.5C, solid black lines).

DXMS experiments and structural insights of wild-type laforin.

Prior to substrate binding experiments, wild-type laforin without substrate (APO) was analyzed using DXMS in order to determine regions of the protein that exhibit secondary structure and/or are buried and thus protected from exchange. The exchange rate of peptides across laforin following 10-10,000 s of D_2O exposure was studied in order to distinguish exchange of free amide hydrogens resulting from solvent exposure of unstructured regions, which occurs on the order of seconds, from regions of slower exchange that indicate secondary structure. We monitored each peptide following laforin incubation in D_2O buffer. We obtained a mass spectra for each time point that shifted to a higher m/z ratio than seen with undeuterated peptide when exchange occurred (Figure 6.6). The average centroid values for each time point spectra were then used to determine exchange over time for each peptide across the entire laforin protein. Combination of this information with the predicted secondary structure of laforin (Figure 6.7A) was then used to confirm the presence of secondary structural elements in laforin.

Both the CBM and DSP of APO wild-type laforin exhibited regions of high exchange (≥50% deuteration after 300 s) between areas of predicted secondary structure (Figure 6.7A). This high degree of exchange between predicted secondary structure at early time points indicates that these regions are highly solvent accessible in addition to being free from hydrogen bonding, supporting structural predictions.

The CBM domains of the members of the CBM20 family that laforin belongs to are highly heterogeneous at the amino acid level and lack invariant residues, but contain moderately well-conserved aromatic residues that coordinate ligand binding (*99*). Within the CBM, three of the aromatic residues predicted to be integral for glucan binding (*55, 166*) (Trp32, Trp60, and Trp99; indicated by asterisks in Figure 6.7A) were found within unstructured regions that were highly solvent

accessible (peptides 21-52, 60-65, and 98-111, respectively). Similarly, residues in the CBM of SEX4 involved in glucan binding are also found in highly solvent accessible regions (*77*) (Figure 6.7B). These results indicate that these three tryptophan residues in the CBM of laforin are in solvent-exposed loops that likely prime these residues for interaction with substrate.

Areas within the DSP of laforin featuring predicted secondary structure exhibited low exchange, supporting the involvement of the amide hydrogens of the residues in these areas in hydrogen bonding as part of secondary structure. Meanwhile, areas between predicted structure exhibited high exchange at early time points and thus a lack of hydrogen bonding as well as solvent accessibility (Figure 6.7A). The DSP of laforin exhibited less deuteration overall than what is seen in the DSP of SEX4 (*77*) (Figure 6.7B). However, regions predicted to interact with substrate, such as the recognition domain (residues 139-152), the variable loop (residues 193-227), the D loop (residues 231-240), and the PTP loop (residues 265-272) of laforin are in mostly unstructured regions that are highly solvent accessible (Figure 6.7A). The R motif (residues 299-313) of laforin is highly solvent accessible (Figure 6.7A), while the R motif of SEX4 is highly protected (*77*) (Figure 6.7B). The recognition domain, variable loop, D loop, PTP loop, and R motif are all associated with the active site of SEX4 and other DSPs (*2*, *160*). In addition, these areas are known to be in loops and turns in both the crystal structure of SEX4 and the structures of other phosphatases that reside within the protein tyrosine phosphatase family (*4, 38, 154, 160*). Thus, the solvent-accessibility of these regions in SEX4 (Figure 6.7B), found to be crucial in substrate interaction (*77*), supports a similar role for these solvent-accessible regions in the DSP of laforin. However, the unique solvent accessibility of the R motif of laforin where the GH1-like region resides indicates a role for this region in substrate binding and a different binding mechanism from SEX4.

The substrate preference of laforin.

In order to determine the substrate preference of wild-type laforin prior to assessing binding dynamics, we performed DXMS of laforin with the structurally

distinct glucans amylopectin, glycogen, and β-cyclodextrin. For each peptide across laforin, we determined the maximum changes in average deuteration at any time point between the APO and glucan condition. Based on previous work utilizing DXMS to study substrate binding, we defined a >10% change in deuteration between the APO and glucan conditions as significant (*64, 128*) (Figure 6.8). In comparing the DXMS results of laforin with the three glucans, we sought regions of laforin that exhibited decreases in deuteration. A significant decrease in deuteration in laforin peptides in the presence of glucan most likely results from the protection of the amino acids in the peptide from deuteration due to interaction with the glucan. More importantly, we sought to define which glucan substrate providing the greatest amount of protection, which would indicate the preferred substrate of laforin. This substrate would then be utilized in subsequent experiments with laforin mutants.

Within the CBM of laforin, incubation with glycogen yielded the most significant decreases in deuteration in peptides encompassing three of the four residues proposed to be crucial for substrate binding (Trp32, Trp60, and Trp99) (Figure 6.8B). Only the peptides encompassing the Lys87 and Trp99 residues in the CBM exhibited significant protection from deuteration when amylopectin (Figure 6.8A) or β-cyclodextrin (Figure 6.8C) were utilized. Binding of laforin to glycogen also gave the greatest decreases in deuteration across most regions of the DSP (Figure 6.8B) compared to amylopectin (Figure 6.8A), indicating more extensive interaction with glycogen. Binding to β-cyclodextrin did not lead to any significant changes in deuteration in the DSP (Figure 6.8C), indicating that the DSP of laforin cannot interact with this substrate. Altogether, these results demonstrate that the CBM and DSP of laforin make the greatest degree of contact with glycogen, the physiological substrate of laforin. Thus, glycogen was utilized in all subsequent wild-type and mutant laforin binding experiments. In addition, the binding dynamics of wild-type laforin with glycogen were more closely examined in comparison to the dynamics of SEX4 with its physiological substrate amylopectin, the major component of starch (*77, 91*), in order to assess differences in binding mechanism.

The binding dynamics of laforin with glycogen.

In order to gain insight into the mechanism by which laforin acts upon carbohydrates, we examined the deuteration changes in laforin over time following interaction of laforin with its physiological substrate, glycogen. In the CBM, three peptides demonstrated a >10% change in deuteration for at least one time point following laforin incubation with glycogen (Figure 6.9). These peptides demonstrated only decreases in deuteration, and encompass the conserved Trp32 (Figure 6.9A), Trp60 (Figure 6.9B), and Trp99 (Figure 6.9C) residues, CBM20 residues predicted to be crucial for substrate binding (*55, 166*). These results suggest that these residues are indeed important for laforin interaction with glucan, which protects these peptides from deuteration.

In the DSP, peptides encompassing the recognition domain (Figure 6.10A and B), the variable loop (Figure 6.10C), the D loop (Figure 6.10D and E), the PTP loop (Figure 6.10F), and the R motif (Figure 6.10I and J) all exhibit a >10% change in deuteration for at least one time point following incubation of laforin with glycogen. As with the CBM, only decreases in deuteration were observed when glycogen was present, indicating protection of the indicated regions of the DSP from deuteration due to substrate binding. Interestingly, the peptide encompassing residues 282-289 adjacent to the R motif exhibited the largest decrease in deuteration of the entire laforin protein (Figure 6.10G), indicating that this region may play a role in substrate binding and presentation to the active site. This peptide contains the final residue of the AYLM motif (Figure 6.7A), a conserved sequence motif that is a signature of DSPs (*2*) and has been demonstrated to play a role in interdomain interaction in SEX4 (*160*). This motif lies between predicted secondary structure and is highly solvent accessible (Figure 6.7A), and thus may consist of a solvent-exposed loop that is primed for substrate interaction. To confirm this finding, we examined a peptide encompassing the entire AYLM motif in laforin and found that this peptide also demonstrates a large decrease in deuteration when glycogen is present (Figure 6.10H). Altogether, the protection from deuteration observed in these regions of the DSP indicates a role for these regions in substrate presentation to the active site.

The above changes in deuteration across laforin upon glycogen binding are more easily visualized when the maximum percent deuteration changes at any time point are graphed for each peptide across the protein. Any increases in deuteration when substrate is present then reflect a positive change, while decreases in deuteration are indicated by a negative change. If there are major conformational changes in a protein's structure upon substrate binding, then one observes both positive and negative changes in protein deuteration. We previously demonstrated that SEX4 exhibits only decreases in deuteration when its physiological substrate, amylopectin, is present (*77*) (Figure 6.11A). This result indicates that SEX4 does not undergo major structural rearrangements upon binding, a finding confirmed by the lack of flexibility of SEX4 seen in the crystal structure (*160*). Surprisingly, there are only significant decreases in deuteration in laforin when glycogen is present (Figure 6.11B). Therefore, laforin also undergoes no major structural rearrangement upon binding to its physiological substrate, glycogen. This result is somewhat surprising given the fact that laforin contains a predicted flexible linker between its CBM and DSP. Our results suggest that the linker is not as flexible as predicted and may be integrated into the tertiary structure of the individual domains.

In the CBM of SEX4, all areas containing residues necessary for binding show significant protection upon amylopectin binding (*77*) (Figure 6.11A). Thus, the Trp32, Trp60, and Trp99 residues in the CBM of laforin are likely critical for binding to glycogen. In support of this hypothesis, the W32G mutation abolishes binding of laforin to glucans (Figure 6.4C and D). In the DSP of laforin, regions found previously to be highly solvent-exposed (the recognition domain, variable loop, D loop, PTP loop, AYLM motif, and R motif) (Figure 6.7A) all show decreases in deuteration when glycogen is present (Figure 6.10 and 6.11B). These same regions in the DSP of SEX4, with the exception of the AYLM and R motifs, show significant protection from deuteration when amylopectin is present (*77*) (Figure 6.11A), indicating the importance of these regions in the function of glucan phosphatases as well as other DSPs (*2*).

Wild-type laforin exhibits a lesser degree of protection from deuteration overall with its endogenous substrate (Figure 6.11B) than does SEX4 with its

endogenous substrate (*77*) (Figure 6.11A). In addition, laforin exhibits a lesser degree of protection from deuteration upon binding to amylopectin (Figure 6.8A) than does SEX4 (*77*) (Figure 6.11A). These results indicate that laforin may possess decreased binding affinity and/or increased release from substrate, or faster dynamics, than SEX4. These biophysical properties would result in decreased protection from deuteration by a substrate and may yield an enzyme with a high specific activity. In support of this finding, laforin exhibits a 3 to 10-fold higher rate of glucan dephosphorylation over SEX4 (*55, 138*). The AYLM motif and the R motif of laforin may thus play a role in the faster dynamics of laforin, with the differences in protection from deuteration between laforin and SEX4 indicating a unique mechanism of substrate interaction for the DSP of laforin.

The DXMS method elucidates the pathogenesis of LD mutations in laforin.

To confirm the validity of our experimental design and verify that DXMS was capable of providing data in agreement with established biochemical analyses, the binding of the W32G and G240S LD mutants to glycogen was examined using DXMS. The W32G mutation is reported to abolish glucan binding while the G240S laforin mutant retains this ability (*141*) (Figure 6.4C and D). Therefore, it was expected that the W32G mutant would show minimal changes in deuteration when glycogen is present, while the G240S mutant would exhibit protection from deuteration indicative of glucan binding in a pattern similar to wild-type laforin. For these DXMS experiments, an upgraded DXMS system was utilized that featured an Orbitrap Elite mass spectrometer with enhanced peptide sensitivity in order to better analyze wild-type and mutant laforin. Although wild-type laforin exhibited a lesser degree of overall protection upon glycogen binding following analysis with the Elite (Figure 6.12A) than seen previously using an LCQ Classic mass spectrophotometer (Figure 6.11B), the patterns of protection from deuteration were similar and allowed for comparison with subsequently analyzed mutants.

DXMS analysis of the W32G mutant in the presence of glycogen revealed that both the DSP and the CBM did not interact with glycogen to any substantial degree. There were no significant changes in deuteration when glycogen was present other

than a slightly significant decrease in deuteration of 11% in the peptide encompassing residues 21-52 that may be due to additional undetermined glucan binding residues in this region (Figure 6.12B). Strikingly, the W32G mutant exhibited loss of protection to both the CBM and DSP even though the mutation is within the CBM. These results corroborate the lack of ability of W32G to bind glucans as previously observed (Figure 6.4C and D) and suggest an integrated binding of glucan between the CBM and DSP. These results also provide insight into the pathogenesis of this mutant.

In contrast to W32G, the binding dynamics of the G240S mutant following glycogen binding (Figure 6.12C) were very similar to wild-type (Figure 6.12A). We observed significant protection from deuteration in all regions of laforin confirmed previously (Figure 6.11B). Interestingly, the protection from deuteration seen in the D loop where the G240S mutation resides was not diminished (Figure 6.12C), indicating that the D loop is still able to interact with substrate. Overall, these DXMS results support the biochemical data that the G240S mutation does not dramatically impact substrate binding or activity (Figure 6.4). As the binding of the CBM and DSP of laforin to glycogen are minimally impacted by the G240S mutation, it is likely that another mechanism such as the disruption of protein-protein interactions is responsible for the pathogenesis of this mutant (*141*). The DXMS results pertaining to W32G and G240S are thus supported by our biochemical assays and prior biochemical characterization, indicating the validity of our DXMS experimental approach.

Insights into the binding mechanism of laforin.

Next, we explored the binding dynamics of the inactive C266S laforin mutant in order to assess the deuteration changes of a mutation that we predicted would strengthen binding to glycogen. As the catalytic cysteine residue has been replaced with another small, polar residue in this mutant, we hypothesized that the structure of the active site of laforin would not be disrupted and laforin would retain the ability to bind glycogen. However, because the enzyme would be unable to perform catalysis, we expected that C266S laforin would remain bound to glycogen and

would therefore exhibit increased protection from deuteration across the protein than observed in wild-type laforin upon substrate binding.

Surprisingly, we found that although the CBM of C266S laforin showed significant protection of the Trp32 and Trp99 residues as seen in wild-type laforin when glycogen was present (Figure 6.13A and B), the DSP of the C266S mutant did not exhibit significant protection from deuteration (Figure 6.13B). These results indicate that while the CBM of C266S laforin is able to bind glycogen, the DSP domain has impaired glucan binding ability. It is likely that the C266S mutation alters the structure of the active site and prevents the binding of glycogen by the DSP. However, the C266S mutant is still able to bind glucan to a similar degree as wild-type laforin using glucan-binding assays (Figure 6.4C and D), indicating that the CBM domain alone is sufficient for the interaction of laforin with glucan.

Although contrary to our hypothesis, these results for C266S laforin, together with our findings that the W32G mutation completely abolished glucan binding, provide insight into the overall mechanism of laforin. The W32G mutation in the CBM disrupts glucan binding in both the CBM and DSP domains, while the C266S mutation in the DSP only disrupts binding of the DSP. This suggests that the CBM of laforin is necessary for initial glucan interaction in order bring the DSP into position for binding, indicating synergy between the two domains. The evidence that these domains can interact with glucan independently also supports the presence of a flexible linker between the two domains (Figure 6.7A).

Effects of LD mutations in the GH1-like region on laforin binding dynamics.

We assessed the binding dynamics of the Y294N and P301L LD mutations within the GH1-like region of the R motif of laforin (Figure 6.7A) in order to determine the impact of these mutations on glucan binding. Due to the conservation of the GH1-like region of laforin with the active site of family 1 glycosyl hydrolases, enzymes that bind to and act on carbohydrates, we hypothesized that the GH1-like region in the DSP of laforin is involved in glucan binding. We therefore predicted that the Y294N and P301L mutations would disrupt the binding of the R motif to glycogen.

The Y294N and P301L mutants both exhibited similar patterns of protection from deuteration in the CBM as wild-type laforin when glycogen was present (Figure 6.14), with significant protection of the Trp32, Trp60, and Trp99 residues observed as seen in wild-type laforin (Figure 6.11B). However, the region of the CBM encompassing the Trp99 residue in both Y294N and P301L exhibited a 10-25% greater decrease in deuteration than wild-type laforin (Figure 6.14). Both mutants demonstrated significant protection of the recognition domain, variable loop, and D loop (Figure 6.14B and C) as seen previously in wild-type laforin (Figure 6.11B).

Contrary to our expectations, the Y294N and P301L mutants both exhibited a dramatic 40-55% greater decrease in deuteration in the R motif when glycogen was present compared to wild-type (Figure 6.14). These results indicate that the R motif in Y294N and P301L is interacting much more strongly with glycogen, as the dissociation of this region from substrate to allow deuterium uptake occurs at a slower rate than seen in wild-type. The stronger interaction of the DSP with glycogen may also be prolonging binding by the CBM, leading to the increased protection of the W99 residue observed in both mutants. This result provides additional evidence that the CBM and DSP are working in a synergistic fashion.

We compared the peptides spanning the GH1-like region in the R motif in wild-type laforin that showed a >10% decrease in deuteration with glycogen present (Figure 6.15A) to the peptides in the same region in Y294N (Figure 6.15B) and P301L (Figure 6.15C). This comparison revealed that the peptides encompassing the Y294N and P301L mutations (peptide 290-296 in Figure 6.15B and peptide 295-303 in Figure 6.15C) exhibited the slowest rate of deuterium uptake and thus the strongest association with glycogen. The Y294N and P301L mutants also demonstrated stronger binding to glycogen than wild-type laforin using our glucan-binding assays (Figure 6.4C and D). Altogether, these results indicate that the Tyr294 and Pro301 residues within the GH1-like region of the R motif are optimal for the DSP to interact with glycogen, but in more of a transient manner rather than tight binding. Interestingly, each of these mutants exhibited nearly abolished pNPP activity yet both mutants still exhibit some glucan

phosphatase activity (Figure 6.4B). Proposed mechanisms to explain these results are detailed below.

Homology model of laforin reveals spatial binding dynamics.

To better interpret the deuteration changes in the CBM and DSP of wild-type laforin due to glycogen binding, we determined the spatial orientation of the important regions in each of the domains and mapped the corresponding changes in deuteration onto them. As no crystal structure of laforin or a laforin-like protein is yet available, we generated a homology model of the CBM (residues 1-112) and DSP (residues 152-331) of laforin using the best available structures for each domain. First, we performed BLASTp searches to identify the proteins that were most similar to the laforin CBM and DSP. A BLASTp search of the CBM of laforin identified the CBM of *Geobacillus stearothermophilus* cyclodextrin glycosyltransferase (Protein Data Bank ID: 1CYG) (*92*) as the closest match (5×10^{-26}) with a determined structure, sharing 36% similarity and 20% identity with laforin. Like laforin, this enzyme also belongs to the CBM20 family (*25*).

Meanwhile, the DSP of SEX4 (Protein Data Bank ID: 3NME) (*160*) was the closest match (9×10^{-5}) to the DSP of laforin, sharing 39% similarity and 24% identity with laforin (*55*). Next, we analyzed the sequences of the CBM and DSP of laforin individually using HHpred to identify the most appropriate crystal structures to utilize in our modeling efforts (*145, 146*). HHpred queries alignment and structural databases such as Pfam, SMART, PDB, CDD, and HMMTigr using hidden Markov models to identify the closest determined structure. HHpred identified *G. stearothermophilus* cyclodextrin glycosyltransferase (1CYG) in the top three hits (2×10^{-22}) for the CBM of laforin and SEX4 as the highest hit (5.1×10^{-38}) for the DSP of laforin.

In generating a homology model, one usually performs a sequence alignment between the protein domains of the solved structure and that of the modeled domains. However, because CBM20 domains are very heterogeneous in sequence (*99*) we did not generate an alignment of *G. stearothermophilus* cyclodextrin glucanotransferase and the CBM of laforin. We utilized *G. stearothermophilus*

cyclodextrin glucanotransferase to generate a homology model of the CBM of laforin (Figure 6.16) using the SWISS-MODEL function in Swiss PDB viewer (*5*). Before generating a homology model of the laforin DSP, we first analyzed SEX4 as a DSP template by performing a sequence alignment of the DSP domain of laforin and SEX4 using PROfile Multiple Alignment with predicted Local Structure 3D (PROMALS3D), which utilizes primary, predicted secondary, and available tertiary information to align sequences (*118*). Based on the match of the predicted secondary structure of laforin with the structure of SEX4 (Figure 6.17A), we utilized the crystal structure of SEX4 to generate a homology model of the DSP of laforin (Figure 6.17).

CBM20 domains typically consist of seven β-strands that form an open-sided distorted β-barrel, with aromatic residues interacting with glucan chains rather than crystalline glucans as seen in other CBM families (*99*). The homology model of the CBM of laforin (Figure 6.16A) suggests that the CBM consists of 6 β-sheets that fold into the characteristic compact β-sandwich composed of anti-parallel β-sheets, with the N-terminus and C-terminus pointing towards opposite ends of the longest axis of the molecule (*98*). The conserved Trp32 and Trp99 residues form a compact, rigid, and surface-exposed hydrophobic site containing inter-ring spacing appropriate for binding to α-1,4-linked glucoses like those found in glycogen. This hydrophobic site forms a shallow pocket on the surface of the CBM that is highly accessible and thus primed for substrate interaction (Figure 6.16B).

To visualize the spatial arrangement of the DXMS results in the CBM of wild-type laforin, the percent decreases in deuteration observed in the CBM following glycogen binding (Figure 6.11B) were overlaid onto the structural model (Figure 6.16). The regions of the hydrophobic binding site encompassing the Trp32 and Trp99 residues exhibited the highest degree of protection observed in the CBM, indicating that the Trp32 and Trp99 residues are crucially positioned for glucan binding. Interestingly, the face of the CBM opposite to the hydrophobic binding site where the Trp60 residue resides also exhibits protection from deuteration upon glycogen binding (Figure 6.16B, inset). As this residue is located far from the

proposed hydrophobic binding site, it is possible that the Trp60 residue is involved in interaction of the CBM with the DSP upon substrate binding, thus leading to its protection.

The structural elements in the homology model of the DSP of laforin that we generated exhibited a match with the predicted secondary structure of laforin (Figure 6.17A and B), indicating that the predicted secondary structure of laforin was correctly interpreted in the model. Members of the DSP family exhibit a characteristic αβα DSP domain fold with the catalytic cysteine of the PTP loop at the base of the active site cleft (*2*). Our *in silico* approach suggests that the laforin DSP domain folds into the αβα fold characteristic of DSPs, exhibiting a five-stranded β-sheet surrounded by seven α-helices (*4*) (Figure 6.17B). As seen in the structures of other DSPs (*160, 177*), the variable loop, D loop, and R motif in the DSP model of laforin are all positioned around the PTP loop, together forming the active site cleft. The catalytic cysteine (Cys266) and the conserved aspartic acid (Asp235) of the D loop both point toward the catalytic groove. Interestingly, the homology model indicates that the variable loop of laforin possesses two unique α-helices that are uncommon to DSPs, but are found in SEX4 (*160*). As the variable loop of other DSPs lacks secondary structure and is in fact a loop (*175, 177*), the α-helical structure of the variable loop in glucan phosphatases may confer the specificity of these enzymes toward glucans and is possibly a defining characteristic of this class of phosphatases.

The regions in the DSP of laforin that demonstrated decreases in deuteration following glycogen binding include the variable loop, D loop, PTP loop, and the R motif (Figure 6.11B). As these regions are integrally associated with the active site in the DSP model (Figure 6.17B), the DXMS results indicate that these regions are likely involved in presentation of the glucan substrate to the active site of laforin. The surface view of the laforin DSP model illustrates the topology of the active site cleft and the concentration of these regions around the active site (Figure 6.17C). Interestingly, the AYLM motif was also protected from deuteration upon glycogen binding (Figure 6.11B), demonstrating the largest decrease in deuteration observed

in the DSP of laforin although it lies on the opposite face of the DSP domain from the active site (Figure 6.17C, inset). This region may be interacting with the Trp60 residue in the CBM domain in order to facilitate the interaction between the CBM and DSP necessary for dephosphorylation of the glucan substrate to occur, indicating synergy between the domains.

Finally, we assessed the spatial impacts of LD mutations in the GH1-like region of the R motif on the binding dynamics of laforin. We mapped the differences in the maximal percent decreases in deuteration following glycogen binding between corresponding regions of wild-type laforin (Figure 6.14A) and P301L (Figure 6.14C) onto the DSP homology model (Figure 6.18). In our DSP model, the Pro301 residue is oriented towards the active site and is thus primed for substrate interaction. The R motif where the P301L mutation resides demonstrated the greatest decrease in deuteration compared to wild-type (Figure 6.18), indicating that the P301L mutation causes increased interaction between the R motif and glycogen. The Y294N mutation also demonstrated similar decreases in deuteration in the same regions as P301L (Figure 6.14B and C), indicating a similar impact for this mutation.

The association of the R motif with the active site of laforin in the DSP model and the increased protection of this region from deuteration following mutation provides further evidence that the Tyr294 and Pro301 residues within the GH1-like region play a crucial role in substrate interaction. Mutation of these residues is thus impacting substrate presentation by the R motif to the active site of laforin, providing insight into the molecular etiology of the Y294N and P301L disease mutations.

Discussion.

Insights into the structure and mechanism of laforin.

Lafora disease is a fatal neurodegenerative disorder resulting from mutation of the glucan phosphatase laforin, the only known vertebrate phosphatase with the ability to bind and dephosphorylate glucans. Although the crystal structure of a

glucan phosphatase in plants known as SEX4 has been solved, this enzyme shares few structural aspects with laforin. We utilized DXMS in conjunction with homology modeling to gain insight into both the structure and mechanism of laforin, as the enzyme likely possesses distinct architecture and unique binding dynamics from SEX4. Our results provide insight into how the CBM and DSP domains of laforin function synergistically in the binding and dephosphorylation of glycogen.

Using DXMS, we found that like SEX4, laforin does not undergo structural rearrangements upon glycogen binding. We also discovered several regions in the both the CBM and DSP of laforin that exhibited significant solvent accessibility. These regions lay between areas of predicted secondary structure, supporting structural predictions as well as indicating areas of the protein that, solvent-exposed and free from structure, likely consist of loops that are primed for substrate interaction. In the laforin CBM, these areas included the peptides encompassing the Trp32, Trp60, and Trp99 residues, conserved CBM20 family residues that are important for glucan binding. Upon glycogen binding, the regions encompassing these residues demonstrated significant protection from deuteration, supporting the role of these residues in glycogen binding. In a homology model of the CBM of laforin, the Trp32 and Trp99 residues form a surface-exposed hydrophobic binding site, with these residues appropriately spaced for the accommodation of glucan chains. We observed that the W32G mutation largely abolished the ability of laforin to bind to glucans, providing evidence that both tryptophan residues within the hydrophobic binding site of the CBM are crucial for glucan binding.

In the DSP of laforin, the recognition domain, variable loop, D loop, PTP loop, AYLM motif, and R motif all exhibited solvent accessibility and lay between regions of predicted secondary structure. The D loop contains the Asp235 residue that makes direct contact with the substrate, acting as the general acid-base catalyst in the dephosphorylation reaction. The recognition domain and the variable loop are both involved in substrate interaction and contribute to the depth of the active site, while the variable loop also assists in orienting the active site arginine to interact with the phosphate of the substrate. The PTP loop possesses the cysteine residue that catalyzes the dephosphorylation reaction, while the AYLM motif, a sequence

motif specific to DSPs, has been demonstrated to play a role in domain interaction in the glucan phosphatase SEX4. Lastly, the R motif possesses a conserved Arg residue specific to DSPs.

These regions in the DSP of laforin all demonstrated significant decreases in deuteration when glycogen was present, indicating that interaction of these regions with substrate is protecting them from deuterium uptake. These regions in SEX4, with the exception of the AYLM motif and R motif, also exhibit protection from deuteration when substrate is present, indicating the importance of these regions in substrate binding. A homology model of the DSP domain of laforin indicates that the variable loop, D loop, PTP loop, and R motif are positioned directly around the active site, together forming the active site cleft. While the recognition domain of laforin could not be modeled in laforin, the recognition domain in addition to the variable loop, D loop, and PTP loop are directly associated with the active site of SEX4, indicating that these regions are crucial for substrate presentation to the active site. Secondary structure predictions and the homology model of laforin indicate that the variable loop of laforin consists of two α-helices as seen in SEX4. As this region is a loop in other DSPs, the α-helices within the variable loop may confer the preference of laforin and SEX4 for glucan substrates.

The protection of the AYLM motif of laforin, which lies on the opposite face of the DSP domain from the active site in the homology model, when glycogen is present suggests that the AYLM motif may not interact with the glucan that is bound at the active site. Interestingly, the Trp60 residue in the CBM of laforin also demonstrates protection from deuteration when glycogen is present, although this residue resides on the opposite face of the CBM from the hydrophobic binding site. Together, these results indicate that Trp60 and the AYLM motif may constitute an interaction site between the CBM and DSP. In support of this hypothesis, the AYLM motif of SEX4 has demonstrated adaptation for interdomain interaction. We observed that the W32G mutation within the CBM of laforin largely abolished glucan binding by both the CBM and DSP domains while the C266S mutation in the DSP affected only glucan binding by the DSP. Thus, the CBM likely makes initial contact

with glucan substrates, bringing the DSP into position for binding and dephosphorylation of the glucans. It is possible that the synergy of the CBM and DSP domains upon glucan binding is mediated by the interaction of the Trp60 residue of the CBM with the AYLM motif in the DSP. Additional biochemical analyses following mutagenesis of the Trp60 residue and the AYLM motif are needed in order to elucidate the role that these motifs play in interdomain interaction in laforin.

Our DXMS analyses indicate that like other CBM20 family members, laforin prefers heterogeneous substrates possessing soluble glucan chains, such as glycogen, rather than insoluble, crystalline glucose polymers such as amylopectin and β-cyclodextrin. Interestingly, laforin exhibits a 3 to 10-fold greater rate in the dephosphorylation of amylopectin than does SEX4. The results indicate that laforin possesses faster binding dynamics, or binding to and release from substrate, than SEX4. In addition, laforin also exhibits less protection from deuteration upon both glycogen and amylopectin binding than observed in SEX4 following amylopectin binding. We observed that the C266S mutation abolished binding of the DSP domain to glucans while the CBM retained the ability, conferring similar binding affinity of C266S to glucans as seen with wild-type laforin. Together these results support the presence of a flexible linker between the CBM and DSP of laforin, which may contribute to the faster dynamics of the protein.

Surprisingly, the R motif of laforin demonstrates protection from deuteration upon glycogen binding while the R motif of SEX4 does not. However, the R motif of SEX4 is positioned directly adjacent to the active site in the crystal structure of SEX4. We discovered a sequence within the R motif shared between laforin, SEX4, and the active site of family 1 glycosyl hydrolases. This glycosyl hydrolase family 1 (GH1)-like sequence was highly conserved among distantly related laforin orthologs, indicating that this conserved sequence plays a role in the interaction of the R motif with glucans in laforin. The Y294N and P301L mutations within the GH1-like region led to an increased interaction of the DSP domain with glycogen, demonstrating that these residues are involved in glucan interaction. The GH1-like sequence within the R motif likely confers the ability of the R motif of laforin to

interact with glucan. This involvement of the R motif of laforin in glucan binding, in addition to the presence of a flexible linker between the CBM and DSP, may contribute to the faster binding dynamics of laforin.

Like SEX4, we observed a role for the AYLM motif in interdomain interaction, indicating that this may be a general feature of the glucan phosphatases. However, the involvement of the R motif of laforin in glucan binding indicates unique binding dynamics of the DSP from glucan phosphatases like SEX4. In addition, we have gained insight into the previously uncharacterized binding mechanism of the CBM20 domain of laforin. A crystal structure of laforin would support these findings, and our DXMS results indicate that the higher substrate preference of laforin for glycogen over other complex carbohydrates should be considered in crystallization attempts.

Insight into the molecular etiology of LD mutations.

Currently, no therapeutic options exist for Lafora disease patients with missense mutations in laforin. Although the impact of several missense mutations on laforin binding and activity has been reported, the conformational changes or mechanistic disruption responsible for these effects has not been studied. We therefore assessed the structural dynamics of the W32G mutation in the CBM of laforin and the G240S, Y294N, and P301L mutations in the DSP domain.

The W32G mutation largely abolished binding of both the CBM and DSP domain to glycogen, indicating that the Trp32 residue, a conserved CBM20 family residue, is absolutely critical for laforin association with glycogen. Our work provides insight into the molecular etiology of this mutation. As this mutation prevents laforin from interacting with glycogen, laforin is likely unable to dephosphorylate glycogen and prevent the formation of LBs.

In contrast to the W32G mutant, the G240S mutation within the D loop did not impact the structural dynamics of laforin. Our DXMS results are in agreement with prior work demonstrating that this mutation impacts the interaction of laforin with PTG, a protein involved in glycogen synthesis. Laforin acts as a scaffold to allow its binding partner malin to ubiquitinate PTG in order to target the protein for

proteasomal degradation. If laforin cannot bind to PTG, the regulation of PTG protein levels and thus the rate of glycogen synthesis by malin is prevented. The agreement of our biochemical and DXMS analyses of W32G and G240S with previously published findings also lends validity to our experimental approach.

We then explored the impact of the Y294N and P301L mutations on the structural dynamics of laforin. As these mutations reside within the GH1-like region of the R motif, a region we propose to be important in glucan binding, we expected that these mutations would disrupt glucan binding by the DSP domain. In support of this hypothesis, previous work has indicated that these mutations completely disrupt both glucan binding and phosphatase activity of laforin. Surprisingly, our glucan binding assays and DXMS results revealed that both the Y294N and P301L mutations cause a strengthened interaction of the R motif with glycogen compared to wild-type laforin and that these proteins still possess some glucan phosphatase activity. This increased interaction of the DSP with glycogen appears to also prolong the interaction of the CBM of laforin, particularly the Trp99 residue, with glycogen. The prolonged interaction of an enzyme with its substrate due to mutation is not a unique phenomenon. Specific mutations in PTP1B lead to an increase in the interaction with its substrate, the insulin receptor, effectively trapping the enzyme with the substrate (*20, 144*)

Our data suggest that the Y294N and P301L mutations cause a breakdown in the normal on/off ability of laforin that potentially disrupts the enzyme's ability to scan for phosphorylated glucans. We propose that the underlying biochemical explanation for LD in these patients is increased and prolonged binding of glucans by laforin. Additional work by our lab studying plant glucan phosphatases suggests that Tyr294 is likely involved in aromatic stacking interactions with the glucose moieties in glycogen. The increased interaction observed with Y294N could be due to hydrogen bonding that occurs between the amide nitrogen of asparagine and the hydroxyl groups present on the glycogen chain. Similarly, the Pro301 residue, shown to be oriented towards the active site in our homology model, may be involved in hydrophobic stacking interactions that are strengthened due to the substitution of this residue with a hydrophobic leucine.

The altered glucan interactions resulting from the Y294N and P301L mutations likely eliminates the normal shuttling of the glucan chain through the laforin active site that occurs via hydrophobic stacking between the chair conformation of each glucose moiety and the aromatic ring. This increased interaction would replace the normal movement of the glucan chain through the laforin active site, causing what Dr. Gentry has defined as a "velcro effect" that inhibits movement of glycogen chains through the DSP-glucan binding channel. As the Y294N and P301L mutants still exhibit some glucan phosphatase activity, the enzyme may be able to perform a few rounds of catalysis before becoming "trapped" in the bound substrate.

Now that we have identified a method to purify large yields of laforin, we can perform a greater range of studies assessing the mechanism of laforin and laforin mutants. Further work using surface plasmon resonance and isothermal titration calorimetry with homogeneous glucan substrates to assess binding affinities and enzyme kinetics will provide further insight into the impact of the Y294N and P301L mutations on the rate of glucan dephosphorylation by laforin.

The insights gained from our work will likely aid in the development of therapies for LD patients. If our hypothesis with Y294N is correct, then LD patients with the Y249N or P301L mutation may be treated by a yet undiscovered laforin inhibitor that could bind weakly to laforin and negate the increased laforin-glucan interaction. This treatment would allow laforin to function more normally, especially considering that much of its interaction is, presumably, based upon binding by its CBM domain.

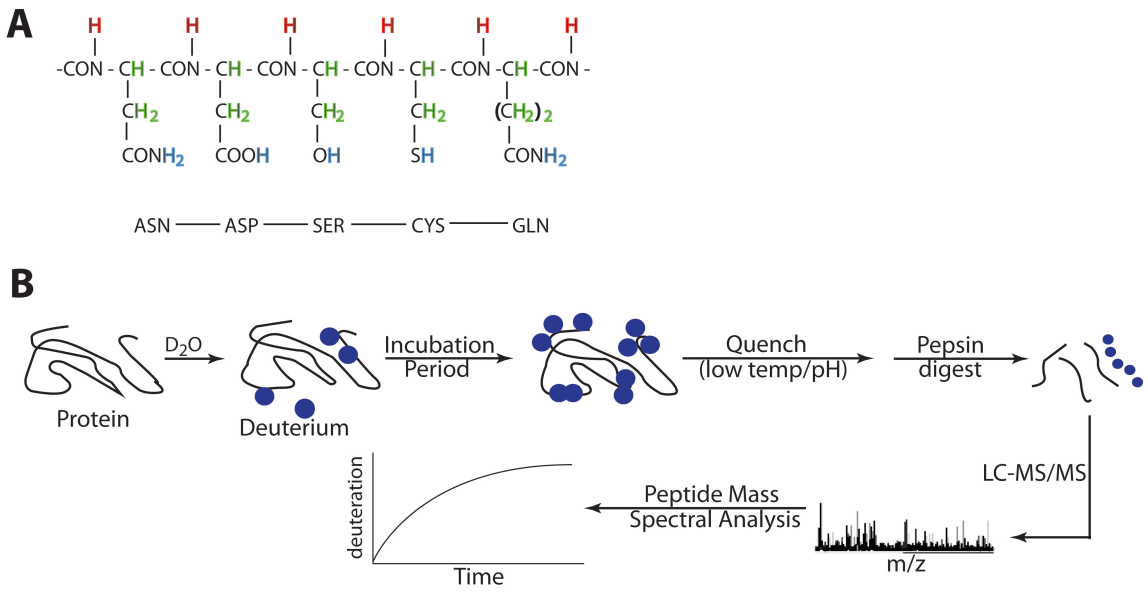

Figure 6.1. Amide hydrogen exchange and DXMS experimental layout.

A. Three main groups of potentially exchangeable hydrogens exist in a protein. Hydrogens covalently attached to carbon atoms (green H) do not exchange. Hydrogens that are part of side chain functional groups (blue H) exchange so rapidly that incorporated deuterium is not retained during processing. The amide hydrogens (red H) do exhibit exchange that can be measured by DXMS (adapted from Hsu) (*76*). **B.** This diagram depicts the general workflow of a typical DXMS experiment. A protein is initially incubated in D_2O buffer for predetermined lengths of time to determine areas of rapid or slow deuterium uptake, after which exchange of deuterium (indicated by blue circles) is quenched using low temperature and pH. Following pepsin proteolysis of the protein and separation of the generated peptides using HPLC, automated sample processing using LC-MS/MS tandem mass spectrometry generates the data used for peptide identification and DXMS analysis to determine the deuteration over time of the generated peptides. Differences in the mass of the pepsin-generated peptides indicates the amount of deuterons (or the number of amino hydrogens that have exchanged) incorporated into the peptide.

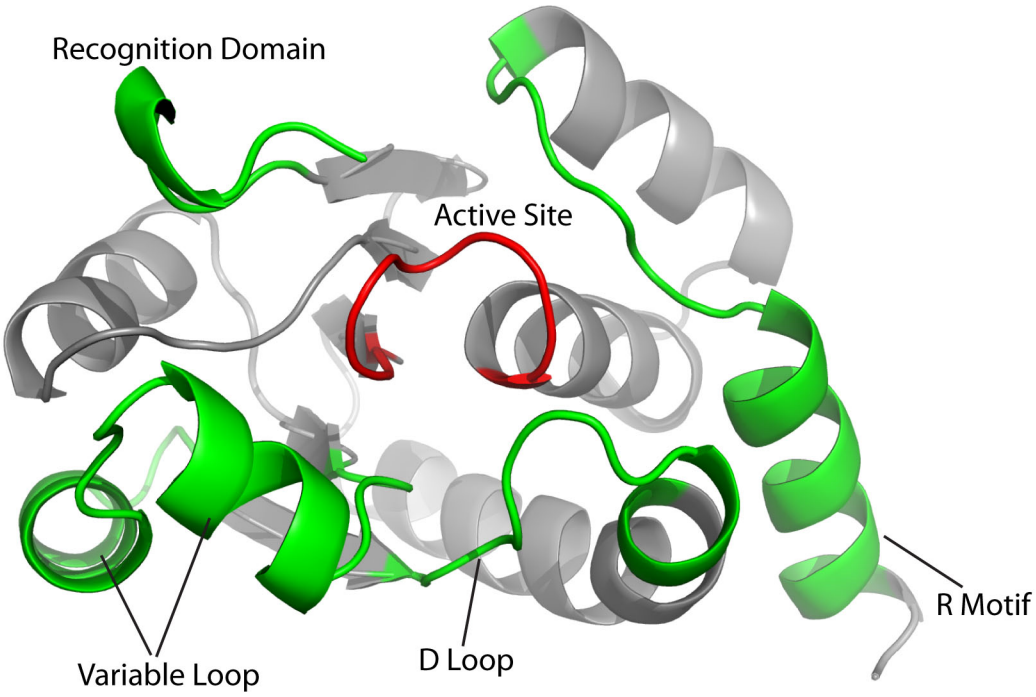

Figure 6.2. The characteristic regions of the DSP domain. The crystal structure of the DSP domain of SEX4 is shown. The important regions characteristic of all DSPs are indicated in green, with the active site depicted in red. The regions together compose the active site cleft.

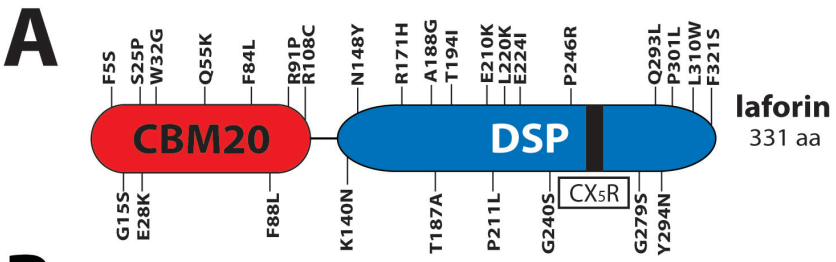

C

Variable Loop of Laforin

	190									200
H. sapiens	A	V	M	N	F	Q	T	E	W	D	I
P. troglodytes	A	V	M	N	F	Q	T	E	W	D	I
M. mulatta	A	V	M	N	F	Q	T	E	W	D	I
M. musculus	A	V	M	N	F	Q	T	E	W	D	I
R. norvegicus	A	V	M	N	F	Q	T	E	W	D	I
G. gallus	A	V	M	N	F	Q	T	E	W	D	I
X. laevis	A	V	L	N	F	Q	T	E	W	D	V
T. nigroviridis	A	V	M	N	F	Q	T	E	A	D	V
B. floridae	A	V	M	N	F	Q	M	D	Y	D	L
N. vectensis	A	V	I	S	L	Q	T	A	S	D	I
E. tenella	V	V	L	N	M	Q	T	A	D	D	M
T. gondii	A	V	V	N	L	Q	T	E	Q	D	L
C. merolae	A	V	L	N	L	Q	T	D	E	D	F

R Motif of Laforin

	300												
H. sapiens	F	L	M	A	K	R	P	A	V	Y	I	D	E
P. troglodytes	F	L	M	A	K	R	P	A	V	Y	I	D	E
M. mulatta	F	L	M	A	K	R	P	A	V	Y	I	D	E
M. musculus	F	I	M	A	K	R	P	A	V	Y	I	D	E
R. norvegicus	F	I	M	A	K	R	P	A	V	Y	I	D	E
G. gallus	F	L	A	S	R	R	P	A	V	Y	I	D	E
X. laevis	F	L	A	S	R	R	P	A	V	Y	I	D	E
T. nigroviridis	F	V	A	A	R	R	P	A	V	Y	I	D	E
B. floridae	Y	L	C	S	R	R	P	V	S	Y	I	D	E
N. vectensis	N	I	C	S	K	R	P	V	A	F	I	D	G
E. tenella	L	V	S	T	K	R	P	V	A	Y	W	D	E
T. gondii	L	I	C	A	R	R	P	V	A	Y	W	D	E
C. merolae	H	V	K	A	R	R	P	V	A	A	V	A	A

D

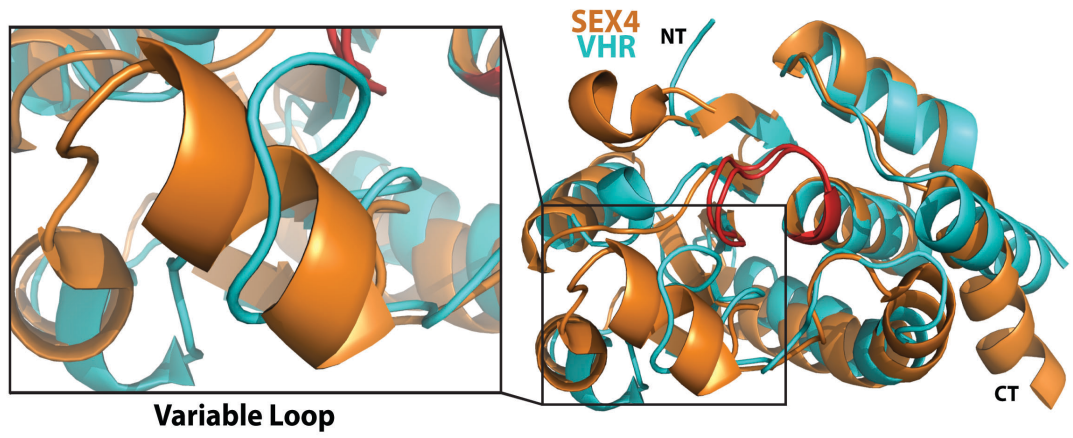

Figure 6.3. The glycosyl hydrolase family 1 active site pattern in the R motif of laforin. A. Laforin possesses an N-terminal carbohydrate binding module family 20 domain (CBM20), an intermediate linker region, and a C-terminal dual-specificity phosphatase (DSP) domain featuring the canonical DSP CX_5R active site motif (indicated by a black bar). Known LD point mutations are equally distributed across the domains of the protein (*78*). **B.** The CBM and DSP domains of SEX4 lie in an orientation opposite to that of laforin. Unlike laforin, SEX4 also contains a domain to target it to the chloroplast (cTP; chloroplast targeting peptide) (*112*) as well as a C-terminal domain (CT) critical for folding (*160*). Although in different families, the CBMs of laforin and SEX4 belong to the same evolutionarily related CBM clan (*25, 35*). **C.** Following bioinformatics analyses of laforin and SEX4 using multiple iterations of PSI-BLASTp and PFAM, we discovered regions within the variable loop and the R motif of the DSP of these enzymes with remote homology to glycosyl hydrolase family 10 (GH10) and family 1 (GH1) enzymes, respectively. Shown are sequence alignments of the GH10-like region in the variable loop and the GH1-like region in the R motif of laforin from a variety of organisms, illustrating the remarkable conservation of these GH-like regions. Residues boxed in dark grey are identical, while residues in light grey indicate conserved substitutions. The number above the sequence indicates the amino acid number of laforin. **D.** The structure of SEX4 (tan) overlaid onto the structure of VHR (teal) with an RMSD of 1.84Å. The inset depicts the differing structure of the variable loop.

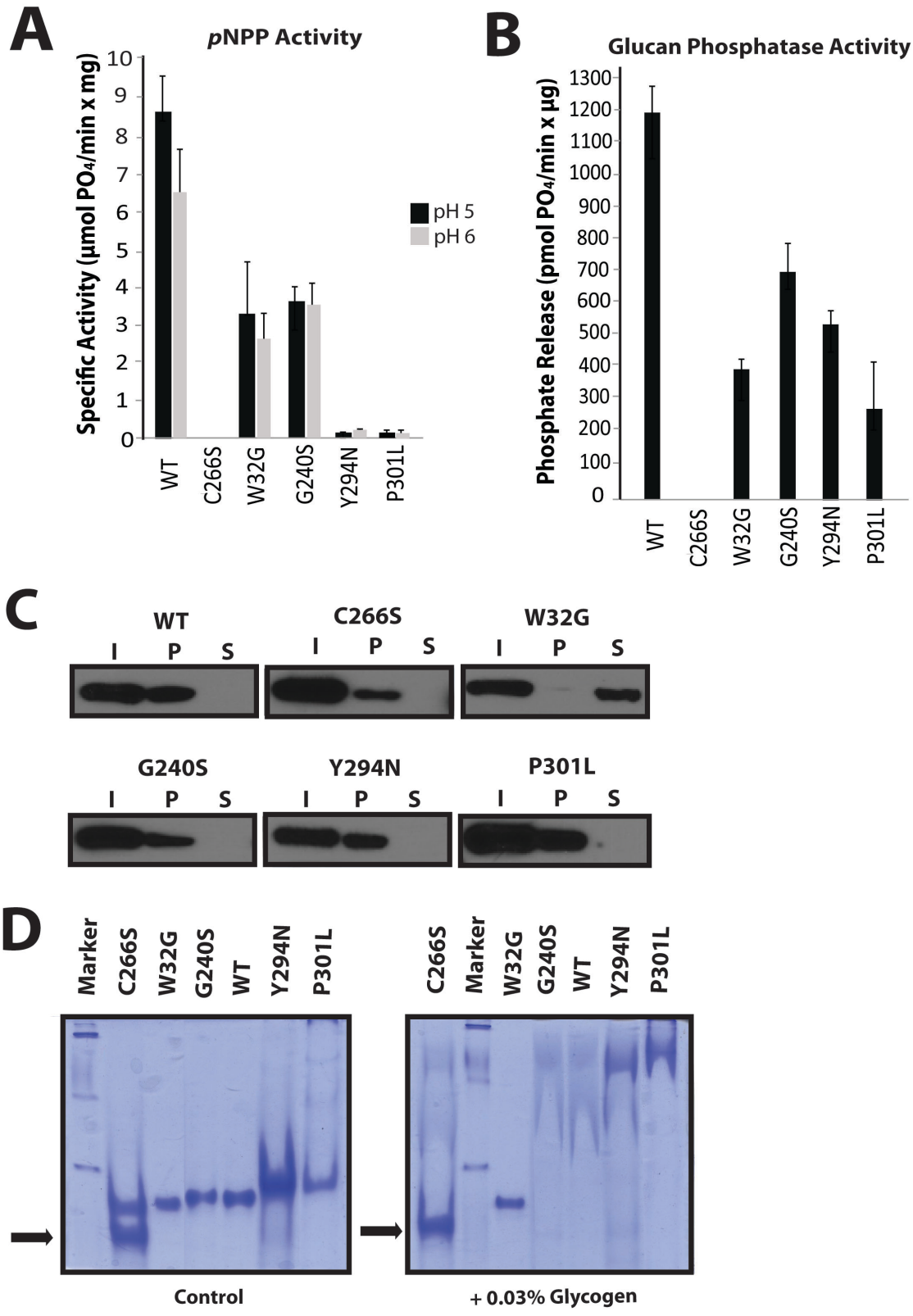
A
pNPP Activity
Specific Activity (µmol PO4/min x mg)
pH 5
pH 6
WT
C266S
W32G
G240S
Y294N
P301L
B
Glucan Phosphatase Activity
Phosphate Release (pmol PO4/min x µg)
C
WT
C266S
W32G
G240S
Y294N
P301L
I
P
S
D
Marker
Control
+ 0.03% Glycogen

Figure 6.4. Biochemical characterization of Ni-NTA purified wild-type laforin and mutants. *p*NPP assays, glucan phosphatase assays, and glucan binding assays were performed using wild-type laforin and laforin mutants. The purity of the proteins utilized in these studies was assessed via Western analysis of the HIS_6 epitope tag using a mouse monoclonal α HIS_6 antibody (Neuromab). Phosphatase activity of mutants was then corrected following densitometric analysis based on the amount of laforin present in equal amounts of total protein for the mutants compared to wild-type laforin. WT, wild-type. **A.** Specific activity of laforin against *p*NPP at pH 5 and 6, the most optimal for laforin activity (*55*). Inactive C266S laforin was used as a control. At least 8 replicates were performed for each protein. Error bars indicate means ± SEM. **B.** Malachite green assay of laforin to measure inorganic phosphate release from amylopectin at pH 7, the optimal pH for laforin (*55*). At least 8 replicates were performed for each protein. Error bars indicate means ± SEM. **C.** The binding of laforin to amylose resin was assessed. Wild-type laforin is able to bind glucan and is pulled down in the amylose-resin pellet (P). Proteins unable to bind glucan are recovered in the supernatant (S). This experiment was repeated three times and the depicted image is a representation. **D**. Glycogen affinity native-PAGE electrophoresis of wild-type laforin and mutants. The right gel contains 0.03% glycogen, while the left gel contains no glycogen. Mutants unable to interact with glycogen move more quickly through the glycogen gel than wild-type laforin, while mutants with stronger binding migrate slower than wild-type. The black arrow indicates the position of a non-laforin protein that co-purified with laforin and does not demonstrate glucan binding. The experiment was repeated three times and the depicted image is a representation.

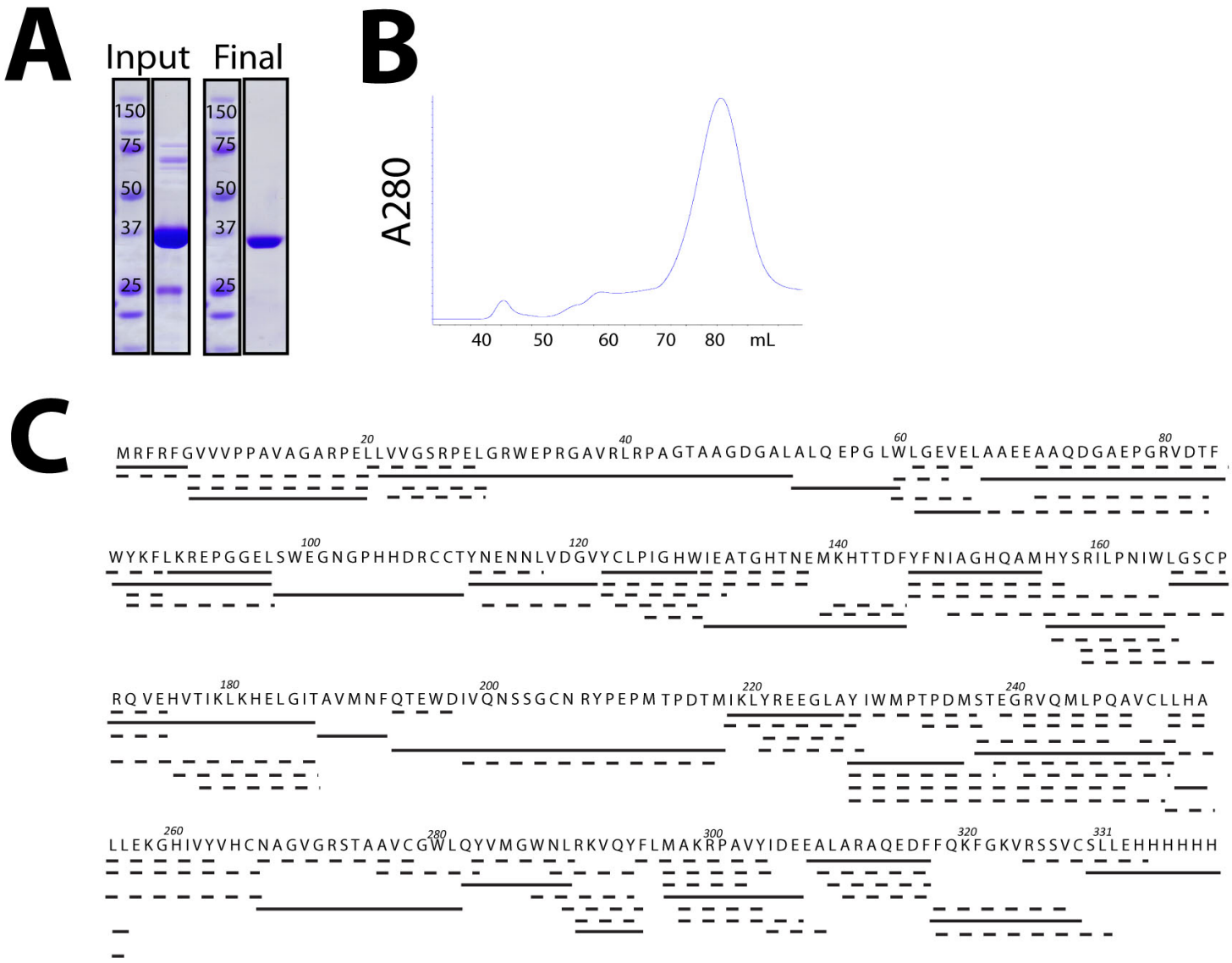
A
Input
Final
150
75
50
37
25
B
A280
40
50
60
70
80
mL
C
MRFRFGVVVPPAVAGARPELLVVGSRPELGRWEPRGAVRLRPAGTAAGDGALALQ EPG LWLGEVELAAEEAAQDGAEPGRVDTF
WYKFLKREPGGELSWEGNGPHHDRCCTYNENNLVDGVYCLPIGHWIEATGHTNEMKHTTDFYFNIAGHQAMHYSRILPNIWLGSCP
RQ VEHVTIKLKHELGITAVMNFQTEWDIVQNSSGCN RYPEPM TPDTMIKLYREEGLAY IWMPTPDMSTEGRVQMLPQAVCLLHA
LLEKGHIVYVHCNAGVGRSTAAVCGWLQYVMGWNLRKVQYFLMAKRPAVYIDEEALARAQEDFFQKFGKVRSSVCSLLEHHHHHH

Figure 6.5. Purification of recombinant wild-type laforin for DXMS and peptide coverage map. **A.** Following expression of laforin in *E. coli* cells and incubation of Ni^{2+}-agarose with cell lysate, the Ni^{2+}-agarose eluate ("Input") was purified to near homogeneity via separation with an S200 gel filtration column ("Final"). **B.** Only the S200 fractions beneath the sharp monomer peak at 80 mL of column eluate were collected for DXMS analysis. **C.** Sequence coverage map of peptides resulting from pepsin digestion of wild-type laforin identified during MS/MS experiments. A total of 134 high-quality peptides were detected. Solid lines indicate the 27 peptides utilized in my analysis, with dashed lines indicating peptides that were not used but were examined for exchange behavior that resembled the selected peptides. Numbers correspond to the amino acid position of laforin.

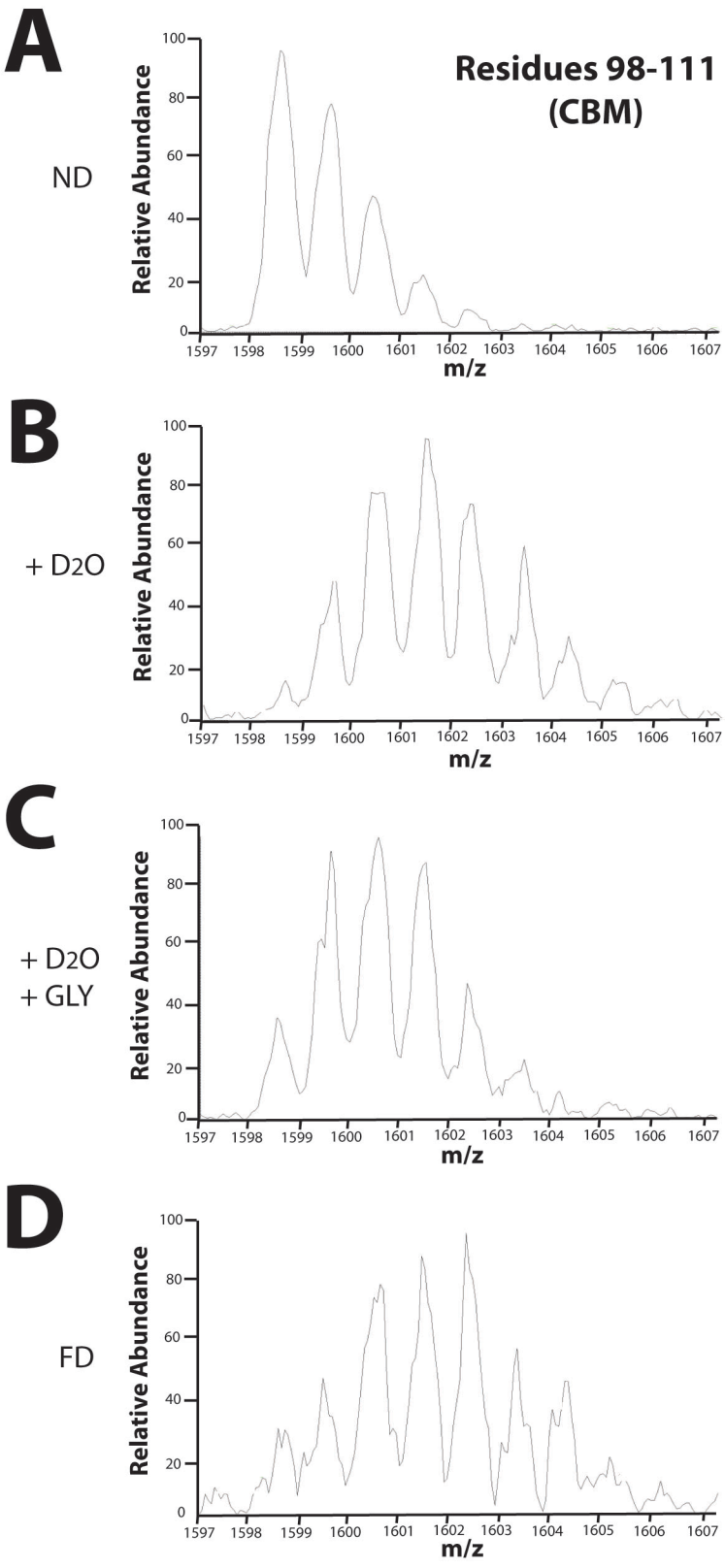
A
ND
Residues 98-111
(CBM)
Relative Abundance
m/z
B
+ D2O
C
+ D2O
+ GLY
D
FD

Figure 6.6. Mass spectra of residues 98-111 of wild-type laforin. The mass spectra of a single peptide encompassing residues 98-111 in the CBM of laforin that exhibited a change in mass following incubation with deuterium alone or with substrate. **A.** The spectra of peptide 98-111 prior to exposure to D_2O. ND; nondeuterated. **B**. The spectra of peptide 98-111 following exposure to D_2O for 10,000 s. The spectra exhibits a shift to the right to a higher m/z ratio as well as an increased complexity of peaks, indicating uptake of deuterium. +D_2O; deuterium present. **C.** The spectra of peptide 98-111 following exposure to D_2O for 10,000 s in the presence of glycogen. +GLY; glycogen present. The spectra demonstrates a shift to the left to a lower m/z charge ratio compared to panel B when substrate is present, indicating that this region of laforin is likely interacting with substrate and is thus protected from deuterium uptake. **D.** The spectra of peptide 98-111 at deuterium exchange equilibrium, indicating the highest possible level of deuteration for this peptide. FD; fully deuterated.

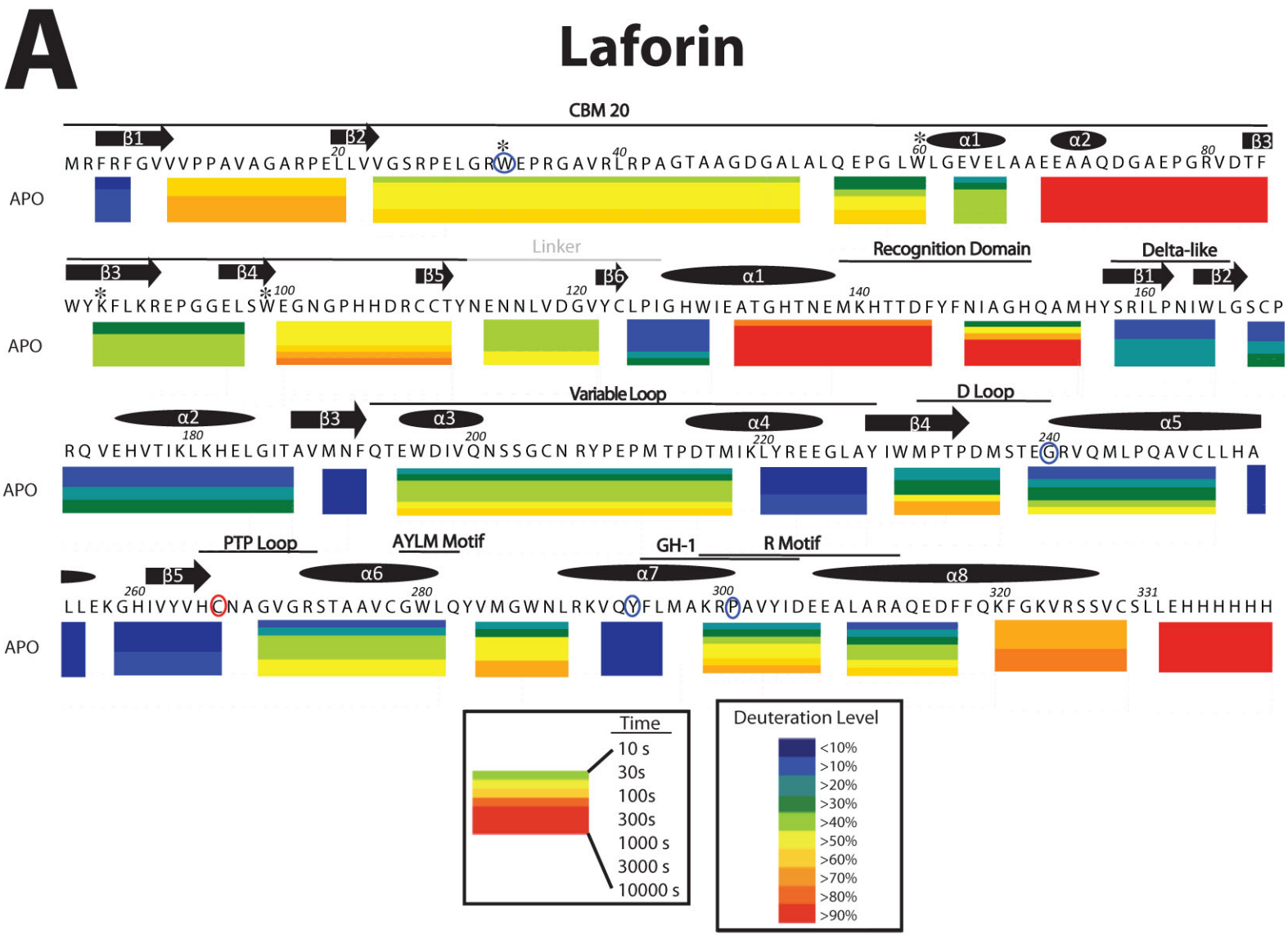
A
Laforin
CBM 20
β1
β2
α1
α2
β3
MRFRFGVVVPPAVAGARPELLVVGSRPELGRWEPRGAVRLRPAGTAAGDGALALQ EPG LWLGEVELAAEEAAQDGAEPGRVDTF
APO
Linker
Recognition Domain
Delta-like
β3
β4
β5
β6
α1
β1
β2
WYKFLKREPGGELSWEGNGPHHDRCCTYNENNLVDGVYCLPIGHWIEATGHTNEMKHTTDFYFNIAGHQAMHYSRILPNIWLGSCP
APO
Variable Loop
D Loop
α2
β3
α3
α4
β4
α5
RQ VEHVTIKLKHELGITAVMNFQTEWDIVQNSSGCN RYPEPM TPDTMIKLYREEGLAY IWMPTPDMSTEGRVQMLPQAVCLLHA
APO
PTP Loop
AYLM Motif
GH-1
R Motif
β5
α6
α7
α8
LLEKGHIVYVHCNAGVGRSTAAVCGWLQYVMGWNLRKVQYFLMAKRPAVYIDEEALARAQEDFFQKFGKVRSSVCSLLEHHHHHH
APO
Time
10 s
30s
100s
300s
1000 s
3000 s
10000 s
Deuteration Level
<10%
>10%
>20%
>30%
>40%
>50%
>60%
>70%
>80%
>90%

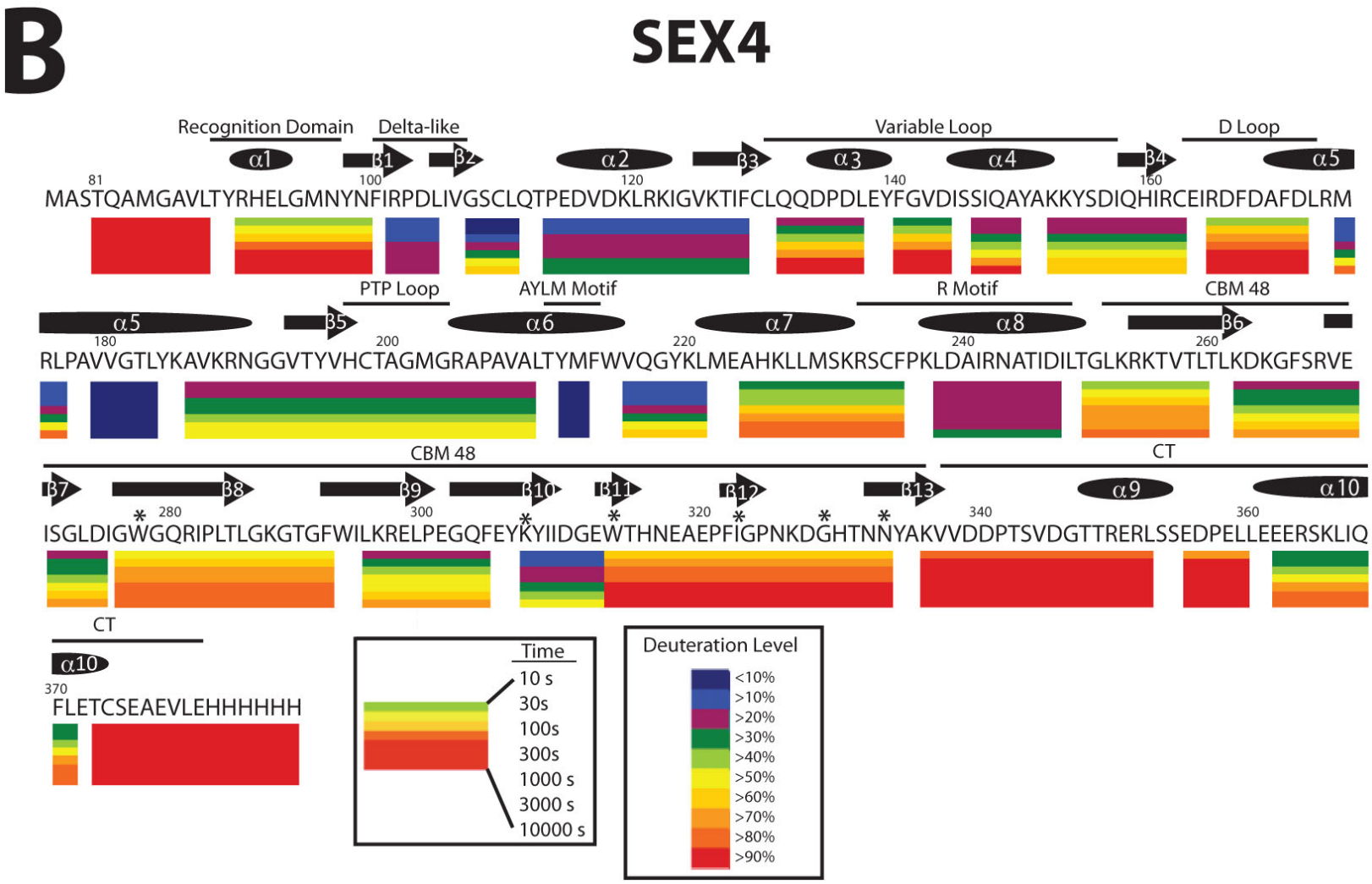
B
SEX4
Recognition Domain
Delta-like
Variable Loop
D Loop
α1
β1
β2
α2
β3
α3
α4
β4
α5
81
100
120
140
160
MASTQAMGAVLTYRHELGMNYNFIRPDLIVGSCLQTPEDVDKLRKIGVKTIFCLQQDPDLEYFGVDISSIQAYAKKYSDIQHIRCEIRDFDAFDLRM
PTP Loop
AYLM Motif
R Motif
CBM 48
α5
β5
α6
α7
α8
β6
180
200
220
240
260
RLPAVVGTLYKAVKRNGGVTYVHCTAGMGRAPAVALTYMFWVQGYKLMEAHKLLMSKRSCFPKLDAIRNATIDILTGLKRKTVTLTLKDKGFSRVE
CBM 48
CT
β7
β8
β9
β10
β11
β12
β13
α9
α10
280
300
320
340
360
ISGLDIGWGQRIPLTLGKGTGFWILKRELPEGQFEYKYIIDGEWTHNEAEPFIGPNKDGHTNNYAKVVDDPTSVDGTTRERLSSEDPELLEEERSKLIQ
CT
α10
370
FLETCSEAEVLEHHHHHH
Time
10 s
30s
100s
300s
1000 s
3000 s
10000 s
Deuteration Level
<10%
>10%
>20%
>30%
>40%
>50%
>60%
>70%
>80%
>90%

Figure 6.7. DXMS results of wild-type laforin and SEX4 without substrate. A. The deuteration level of wild-type laforin from 10-10,000s (see left inset) in the absence of substrate (APO) is shown, with the lowest deuteration level indicated in blue and the highest in red (see right inset). Each block represents one of the 27 peptides chosen for analysis from Figure 6.4B, with each bar within that block representing the average spectra centroid value for an increasing time point with <2% standard deviation. Therefore, >10% changes in deuteration can be deemed statistically significant. The CBM of laforin extends from residues 1-112, with the conserved Trp32, Trp60, Lys87, and Trp99 CBM20 residues predicted to be critical for glucan binding denoted by asterisks (*141, 166*). A predicted linker extends from residues 112-126, and the DSP, with important regions labeled (*54*), extends from residues 127-331. The predicted secondary structure of laforin is indicated above the amino acid sequence, with the α-helices of the DSP domain labeled as per standard nomenclature (*177*). PSIPRED (*85*) was used due to its accuracy in SEX4 structure prediction. The first two amino acids of each peptide lack exchange data, as the first amino acid does not possess an amide hydrogen and the second exchanges too rapidly to retain deuterons (*8*), and so are not included in the figure. The LD-causing missense mutations utilized in this study are circled in blue, with the catalytically inactive artificial C266S mutant circled in red. **B.** The deuteration level of APO SEX4 (the first 80 amino acids encompassing the cTP are missing) from 10-10,000 s is shown. Residues critical for glucan binding in the CBM are denoted by asterisks. The secondary structure of SEX4 is indicated above the amino acid sequence (*160*) and the important DSP regions are labeled.

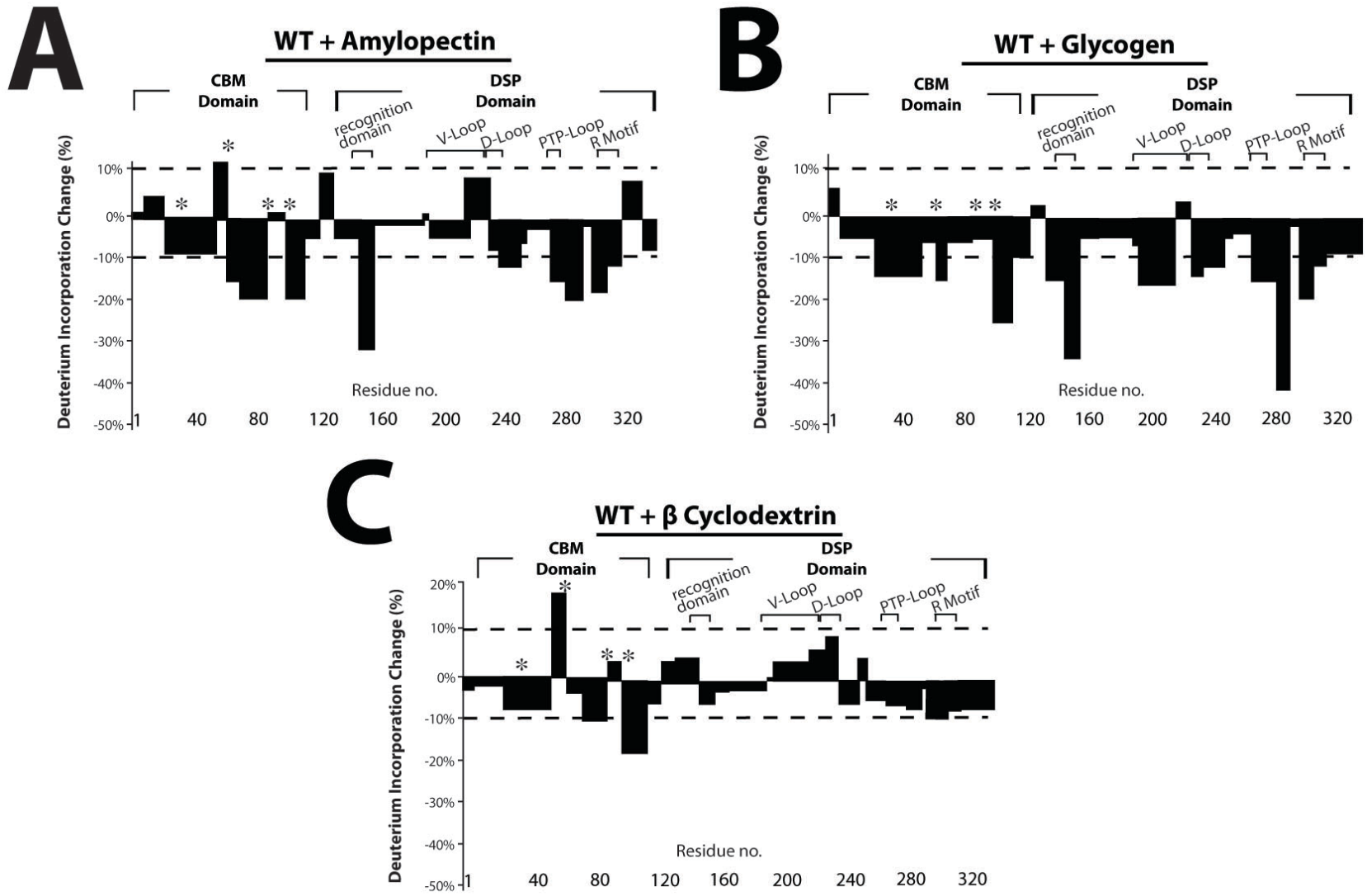
A
WT + Amylopectin
CBM Domain
DSP Domain
recognition domain
V-Loop
D-Loop
PTP-Loop
R Motif
Deuterium Incorporation Change (%)
10%
0%
-10%
-20%
-30%
-40%
-50%
Residue no.
1
40
80
120
160
200
240
280
320
B
WT + Glycogen
CBM Domain
DSP Domain
recognition domain
V-Loop
D-Loop
PTP-Loop
R Motif
Deuterium Incorporation Change (%)
10%
0%
-10%
-20%
-30%
-40%
-50%
Residue no.
1
40
80
120
160
200
240
280
320
C
WT + β Cyclodextrin
CBM Domain
DSP Domain
recognition domain
V-Loop
D-Loop
PTP-Loop
R Motif
Deuterium Incorporation Change (%)
20%
10%
0%
-10%
-20%
-30%
-40%
-50%
Residue no.
1
40
80
120
160
200
240
280
320

Figure 6.8. DXMS results of wild-type laforin with structurally varied glucan substrates. Wild-type laforin was incubated with amylopectin, glycogen, or β-cyclodextrin during DXMS experiments. Maximal percent changes in deuteration at any time point between the substrate-free condition and upon binding to amylopectin (**A**), glycogen (**B**), and β-cyclodextrin (**C**) were calculated for each peptide of laforin. Individual peptides are indicated by single black bars. The different regions of the DSP domain are noted at the top of the graphs and the asterisks indicate the positions of residues within the CBM likely required for glucan binding. In all panels, a positive value for change indicates increased deuteration while a negative value signifies a decrease in deuteration after glucan binding. Changes greater than 10% (dashed lines) are considered to be significant as <2% standard deviation was observed between experimental replicates.

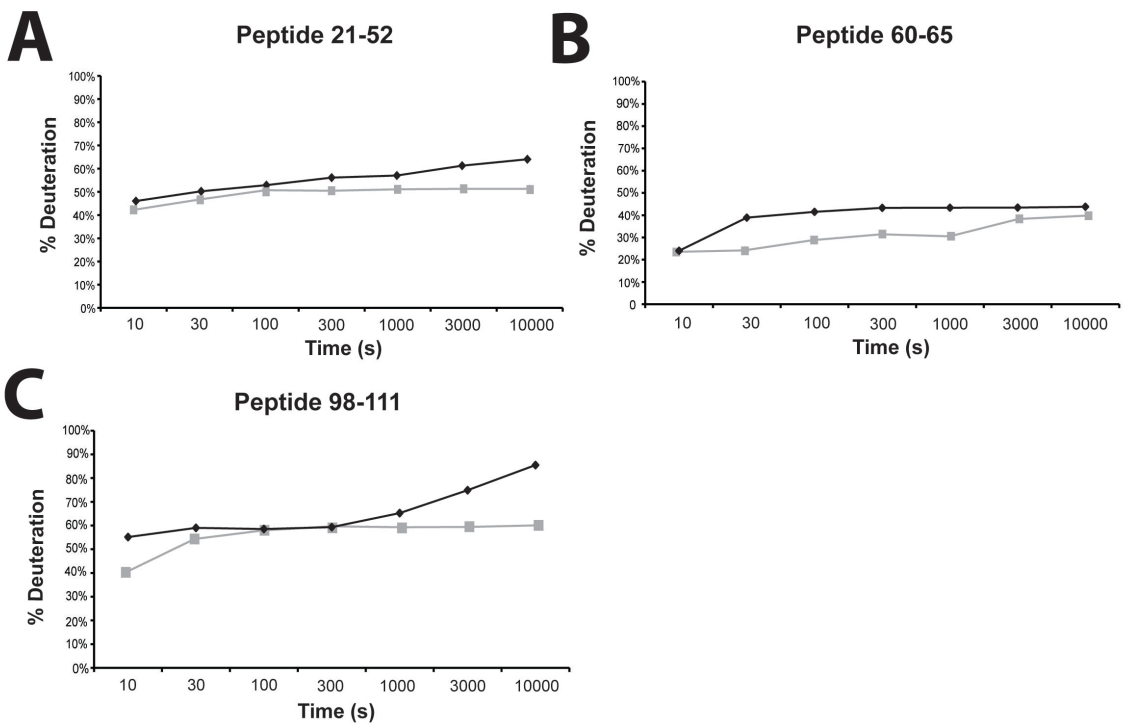

Figure 6.9. Peptides within the CBM of laforin that exhibit deuteration changes after glycogen binding. The percent deuteration of peptides in the CBM of wild-type laforin between the APO and glycogen-bound conditions was examined over time. Each point indicates the centroid value of the mass spectra for the peptide at the indicated time with <2% standard deviation. Black diamonds indicate the APO condition while gray squares indicate the glycogen condition. The x-axis has a log scale. Only the peptides covering residues (**A**) 21-52, (**B**) 60-65, and (**C**) 98-111 exhibited a >10% change in deuteration between the APO and glycogen conditions.

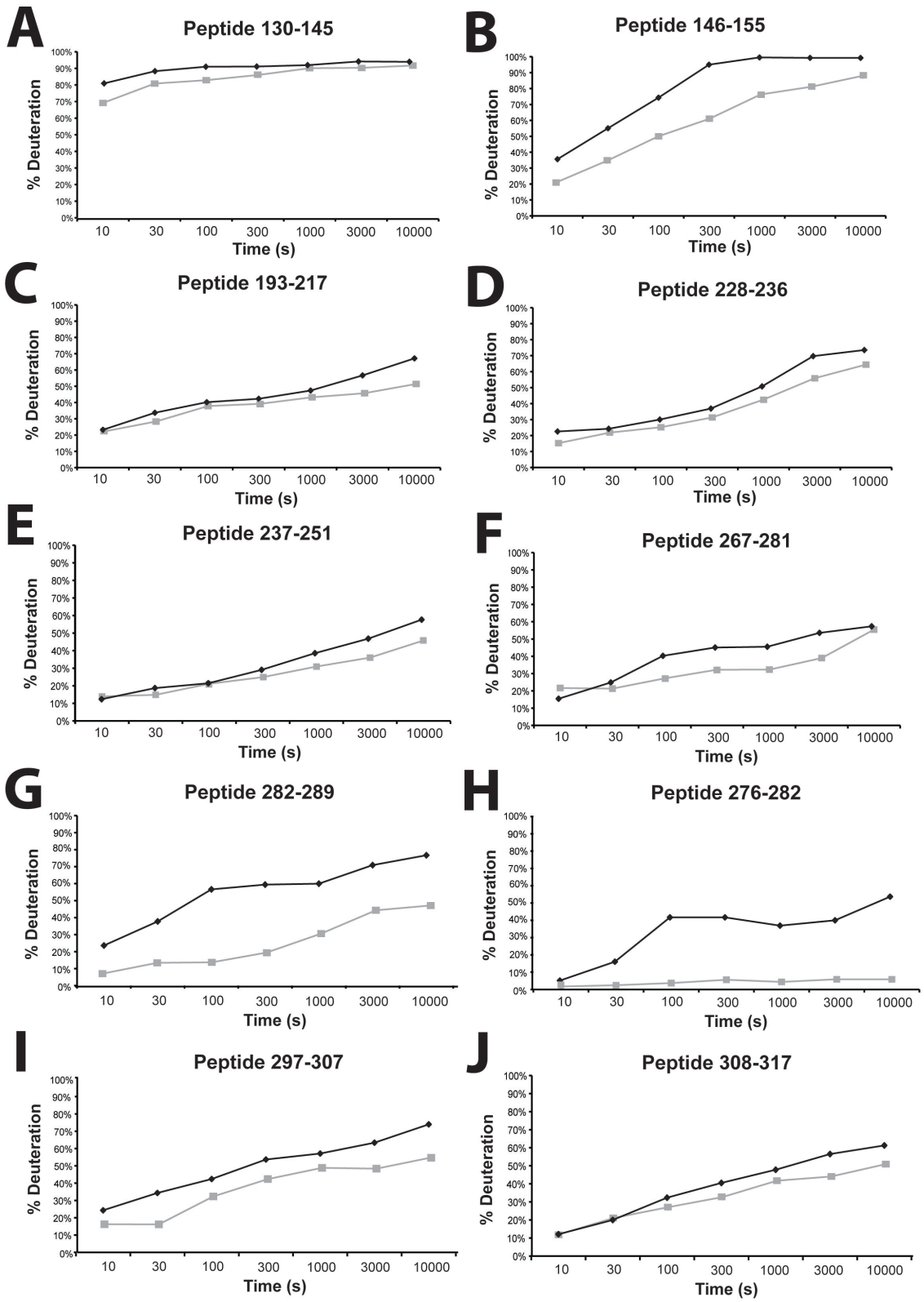
A
Peptide 130-145
B
Peptide 146-155
C
Peptide 193-217
D
Peptide 228-236
E
Peptide 237-251
F
Peptide 267-281
G
Peptide 282-289
H
Peptide 276-282
I
Peptide 297-307
J
Peptide 308-317
% Deuteration
Time (s)
10
30
100
300
1000
3000
10000

Figure 6.10. Peptides within the DSP of laforin that exhibit deuteration changes after glycogen binding. The percent deuteration of peptides in the DSP of wild-type laforin between the APO and glycogen-bound conditions was examined over time. Each point indicates the centroid value of the mass spectra for the peptide at the indicated time with <2% standard deviation. Black diamonds indicate the APO condition while gray squares indicate the glycogen condition. The x-axis has a log scale. Peptides covering residues (**A**) 130-145 and (**B**) 146-155 in the recognition domain, (**C**) 193-217 in the variable loop, (**D**) 228-236 and (**E**) 237-251 in the D loop, (**F**) 267-281 in the PTP loop, (**G**) 282-289 and (**H**) 276-282 in the AYLM motif, and (**I**) 297-307 and (**J**) 308-317 of the R motif exhibited a >10% change in deuteration between the APO and glycogen conditions.

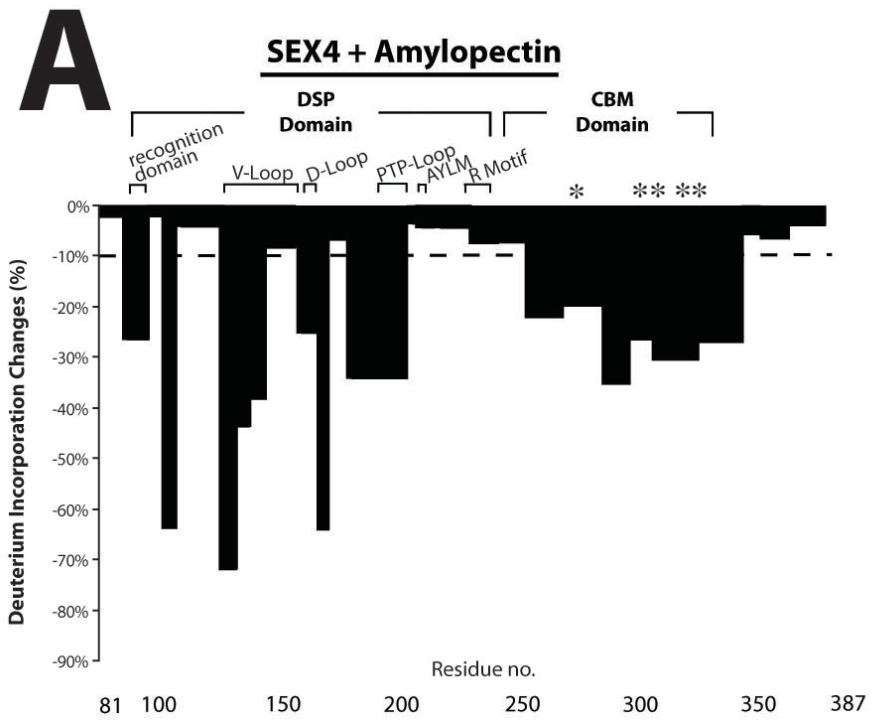
A
SEX4 + Amylopectin
DSP Domain
CBM Domain
recognition domain
V-Loop
D-Loop
PTP-Loop
AYLM
R Motif
Deuterium Incorporation Changes (%)
0%
-10%
-20%
-30%
-40%
-50%
-60%
-70%
-80%
-90%
Residue no.
81
100
150
200
250
300
350
387

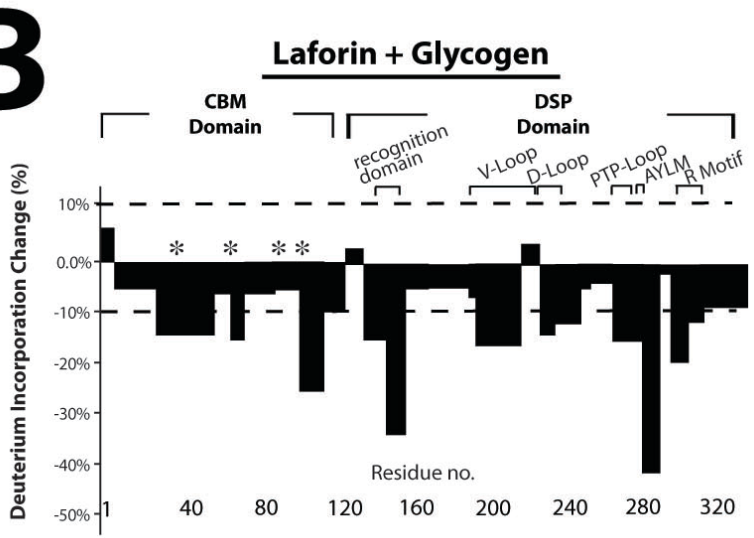
B
Laforin + Glycogen
CBM Domain
DSP Domain
recognition domain
V-Loop
D-Loop
PTP-Loop
AYLM
R Motif
Deuterium Incorporation Change (%)
10%
0.0%
-10%
-20%
-30%
-40%
-50%
Residue no.
1
40
80
120
160
200
240
280
320

Figure 6.11. Maximal percent decreases in deuteration of SEX4 and laforin upon substrate binding. For each peptide across the proteins, the maximum percent changes in deuteration for any time point was determined following SEX4 incubation with amylopectin (**A**) and laforin incubation with glycogen (**B**). Individual peptides are indicated by single black bars. Asterisks indicate the location of CBM residues necessary for substrate binding, with the important regions of the DSP domain labeled. In both panels, a positive value for change indicates increased deuteration while a negative value signifies a decrease in deuteration after glucan binding. Changes greater than 10% (dashed lines) are considered to be significant as <2% standard deviation was observed between experimental replicates.

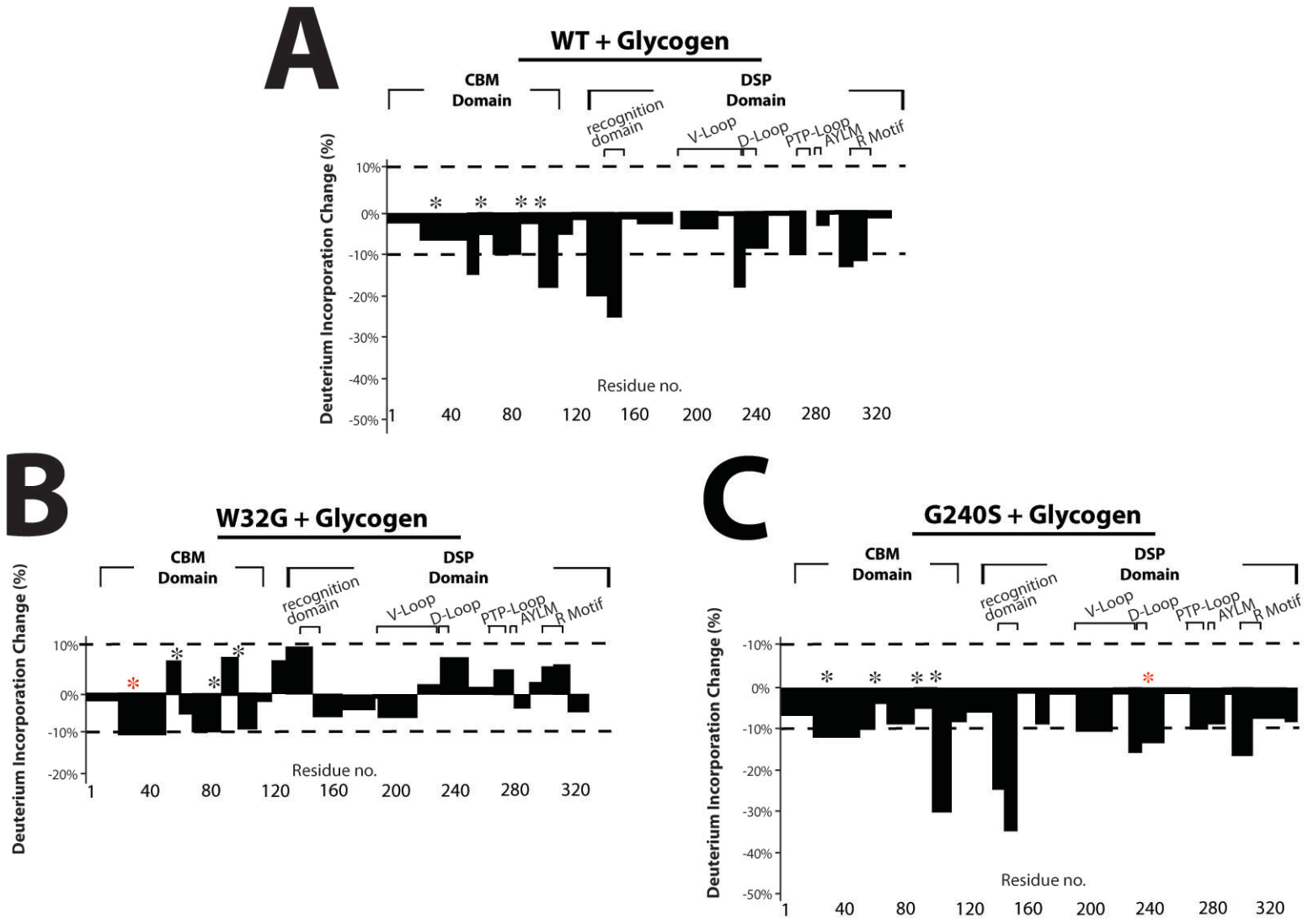
A
WT + Glycogen
CBM Domain
DSP Domain
recognition domain
V-Loop
D-Loop
PTP-Loop
AYLM
R Motif
Deuterium Incorporation Change (%)
10%
0%
-10%
-20%
-30%
-40%
-50%
Residue no.
1
40
80
120
160
200
240
280
320
B
W32G + Glycogen
CBM Domain
DSP Domain
recognition domain
V-Loop
D-Loop
PTP-Loop
AYLM
R Motif
Deuterium Incorporation Change (%)
10%
0%
-10%
-20%
Residue no.
1
40
80
120
160
200
240
280
320
C
G240S + Glycogen
CBM Domain
DSP Domain
recognition domain
V-Loop
D-Loop
PTP-Loop
AYLM
R Motif
Deuterium Incorporation Change (%)
-10%
0%
-10%
-20%
-30%
-40%
-50%
Residue no.
1
40
80
120
160
200
240
280
320

Figure 6.12. The laforin W32G CBM mutant and DSP mutant G240S validate the DXMS method. For each peptide across the proteins, the maximum percent changes in deuteration for any time point was determined following incubation of wild-type laforin (**A**), W32G laforin (**B**), and G240S laforin (**C**) with glycogen. Individual peptides are indicated by single black bars. Black asterisks indicate the location of CBM residues necessary for substrate binding, with the important regions of the DSP domain labeled. In both panels, a positive value for change indicates increased deuteration while a negative value signifies a decrease in deuteration after glucan binding. Changes greater than 10% (dashed lines) are considered to be significant as <2% standard deviation was observed between experimental replicates. The red asterisk in panels **B** and **C** indicates the location of the respective mutation.

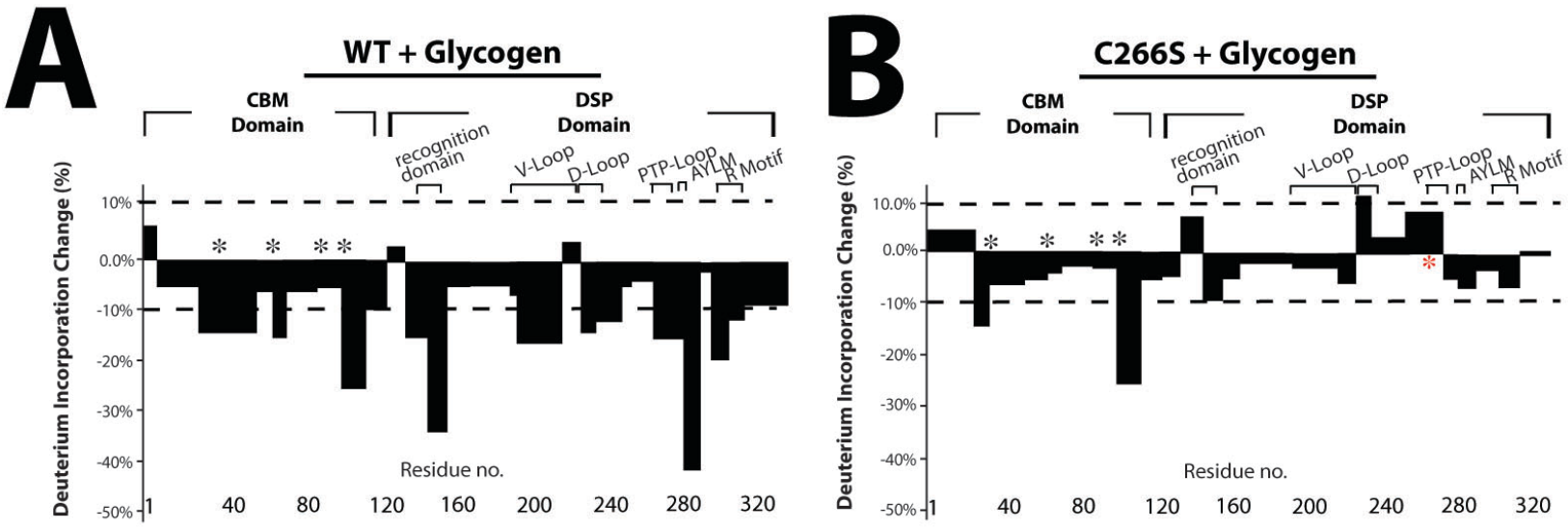
A
WT + Glycogen
CBM Domain
DSP Domain
recognition domain
V-Loop
D-Loop
PTP-Loop
AYLM
R Motif
Deuterium Incorporation Change (%)
10%
0.0%
-10%
-20%
-30%
-40%
-50%
Residue no.
1
40
80
120
160
200
240
280
320
B
C266S + Glycogen
CBM Domain
DSP Domain
recognition domain
V-Loop
D-Loop
PTP-Loop
AYLM
R Motif
Deuterium Incorporation Change (%)
10.0%
0.0%
-10%
-20%
-30%
-40%
-50%
Residue no.
1
40
80
120
160
200
240
280
320

Figure 6.13. The DSP of C266S laforin exhibits disrupted glycogen binding. For each peptide across the proteins, the maximum percent changes in deuteration for any time point was determined following incubation of wild-type laforin (**A**) or inactive C266S laforin (**B**) with glycogen. Individual peptides are indicated by single black bars. Black asterisks indicate the location of CBM residues necessary for substrate binding, with the important regions of the DSP domain labeled. In both panels, a positive value for change indicates increased deuteration while a negative value signifies a decrease in deuteration after glucan binding. Changes greater than 10% (dashed lines) are considered to be significant as <2% standard deviation was observed between experimental replicates. The location of the C266S mutation is denoted by a red asterisk in panel **B**.

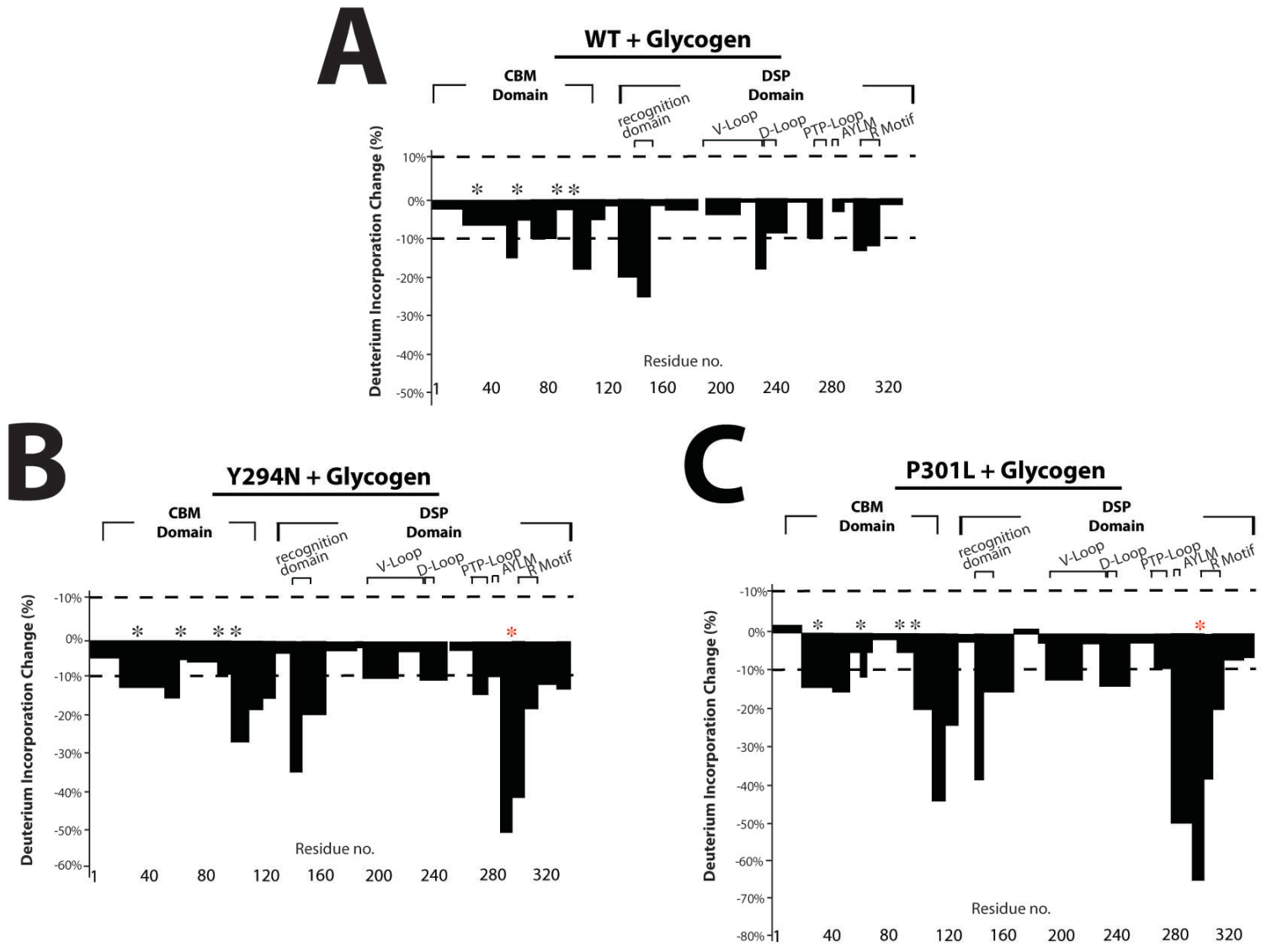
A
WT + Glycogen
CBM Domain
DSP Domain
recognition domain
V-Loop
D-Loop
PTP-Loop
AYLM
R Motif
Deuterium Incorporation Change (%)
10%
0%
-10%
-20%
-30%
-40%
-50%
Residue no.
1
40
80
120
160
200
240
280
320
B
Y294N + Glycogen
CBM Domain
DSP Domain
recognition domain
V-Loop
D-Loop
PTP-Loop
AYLM
R Motif
Deuterium Incorporation Change (%)
-10%
0%
-10%
-20%
-30%
-40%
-50%
-60%
Residue no.
1
40
80
120
160
200
240
280
320
C
P301L + Glycogen
CBM Domain
DSP Domain
recognition domain
V-Loop
D-Loop
PTP-Loop
AYLM
R Motif
Deuterium Incorporation Change (%)
-10%
0%
-10%
-20%
-30%
-40%
-50%
-60%
-70%
-80%
Residue no.
1
40
80
120
160
200
240
280
320

Figure 6.14. The Y294N and P301L mutants exhibit strengthened glycogen binding. For each peptide across the proteins, the maximum percent changes in deuteration for any time point was determined following incubation of wild-type laforin (**A**), Y294N laforin (**B**), and P301L laforin (**C**) with glycogen. Individual peptides are indicated by single black bars. Black asterisks indicate the location of CBM residues necessary for substrate binding, with the important regions of the DSP domain labeled. In both panels, a positive value for change indicates increased deuteration while a negative value signifies a decrease in deuteration after glucan binding. Changes greater than 10% (dashed lines) are considered to be significant as <2% standard deviation was observed between experimental replicates. The red asterisk in panels **B** and **C** indicates the location of the respective mutation.

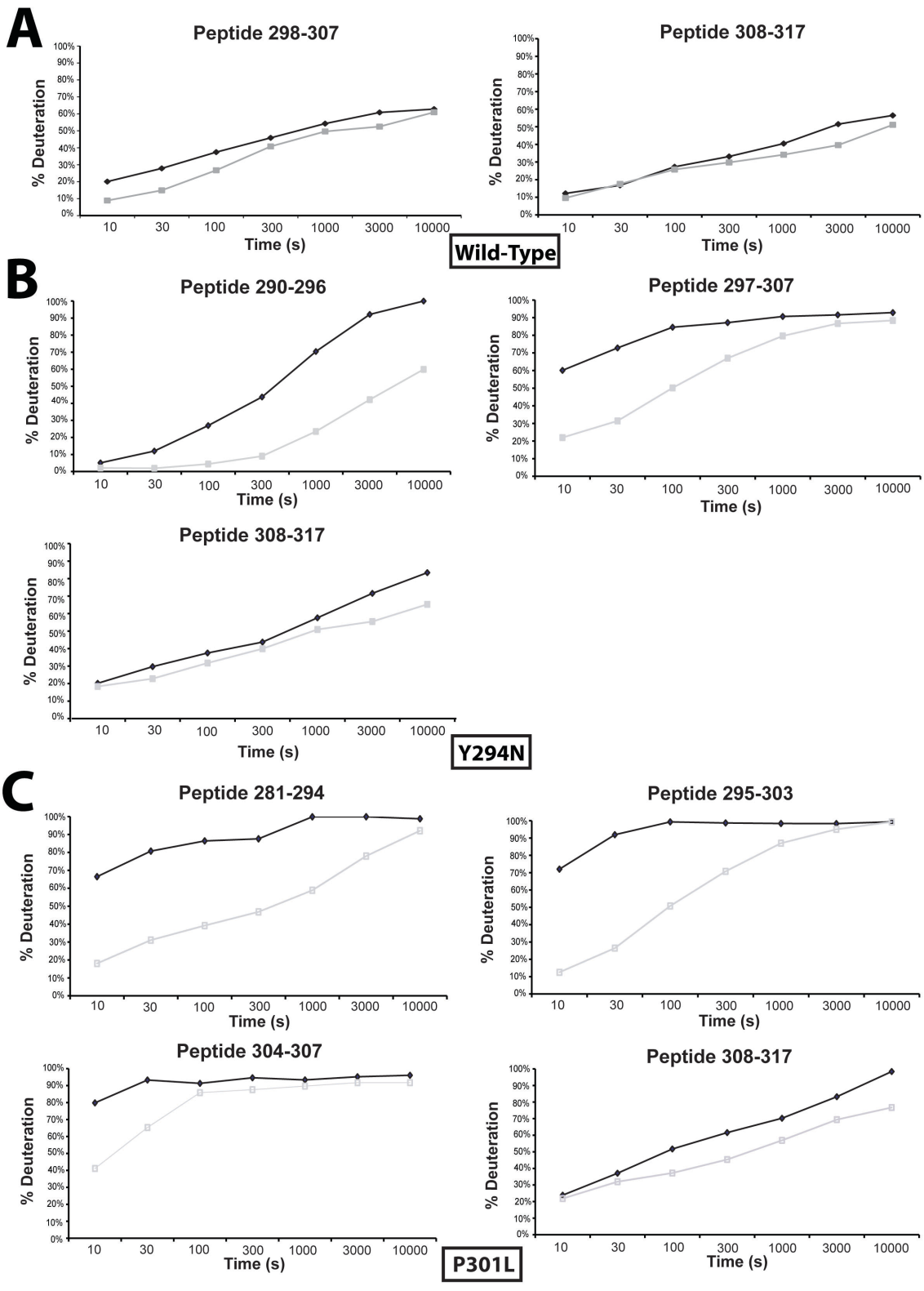
A
Peptide 298-307
Peptide 308-317
% Deuteration
Time (s)
Wild-Type
B
Peptide 290-296
Peptide 297-307
Peptide 308-317
Y294N
C
Peptide 281-294
Peptide 295-303
Peptide 304-307
Peptide 308-317
P301L

Figure 6.15. Peptides within the R motif of the Y294N and P301L mutants that exhibit decreases in deuteration after glycogen binding. The peptides in the R motif of wild-type laforin (**A**), Y294N laforin (**B**), and P301L laforin (**C**) that exhibited a >10% change in deuteration between the APO and glycogen conditions. Each point indicates the centroid value of the mass spectra for the peptide at the indicated time with <2% standard deviation. Black diamonds indicate the APO condition while gray squares indicate the glycogen condition. The x-axis has a log scale. **A.** Peptides covering residues 298-307 and 308-317 of wild-type laforin. **B.** Peptides covering residues 290-296, 297-307, and 308-317 of Y294N laforin. **C.** Peptides covering residues 281-294, 295-303, 304-307, 308-317 of P301L laforin.

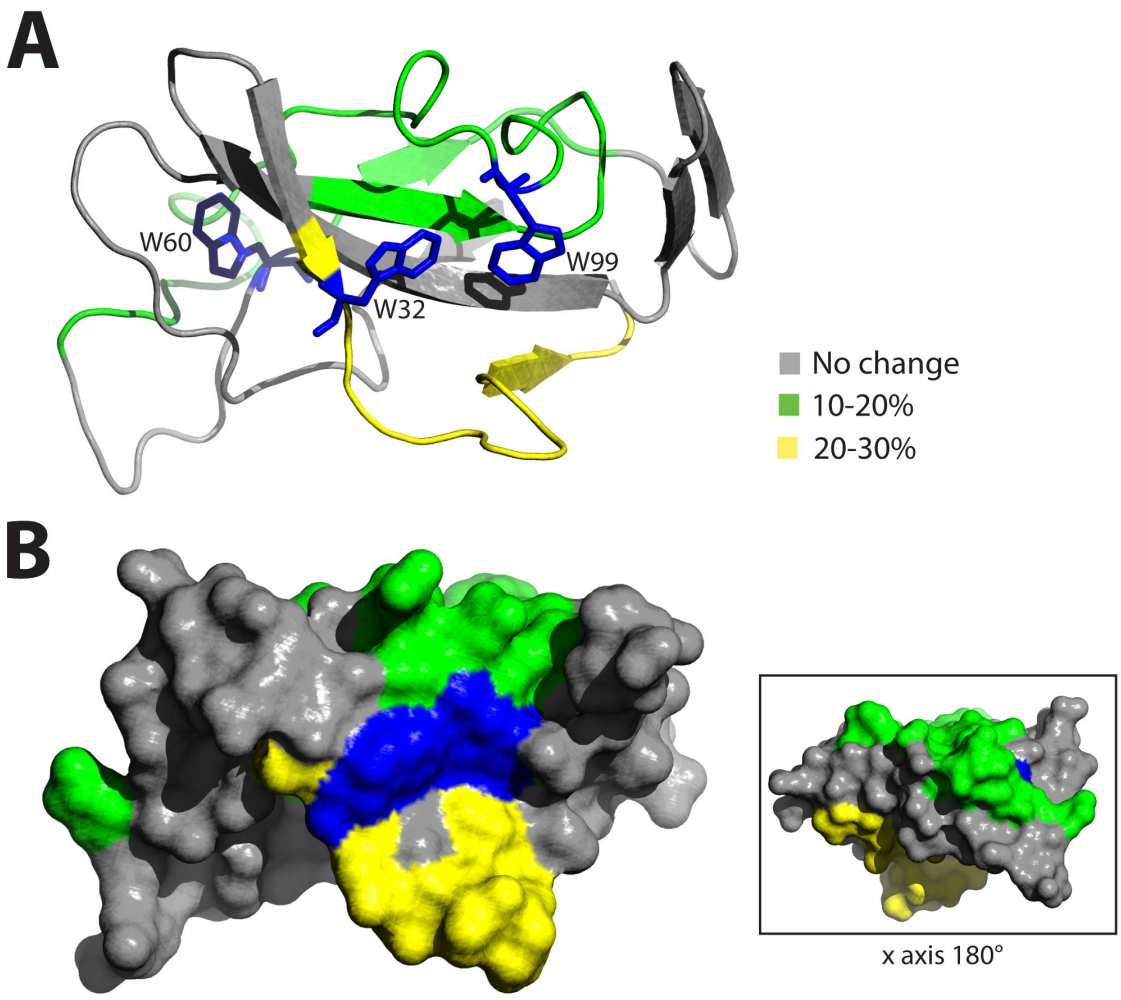

Figure 6.16. Homology model of the CBM of wild-type laforin with binding dynamics. A. Ribbon structure of the laforin CBM homology model with the percent decreases in deuteration from Figure 6.10B mapped onto it. The percent change corresponds to the inset. The Trp32, Trp60, and Trp99 residues are indicated in blue. **B**. Surface view of the laforin CBM model with the percent decreases in deuteration mapped onto it. Percent change colors are as in panel A. The inset is a view of the surface after the model has been rotated 180° on the x-axis.

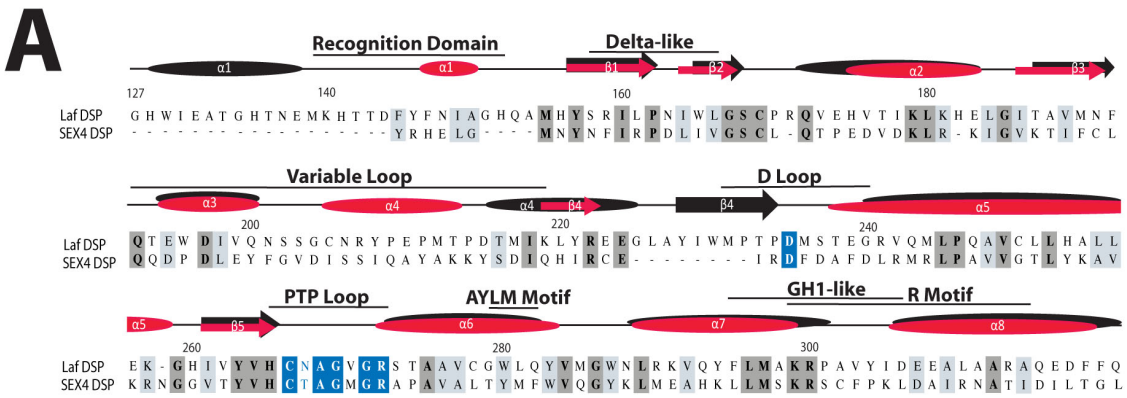
A
Recognition Domain
Delta-like
Variable Loop
D Loop
PTP Loop
AYLM Motif
GH1-like
R Motif
Laf DSP
SEX4 DSP

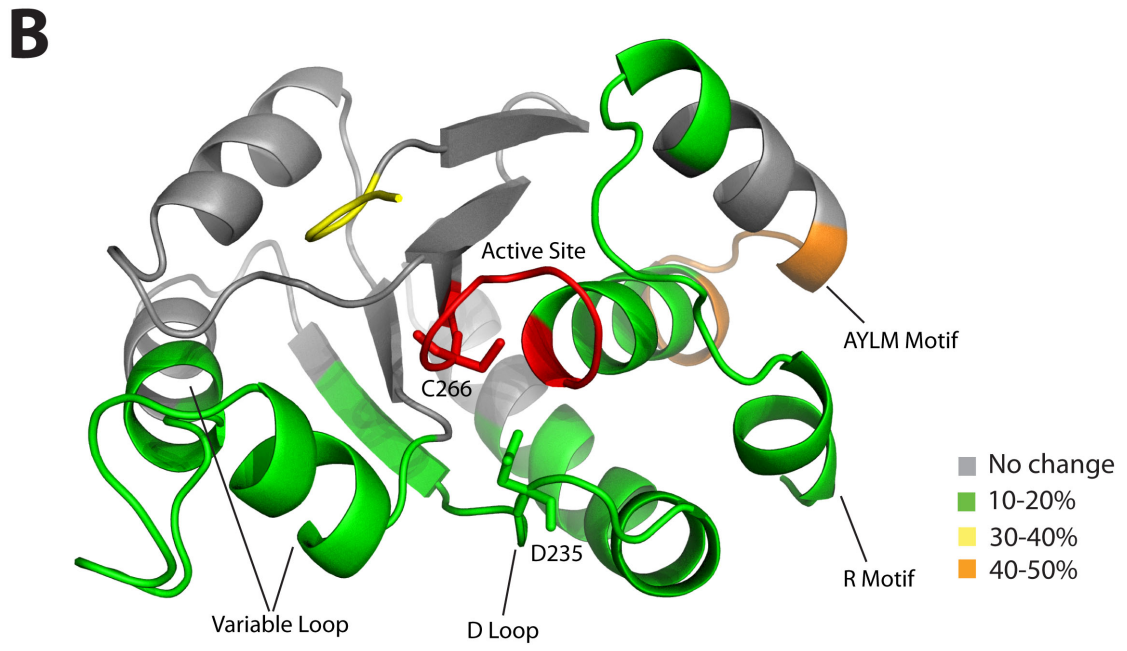
B
Active Site
C266
AYLM Motif
R Motif
D235
Variable Loop
D Loop
No change
10-20%
30-40%
40-50%

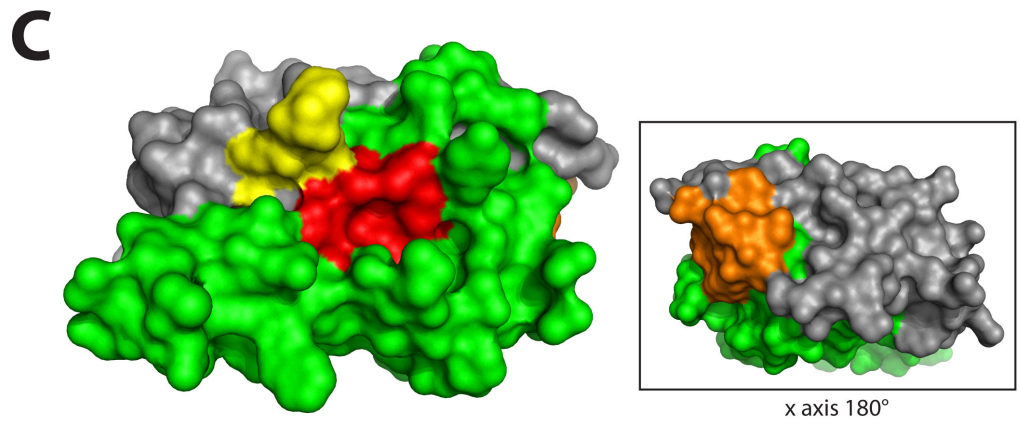
C
x axis 180°

Figure 6.17. Homology model of the DSP of wild-type laforin with binding dynamics. A. Alignment of the DSP domain of laforin and SEX4. Above the amino acids is the comparison between the predicted secondary structure of laforin (shown in black) and the known structure of SEX4 (shown in red). The α-helices and β-sheets are numbered per accepted DSP domain nomenclature (*2*). The residues boxed in blue are invariant DSP residues (*55*). **B**. Ribbon structure of the laforin DSP homology model with the percent decreases in deuteration from Figure 6.10B mapped onto it. The percent change in deuteration corresponds to the inset. The DSP regions of interest are labeled and the active site highlighted in red. The recognition domain is not included in the model due to low sequence similarity with SEX4. The residues in the active site also exhibit a 10-20% decrease in deuteration as shown in green. The position of the catalytic Cys266 residue in the PTP loop and the invariant Asp235 residue in the D loop are indicated. **C**. Surface view of the laforin DSP model with the percent decreases in deuteration mapped onto it. Percent change colors are as in panel B. The inset is a view of the surface after the model has been rotated 180° on the x-axis.

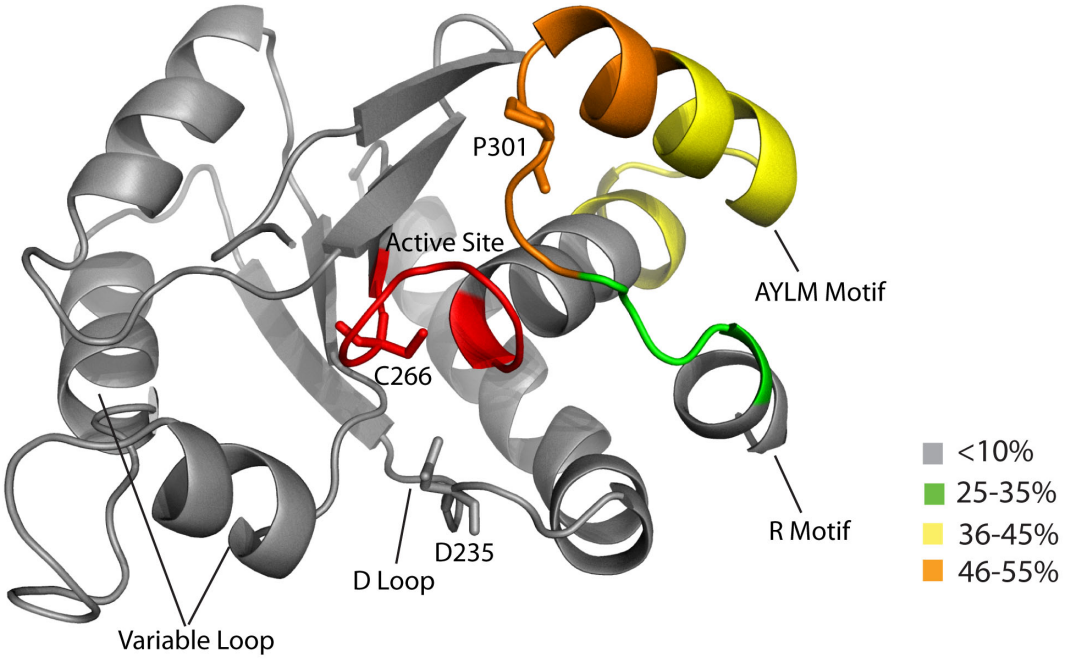

Figure 6.18. Alteration of the binding dynamics of laforin resulting from the P301L mutation. The difference in the maximal percent change in deuteration between corresponding regions of wild-type laforin and the P301L mutant from Figure 6.13 was calculated and mapped onto the laforin DSP model. The difference in maximal deuteration is indicated by the inset. The DSP regions of interest are labeled and the location of the catalytic Cys266, invariant Asp235, and mutated Pro301 indicated. The active site is highlighted in red.

CHAPTER 7: CONCLUSIONS AND FUTURE DIRECTIONS

Application of the laforin bioassay with Lafora disease patients.

Currently, experimental therapies for Lafora disease (LD) patients are still in the early stages of development. Putative therapies include the downregulation of protein targeting to glycogen (PTG), the glycogen-targeting subunit of PP1, a protein directly involved in the regulation of glycogen metabolism. Depletion of PTG in a mouse model lacking laforin resulted in the downregulation of glycogen synthesis concurrent with an almost complete disappearance of LBs. These mice also exhibited decreased neuronal cell death and myoclonus (*156*). Similar decreases in epilepsy and the formation of LBs, and more importantly, a lack of neurodegeneration, is observed in laforin-deficient mice in which glycogen synthase is also lacking (*117*). The compound sirolimus is known to partially inhibit glycogen synthase, and is currently in clinical use for another neurological disease known as tuberous sclerosis (*7*). Sirolimus may thus prove applicable in preventing the progression of LD.

Additionally, the use of gene therapy to express the *EPM2A* and *EPM2B* genes and the delivery of these genes using Trojan horse liposomes (also called PEGylated immunoliposomes) are currently being explored (*115*). Dr. Eain Cornford of the Brentwood Biomedical Research Institute is currently exploring the efficacy of *EPM2A* gene delivery to the brains of mice lacking laforin using intravenous administration of immunoliposomes (http://projectreporter.nih.gov). If this non-viral delivery system is successful in animal models in terms of alleviation of the LD phenotype, an immunoliposome-based cure for LD could be developed for clinical use. The laforin bioassay that we developed could be used to monitor expression of the *EPM2A* gene and/or delivery of protein via immunoliposomes. One could collect tissue from the brains of mice receiving viral-based therapies and/or immunoliposome-based therapy to determine the successful delivery of the *EPM2A* gene to the brain.

In Chapter 5: Effects of Aminoglycosides on Nonsense Mutations in Laforin and Malin as a Therapeutic Option for Lafora Disease, we assessed the efficacy of

aminoglycosides for the readthrough of nonsense mutations in laforin and malin that cause LD. As our i*n vitro* readthrough model was not optimal for the assessment of gentamicin, amikacin, or PTC124-mediated readthrough, fibroblasts collected from LD patients possessing nonsense mutations will be required to fully assess the efficacy of these compounds. We are currently collaborating with Dr. Antonio Delgado-Escueta at the University of California Los Angeles School of Medicine in initiating a clinical trial involving the application of intravenous gentamicin to LD patients possessing nonsense mutations.

This phase I clinical study will evaluate both the safety and efficacy of a dose-escalation protocol of gentamicin application. Over the course of a year, six LD patients possessing several different nonsense mutations in *EPM2A* will be treated with intravenous gentamicin for ten day blocks every three months. Each patient would receive 7 mg/kg gentamicin in 100 mL 5% dextrose for 30 minutes every 24 hours. The pharmacokinetic response of each patient will be used to adjust the applied dose in order to achieve the peak serum concentration of 30 μg/mL found to be effective in other trials (*131, 165*). This protocol will define the dose response relationship for short-term safety as well as preliminary efficacy effects.

Prior to gentamicin application in patients, the response of individual patients to the drug will be assessed following collection and treatment of fibroblasts. Our bioassay for laforin activity can then be applied to measure an increase in functional laforin protein levels following treatment. If *in vitro* work in LD patient fibroblasts demonstrates a response to gentamicin treatment, is it likely that gentamicin will cause readthrough in the patient, as *in vitro* and *in vivo* readthrough of specific nonsense mutations causing cystic fibrosis and Duchenne muscular dystrophy has been found to correlate (*15, 131*). In addition to assessing the efficacy of intravenous gentamicin application in LD patients based on the electroclinical and neurologic state of each patient, a biopsy of skin fibroblasts will be obtained following each dosing regimen in order to determine an increase in laforin glucan phosphatase activity using the laforin bioassay.

Structural aspects of laforin and the impact of disease mutations.

Our work examining the structure and binding aspects of the glucan phosphatase laforin revealed that while this human protein exhibits some mechanistic similarities with the well-characterized plant glucan phosphatase SEX4, laforin also exhibits critical structural and mechanistic idiosyncrasies. The crystal structure of SEX4 reveals that the AYLM motif in the DSP of SEX4 has been adapted for interdomain interaction (*160*). Similarly, the AYLM motif of laforin may interact with the Trp60 residue of the CBM in order to facilitate the association of the CBM and DSP domains of laforin. Likewise, additional conserved domains within the DSP domains of laforin and SEX4 are necessary for the binding of the DSP domain to glucans and presentation of these glucans to the active site.

However, laforin exhibits distinct mechanistic differences with SEX4 in the DSP domain. Using DXMS, we found that the R motif in the DSP of laforin is involved in substrate interaction, while the R motif does not play such a role in SEX4 (*77*). In addition, laforin possesses a CBM20 domain while SEX4 possesses a CBM48 domain. While these CBM domains are within the same evolutionarily related clan (*25, 35*), SEX4 possesses residues in the CBM involved in glucan binding (*160*) that laforin does not. Our DXMS results and homology model of laforin provide insight into the uncharacterized binding mechanism of the CBM domain of laforin and the importance of the Trp32 and Trp99 residues in forming a hydrophobic glucan binding site. We found that laforin prefers soluble glucan chains such as those found in glycogen over insoluble, crystalline glucans, similar to other enzymes featuring CBM20 domains (*99*). We also observed that the Tyr294 and Pro301 residues in the DSP domain of laforin appear to be crucial for shuttling of these chains through the active site. The hydrophobic binding site in the CBM of laforin may therefore form a contiguous glucan-binding channel with the DSP domain as seen in SEX4 (*160*).

The biochemical and DXMS analyses of the W32G mutation within the CBM of laforin and the C266S mutation within the DSP of laforin provide evidence that the two domains can function independently, but may perform synergistic action via interaction between Trp60 and the AYLM motif. The fact that these domains can function independently supports the presence of a flexible linker between the CBM

and DSP domain of laforin, a structural feature not present in SEX4 (*160*). This flexible linker in addition to the unique involvement of the R motif of laforin in substrate interaction may contribute to the faster on/off substrate binding dynamics that laforin exhibits over SEX4. However, in order to confirm the above hypotheses, a crystal structure of laforin is required.

Our DXMS analyses of wild-type laforin reveal that the C-terminal end of the protein encompassing residues 318-331 of laforin and the HIS_6 epitope tag utilized to purify the protein is >70% deuterated at the earliest time point studied. This finding indicates that residues 318-331 of laforin in addition to those of the C-terminal HIS_6 tag are unstructured and highly exposed to solvent, and likely exhibit significant thermodynamic fluctuations in solution. We hypothesized that this highly mobile segment of laforin would likely obstruct the packing of proteins required for crystal formation. In addition, we recently demonstrated that the Cys329 residue plays a role in laforin dimerization (*125*). It is possible that laforin does not crystallize because of its dimerization. Therefore, we generated a C329X mutant of laforin featuring an adjacent protease site to remove the C-terminal HIS_6 tag utilized for purification. We found that this construct yields crystals for which we have obtained data at a resolution of 2.3Å. However, we have not yet been unable to determine the structure of laforin. Laforin is different enough from other phosphatases (including SEX4) that molecular replacement is not useful. Additionally, we have been unable to generate crystals from protein with selenium incorporated. Therefore, we will attempt to soak laforin crystals in heavy atoms in order to obtain a dataset that will allow us to solve the phase problem.

Upon obtaining the crystal structure of laforin, we can assess the presence of a flexible linker as well as the interaction of the Trp60 residue of the CBM with the AYLM motif of the DSP. The role of the AYLM motif in interdomain interaction in laforin as well as SEX4 may then prove a general feature of glucan phosphatases. The crystal structure of SEX4 illustrates that the variable loop of the protein possesses α-helical structure, while this region is an unstructured loop in other protein DSPs such as VHR (*160, 177*). Our homology model of the DSP of laforin

indicates that the variable loop of laforin also possesses α-helical structure. A crystal structure of laforin would confirm this observation, and support our hypothesis that the α-helical structure of the variable loop is a feature specific to the glucan phosphatases and may confer specificity for glucan substrates.

Our study of the W32G and C266S mutations in laforin also suggests that the CBM of laforin makes initial contact with glucan substrates, bringing the DSP into proximity to the glucan to allow binding by the DSP to occur. We propose mutagenesis and DXMS studies of the AYLM motif of laforin in order to determine if the disruption of this motif prevents the synergy of the CBM and DSP domain necessary for interaction of the DSP with glucan. If we also observe that mutation of Trp60 in the CBM does not impact binding of the CBM while disrupting binding of the DSP, we can confirm the importance of the AYLM motif of laforin in interdomain interaction.

Our bioinformatics analyses of laforin and SEX4 indicate that the R motif and variable loop within the DSP domains of these enzymes share sequence homology with the active sites of glycosyl hydrolases. To examine the role these sequences play in substrate interaction by the DSP, we determined the impact of the Y294N and P301L LD mutations within the GH-like region in the R motif of laforin on glucan binding. Our biochemical and DXMS analyses indicate that these mutations drastically alter the interaction of laforin with glycogen, supporting a role of this GH-like sequences in glucan binding. In utilizing a crystal structure of laforin, we could determine if the GH-like residues in the R motif are indeed positioned to interact with substrate as our DXMS work and homology model suggest.

Our lab has also worked to characterize the GH-like domain in the variable loop. This GH domain is shared between laforin and SEX4 and now a recently discovered glucan phosphatase found in *Arabidopsis*, Like SEX4 2 (LSF2). LSF2 features all of the domains found in SEX4 with the notable exception of the CBM domain (Figure 7.1A). How this protein is this able to bind glucans (Figure 7.1B) in the absence of a CBM domain is curious. Our lab discovered that aromatic residues within the variable loop make direct contact with a glucan substrate in the LSF2

crystal structure (*104*). Additional work by David Meekins in our lab has demonstrated that aromatic residues within the variable loop are required for glucan phosphatase activity (Figure 7.1C). These results support a role of the GH-like sequences in glucan binding in the glucan phosphatases. These GH-like regions may also prove to be a general feature of glucan phosphatases.

Our studies of the Y294N and P301L mutations in laforin indicate that these mutations cause laforin to become trapped in glycogen. Now that we have generated a method to purify large yields of laforin, we can perform additional experiments with wild-type laforin and the Y294N and P301L mutants in order to determine the impact of the strengthened glucan binding observed in these mutants. We will determine the glucan-binding constants and kinetics of these LD mutations using Surface Plasmon Resonance (SPR) and Isothermal Titration Calorimetry (ITC) with our collaborator and expert in determining the binding constants and kinetics of glucan phosphatases, Dr. Birte Svensson. This work, in conjunction with a crystal structure of laforin, will aid in the design of small molecules that could decrease the affinity of laforin for glycogen and thus alleviate the LD phenotype.

We have designed and optimized methodologies to immobilize laforin on SPR chips in order to perform binding experiments. We will utilize multiple oligosaccharides in conjunction with a Biacore T100 (GE Healthcare), and independently verify our results utilizing an ITC_{200} calorimeter (GE Healthcare). These experiments, performed using structurally varied glucans such as β-cyclodextrin, glycogen, and amylopectin, will determine the binding affinities and kinetic constants of wild-type laforin for the various glucan substrates. This work will also define the interaction of the Y294N and P301L mutants with multiple glucans at a molecular resolution.

The biochemical and structural analyses that we have performed in this work provide important insight into the molecular etiology behind several LD mutations that impact a range of laforin functions, including CBM interaction with glucans, shuttling of glucan chains through the DSP active site, and interaction with binding partners. We have also identified potential therapeutics for a subset of LD patients,

as well as a means to assess the efficacy of these treatments. While additional work is required to lend support to our findings, our current work has provided important initial analyses that will facilitate the development of crucial therapies for a devastating disease.

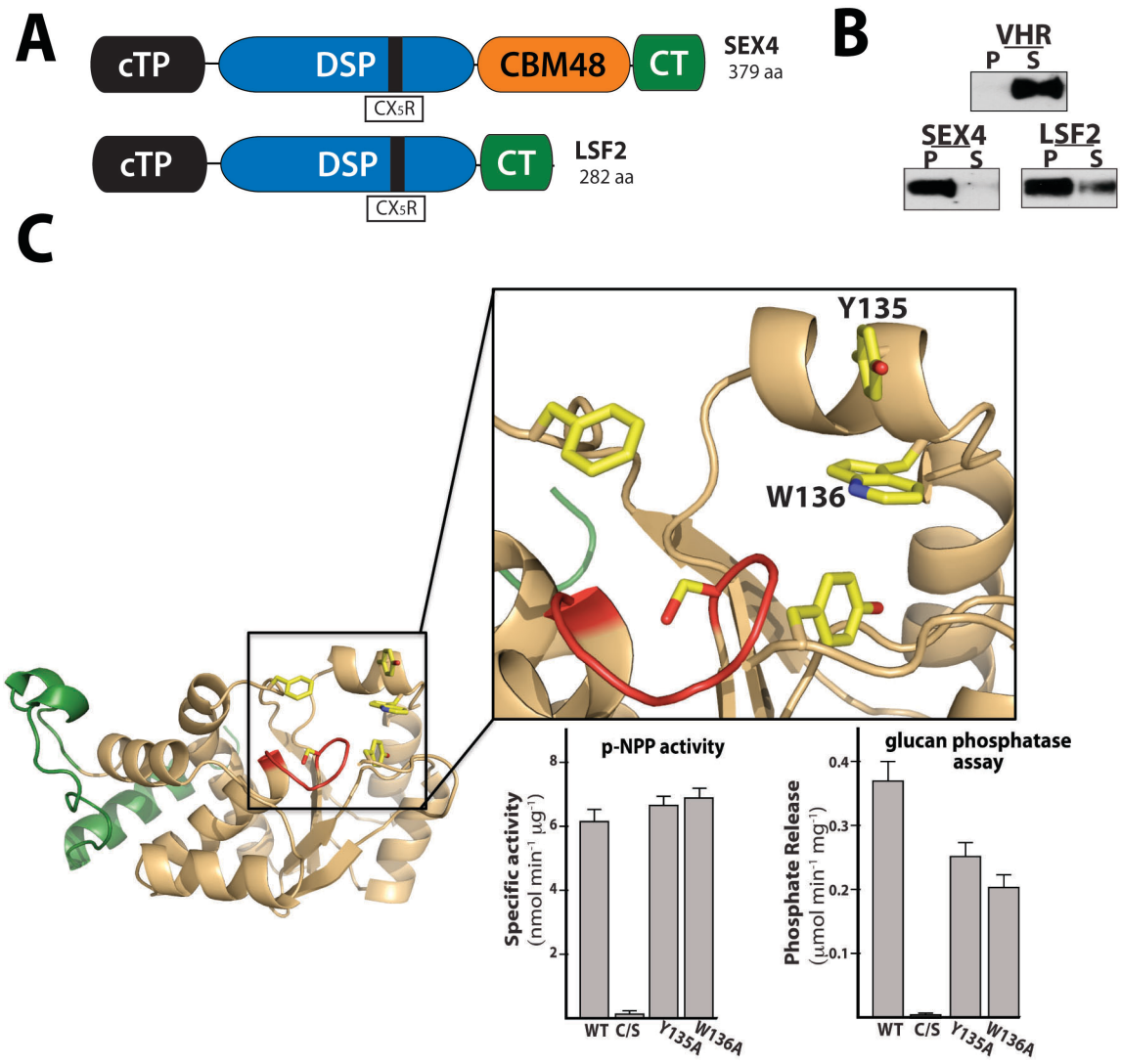
A
cTP
DSP
CBM48
CT
SEX4
379 aa
CX5R
cTP
DSP
CT
LSF2
282 aa
CX5R
B
VHR
P S
SEX4
P S
LSF2
P S
C
Y135
W136
p-NPP activity
Specific activity
(nmol min-1 µg-1)
8
6
4
2
WT C/S Y135A W136A
glucan phosphatase
assay
Phosphate Release
(µmol min-1 mg-1)
0.4
0.3
0.2
0.1
WT C/S Y135A W136A

Figure 7.1. The role of the GH-like motif in the variable loop of LSF2. A. SEX4 contains an N-terminal domain to target it to the chloroplast (cTP; chloroplast targeting peptide) (*112*), a dual-specificity phosphatase (DSP) domain featuring the canonical DSP CX_5R active site motif (indicated by a black bar), a CBM48 domain, and a C-terminal domain (CT) critical for folding (*160*). LSF2 contains the same domains as SEX4 and in the same orientation, although the CBM48 domain is missing (*104*). **B**. A glucan binding assay utilizing amylose resin was performed using LSF2 and SEX4. VHR, which is unable to bind glucans, was used a control. Like SEX4, LSF is pulled down in the amylose pellet, while VHR remains in the supernatant as expected. P; pellet. S; supernatant. **C**. The crystal structure of LSF2 lacking the cTP is depicted, with tan coloring indicating the DSP domain and green coloring indicating the CT domain. The active site is shown in red. The inset highlights the variable loop of LSF2 possessing the GH-like motif. The aromatic residues Tyr135 and Trp136 are indicated. The *p*NPP and specific glucan phosphatase activity of LSF2 following mutation of these residues to alanine is depicted. Wild-type and inactive C193S LSF2 were included in these assays as a control. Specific glucan phosphatase activity is decreased when Tyr135 and Trp136 are mutated to alanine, while *p*NPP activity is not changed. These results indicate that these residues are specifically involved in glucan binding and not catalysis. The above work was performed by David Meekins.

APPENDIX 1: SUPPLEMENTARY PROTOCOLS

pNPP Assay.

Reagents.

4-Nitrophenylphosphate di(tris) salt (Sigma, St. Louis, MO, USA)

DL-Dithiothreitol (Sigma, St. Louis, MO, USA)

Sodium Acetate (Sigma, St. Louis, MO, USA)

Trizma (Tris) Base (Sigma, St. Louis, MO, USA)

Bis-Tris (Sigma, St. Louis, MO, USA)

Sodium Hydroxide (Fisher Scientific, New Jersey, USA)

TrUView Cuvettes (Bio Rad, USA)

0.5 mL Eppendorf tubes (USA Scientific, Orlando, FL, USA)

0.2 μ syringe filter (Millipore, Billerica, MD, USA)

10 mL syringes (BD, Franklin Lakes, NY, USA)

Procedure.

1) Thaw enzyme aliquots on wet ice.
2) Prepare 1X assay buffer for each pH to be tested, adding DTT to a final concentration of 1 mM.
3) Dilute enzymes to 50 to 1000 ng/μL with appropriate 1X assay buffer(s). The dilution of each enzyme is based upon its purity and rate of activity so that product formation remains in the linear range of detection during the assay.
4) Each reaction replicate is performed in a final volume of 50 μL, with a set of at least 3 replicates for each enzyme and pH to be analyzed. If 1 μl of diluted enzyme is to be added, then each reaction consists of:

- 33 μL H_2O
- 10 μL 5X assay buffer of optimal enzyme pH
- 1 μL 100 mM DTT
- 5 μL 0.5 M *p*NPP

5) Add 1 μL of diluted enzyme to each reaction, vortex thoroughly to mix, and place the tube at 37°C. Begin timing the reaction once enzyme is added to the first tube, and be consistent with timing as enzyme is added to subsequent reactions. Four replicates per enzyme/ pH with a time interval of 15 seconds for enzyme addition to each replicate is suggested.
6) Incubate the reactions at 37°C for 10 minutes. After 10 minutes, add 200 μL of 0.25N NaOH to quench the reactions. Vortex the tubes on their sides to mix any liquid that has evaporated to the lid. Be sure to add the base at identical time intervals as the protein was added to the reactions and in the same order.
7) Read the absorbance (*A*) of the reactions at 410 nm, using the appropriate blank (such as a control reaction with an inactive phosphatase). Cuvettes can be rinsed and reused.
8) The molar absorption coefficient (ε) of the product phenolate ion is 17,800 M^{-1} cm^{-1}. Use Beer's Law ($A=\varepsilon lc$) with a path length (l) of 1 cm to find the concentration of phenolate ion in moles per liter (c) and finally the activity (μmol phosphate released/min per μmol of protein) of each replicate, taking the average.

Tips for success.

1) While unessential, adding EDTA to 5X assay buffer will chelate iron, which can react with thiols (DTT) to form free radicals that inactivate PTPs (*108*).
2) Although unessential, use of uncharged reaction tubes composed of uncoated polypropylene or polystyrene and addition of Triton-X-100 (peroxide free) or BSA (1 mg/mL) to an optimal concentration of 0.01% prevents binding of a phosphatase to itself or to reaction tubes to preserve phosphatase activity over time (*108*).
3) The pK_a of buffer salts for the phosphatase assay buffer (common buffers include HEPES, acetate, glycine, or Tris) for each phosphatase studied should correlate with the optimal pH of that phosphatase ±0.5 units. A mixture of

buffer salts is also desirable in pH studies to maintain buffering over a wide pH range, using the lowest concentrations of these salts possible to maintain pH during the dephosphorylation reaction (*16, 103*).

4) While unessential for phosphatase activity, adjustment of the ionic strength of the assay buffer to 150 mM with sodium chloride to mimic conditions in the cell can affect inhibitor potency or substrate affinity either positively or negatively (*108*).
5) The absorption measurement of the terminated phosphatase reaction must be within the linear range of the spectrophotometer (*108*). If the absorption is too high, decrease the incubation time of the reaction and/or the amount of protein used to ensure product formation is linear over the reaction time.
6) Tubes can be prewarmed to 37°C for shorter reaction times.

Recipes.

* All prepared in MilliQ H_2O 18.2 MΩcm

* Be sure to allow *p*NPP to warm to room temp prior to opening, as the compound is hydroscopic. *p*NPP stock solutions should be stored at -20°C to prevent non-enzymatic hydrolysis (*103*), and should not be added to assay buffer until experiments (*108*).

<u>5X Stock Assay Buffer (Store 22°C).</u>

0.5 M Sodium Acetate

0.25 M Bis-Tris

0.25 M Tris

pH to desired pH with HCl

<u>0.5M *p*NPP and 100 mM DTT (Store -20°C).</u>

Prepared by dissolving into MilliQ H_2O 18.2 MΩcm. Sterile-filter prior to use.

Troubleshooting.

1) Little to no phosphatase activity.

While most buffers are compatible with phosphatases (*103*), buffering components should be tested for an effect on phosphatase activity. When assaying activity of any enzyme, it is important to consider pH, ionic strength, and buffer choice, as these attributes can affect the kinetic parameters of an enzyme. Phosphatases are typically active in a wide pH range (pH 4 to 9), so buffer choice to maintain desired pH during the phosphatase reaction is essential. The presence of a reducing agent during PTP purification, storage, and analysis is also necessary to prevent inactivation of the catalytic cysteine residue by oxidation (*103, 109*). Also, be sure to vortex the reaction thoroughly prior to incubation at 37°C. Finally, use varying amounts of enzyme to determine how much enzyme is required to obtain detectable linear activity over time. Alternatively, reaction time can be varied while the amount of enzyme is held constant.

Equipment.

Beckman Coulter DU370 UV/Vis Spectrophotometer (Beckman Coulter, Indianapolis, IN, USA)

Temperature-controlled hotplate (Fisher Scientific, New Jersey, USA)

Malachite Green Standard Curve and Assay.

Reagents.

Potassium Phosphate Monobasic (Fisher, Scientific, New Jersey, USA)
Sodium Hydroxide (Fisher Scientific, New Jersey, USA)
Ammonium Molybdate Tetrahydrate (Sigma, St. Louis, MO, USA)
Malachite Green Carbinol Hydrochloride (Sigma, St. Louis, MO, USA)
Tween 20 (Acros, New Jersey, USA)
Grade 5 Filter Paper (Whatman, Clifton, NJ, USA)
4N Hydrochloric Acid (Fisher Scientific, New Jersey, USA)
0.5 mL Eppendorf tubes (USA Scientific, Orlando, FL, USA)
0.2 μm syringe filter (Millipore, Billerica, MD, USA)
10 mL syringes (BD, Franklin Lakes, NY, USA)
TrUView Cuvettes (Bio Rad, USA)
N-Ethylmaleimide (Fluka, St. Louis, Mo, USA)
DL-Dithiothreitol (Sigma, St. Louis, MO, USA)
Sodium Acetate (Sigma, St. Louis, MO, USA)
Trizma (Tris) Base (Sigma, St. Louis, MO, USA)
Bis-Tris (Sigma, St. Louis, MO, USA)
Amylopectin (from potato starch) (Fluka, St. Louis, MO, USA)
100% Ethanol (Decon Laboratories, King of Prussia, PA, USA)

Malachite green standard curve.

The phosphate released during a malachite green assay with an active or potentially active enzyme is quantified by comparison to a standard curve. The standard curve is a ten-point curve from 100 pmol to 1nmol in 100 pmol increments.

1) Make a 100 mM stock solution of KH_2PO_4 in MilliQ H_2O or enzyme reaction buffer.

2) Make a 1:100 dilution in purified H_2O to create a 1 mM working solution. This solution will be used to make solutions from 100 pmol to 1nmol per 50 μL. A volume less than 50 μL is difficult to read in the spectrophotometer.

Solutions (μM)	pmol/50 μL
MilliQ H_2O	0
2	100
4	200
6	300
8	400
10	500
12	600
14	700
16	800
18	900
20	1000

3) The above table lists the required solutions for the standard curve and the moles of phosphate present in 50 μL of that solution. Prepare each of the solutions listed by first diluting a fraction of the 1 mM working solution to 1 mL with purified water. For example, to make a 2 μM solution from the 1mM stock solution, add 2 μL of the stock to 998 μL of QH_2O. Make and vortex all ten solutions well before analyzing.

4) Add 0.01% v/v Tween 20 (from a 10% stock solution) to an aliquot of malachite green reagent prior to use (10 μL per 10 mL). Keep on wet ice.

5) Put 50 μL of each solution into a 0.5 mL eppendorf tube, add 100 μL malachite green reagent + Tween 20, vortex, and incubate at room temperature for 30 minutes (these proportions are similar to the final proportions of samples for assay). Reactions are typically performed in triplicate.

6) Read all samples at 620nm at 30 minutes, and read again at 40 minutes. Cuvettes can be rinsed to avoid staining and reused.

7) Make a plot of mean absorbance at 620 nm, using a 0 pmol standard as the blank, (y axis), vs. pmol inorganic phosphate (x axis) for each dilution sample, and find the best fit line using a computer generated four parameter logistic (4-PL) curve fit. This can be done using most graphing software (e.g., Microsoft Excel) to give the linear equation y= mx+b. Using the standard curve values for the y-intercept (b) and the slope (m) of the regression line, the concentration of phosphate released (x) can be calculated using the experimental absorbance value (y).

Malachite green assay.

1) Add 0.01% v/v Tween 20 (from 10% stock solution) to an aliquot of malachite green reagent prior to use (10 μL per 10 mL). Keep on wet ice.
2) Thaw enzyme aliquots on wet ice.
3) Prepare 1X assay buffer for each pH to be tested, adding DTT to a final concentration of 1 mM.
4) Dilute enzymes to 50 to 1000 ng/μL with appropriate 1X assay buffer(s). The dilution of each enzyme is based upon its purity and rate of activity so that product formation remains in the linear range of detection during the assay.
5) Each reaction replicate is performed in a final volume of 20 μL, with a set of at least 3 replicates for each enzyme/ pH to be analyzed. When adding 1 μL of diluted enzyme, each reaction consists of:

- 4 μL H_2O
- 4 μL 5X assay buffer of optimal enzyme pH
- 2 μL 100 mM DTT
- 9 μL 5 mg/mL amylopectin

6) Add 1 μL of diluted enzyme to each reaction and vortex to mix thoroughly, placing the tube at 37°C. Begin timing once enzyme is added to the first tube, and be consistent with timing as enzyme is added to subsequent reactions. Four replicates per enzyme/ pH with a time interval of 15 seconds for enzyme addition to each replicate is suggested.

7) Incubate the reactions at 37°C for 10 minutes. After 10 minutes, add 20 μL of 0.1M NEM to quench PTP reactions or 80 μL malachite green reagent + Tween 20 to quench non-PTP reactions. Vortex tubes thoroughly on their sides to ensure any evaporated liquid is mixed. Add NEM or malachite green reagent + Tween 20 at identical time intervals as enzyme was added to the reactions and in the same order. As soon as malachite green reagent + Tween 20 is added to the first non-PTP tube, begin timing.
8) Add 80 μL malachite green reagent + Tween 20 to the PTP reactions quenched with NEM, vortex tubes on their sides, and begin timing immediately.
9) Incubate the reactions at 22°C for 30 to 40 minutes to develop color. The time of incubation is determined by the time of incubation utilized to generate the standard curve.
10) Measure the absorbance of the reactions at 620 nm in similar time intervals to the addition of malachite green reagent + Tween 20, using the appropriate blank (such as a control reaction with an inactive phosphatase). Cuvettes can be rinsed and reused to avoid staining.
11) Utilizing the values calculated from the standard curve, use the experimental absorbance value to determine the pmoles of phosphate released/min per nmol of protein.

Recipes.

***** All prepared in MilliQ H_2O 18.2 MΩcm

<u>5X Stock Assay Buffer (Store 22°C)</u>

0.5 M Sodium Acetate

0.25 M Bis-Tris

0.25 M Tris

pH to desired pH with HCl

5 mg/mL amylopectin in H_2O (Store 22°C).

1) Resuspend 5 mg/mL of amylopectin in H_2O.
2) Heat the suspension at 65˚C-95˚C until amylopectin goes into solution (previously opaque, the solution will become clear). Vortexing aids solubility.
3) Store at 22°C. If amylopectin precipitates over time (solution becomes opaque), heat it again until the solution becomes clear.

5 mg/mL amylopectin (Roach Method) (Store 22°C).

1) Combine 400 μl 100% ethanol, 1 mL H_2O, and 1 mL 2M NaOH.
2) Add 50 mg amylopectin.
3) Add 2 mL H_2O and adjust the pH to 6.5 with approximately 800 μl 2M HCl.
4) Bring the volume up to 10 mL with H_2O.

0.1M NEM and 100 mM DTT (store -20°C).

Prepared by dissolving stock in MilliQ H_2O 18.2 MΩcm. Sterile-filter prior to use.

Malachite green reagent (store 4˚C for up to 12 months).

1) Begin with 1 volume 4.2% w/v ammonium molybdate tetrahydrate ($(NH_4)_6Mo_7O_{24}.4H_2O$) in 4N HCl.
2) Add 3 volumes 0.045% w/v malachite green carbinol hydrochloride.
3) Stir for 30 minutes and filter with Whatman grade 5 filter paper.
4) Sterile-filter reagent. Store at 4˚C away from light. Malachite green solution is stable for up to 12 months.
5) Add 0.01% v/v Tween20 to malachite green reagent right before use (stock Tween20 should be 10% v/v).

Troubleshooting.

1) Malachite green reagent is green or brown, and not yellow in color.

Malachite green reagent is light sensitive, and also precipitates over time. It is essential to store the solution at 4˚C away from light. Precipitation can be removed by gentle heating, and reagent should be shaken well before use.

2) Blank OD value at 620 nm is 0.2 or higher.

Be sure to use double distilled water to prepare all reaction components and ensure lab wares are thoroughly washed to prevent contamination of enzyme preparations and assay buffers by free phosphate.

3) Standard or sample reactions precipitate upon incubation with malachite green reagent.

At high concentrations of phosphate (>100 μM), formation of precipitates may occur. Samples should be diluted and assays repeated. Divalent cations such manganese, magnesium, and calcium can form insoluble phosphate salts, so the lowest possible concentrations of these cations should be used in phosphatase buffers.

Equipment.

Beckman Coulter DU370 UV/Vis Spectrophotometer (Beckman Coulter, Indianapolis, IN, USA)

Temperature-controlled hotplate (Fisher Scientific, New Jersey, USA)

REFERENCES

1. (2010) About Epilepsy and Seizures, (Board, P. A., Ed.), Epilepsy Foundation, Landover.
2. Alonso, A., Rojas, A., Godzik, A., and Mustelin, T. (2003) *The dual-specific protein tyrosine phosphatase family*, Vol. 5, Springer, Berlin.
3. Alonso, A., Sasin, J., Bottini, N., Friedberg, I., Friedberg, I., Osterman, A., Godzik, A., Hunter, T., Dixon, J., and Mustelin, T. (2004) Protein Tyrosine Phosphatases in the Human Genome, *Cell 117*, 699.
4. Andersen, J. N., Mortensen, O. H., Peters, G. H., Drake, P. G., Iversen, L. F., Olsen, O. H., Jansen, P. G., Andersen, H. S., Tonks, N. K., and Moller, N. P. (2001) Structural and evolutionary relationships among protein tyrosine phosphatase domains, *Mol Cell Biol 21*, 7117-7136.
5. Arnold, K., Bordoli, L., Kopp, J., and Schwede, T. (2006) The SWISS-MODEL workspace: a web-based environment for protein structure homology modelling, *Bioinformatics 22*, 195-201.
6. Asante-Appiah, E., Ball, K., Bateman, K., Skorey, K., Friesen, R., Desponts, C., Payette, P., Bayly, C., Zamboni, R., Scapin, G., Ramachandran, C., and Kennedy, B. P. (2001) The YRD motif is a major determinant of substrate and inhibitor specificity in T-cell protein-tyrosine phosphatase, *J Biol Chem 276*, 26036-26043.
7. Ashe, K. M., Taylor, K. M., Chu, Q., Meyers, E., Ellis, A., Jingozyan, V., Klinger, K., Finn, P. F., Cooper, C. G., Chuang, W. L., Marshall, J., McPherson, J. M., Mattaliano, R. J., Cheng, S. H., Scheule, R. K., and Moreland, R. J. (2010) Inhibition of glycogen biosynthesis via mTORC1 suppression as an adjunct therapy for Pompe disease, *Mol Genet Metab 100*, 309-315.
8. Bai, Y., Milne, J. S., Mayne, L., and Englander, S. W. (1993) Primary structure effects on peptide group hydrogen exchange, *Proteins 17*, 75-86.
9. Bai, Y., Milne, J. S., Mayne, L., and Englander, S. W. (1994) Protein stability parameters measured by hydrogen exchange, *Proteins 20*, 4-14.

10. Bartal, C., Danon, A., Schlaeffer, F., Reisenberg, K., Alkan, M., Smoliakov, R., Sidi, A., and Almog, Y. (2003) Pharmacokinetic dosing of aminoglycosides: a controlled trial, *Am J Med 114*, 194-198.
11. Bedwell, D. M., Kaenjak, A., Benos, D. J., Bebok, Z., Bubien, J. K., Hong, J., Tousson, A., Clancy, J. P., and Sorscher, E. J. (1997) Suppression of a CFTR premature stop mutation in a bronchial epithelial cell line, *Nat Med 3*, 1280-1284.
12. Begley, M. J., Taylor, G. S., Brock, M. A., Ghosh, P., Woods, V. L., and Dixon, J. E. (2006) Molecular basis for substrate recognition by MTMR2, a myotubularin family phosphoinositide phosphatase, *Proc Natl Acad Sci U S A 103*, 927-932.
13. Berkovic, S. F., Andermann, F., Carpenter, S., and Wolfe, L. S. (1986) Progressive myoclonus epilepsies: specific causes and diagnosis, *N Engl J Med 315*, 296-305.
14. Berkovic, S. F., So, N. K., and Andermann, F. (1991) Progressive myoclonus epilepsies: clinical and neurophysiological diagnosis, *J Clin Neurophysiol 8*, 261-274.
15. Bidou, L., Hatin, I., Perez, N., Allamand, V., Panthier, J. J., and Rousset, J. P. (2004) Premature stop codons involved in muscular dystrophies show a broad spectrum of readthrough efficiencies in response to gentamicin treatment, *Gene Ther 11*, 619-627.
16. Blanchard, J. S. (1984) Buffers for enzymes, *Methods Enzymol 104*, 404-414.
17. Bollen, M., Peti, W., Ragusa, M. J., and Beullens, M. (2010) The extended PP1 toolkit: designed to create specificity, *Trends Biochem Sci 35*, 450-458.
18. Boraston, A. B., Bolam, D. N., Gilbert, H. J., and Daview, G. J. (2004) Carbohydrate-binding modules: fine-tuning polysaccharide recognition., The Biochemical Journal 382, 769-781.
19. Borden, K. L. a. P. S. F. (1996) The RING finger domain: a recent example of a sequence-structure family, *Current Opinion in Structural Biology 6*, 395-401.
20. Boubekeur, S., Boute, N., Pagesy, P., Zilberfarb, V., Christeff, N., and Issad, T. (2011) A new highly efficient substrate-trapping mutant of protein tyrosine

phosphatase 1B (PTP1B) reveals full autoactivation of the insulin receptor precursor, *J Biol Chem 286*, 19373-19380.

21. Brendel, C., Belakhov, V., Werner, H., Wegener, E., Gartner, J., Nudelman, I., Baasov, T., and Huppke, P. (2011) Readthrough of nonsense mutations in Rett syndrome: evaluation of novel aminoglycosides and generation of a new mouse model, *J Mol Med (Berl) 89*, 389-398.
22. Brendel, C., Klahold, E., Gartner, J., and Huppke, P. (2009) Suppression of nonsense mutations in Rett syndrome by aminoglycoside antibiotics, *Pediatr Res 65*, 520-523.
23. Brock, M., Fan, F., Mei, F. C., Li, S., Gessner, C., Woods, V. L., Jr., and Cheng, X. (2007) Conformational analysis of Epac activation using amide hydrogen/deuterium exchange mass spectrometry, *J Biol Chem 282*, 32256-32263.
24. Buleon, A., Colonna, P., Planchot, V., and Ball, S. (1998) Starch granules: structure and biosynthesis, *Int J Biol Macromol 23*, 85-112.
25. Cantarel, B. L., Coutinho, P. M., Rancurel, C., Bernard, T., Lombard, V., and Henrissat, B. (2009) The Carbohydrate-Active EnZymes database (CAZy): an expert resource for Glycogenomics, *Nucleic Acids Res 37*, D233-238.
26. Cao, J., Hsu, Y. H., Li, S., Woods, V. L., and Dennis, E. A. (2011) Lipoprotein-associated phospholipase A(2) interacts with phospholipid vesicles via a surface-disposed hydrophobic alpha-helix, *Biochemistry 50*, 5314-5321.
27. Carpenter, S., and Karpati, G. (1981) Sweat gland duct cells in Lafora disease: diagnosis by skin biopsy, *Neurology 31*, 1564-1568.
28. Chan, E. M., Ackerley, C. A., Lohi, H., Ianzano, L., Cortez, M. A., Shannon, P., Scherer, S. W., and Minassian, B. A. (2004) Laforin preferentially binds the neurotoxic starch-like polyglucosans, which form in its absence in progressive myoclonus epilepsy, *Hum Mol Genet 13*, 1117-1129.
29. Chan, E. M., Young, E. J., Ianzano, L., Munteanu, I., Zhao, X., Christopoulos, C. C., Avanzini, G., Elia, M., Ackerley, C. A., Jovic, N. J., Bohlega, S., Andermann, E., Rouleau, G. A., Delgado-Escueta, A. V., Minassian, B. A., and Scherer, S. W.

(2003) Mutations in NHLRC1 cause progressive myoclonus epilepsy, *Nat Genet 35*, 125-127.

30. Cheng, A., Zhang, M., Gentry, M. S., Worby, C. A., Dixon, J. E., and Saltiel, A. R. (2007) A role for AGL ubiquitination in the glycogen storage disorders of Lafora and Cori's disease, *Genes Dev. 21*, 2399-2409.
31. Christen, M., Hunenberger, P. H., Bakowies, D., Baron, R., Burgi, R., Geerke, D. P., Heinz, T. N., Kastenholz, M. A., Krautler, V., Oostenbrink, C., Peter, C., Trzesniak, D., and van Gunsteren, W. F. (2005) The GROMOS software for biomolecular simulation: GROMOS05, *J Comput Chem 26*, 1719-1751.
32. Clancy, J. P., Bebok, Z., Ruiz, F., King, C., Jones, J., Walker, L., Greer, H., Hong, J., Wing, L., Macaluso, M., Lyrene, R., Sorscher, E. J., and Bedwell, D. M. (2001) Evidence that systemic gentamicin suppresses premature stop mutations in patients with cystic fibrosis, *Am J Respir Crit Care Med 163*, 1683-1692.
33. Coleman, J. E. (1992) Structure and mechanism of alkaline phosphatase, *Annu Rev Biophys Biomol Struct 21*, 441-483.
34. Connelly, G. P., Bai, Y., Jeng, M. F., and Englander, S. W. (1993) Isotope effects in peptide group hydrogen exchange, *Proteins 17*, 87-92.
35. Coutinho, P. M., and Henrissat, B. (1999) Carbohydrate-active enzymes: an integrated database approach., In *Recent Advances in Carbohydrate Bioengineering* (H.J. Gilbert, G. D., B. Henrissat and B. Svensson Ed.), pp 3-12, The Royal Society of Chemistry, Cambridge.
36. Damo, S. M., Phillips, A. H., Young, A. L., Li, S., Woods, V. L., Jr., and Wemmer, D. E. (2010) Probing the conformation of a prion protein fibril with hydrogen exchange, *J Biol Chem 285*, 32303-32311.
37. Delgado-Escueta, A. V., Ganesh, S., and Yamakawa, K. (2001) Advances in the genetics of progressive myoclonus epilepsy, *Am J Med Genet 106*, 129-138.
38. Denu, J. M., Stuckey, J. A., Saper, M. A., and Dixon, J. E. (1996) Form and Function in Protein Dephosphorylation, *Cell 87*, 361.
39. Denu, J. M., Zhou, G., Wu, L., Zhao, R., Yuvaniyama, J., Saper, M. A., and Dixon, J. E. (1995) The Purification and Characterization of a Human Dual-specific Protein Tyrosine Phosphatase, *J. Biol. Chem. 270*, 3796-3803.

40. DePaoli-Roach, A. A., Tagliabracci, V. S., Segvich, D. M., Meyer, C. M., Irimia, J. M., and Roach, P. J. (2010) Genetic depletion of the malin E3 ubiquitin ligase in mice leads to lafora bodies and the accumulation of insoluble laforin, *J Biol Chem 285*, 25372-25381.
41. Du, M., Keeling, K. M., Fan, L., Liu, X., Kovacs, T., Sorscher, E., and Bedwell, D. M. (2006) Clinical doses of amikacin provide more effective suppression of the human CFTR-G542X stop mutation than gentamicin in a transgenic CF mouse model, *J Mol Med (Berl) 84*, 573-582.
42. Dukhande, V. V., Sherwood, A. R., and Gentry, M. S. (2010) Laforin- Nature Molecule Page, *Nature Molecule Pages*.
43. Englander, J. J., Del Mar, C., Li, W., Englander, S. W., Kim, J. S., Stranz, D. D., Hamuro, Y., and Woods, V. L., Jr. (2003) Protein structure change studied by hydrogen-deuterium exchange, functional labeling, and mass spectrometry, *Proc Natl Acad Sci U S A 100*, 7057-7062.
44. Englander, S. W., Mayne, L., Bai, Y., and Sosnick, T. R. (1997) Hydrogen exchange: the modern legacy of Linderstrom-Lang, *Protein Sci 6*, 1101-1109.
45. Feng, Q., Sekula, D., Muller, R., Freemantle, S. J., and Dmitrovsky, E. (2007) Uncovering residues that regulate cyclin D1 proteasomal degradation, *Oncogene 26*, 5098-5106.
46. Fernandez-Sanchez, M. E., Criado-Garcia, O., Heath, K. E., Garcia-Fojeda, B., Medrano-Fernandez, I., Gomez-Garre, P., Sanz, P., Serratosa, J. M., and Rodriguez de Cordoba, S. (2003) Laforin, the dual-phosphatase responsible for Lafora disease, interacts with R5 (PTG), a regulatory subunit of protein phosphatase-1 that enhances glycogen accumulation, *Hum Mol Genet 12*, 3161-3171.
47. Floquet, C., Hatin, I., Rousset, J. P., and Bidou, L. (2012) Statistical analysis of readthrough levels for nonsense mutations in mammalian cells reveals a major determinant of response to gentamicin, *PLoS Genet 8*, e1002608.
48. Forge, A., and Schacht, J. (2000) Aminoglycoside antibiotics, *Audiol Neurootol 5*, 3-22.

49. Ganesh, S., Agarwala, K. L., Amano, K., Suzuki, T., Delgado-Escueta, A. V., and Yamakawa, K. (2001) Regional and developmental expression of Epm2a gene and its evolutionary conservation, *Biochem Biophys Res Commun 283*, 1046-1053.

50. Ganesh, S., Delgado-Escueta, A. V., Sakamoto, T., Avila, M. R., Machado-Salas, J., Hoshii, Y., Akagi, T., Gomi, H., Suzuki, T., Amano, K., Agarwala, K. L., Hasegawa, Y., Bai, D. S., Ishihara, T., Hashikawa, T., Itohara, S., Cornford, E. M., Niki, H., and Yamakawa, K. (2002) Targeted disruption of the Epm2a gene causes formation of Lafora inclusion bodies, neurodegeneration, ataxia, myoclonus epilepsy and impaired behavioral response in mice, *Hum Mol Genet 11*, 1251-1262.

51. Ganesh, S., Delgado-Escueta, A. V., Suzuki, T., Francheschetti, S., Riggio, C., Avanzini, G., Rabinowicz, A., Bohlega, S., Bailey, J., Alonso, M. E., Rasmussen, A., Thomson, A. E., Ochoa, A., Prado, A. J., Medina, M. T., and Yamakawa, K. (2002) Genotype-phenotype correlations for EPM2A mutations in Lafora's progressive myoclonus epilepsy: exon 1 mutations associate with an early-onset cognitive deficit subphenotype, *Hum Mol Genet 11*, 1263-1271.

52. Ganesh, S., Puri, R., Singh, S., Mittal, S., and Dubey, D. (2006) Recent advances in the molecular basis of Lafora's progressive myoclonus epilepsy, *J Hum Genet 51*, 1-8.

53. Garcia, R. A., Pantazatos, D., and Villarreal, F. J. (2004) Hydrogen/deuterium exchange mass spectrometry for investigating protein-ligand interactions, *Assay Drug Dev Technol 2*, 81-91.

54. Gentry, M. S., Dixon, J. E., and Worby, C. A. (2009) Lafora disease: insights into neurodegeneration from plant metabolism, *Trends Biochem Sci 34*, 628-639.

55. Gentry, M. S., Dowen, R. H., 3rd, Worby, C. A., Mattoo, S., Ecker, J. R., and Dixon, J. E. (2007) The phosphatase laforin crosses evolutionary boundaries and links carbohydrate metabolism to neuronal disease, *J Cell Biol 178*, 477-488.

56. Gentry, M. S., and Pace, R. M. (2009) Conservation of the glucan phosphatase laforin is linked to rates of molecular evolution and the glycogen metabolism of the organism, *BMC Evol Biol 9*, 138.
57. Gentry, M. S., Roma-Mateo, C., and Sanz, P. (2013) Laforin, a protein with many faces: glucan phosphatase, adapter protein, et alii, *FEBS J 280*, 525-537.
58. Gentry, M. S., Worby, C. A., and Dixon, J. E. (2005) Insights into Lafora disease: malin is an E3 ubiquitin ligase that ubiquitinates and promotes the degradation of laforin, *Proc Natl Acad Sci U S A 102*, 8501-8506.
59. Glaring, M. A., Baumann, M. J., Abou Hachem, M., Nakai, H., Nakai, N., Santelia, D., Sigurskjold, B. W., Zeeman, S. C., Blennow, A., and Svensson, B. (2011) Starch-binding domains in the CBM45 family--low-affinity domains from glucan, water dikinase and alpha-amylase involved in plastidial starch metabolism, *FEBS J 278*, 1175-1185.
60. Guan, K. L., and Dixon, J. E. (1993) Bacterial and viral protein tyrosine phosphatases, *Semin Cell Biol 4*, 389-396.
61. Gunja-Smith, Z., Marshall, J. J., Mercier, C., Smith, E. E., and Whelan, W. J. (1970) A revision of the Meyer-Bernfeld model of glycogen and amylopectin, *FEBS Lett 12*, 101-104.
62. Ham, M. W. V. H. T. (1975) Lafora disease, a form of progressive myoclonus epilepsy., In *The Epilepsies. Handbook of Clinical Neurology.* (Bruyn, P. J. V. a. G. W., Ed.), pp 382-422., North-Holland, Amsterdam.
63. Hamuro, Y., Anand, G. S., Kim, J. S., Juliano, C., Stranz, D. D., Taylor, S. S., and Woods, V. L., Jr. (2004) Mapping intersubunit interactions of the regulatory subunit (RIalpha) in the type I holoenzyme of protein kinase A by amide hydrogen/deuterium exchange mass spectrometry (DXMS), *J Mol Biol 340*, 1185-1196.
64. Hamuro, Y., Coales, S. J., Morrow, J. A., Molnar, K. S., Tuske, S. J., Southern, M. R., and Griffin, P. R. (2006) Hydrogen/deuterium-exchange (H/D-Ex) of PPARgamma LBD in the presence of various modulators, *Protein Sci 15*, 1883-1892.

65. Hamuro, Y., Coales, S. J., Southern, M. R., Nemeth-Cawley, J. F., Stranz, D. D., and Griffin, P. R. (2003) Rapid analysis of protein structure and dynamics by hydrogen/deuterium exchange mass spectrometry, *J Biomol Tech 14*, 171-182.

66. Hamuro, Y., Zawadzki, K. M., Kim, J. S., Stranz, D. D., Taylor, S. S., and Woods, V. L., Jr. (2003) Dynamics of cAPK type IIbeta activation revealed by enhanced amide H/2H exchange mass spectrometry (DXMS), *J Mol Biol 327*, 1065-1076.

67. Harder, K. W., Owen, P., Wong, L. K., Aebersold, R., Clark-Lewis, I., and Jirik, F. R. (1994) Characterization and kinetic analysis of the intracellular domain of human protein tyrosine phosphatase beta (HPTP beta) using synthetic phosphopeptides, *Biochem J 298 (Pt 2)*, 395-401.

68. Harriman, D. G., Millar, J. H., and Stevenson, A. C. (1955) Progressive familial myoclonic epilepsy in three families: its clinical features and pathological basis, *Brain 78*, 325-349.

69. Henrissat, B. (1991) A classification of glycosyl hydrolases based on amino acid sequence similarities, *Biochem J 280 (Pt 2)*, 309-316.

70. Henrissat, B., and Bairoch, A. (1993) New families in the classification of glycosyl hydrolases based on amino acid sequence similarities, *Biochem J 293 (Pt 3)*, 781-788.

71. Hershko, A., and Ciechanover, A. (1998) The ubiquitin system, *Annu Rev Biochem 67*, 425-479.

72. Hirawat, S., Welch, E. M., Elfring, G. L., Northcutt, V. J., Paushkin, S., Hwang, S., Leonard, E. M., Almstead, N. G., Ju, W., Peltz, S. W., and Miller, L. L. (2007) Safety, tolerability, and pharmacokinetics of PTC124, a nonaminoglycoside nonsense mutation suppressor, following single- and multiple-dose administration to healthy male and female adult volunteers, *J Clin Pharmacol 47*, 430-444.

73. Howard, M., Frizzell, R. A., and Bedwell, D. M. (1996) Aminoglycoside antibiotics restore CFTR function by overcoming premature stop mutations, *Nat Med 2*, 467-469.

74. Howard, M. T., Anderson, C. B., Fass, U., Khatri, S., Gesteland, R. F., Atkins, J. F., and Flanigan, K. M. (2004) Readthrough of dystrophin stop codon mutations induced by aminoglycosides, *Ann Neurol 55*, 422-426.
75. Howard, M. T., Shirts, B. H., Petros, L. M., Flanigan, K. M., Gesteland, R. F., and Atkins, J. F. (2000) Sequence specificity of aminoglycoside-induced stop condon readthrough: potential implications for treatment of Duchenne muscular dystrophy, *Ann Neurol 48*, 164-169.
76. Hsu, S. (2008) Hydrogen/Deuterium-exchange (DXMS) Analysis of the Carbohydrate Phosphatase, Starch-Excess 4, In *Department of Medicine and Biomedical Sciences Graduate Program*, University of California, San Diego, La Jolla, CA.
77. Hsu, S., Kim, Y., Li, S., Durrant, E. S., Pace, R. M., Woods, V. L., and Gentry, M. S. (2009) Structural Insights of Glucan Phosphatase Dynamics using Amide Hydrogen/Deuterium Exchange Mass Spectrometry, *Biochemistry*.
78. Ianzano, L., Zhang, J., Chan, E. M., Zhao, X., Lohi, H., Scherer, S. W., and Minassian, B. A. (2005) Lafora progressive myoclonus epilepsy mutation database-EPM2A and NHLRC1 (EMP2B) genes, *Human Mutation 26*, 397.
79. Ianzano, L., Zhang, J., Chan, E. M., Zhao, X. C., Lohi, H., Scherer, S. W., and Minassian, B. A. (2005) Lafora progressive Myoclonus Epilepsy mutation database-EPM2A and NHLRC1 (EPM2B) genes, *Hum Mutat 26*, 397.
80. Itaya, K., and Ui, M. (1966) A new micromethod for the colorimetric determination of inorganic phosphate, *Clin Chim Acta 14*, 361-366.
81. Janecek, S., and Sevcik, J. (1999) The evolution of starch-binding domain, *FEBS Lett 456*, 119-125.
82. Janecek, S., Svensson, B., and MacGregor, E. A. (2011) Structural and evolutionary aspects of two families of non-catalytic domains present in starch and glycogen binding proteins from microbes, plants and animals, *Enzyme Microb Technol 49*, 429-440.
83. Janeway, R., Ravens, J. R., Pearce, L. A., Odor, D. L., and Suzuki, K. (1967) Progressive myoclonus epilepsy with Lafora inclusion bodies. I. Clinical, genetic, histopathologic, and biochemical aspects, *Arch Neurol 16*, 565-582.

84. Jia, Z., Barford, D., Flint, A. J., and Tonks, N. K. (1995) Structural basis for phosphotyrosine peptide recognition by protein tyrosine phosphatase 1B, *Science 268*, 1754-1758.
85. Jones, D. T. (1999) Protein secondary structure prediction based on position-specific scoring matrices, *J Mol Biol 292*, 195-202.
86. Keeling, K. M., and Bedwell, D. M. (2002) Clinically relevant aminoglycosides can suppress disease-associated premature stop mutations in the IDUA and P53 cDNAs in a mammalian translation system, *J Mol Med (Berl) 80*, 367-376.
87. Kerem, E., Hirawat, S., Armoni, S., Yaakov, Y., Shoseyov, D., Cohen, M., Nissim-Rafinia, M., Blau, H., Rivlin, J., Aviram, M., Elfring, G. L., Northcutt, V. J., Miller, L. L., Kerem, B., and Wilschanski, M. (2008) Effectiveness of PTC124 treatment of cystic fibrosis caused by nonsense mutations: a prospective phase II trial, *Lancet 372*, 719-727.
88. Kervestin, S., and Jacobson, A. (2012) NMD: a multifaceted response to premature translational termination, *Nat Rev Mol Cell Biol 13*, 700-712.
89. Kim, Y., Gentry, M. S., Harris, T. E., Wiley, S. E., Lawrence, J. C., Jr., and Dixon, J. E. (2007) A conserved phosphatase cascade that regulates nuclear membrane biogenesis, *Proc Natl Acad Sci U S A 104*, 6596-6601.
90. Konermann, L., Pan, J., and Liu, Y. H. (2011) Hydrogen exchange mass spectrometry for studying protein structure and dynamics, *Chem Soc Rev 40*, 1224-1234.
91. Kotting, O., Santelia, D., Edner, C., Eicke, S., Marthaler, T., Gentry, M. S., Comparot-Moss, S., Chen, J., Smith, A. M., Steup, M., Ritte, G., and Zeeman, S. C. (2009) STARCH-EXCESS4 Is a Laforin-Like Phosphoglucan Phosphatase Required for Starch Degradation in Arabidopsis thaliana, *Plant Cell 21*, 334-346.
92. Kubota, M., Mikami, B., Tsujisaka, Y., and Morita, Y. (1988) Crystallization of and preliminary crystallographic data for Bacillus stearothermophilus cyclodextrin glucanotransferase, *J Biochem 104*, 12-13.

93. Lanzetta, P. A., Alvarez, L. J., Reinach, P. S., and Candia, O. A. (1979) An improved assay for nanomole amounts of inorganic phosphate, *Anal Biochem 100*, 95-97.
94. Linde, L., and Kerem, B. (2008) Introducing sense into nonsense in treatments of human genetic diseases, *Trends Genet 24*, 552-563.
95. Liu, Y., Wang, Y., Wu, C., and Zheng, P. (2009) Deletions and missense mutations of EPM2A exacerbate unfolded protein response and apoptosis of neuronal cells induced by endoplasm reticulum stress, *Hum Mol Genet 18*, 2622-2631.
96. Lomako, J., Lomako, W. M., Kirkman, B. R., and Whelan, W. J. (1994) The role of phosphate in muscle glycogen, *Biofactors 4*, 167-171.
97. Luthy, R., Bowie, J. U., and Eisenberg, D. (1992) Assessment of protein models with three-dimensional profiles, *Nature 356*, 83-85.
98. Machovic, M., and Janecek, S. (2006) Starch-binding domains in the post-genome era, *Cell Mol Life Sci 63*, 2710-2724.
99. Machovic, M., Svensson, B., MacGregor, E. A., and Janecek, S. (2005) A new clan of CBM families based on bioinformatics of starch-binding domains from families CBM20 and CBM21, *FEBS J 272*, 5497-5513.
100. Maehama, T., and Dixon, J. E. (1998) The Tumor Suppressor, PTEN/MMAC1, Dephosphorylates the Lipid Second Messenger, Phosphatidylinositol 3,4,5-Trisphosphate, *J. Biol. Chem. 273*, 13375-13378.
101. Maehama, T., Taylor, G. S., Slama, J. T., and Dixon, J. E. (2000) A Sensitive Assay for Phosphoinositide Phosphatases, *Analytical Biochemistry 279*, 248-250.
102. Manuvakhova, M., Keeling, K., and Bedwell, D. M. (2000) Aminoglycoside antibiotics mediate context-dependent suppression of termination codons in a mammalian translation system, *RNA 6*, 1044-1055.
103. McCain, D. F., and Zhang, Z. Y. (2002) Assays for protein-tyrosine phosphatases, *Methods Enzymol 345*, 507-518.
104. Meekins, D. A., Guo, H. F., Husodo, S., Paasch, B. C., Bridges, T. M., Santelia, D., Kotting, O., Vander Kooi, C. W., and Gentry, M. S. (2013) Structure of the

Arabidopsis glucan phosphatase like sex four2 reveals a unique mechanism for starch dephosphorylation, *Plant Cell 25*, 2302-2314.

105. Minassian, B. A. (2001) Lafora's disease: towards a clinical, pathologic, and molecular synthesis, *Pediatr Neurol 25*, 21-29.
106. Minassian, B. A., Lee, J. R., Herbrick, J. A., Huizenga, J., Soder, S., Mungall, A. J., Dunham, I., Gardner, R., Fong, C. Y., Carpenter, S., Jardim, L., Satishchandra, P., Andermann, E., Snead, O. C., 3rd, Lopes-Cendes, I., Tsui, L. C., Delgado-Escueta, A. V., Rouleau, G. A., and Scherer, S. W. (1998) Mutations in a gene encoding a novel protein tyrosine phosphatase cause progressive myoclonus epilepsy, *Nat Genet 20*, 171-174.
107. Monaghan, T. S., and Delanty, N. (2010) Lafora disease: epidemiology, pathophysiology and management, *CNS Drugs 24*, 549-561.
108. Montalibet, J., Skorey, K. I., and Kennedy, B. P. (2005) Protein tyrosine phosphatase: enzymatic assays, *Methods 35*, 2-8.
109. Moorhead, G. B., De Wever, V., Templeton, G., and Kerk, D. (2009) Evolution of protein phosphatases in plants and animals, *Biochem J 417*, 401-409.
110. Morais, S., Lamed, R., and Bayer, E. A. (2012) Affinity electrophoresis as a method for determining substrate-binding specificity of carbohydrate-active enzymes for soluble polysaccharides, *Methods Mol Biol 908*, 119-127.
111. Moreno, D., Towler, M. C., Hardie, D. G., Knecht, E., and Sanz, P. (2010) The laforin-malin complex, involved in Lafora disease, promotes the incorporation of K63-linked ubiquitin chains into AMP-activated protein kinase beta subunits, *Mol Biol Cell 21*, 2578-2588.
112. Niittyla, T., Comparot-Moss, S., Lue, W.-L., Messerli, G., Trevisan, M., Seymour, M. D. J., Gatehouse, J. A., Villadsen, D., Smith, S. M., Chen, J., Zeeman, S. C., and Smith, A. M. (2006) Similar protein phosphatases control starch metabolism in plants and glycogen metabolism in mammals, *J. Biol. Chem. 281*, 11815-11818.
113. Nitschke, F., Wang, P., Schmieder, P., Girard, J. M., Awrey, D. E., Wang, T., Israelian, J., Zhao, X., Turnbull, J., Heydenreich, M., Kleinpeter, E., Steup, M., and Minassian, B. A. (2013) Hyperphosphorylation of glucosyl C6 carbons

and altered structure of glycogen in the neurodegenerative epilepsy Lafora disease, *Cell Metab 17*, 756-767.

114. Pantazatos, D., Kim, J. S., Klock, H. E., Stevens, R. C., Wilson, I. A., Lesley, S. A., and Woods, V. L., Jr. (2004) Rapid refinement of crystallographic protein construct definition employing enhanced hydrogen/deuterium exchange MS, *Proc Natl Acad Sci U S A 101*, 751-756.
115. Pardridge, W. M. (2010) Preparation of Trojan horse liposomes (THLs) for gene transfer across the blood-brain barrier, *Cold Spring Harb Protoc 2010*, pdb prot5407.
116. Patterson, K. I., Brummer, T., O'Brien, P. M., and Daly, R. J. (2009) Dual-specificity phosphatases: critical regulators with diverse cellular targets, *Biochem J 418*, 475-489.
117. Pederson, B. A., Turnbull, J., Epp, J. R., Weaver, S. A., Zhao, X., Pencea, N., Roach, P. J., Frankland, P., Ackerley, C. A., and Minassian, B. A. (2013) Inhibiting glycogen synthesis prevents lafora disease in a mouse model, *Ann Neurol*.
118. Pei, J., Kim, B. H., and Grishin, N. V. (2008) PROMALS3D: a tool for multiple protein sequence and structure alignments, *Nucleic Acids Res 36*, 2295-2300.
119. Prasad, A. N., and Hoffmann, G. F. (2010) Early onset epilepsy and inherited metabolic disorders: diagnosis and management, *Can J Neurol Sci 37*, 350-358.
120. Ramalho, A. S., Beck, S., Meyer, M., Penque, D., Cutting, G. R., and Amaral, M. D. (2002) Five percent of normal cystic fibrosis transmembrane conductance regulator mRNA ameliorates the severity of pulmonary disease in cystic fibrosis, *Am J Respir Cell Mol Biol 27*, 619-627.
121. Roach, P. J., Skurat, A. V., and Harris, R. A. (2001) Regulation of glycogen metabolism., In *The Endocrine Pancreas and Regulation of Metabolism* (Jefferson, L. S., and Cherrington, A. D., Eds.), pp 609-647, Oxford University Press, Inc New York, NY.

122. Roma-Mateo, C., Moreno, D., Vernia, S., Rubio, T., Bridges, T. M., Gentry, M. S., and Sanz, P. (2011) Lafora disease E3-ubiquitin ligase malin is related to TRIM32 at both the phylogenetic and functional level, *BMC Evol Biol 11*, 225.
123. Roy, J., and Cyert, M. S. (2009) Cracking the phosphatase code: docking interactions determine substrate specificity, *Sci Signal 2*, re9.
124. Sakai, M., Austin, J., Witmer, F., and Trueb, L. (1970) Studies in myoclonus epilepsy (Lafora body form). II. Polyglucosans in the systemic deposits of myoclonus epilepsy and in corpora amylacea, *Neurology 20*, 160-176.
125. Sanchez-Martin, P., Raththagala, M., Bridges, T. M., Husodo, S., Gentry, M. S., Sanz, P., and Roma-Mateo, C. (2013) Dimerization of the glucan phosphatase laforin requires the participation of cysteine 329, *PLoS One 8*, e69523.
126. Santelia, D., Kotting, O., Seung, D., Schubert, M., Thalmann, M., Bischof, S., Meekins, D. A., Lutz, A., Patron, N., Gentry, M. S., Allain, F. H., and Zeeman, S. C. (2011) The phosphoglucan phosphatase like sex Four2 dephosphorylates starch at the C3-position in Arabidopsis, *Plant Cell 23*, 4096-4111.
127. Santelia, K. O., Seung D, Schubert M, Thalmann M, Bischof S, Meekins S, Lutz A, Patron N, Gentry MS, Allain FHT and Zeeman S. (2011) Inhibition of phosphoglucan phosphatase LSF2 (Like Sex Four 2) in Arabidopsis leads to modified starch with elevated C3-bound phosphate content, *Plant Cell*.
128. Schuster, M. C., Ricklin, D., Papp, K., Molnar, K. S., Coales, S. J., Hamuro, Y., Sfyroera, G., Chen, H., Winters, M. S., and Lambris, J. D. (2008) Dynamic structural changes during complement C3 activation analyzed by hydrogen/deuterium exchange mass spectrometry, *Mol Immunol 45*, 3142-3151.
129. Schwarz, G. A., and Yanoff, M. (1965) Lafora's Disease. Distinct Clinico-Pathologic Form of Unverricht's Syndrome, *Archives of neurology 12*, 172-188.
130. Sermet-Gaudelus, I., Boeck, K. D., Casimir, G. J., Vermeulen, F., Leal, T., Mogenet, A., Roussel, D., Fritsch, J., Hanssens, L., Hirawat, S., Miller, N. L., Constantine, S., Reha, A., Ajayi, T., Elfring, G. L., and Miller, L. L. (2010) Ataluren (PTC124) induces cystic fibrosis transmembrane conductance

regulator protein expression and activity in children with nonsense mutation cystic fibrosis, *Am J Respir Crit Care Med 182*, 1262-1272.

131. Sermet-Gaudelus, I., Renouil, M., Fajac, A., Bidou, L., Parbaille, B., Pierrot, S., Davy, N., Bismuth, E., Reinert, P., Lenoir, G., Lesure, J. F., Rousset, J. P., and Edelman, A. (2007) In vitro prediction of stop-codon suppression by intravenous gentamicin in patients with cystic fibrosis: a pilot study, *BMC Med 5*, 5.
132. Serratosa, J. M. (1995) [Genetic molecular basis of epilepsy], *Rev Neurol 23*, 1290-1291.
133. Serratosa, J. M., Gomez-Garre, P., Gallardo, M. E., Anta, B., de Bernabe, D. B., Lindhout, D., Augustijn, P. B., Tassinari, C. A., Malafosse, R. M., Topcu, M., Grid, D., Dravet, C., Berkovic, S. F., and de Cordoba, S. R. (1999) A novel protein tyrosine phosphatase gene is mutated in progressive myoclonus epilepsy of the Lafora type (EPM2), *Hum Mol Genet 8*, 345-352.
134. Serratosa, J. M., Minassian, B. A., and Ganesh, S. (2012) Progressive myoclonus epilepsy of Lafora.
135. Sharma, J., Rao, S. N., Shankar, S. K., Satishchandra, P., and Jana, N. R. (2011) Lafora disease ubiquitin ligase malin promotes proteasomal degradation of neuronatin and regulates glycogen synthesis, *Neurobiol Dis 44*, 133-141.
136. Shen, J. J., and Chen, Y. T. (2002) Molecular characterization of glycogen storage disease type III, *Curr Mol Med 2*, 167-175.
137. Sherwood, A. R., Johnson, M. B., Delgado-Escueta, A. V., and Gentry, M. S. (2013) A bioassay for Lafora disease and laforin glucan phosphatase activity, *Clin Biochem*. In press.
138. Sherwood, A. R., Paasch, B. C., Worby, C. A., and Gentry, M. S. (2013) A Malachite Green-Based Assay to Assess Glucan Phosphatase Activity, *Anal Biochem 435*, 54-56.
139. Shi, N., and Pardridge, W. M. (2000) Noninvasive gene targeting to the brain, *Proc Natl Acad Sci U S A 97*, 7567-7572.
140. Shi, Y. (2009) Serine/threonine phosphatases: mechanism through structure, *Cell 139*, 468-484.

141. Singh, S., and Ganesh, S. (2009) Lafora progressive myoclonus epilepsy: a meta-analysis of reported mutations in the first decade following the discovery of the EPM2A and NHLRC1 genes, *Hum Mutat 30*, 715-723.
142. Skinner, J. J., Lim, W. K., Bedard, S., Black, B. E., and Englander, S. W. (2012) Protein dynamics viewed by hydrogen exchange, *Protein Sci 21*, 996-1005.
143. Slack, F. J., and Ruvkun, G. (1998) A novel repeat domain that is often associated with RING finger and B-box motifs, *Trends Biochem Sci 23*, 474-475.
144. Snider, N. T., Park, H., and Omary, M. B. (2013) A Conserved Rod Domain Phosphotyrosine That Is Targeted by the Phosphatase PTP1B Promotes Keratin 8 Protein Insolubility and Filament Organization, *J Biol Chem 288*, 31329-31337.
145. Soding, J. (2005) Protein homology detection by HMM-HMM comparison, *Bioinformatics 21*, 951-960.
146. Soding, J., Biegert, A., and Lupas, A. N. (2005) The HHpred interactive server for protein homology detection and structure prediction, *Nucleic Acids Res 33*, W244-248.
147. Solaz-Fuster, M. C., Gimeno-Alcaniz, J. V., Ros, S., Fernandez-Sanchez, M. E., Garcia-Fojeda, B., Criado Garcia, O., Vilchez, D., Dominguez, J., Garcia-Rocha, M., Sanchez-Piris, M., Aguado, C., Knecht, E., Serratosa, J., Guinovart, J. J., Sanz, P., and Rodriguez de Cordoba, S. (2008) Regulation of glycogen synthesis by the laforin-malin complex is modulated by the AMP-activated protein kinase pathway, *Hum Mol Genet 17*, 667-678.
148. Strausbaugh, L. J., and Brinker, G. S. (1983) Effect of osmotic blood-brain barrier disruption on gentamicin penetration into the cerebrospinal fluid and brains of normal rabbits, *Antimicrob Agents Chemother 24*, 147-150.
149. Tagliabracci, V. S., Girard, J. M., Segvich, D., Meyer, C., Turnbull, J., Zhao, X., Minassian, B. A., Depaoli-Roach, A. A., and Roach, P. J. (2008) Abnormal metabolism of glycogen phosphate as a cause for lafora disease, *J Biol Chem 283*, 33816-33825.

150. Tagliabracci, V. S., Girard, J. M., Segvich, D., Meyer, C., Turnbull, J., Zhao, X., Minassian, B. A., Depaoli-Roach, A. A., and Roach, P. J. (2008) Abnormal metabolism of glycogen phosphate as a cause for Lafora disease, *J Biol Chem 283*, 33816-33825.
151. Tagliabracci, V. S., Heiss, C., Karthik, C., Contreras, C. J., Glushka, J., Ishihara, M., Azadi, P., Hurley, T. D., DePaoli-Roach, A. A., and Roach, P. J. (2011) Phosphate incorporation during glycogen synthesis and Lafora disease, *Cell Metab 13*, 274-282.
152. Tagliabracci, V. S., Turnbull, J., Wang, W., Girard, J. M., Zhao, X., Skurat, A. V., Delgado-Escueta, A. V., Minassian, B. A., Depaoli-Roach, A. A., and Roach, P. J. (2007) Laforin is a glycogen phosphatase, deficiency of which leads to elevated phosphorylation of glycogen in vivo, *Proc Natl Acad Sci U S A 104*, 19262-19266.
153. Tonks, N. K. (2013) Protein tyrosine phosphatases--from housekeeping enzymes to master regulators of signal transduction, *FEBS J 280*, 346-378.
154. Tonks, N. K. (2006) Protein tyrosine phosphatases: from genes, to function, to disease, *Nat Rev Mol Cell Biol 7*, 833-846.
155. Tsutsui, Y., and Wintrode, P. L. (2007) Hydrogen/deuterium exchange-mass spectrometry: a powerful tool for probing protein structure, dynamics and interactions, *Curr Med Chem 14*, 2344-2358.
156. Turnbull, J., DePaoli-Roach, A. A., Zhao, X., Cortez, M. A., Pencea, N., Tiberia, E., Piliguian, M., Roach, P. J., Wang, P., Ackerley, C. A., and Minassian, B. A. (2011) PTG depletion removes Lafora bodies and rescues the fatal epilepsy of Lafora disease, *PLoS Genet 7*, e1002037.
157. Turnbull, J., Wang, P., Girard, J. M., Ruggieri, A., Wang, T. J., Draginov, A. G., Kameka, A. P., Pencea, N., Zhao, X., Ackerley, C. A., and Minassian, B. A. (2010) Glycogen hyperphosphorylation underlies lafora body formation, *Ann Neurol 68*, 925-933.
158. Tyers, M. a. A. R. W. (1999) One Ring to Rule a Superfamily of E3 Ubiquitin Ligases, *Science 284*, 601-604.

159. Valles-Ortega, J., Duran, J., Garcia-Rocha, M., Bosch, C., Saez, I., Pujadas, L., Serafin, A., Canas, X., Soriano, E., Delgado-Garcia, J. M., Gruart, A., and Guinovart, J. J. (2011) Neurodegeneration and functional impairments associated with glycogen synthase accumulation in a mouse model of Lafora disease, *EMBO Mol Med 3*, 667-681.

160. Vander Kooi, C. W., Taylor, A. O., Pace, R. M., Meekins, D. A., Guo, H. F., Kim, Y., and Gentry, M. S. (2010) Structural basis for the glucan phosphatase activity of Starch Excess4, *Proc Natl Acad Sci U S A 107*, 15379-15384.

161. Vernia, S., Rubio, T., Heredia, M., Rodriguez de Cordoba, S., and Sanz, P. (2009) Increased endoplasmic reticulum stress and decreased proteasomal function in lafora disease models lacking the phosphatase laforin, *PLoS One 4*, e5907.

162. Vernia, S., Solaz-Fuster, M. C., Gimeno-Alcaniz, J. V., Rubio, T., Garcia-Haro, L., Foretz, M., Rodriguez de Cordoba, S., and Sanz, P. (2009) AMP-activated protein kinase phosphorylates R5/PTG, the glycogen targeting subunt of the R5/PTG-PP1 holoenzyme and accelerates its downregulation by the laforin-malin complex, *J Biol Chem*.

163. Vilchez, D., Ros, S., Cifuentes, D., Pujadas, L., Valles, J., Garcia-Fojeda, B., Criado-Garcia, O., Fernandez-Sanchez, E., Medrano-Fernandez, I., Dominguez, J., Garcia-Rocha, M., Soriano, E., Rodriguez de Cordoba, S., and Guinovart, J. J. (2007) Mechanism suppressing glycogen synthesis in neurons and its demise in progressive myoclonus epilepsy, *Nat Neurosci 10*, 1407-1413.

164. Virshup, D. M., and Shenolikar, S. (2009) From promiscuity to precision: protein phosphatases get a makeover, *Mol Cell 33*, 537-545.

165. Wagner, K. R., Hamed, S., Hadley, D. W., Gropman, A. L., Burstein, A. H., Escolar, D. M., Hoffman, E. P., and Fischbeck, K. H. (2001) Gentamicin treatment of Duchenne and Becker muscular dystrophy due to nonsense mutations, *Ann Neurol 49*, 706-711.

166. Wang, J., Stuckey, J. A., Wishart, M. J., and Dixon, J. E. (2002) A unique carbohydrate binding domain targets the lafora disease phosphatase to glycogen, *J Biol Chem 277*, 2377-2380.

167. Wang, W., Parker, G. E., Skurat, A. V., Raben, N., DePaoli-Roach, A. A., and Roach, P. J. (2006) Relationship between glycogen accumulation and the laforin dual specificity phosphatase, *Biochem Biophys Res Commun 350*, 588-592.

168. Weinreb, P. H., Li, S., Gao, S. X., Liu, T., Pepinsky, R. B., Caravella, J. A., Lee, J. H., and Woods, V. L., Jr. (2012) Dynamic structural changes are observed upon collagen and metal ion binding to the integrin alpha1 I domain, *J Biol Chem 287*, 32897-32912.

169. Welch, E. M., Barton, E. R., Zhuo, J., Tomizawa, Y., Friesen, W. J., Trifillis, P., Paushkin, S., Patel, M., Trotta, C. R., Hwang, S., Wilde, R. G., Karp, G., Takasugi, J., Chen, G., Jones, S., Ren, H., Moon, Y. C., Corson, D., Turpoff, A. A., Campbell, J. A., Conn, M. M., Khan, A., Almstead, N. G., Hedrick, J., Mollin, A., Risher, N., Weetall, M., Yeh, S., Branstrom, A. A., Colacino, J. M., Babiak, J., Ju, W. D., Hirawat, S., Northcutt, V. J., Miller, L. L., Spatrick, P., He, F., Kawana, M., Feng, H., Jacobson, A., Peltz, S. W., and Sweeney, H. L. (2007) PTC124 targets genetic disorders caused by nonsense mutations, *Nature 447*, 87-91.

170. Wilschanski, M., Miller, L. L., Shoseyov, D., Blau, H., Rivlin, J., Aviram, M., Cohen, M., Armoni, S., Yaakov, Y., Pugatsch, T., Cohen-Cymberknoh, M., Miller, N. L., Reha, A., Northcutt, V. J., Hirawat, S., Donnelly, K., Elfring, G. L., Ajayi, T., and Kerem, E. (2011) Chronic ataluren (PTC124) treatment of nonsense mutation cystic fibrosis, *Eur Respir J 38*, 59-69.

171. Wilschanski, M., Yahav, Y., Yaacov, Y., Blau, H., Bentur, L., Rivlin, J., Aviram, M., Bdolah-Abram, T., Bebok, Z., Shushi, L., Kerem, B., and Kerem, E. (2003) Gentamicin-induced correction of CFTR function in patients with cystic fibrosis and CFTR stop mutations, *N Engl J Med 349*, 1433-1441.

172. Worby, C. A., Gentry, M. S., and Dixon, J. E. (2006) Laforin, a dual specificity phosphatase that dephosphorylates complex carbohydrates, *J Biol Chem 281*, 30412-30418.

173. Worby, C. A., Gentry, M. S., and Dixon, J. E. (2006) Laforin: A dual specificity phosphatase that dephosphorylates complex carbohydrates, *J. Biol. Chem. 281*, 30412-30418.

174. Worby, C. A., Gentry, M. S., and Dixon, J. E. (2008) Malin decreases glycogen accumulation by promoting the degradation of protein targeting to glycogen (PTG), *J Biol Chem 283*, 4069-4076.
175. Xiao, J., Engel, J. L., Zhang, J., Chen, M. J., Manning, G., and Dixon, J. E. (2011) Structural and functional analysis of PTPMT1, a phosphatase required for cardiolipin synthesis, *Proc Natl Acad Sci U S A 108*, 11860-11865.
176. Yokoi, S., Austin, J., Witmer, F., and Sakai, M. (1968) Studies in myoclonus epilepsy (Lafora body form). I. Isolation and preliminary characterization of Lafora bodies in two cases, *Arch Neurol 19*, 15-33.
177. Yuvaniyama, J., Denu, J. M., Dixon, J. E., and Saper, M. A. (1996) Crystal structure of the dual specificity protein phosphatase VHR, *Science 272*, 1328-1331.
178. Zhang, Z., and Smith, D. L. (1993) Determination of amide hydrogen exchange by mass spectrometry: a new tool for protein structure elucidation, *Protein Sci 2*, 522-531.
179. Zhang, Z. Y., Clemens, J. C., Schubert, H. L., Stuckey, J. A., Fischer, M. W., Hume, D. M., Saper, M. A., and Dixon, J. E. (1992) Expression, purification, and physicochemical characterization of a recombinant Yersinia protein tyrosine phosphatase, *J Biol Chem 267*, 23759-23766.

VITA

Amanda Renee Sherwood

Hometown: San Antonio, Texas, USA

EDUCATION

B.S., Biology, Centre College, Danville Kentucky, 2008

AWARDS AND FELLOWSHIPS

Center for Clinical and Translational Science Seed Grant Award, UK, 2012-2013
Predoctoral Travel Award, UK Graduate School, 2012
Graduate Certificate in Clinical and Translational Science, UK, 2012
NIH/NCRR CTSA T32 Predoctoral Fellowship Award, 2011-2013
Presidential Fellowship Nominee, 2010
Predoctoral Travel Award, UK Graduate School, 2009
Good Standing, University of Kentucky College of Medicine, 2008-2013
Tri Beta Honor Society (Biology), Centre College, 2007-2008
KBRIN-REU (Research Experience For Undergraduates) Fellow, UK, 2007
First Place Undergraduate Poster in Cellular and Molecular Biology, Kentucky Academy of Sciences, 2007
The Monnie McChord Scholarship Prize, Centre College, 2006

PUBLICATIONS

Amanda R Sherwood, Antonio V Delgado-Escueta, and Matthew S Gentry. Suppression of Nonsense Mutations in Laforin and Malin as a Therapeutic Option for Lafora Disease. (Manuscript in preparation).

Amanda R Sherwood, Mary Beth Johnson, Antonio V Delgado-Escueta, and Matthew S Gentry. A Bioassay for Lafora Disease and Laforin Glucan Phosphatase Activity. Accepted in *Clinical Biochemistry* (2013). In press. (doi: 10.1016/j.clinbiochem.2013.08.016)

Amanda R Sherwood, Bradley C Paasch, Carolyn A Worby, and Matthew S Gentry. A Malachite Green-Based Assay to Assess Glucan Phosphatase Activity. *Analytical Biochemistry* (2013). 435:1, pp 54-56.

Amanda R Sherwood, Vikas V Dukhande, and Matthew S Gentry. Laforin: Function and Action of a Glucan Phosphatase. *Encyclopedia of Signaling Molecules* (2012). Springer. Vol 1: pp 1003-1010. (doi: 10.1007/978-1-4419-0461-4_603).

Vikas V Dukhande, **Amanda R Sherwood**, and Matthew S Gentry. Laforin. *UCSD-Nature Molecule Pages* (2010). (doi: 10.1038/mp.a000032.01).

INVITED PRESENTATIONS

Deciphering Lafora Disease Using Translational and Biophysical Approaches.
Centre College, Danville, KY. *A*pril 2013.

Structural Dynamics of the Glucan Phosphatase Laforin and a Biomarker for Activity.
University of Kentucky, Lexington, KY. March 2012.

Amanda Renee Sherwood

November 27, 2013